A SOLUTION AND SOLID STATE STUDY OF VANADIUM COMPLEXES

by

CARLA PRETORIUS

A dissertation submitted to meet the requirements for the degree of

MAGISTER SCIENTIAE

in the

DEPARTMENT OF CHEMISTRY

FACULTY OF NATURAL-AND AGRICULTURAL SCIENCES

at the

UNIVERSITY OF THE FREE STATE

Supervisor

Prof. Andreas Roodt

Co-Supervisor

Dr. Johan A. Venter

JANUARY 2012

Acknowledgements

Firstly, I would like to thank God for all the blessings that have been bestowed upon me in my life. For carrying me when I couldn't think of taking another step. My life is filled with love from family and friends that You have placed in my life and Your amazing works inspire me daily.

My parents, Pierre and Ronelle Pretorius. You have given me so much in life- from material things to inspiration through your hard work and dedication in every aspect of life. I cannot say enough how much I love and look up to you for being my safe place when I need it.

Jacques, Ricky, family and friends. Jacques- your jokes bring the much needed relief after a hard day's work. Ricky- you are as dependable as a rock, always there when needed and for that I say thank you. To all who have entered my life and enriched it over the years- thank you for adding true meaning to life.

Mrs. Dreyer, as my high school science teacher you instilled in me the enthusiasm I have today for science. Through your passion which was so contagious I fell in love with this discipline. You could have stood your ground against any professor in chemistry and I hope you continue to inspire many more students.

Prof. A. Roodt, could I have asked for a more remarkable supervisor? Your knowledge is incredible and yet I respect you most for the humility you show. For treating your students with such respect. For never laughing at our ideas and pushing us in the right directions to learn as much as we can from our work. Thank you for all the effort in the research presented here and I hope to learn much more in the years to come.

Dr. J. A. Venter, thank you so much for the kind words when needed and the ear you are always willing to lend to your students. I can without a doubt say you have been one of my favourite lecturers during my studies and it was a privilege to work together on this research project.

SASOL, University of the Free State and the South African National Research Foundation (NRF) are gratefully acknowledged for financial assistance and for making this project possible.

The Chemistry people I need to thank- Ricky Kotze (collection of crystals on the XRD and being the go-to person when I need some answers), Truidie (Translations and the hours in the NMR room) and the entire Inorganic Chemistry group for their contributions to this work.

Lastly, this work would never have come to this point if it wasn't for the inspiration of one person in particular, Johannes Petrus (JP) Pretorius. I miss you and it was you that believed in me to pursue my studies. For believing I was more than what meets the eye and for teaching me so much.

TABLE OF CONTENTS

Abbreviations and Symbols

Abbreviation	Meaning
acac	Acetylacetonate
Et-acac	3-Ethyl-2,4-pentanedionate
Me-acac	3-Methyl-2,4-pentanedionate
dbm	Dibenzoylmethane
thtfac	Thenoyltrifluoroacetone
trop	Tropolone
cupf	Cupferron
Ox	8-Hydroxyquinoline
Z	Number of molecules in a unit cell
Å	Angstrom
NMR	Nuclear Magnetic Resonance spectroscopy
KMR	Kern Magnetiese Resonans spekstroskopie
IR	Infrared spectroscopy
ν	Stretching frequency on IR
δ	Chemical shift
ppm	Parts per million
π	pi
σ	sigma
α	Alpha
β	Beta
γ	Gamma
λ	Wavelength
Θ	Thetha
°	Degrees
°C	Degrees Celsius
ε	Extinction coefficient
g	Gram
M	$mol.dm^{-3}$
mM	Millimolar
mg	Milligram
ΔH	Enthalpy of activation
ΔS	Entropy of activation
h	Planck's constant
k_B	Boltzman's constant
k_{obs}	Observed pseudo-first order rate constant
K	Equilibrium constant
pK_a	Acid dissociation constant
pH	Measure of acidity
Me	Methyl
Ph	Phenyl
T	Temperature
UV	Ultraviolet region in light spectrum
Vis	Visible region in light spectrum
DMSO-d^6	Dimethyl sufoxide
$CDCl_3$	Deuterated chloroform
D_2O	Deuterium oxide
TMS	Tetramethylsilane
MeOH	Methanol
bpy	2,2 bipyridine
pic	Picolinic acid
2,3 dipic	2,3-pyridinedicarboxylic acid
2,6 dipic	2,6-pyridinedicarboxylic acid

ABSTRACT

Vanadium is an early first-row transition metal that is known for the beautiful coloured compounds that it forms in a wide range of oxidation states. In high oxidation states, vanadium is very oxophilic whilst at low oxidation states, π-donating ligands are preferred. It is the only element in the periodic table to be named after a goddess (the Nordic goddess Vanadis), and perhaps with this legacy in mind some unpredictable and surprising chemistry might be expected.

This research study focussed on the rich and diverse coordination chemistry of vanadium. Various vanadium(IV) and vanadium(V) compounds were successfully synthesized with O,O^- and N,O^--Bid ligand systems (Bid= five or six membered chelating ligand *via* O,O' or N,O-donor atoms). These ligands were chosen for their wide application in terms of industrial use in the development of catalysts as well as their biological activity for pharmacological application. To achieve the above mentioned aim various characterization techniques were mastered such as IR, UV/Vis, NMR and single crystal X-ray diffraction. To this regard four vanadium complexes were successfully characterized by XRD namely [VO(dbm)$_2$], [VO(dbm)$_2$(MeOH)]•2MeOH, [VO(dbm)$_2$py] and (C$_9$H$_{17}$O$_2$)[VO$_2$(cupf)$_2$]. The three diketonato containing complexes provided unique stereo-electronic changes in each case and the effect upon distortion of the vanadium centre as well as the *trans* effect of the oxido bond could be evaluated. The last mentioned compound was of special interest as the novel 2,2,6,6-tetramethyldihydropyran-4-onium that acts as cation for the anionic vanadium complex was speculated to have formed either by cyclization of acetone during the reaction or by action of the vanadium present.

In addition to the synthesis component of the research a kinetic substitution study was instigated. The complex solution chemistry of vanadium resulted in a wide array of experiments to evaluate the effects of not only ligand concentration on reaction rates but also pH dependence of certain species in solution. This culminated in a proposed reaction mechanism and rate law that accounts for various pH, pK$_a$ and concentration effects.

As vanadium is known for its biological activity, selected complexes synthesized from this study was investigated for *in vitro* cancer screening. These results were concluded as not being positive but provided valuable insight for future ligand and complex design.

^{51}V NMR was effectively used in this study both in the synthesis component as well as the kinetic study conducted. Valuable insight into the electronic environment experienced by the vanadium centre was obtained and correlations could be established between steric strain within a complex and the amount of shielding experienced by the vanadium centre. Additionally, experiments such as in the kinetic study could be followed over time on ^{51}V NMR and revealed important information regarding product formation and the identification of an intermediate $[VO(O_2)(2,3\text{-dipic})]^{2-}$ in the reaction which was vital in construction of the reaction mechanism.

OPSOMMING

Vanadium is `n vroeg eerste ry oorgangsmetaal wat bekend is vir die pragtige gekleurde komplekse wat dit vorm in `n wye reeks oksidasietoestande. In `n hoë oksidasietoestand is vanadium baie oksofilies terwyl $\pi$-skenkende ligande verkies word by lae oksidasietoestande. Dit is die enigste element wat na `n godin vernoem is (die Noordiese Vanadis), en bring dalk saam met hierdie erfenis `n gevoel van onvoorspelbare en verrassende chemie.

Hierdie navorsingstudie fokus op die ryk en uiteenlopende koördinasiechemie van vanadium. Verskeie vanadium(IV) en vanadium(V) komplekse is suksesvol vervaardig met O,O^- en N,O^--Bid ligandstelsels (Bid= vyf-of seslid chelerende ligande via 'n O,O'-of N,O-donerende paar). Hierdie ligande is gekies vir hulle wye verskeidenheid gebruike in terme van industriële toepassings in die ontwikkeling van kataliste asook hulle biologiese aktiwiteit vir farmakologiese toepassing. Om die bogenoemde doel te behaal is verskeie tegnieke, soos IR, UV/Vis, KMR en enkelkristal X-straaldiffraksie, bemeester. In hierdie verband is vier vanadium komplekse suksesvol gekarakteriseer deur XRD, naamlik $[VO(dbm)_2]$, $[VO(dbm)_2(MeOH)] \cdot 2MeOH$, $[VO(dbm)_2py]$ en $(C_9H_{17}O_2)[VO_2(cupf)_2]$. Die drie diketonato-bevattende komplekse het in elke geval unieke stereo-elektroniese veranderinge geopenbaar en die effek van vervorming van die vanadiumkern asook die *trans* effek van die oksido binding kon nagevors word. Die laasgenoemde kompleks is van spesiale belang aangesien gespekuleer word dat die unieke 2,2,6,6, tetrametielpironium wat optree as katioon vir die anioniese vanadium kompleks gevorm is òf deur siklisering van asetoon gedurende die reaksie, òf deur die aksie van die vanadium teenwoordig.

Byvoegend tot die sintetiese aspek van hierdie projek is `n studie van `n kinetiese substitusie geïnisieer. Die ingewikkelde oplossingschemie van vanadium het gelei tot `n wye reeks eksperimente om nie net die effek van ligand konsentrasie op reaksietempo nie, maar ook pH-afhanklikheid van sekere spesies in oplossing vas te stel.   Dit het uitgeloop op die voorgestelde reaksiemeganisme en tempowet wat verskillende pH, pK_a en konsentrasie effekte in ag neem.

Aangesien vanadium bekend is vir biologiese aktiwiteit is gekose komplekse wat vir hierdie studie vervaardig is ondersoek vir *in vitro* kanker sifting. Hierdie resultate is gevind as nie positief nie, maar het waardevolle insigte verskaf ten opsigte van toekomstige ligand- en kompleksontwerpe.

^{51}V KMR is effektief in hierdie studie gebruik in beide die sintetiese komponent en die kinetiese studie en waardevolle inligting is ingewin aangaande die elektroniese omgewing wat deur die vanadium kern ervaar word. Korrelasies kon vasgestel word tussen die steriese stremming binne die kompleks en die hoeveelheid skerming deur die vanadium kern ervaar. Daarbenewens kon eksperimente soos die kinetiese studie oor `n tydperk gevolg word wat belangrike inligting verskaf het aangaande produkvorming en die identifikasie van intermediêre die $[VO(O_2)(2,3\text{-dipic})]^{2-}$, wat uiters belangrik was in die konstruksie van die reaksiemeganisme.

Chapter 1: Introduction

1.1   Introduction

The element vanadium offers a rich and diverse chemistry that has seen an influx of interest over the last two decades. This can be attributed to recent discoveries of vanadium-containing enzymes and a range of catalytic applications for vanadium complexes.

Various novel vanadium complexes have been researched for insulin mimicking action in the fight against diabetes with these studies bearing fruit in the form of the bis(maltolato)oxovanadium(IV) complex that has recently entered clinical trials.[1] Additionally, peroxovandates have shown great potential as insulin mimics and are extensively being studied for further improvement in the reduction of side-effects once administered.

Vanadium has also found a prominent role to be played in the world's search for greener living. As part of a 'green chemistry' project, water-soluble polyoxovanadates are being investigated as oxo-transfer catalysts that require small energy inputs and result in few waste products.[2]

Inorganic and organovanadium compounds have shown great versatility in terms of application in the biological and medicinal fields, as well as in material sciences and catalysis, prompting much needed research into basic vanadium chemistry. This will in turn assist future work in developing and understanding complex systems that vanadium is involved in.

[1] McNeill, J. H., Yuen, V. G., Hoveyda, H. R., Orvig, C., *J. Med. Chem.*, **1992**, *35*, 1489.
[2] Love, J. B., *Annu. Rep. Prog. Chem., Sect. A.*, **2004**, *100*, 163.

1.2 Application of Vanadium in Industry

1.2.1 Industrial Processes

Vanadium is utilized in industry for a wide range of applications. Apart from its usage in steel production, vanadium is used as a corrosion inhibitor for reactor vessels where surface films of vanadium oxides form in order to protect the steel walls.[3]

In the Stredford and Sulfolin processes vanadium(V) is utilized to oxidize H_2S, found in fossil fuels, to S^0. Sulphur as a serious pollutant must be removed from fossil fuels before burning in order to prevent release into the atmosphere.[4] The best known industrial process to employ vanadium remains however the contact process for the production of sulphuric acid, having replaced platinum due to its effectiveness and relatively low cost.[5]

1.2.2 Catalytic Investigations

Most vanadium catalysts have been designed with a focus on its redox chemistry, but recent developments has now shifted the attention to peroxovanadates. These complexes can initialize a variety of two-electron oxidation reactions as shown in Scheme 1.1.[6] Alkenes and allylic alcohols are epoxidized while sulfides are oxidized to sulfoxides and sulfones. Arenes and alkanes along with benzene can be hydroxylated whilst primary and secondary alcohols will yield aldehydes and ketones respectively.[7] This has sparked interest in developing these complexes with various combinations of ligands to test whether differences in reactivity may be fine-tuned for a specific reaction.

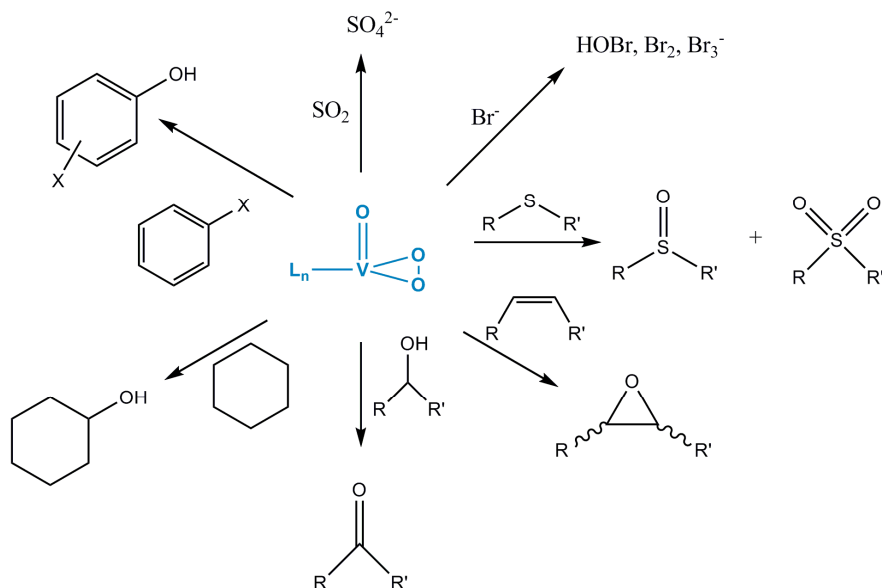[3] Greenwood, N. N., Earnshaw, A., *A Chemistry of the Elements*, Buttersworth/ Heinnemann, **1997**, 976.
[4] Van Vuuren, M. J. J., *PhD Thesis*, University of the Free State, **1996**, 2.
[5] Rehder, D., *Bioinorganic Vanadium Chemistry*, Wiley & Sons, **2008**, 8.
[6] Conte, V., Floris, B., *Inorganica Chimica Acta*, **2010**, *363*, 1935.
[7] Butler, A., Clague, M. J., Meister, G. E., *Chem. Rev*., **1994**, *94*, 625.

Scheme 1.1: Different oxidation reactions with peroxovandate species as catalyst. L represents an organic ligand or solvent molecule with n = 3 or 4.

A surprising discovery by Reis in 2003 was made with a single-pot conversion of methane to acetic acid using a vanadium catalyst in the absence of CO.[8] These complexes were based on vanadium in the +4 and +5 oxidation states with functionalities of *O,O* and *N,O* ligands such as amavadine.[2] This compound is of particular interest as it is found naturally in certain mushrooms of the *Amanita* species, acting as catalyst for oxidation reactions of thiols.[8] The discovery holds promising application to replace current industrial methods in the conversion of methane, as advantages include a one-step reaction, avoidance of CO, low energy requirements and cheap catalysts.[2]

1.3 Vanadium in Biological Systems

The chemistry involving vanadium in its biological role has been investigated in the study of haloperoxidases and nitrogenases as well as the activity of vanadium at a physiological level. More detail surrounding this research will be given in Chapter 2.

Studies to evaluate the kinetics and mechanism of ligand substitution in five-coordinated, bis-chelate oxovanadium(V) compounds have been undertaken. The results of such studies will assist in the understanding of how vanadium interacts on a physiological level

---

[8] Reis, P. M. *et al.*, *Angew. Chem. Int. Ed.*, **2003**, *42*, 821.

and will hopefully lead to correlations between Lewis acidity and ligand basicity for ligand substitutions.[2]

1.4 Aims of Project

The overarching aim of this project was to investigate some of the basic concepts of vanadium coordination chemistry as this would assist in understanding the observed, but not always understood complex interactions in biological as well as industrial systems. The focus will be placed on vanadium in the +4 and +5 oxidation states as these are the oxidation states mostly encountered in successful catalysts and in biological systems. The coordination chemistry of vanadium with various *O,O* and *N,O* bidentate donor ligands (in general indicated as L,L'-Bid ligands where L,L' represent the donor atoms) will be studied to effectively evaluate the influence of ring size as well as basicity on the V(IV) and V(V) metal centres.

Taking into account the above mentioned scope of the study, the specific project aims are defined as:

i.   Synthesis of novel vanadium compounds with ligand systems that contain *O,O*- and *N,O*-Bid donor functionalities and to study the solid state and solution properties of said compounds.

ii. Utilize the following techniques in order to achieve the above mentioned goal: X-ray crystallography, NMR (including multinuclear NMR), UV/Vis and infrared spectroscopy to further the knowledge base on the coordination ability of vanadium.

iii. Initialize a kinetic study on the substitution reaction of $[VO(O_2)_2bpy]^-$ with 2,3-pyridinedicarboxylic acid to determine the reaction mechanism and derive a rate law by taking into account various factors such as concentration as well as pH on reaction rates.

iv. The study of synthesized vanadium(IV) and vanadium(V) complexes via ^{51}V NMR to study the electronic effects of various ligand systems surrounding the vanadium centre, as well as employing this technique to resolve solution kinetic behaviour of $[VO(O_2)_2bpy]^-$ under various conditions.

In the following chapters the above mentioned project aims will be addressed through a detailed literature review of basic vanadium chemistry and background on its biological role and ^{51}V NMR. The theory on the characterization techniques chosen for this study is discussed which is followed by the details of the synthesis of various vanadium(IV) and vanadium(V) compounds in Chapter 4. This is followed by a structural study of four vanadium complexes that were analyzed by single crystal X-ray diffraction. To meet goal three of this research project a substitution reaction of the $[VO(O_2)_2bpy]^-$ complex was investigated *via* slow UV/Vis techniques as well as ^{51}V NMR. Lastly, a study of a few of the synthesized complexes in cancer screening tests was performed and the results discussed. In conclusion, the successes and failures of this project were evaluated in Chapter 8 with future work outlined.

Chapter 2: Literature Review of Relevant Vanadium Chemistry

2.1　Introduction

An overview on some of the most important aspects of vanadium chemistry will be given in this chapter. The discovery and history are shortly highlighted after which an introduction to the rich and often complex aqueous chemistry of the element follows. The role vanadium plays within the biological world is discussed with a focus on the activity of vanadium in treatment of diabetes and cancer. A brief summary of the principles in ^{51}V NMR as well as its relevance to this project will be given and lastly, some background on the type of coordination complexes, aimed at the syntheses in this study is given.

2.2　Discovery and Abundance of Vanadium

2.2.1 Discovery of Vanadium

In 1801 a Spanish mineralogist A. M. del Rio discovered a new element in a sample of lead ore from Zimapán, Mexico.[1] The new element was initially named *panchromium* as Del Rio had observed a variety of different coloured salts of the new element. He changed his mind, however, after observing the sample turn a brilliant red colour upon acidification, and decided to call it *erythronium* instead.[2]

His claim for the previously unknown element 23 was withdrawn in 1805 when the Frenchman, H. V. Collett-Descotils (erroneously) convinced del Rio that the sample was in fact basic lead chromate. This then led to a "rediscovery'' of vanadium in 1830 by the Swedish scientist, N. G. Sefström. The fascination with the widely coloured complexes of the element led Sefström as with del Rio to name the element for its beauty. The element was named vanadium after the Scandinavian goddess of beauty and fertility, Vanadis.[3]

---

[1] Rehder, D., *Bioinorganic Vanadium Chemistry*, John Wiley & Sons, **2008**, 1.
[2] Greenwood, N. N., *Catalysis Today*, **2003**, *78*, 5.
[3] Greenwood, N. N., Earnshaw, A., *Chemistry of the Elements*, Buttersworth/Heinemann, **1997**, 976.

2.2.2 Abundance and Uses

Vanadium comprises about 136 ppm (0.0136 %) of the earth's crust. Approximately 152 minerals contain vanadium within their structure, with economically the most significant being patronite (VS_4), vanadinite [$Pb_5(VO_4)_3Cl$] and carnotite [$K_2(UO_2)_2(VO_4)_2$]•$3H_2O$.[4] It is perhaps the mineral beryl [$Be_3Al_2(SiO_3)_6$], however, that is most famous amongst this list as the precious gemstone emerald with trace amounts of vanadium acting as a chromophore.[5] Of these naturally occurring minerals the most common oxidation states of vanadium are III, IV and V.[6]

Extraterrestrial vanadium compounds are also quite common and typically found in the low oxidation states of II and III. The coma of comet Wild 2 contains osbornite (TiN) with the titanium replaced with as much as 63 % vanadium. The atmospheres of hot exoplanets as well as red dwarfs have been shown to contain vanadium(II) oxide and it is speculated that these species act as catalysts.[7]

Also commonly found in fossil fuels, vanadium is complexed by various organic ligands and as a result can be concentrated up to a few percent in oil reserves.[8] The burning of vanadium-rich oils from Venezuela in the absence of any precautions can lead to airborne vanadium being released with serious health concerns.[9]

The 58 600 tonnes of vanadium produced each year is mainly sourced from China, eastern Russia and South Africa. On average, 33 000 tonnes is used in the steel industry as an additive in alloys that allows for increased strength. Ferrovanadium is in high demand due to the finely dispersed V_4C_3 in the alloys. Vanadium as additive to titanium further accounts for 50 % of all commercially available alloys.[10]

The major use of vanadium, however, remains its use as an industrial catalyst. Having replaced platinum as catalyst in the production of sulphuric acid, many organic reactions

---

[4] Magee, J. S., Mitchel, M. M., *Stud. Surf. Sci. Catal.,* **1993**, *76*, 5.

[5] Thomas, A., *Gemstones: Properties, Identification and Use*, New Holland Publishers, **2008**, 77.

[6] Nriagu, J. O., *Vanadium in the Environment in Adv. Environ. Science Technol.*, John Wiley & Sons, **1998**, Vols. 30 and 31.

[7] Rehder, D., *Coord. Chem. Rev.*, In press, **2011**.

[8] Roberts, W. L., Campbell, T. J., Rapp, G. R., *Encyclopedia of Minerals 2nd edition*, Van Nostrand Reinholdt Company, **1990**.

[9] Sabbioni, E., Kueera, J. Pietra, R., Vesterberg, O., *The Science of the Total Environment*, **1996**, *188*, 49.

[10] Enghag, P, *Encyclopedia of the Elements*, John Wiley & Sons, **2004**, 546.

are now also catalyzed by vanadium.[11] Some of the most important catalytic processes featuring vanadium are summarized in Table 2.1.

Table 2.1: Industrial catalytic processes involving vanadium oxides.

Industrial Process	Catalyst used
Oxidation of SO_2 to SO_3 in sulphuric acid production	V_2O_5
Oxidation of benzene to maleic anhydride	V_2O_5
Oxidation of naphthalene to phthalic anhydride	V oxides
Reduction of NO_x with NH_3	V_2O_5

The number of applications in which vanadium can be used as catalyst compared to other transition metal centres is illustrated in Figure 2.1.[12] The chart displays the amount of literature devoted to different metal catalysts in the period of 1967 to 2000. Most vanadium catalysts are based on oxides with many new developments aimed towards heterogeneous catalysis and with supports such as SiO_2 and Al_2O_3 for increased surface areas and mechanical strength of the catalyst.[13]
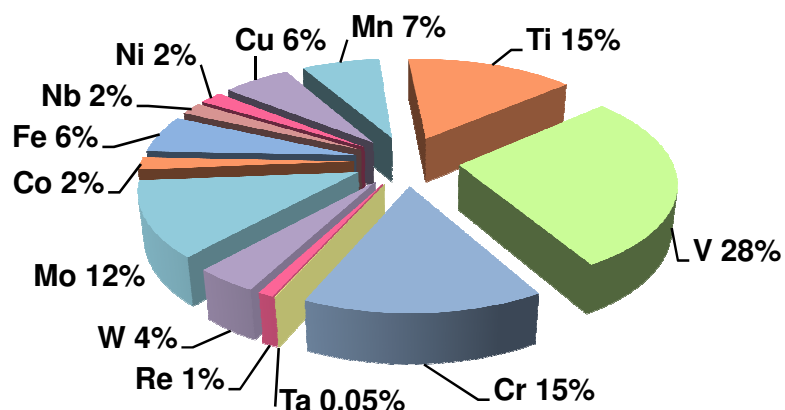
Figure 2.1: Overview of the number of published articles between 1967 and 2000 with regard to different metal oxide catalysts.

[11] Deo, G, Wachs, I. E., Habeer, J., *Crit. Rev. Surf. Chem.*, **1994**, *4*, 141.
[12] Weckhuysen, B. M., Keller, D. E., *Catalysis Today*, **2003**, *78*, 25.
[13] Trifiro, F., Crzybowska, B., *Appl. Catal. A Gen.*, **1997**, *157*, 195.

2.3   Overview of Vanadium Chemistry

2.3.1 Atomic and Physical Properties

The elements of Group 5 have few naturally occurring isotopes due to their odd atomic numbers. Niobium has only one isotope whilst Tantalum and Vanadium have two. To date 24 isotopes of vanadium have been identified, but it is expected that a further 13 could still be discovered.[14] The two naturally occurring isotopes are ^{50}V and ^{51}V. ^{50}V has a natural abundance of merely 0.250 % and is slightly radioactive with a half-life of 3.9 x 10^{17} years with decay by electron capture/ positron emission.[15]

Comparing the elements in the group with the corresponding elements of Group 4, some trends are to be expected. The three elements are slightly less electropositive and smaller than their counterparts in Group 4. The extra *d* electron contributes to a stronger metal-metal bonding that result in higher melting and boiling points as well as enthalpy of atomization.[3]

Vanadium is the last element in the first transition series before the *(n-1)d* electrons enter the inert electron-core of the atom and become unavailable for bonding. Consequently, vanadium is the element with the highest melting point in the series, as well as being the last element in the group whose compounds are not strongly oxidizing. A comparison between the properties of the three elements in Group 5 is given in Table 2.2.[3]

---

[14] Shore, A., Fritsch, A., Heim, M., Schuh, A., Thoennensen, M., *Atomic Data and Nuclear Data Tables*, **2010**, *96*, 351.
[15] De Groot, P. A., *Handbook of Stable Isotope Analytical Techniques vol. 2*, Elsevier, **2009**, 819.

Table 2.2: Important properties of the Group 5 elements.

Property	V	Nb	Ta
Atomic number	23	41	73
No. of naturally occurring isotopes	2	1	2
Atomic weight	50.9415 (1)	92.90638 (2)	180.9479 (1)
Electronic configuration	$[Ar]3d^3 4s^2$	$[Kr]4d^3 5s^2$	$[Xe]4f^{14} 5d^3 6s^2$
Electronegativity	1.6	1.6	1.5
Metal radius 12-coordinate (pm)	134	146	146
Ionic radius 6-coordinate (pm) V	54	64	64
IV	58	68	68
III	64	72	72
II	79	-	-
MP (°C)	1915	2468	2980
BP (°C)	3350	4758	5534
ΔH_{fus} (kJ.mol^{-1})	17.5	26.8	24.7
ΔH_{vap} (kJ.mol^{-1})	459.7	680.2	758.2
ΔH_f **monoatomic gas** (kJ.mol^{-1})	510	724	782
Density **20 °C** g/cm^3	6.11	8.57	16.65
Electrical resistivity **20 °C** (μohm.cm)	~25	~12.5	12.4

2.3.2 Chemical Reactivity and Trends

Similar to the elements of Group 4, Vanadium reacts with most non-metals yielding products that are non-stoichiometric. One of the most common uses of the metal, as corrosion inhibitor can be attributed to the formation of oxide surface films. Of the formal oxidation states cited in literature for vanadium, between +5 and -3, it is the +4 oxidation state which is most stable.[3,16]

The VO^{2+} (vanadyl) ion which is part of many vanadium complexes has been given the title of most stable diatomic ion known within literature sources and retains its identity in many complexes.[3] Earning a place in the Irving-Williams metal ion series that is based on

---

[16] Hirao, T., *Encyclopedia of Inorganic Chemistry: Vanadium: Organometallic Chemistry 2nd edition*, **2006**, 1.

the stability of complexes with acetylacetone, salicylaldehyde and oxalate, the following trend has been set: $VO^{2+}> Cu^{2+}> Ni^{2+}> Co^{2+}>Fe^{2+}> Mn^{2+}$.[17]

As vanadium has 9 oxidation states, a wide range of stereochemistries can be found for different coordination complexes, of which a few examples are given in Table 2.3. [3,18]

Table 2.3: Some oxidation states of vanadium and their various geometries.

Oxidation state	Coordination number	Stereochemistry	Compound
-3	5	-	$[V(CO)_5]^{3-}$
-1	6	Octahedral	$[V(CO)_6]^-$
0	6	Octahedral	$[V(CO)_6]$, $[V(bpy)_3]$
1	6	Octahedral	$[V(bpy)_3]^+$
2	6	Octahedral	$[V(CN)_6]^{4-}$
		Trigonal prismatic	VS
3	4	Tetrahedral	$[VCl_4]^-$
	5	Trigonal bipyramidal	$[VCl_3(NMe_3)_2]$
	6	Octahedral	$[V(ox)_3]^{3-}$
4	4	Tetrahedral	$[VCl_4]$
	5	Trigonal bipyramidal	$[VOCl_2(NMe_3)_2]$
		Square pyramidal	$[VO(acac)_2]$
	6	Octahedral	$[VCl_4(bpy)]$
	8	Dodecahedral	$[VCl_4(diars)_2]$
5	4	Tetrahedral	$[VOCl_3]$
	5	Trigonal bipyramidal	$[VCl_5]$
		Square pyramidal	$[VOF_4]^-$
	6	Octahedral	$[VF_6]^-$
	7	Pentagonal bipyramidal	$[VO(S_2CNEt_2)_3]$
	8	Dodecahedral	$[V(O_2)_4]^{3-}$

[**(bpy)**= 2,2-bipyridine, **(NMe₃)**= trimethylamino, **(ox)**= oxalate, **(acac)**= acetylacetonato, **(diars)**= dimethylarseno, **(S₂CNEt₂)**= μ_3-N,N-diethyldithiocarbamato, **(O₂)**= peroxo]

2.3.3 Oxides of Vanadium

Vanadium has four known oxide forms with V_2O_5 the most notable. The most prominent oxides of vanadium are given in Table 2.4 as the light grey monoxide, VO; the blue black dioxide, VO_2; the black sesquioxide, V_2O_3 and the yellow-orange V_2O_5.[19] The last mentioned oxide, V_2O_5, is the final product when the pure metal is heated in the presence of oxygen.

---

[17] Selbin, J., *Chem. Rev*., **1965**, *65*, 153.
[18] Cotton, F. A., Wilkinson, G., Murillo, C. A., Bochman, M., *Advanced Inorganic Chemistry 6th edition*, Wiley Interscience, **1999,** 715.
[19] Patnaik, P., *Handbook of Inorganic Chemicals*, McGraw-Hill, **2003**, 964.

Table 2.4: Oxides of various oxidation states of vanadium.

Oxidation State	Vanadium oxide
+2	VO
+3	V_2O_3
+4	VO_2
+5	V_2O_5

As mentioned in Section 2.2, vanadium has particularly good application in catalysis and this holds true for many of the oxides. V_2O_5 is most famously used to catalyze the reaction in which sulphuric acid is produced, but another often overlooked reaction in which V_2O_5 is involved is the important conversion of ethanol to acetaldehyde.[20]

The pentavalent oxide has the ability to block UV light when combined with glass and is used in the production of commercially available glass windows. The tetravalent oxide in contrast has the ability to block infrared rays. Vanadium pentoxide is also used as photographic developer and as a dye in textiles.[21,22]

Due to its high oxidation state, V_2O_5 is an amphoteric oxide as well as an oxidizing agent. An example of its amphoteric character is given in Eq. 2.1. Reaction with strong non-reducing acids results in pale yellow salts containing dioxovanadium centres. Polyoxovanadates are formed upon reaction with alkalis and are heavily dependent upon pH.

$$V_2O_5 + 2HNO_3 \rightarrow 2VO_2NO_3 + H_2O \qquad\qquad \text{(Eq. 2.1)}$$
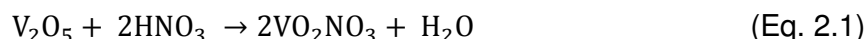
Simple radius to ratio calculations would suggest vanadium(V) to be rather large for a tetrahedral coordination to oxygen and too small for octahedral geometries. The structures of V_2O_5 and NH_4VO_3 consist of distorted trigonal bipyramids forming zigzag double chains with VO_5 fragments sharing edges. These tetrahedral shapes are illustrated in Figure 2.2.

---

[20] Quaranta, N. E., Soria, J., Cortés Corberán, V., Fierro, J. L. G., *Journal of Catalysis*, **1997**, *171*, 1.

[21] Siligardi, C., Wu, J. P., Boccaccini, A. R., *Materials Letters*, **2006**, *60*, 1607.

[22] Krebs, R. E., *The History and Use of Our Earth's Chemical Elements 2nd edition*, Greenwood Press, **2006**, 94.

a   **b**
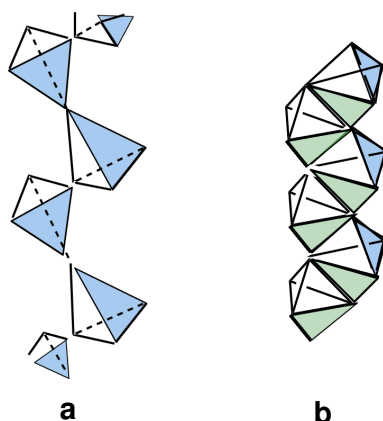
Figure 2.2: Structures of isopolyvanadates in solid state, each polyhedron contains a metal atom and each vertex of a polyhedron illustrates an oxygen; a) anhydrous metavanadate as well as V_2O_5 consisting of infinite chains, b) hydrated metavanadate with infinite chains of VO_5 trigonal bipyramids.

2.4 Aqueous Vanadium Chemistry

When vanadium compounds in oxidation states of III, IV and V are dissolved in water various hydrolytic, acid/base, condensation and redox reactions can occur. The species rarely maintain their solid-state structure once dissolved. Complexity arises in determining the solution structure of a species as vanadium(III) and (IV) species become cationic whilst vanadium(V) species are anionic in solution. Pourbaix diagrams such as the one illustrated in Figure 2.3 has aided in the identification of species in solution.[23] Figure 2.4 illustrates the species distribution in solution for vanadium(V) systems as a function of pH and concentration.[24]

---

[23] McCleverty, J. A., Meyer, T. J., *Comprehensive Coordination Chemistry II vol. 4*, Elsevier, **2005**, 176.
[24] Van Vuuren, M. J. J., *PhD Thesis*, University of the Free State, **1996**, 22.
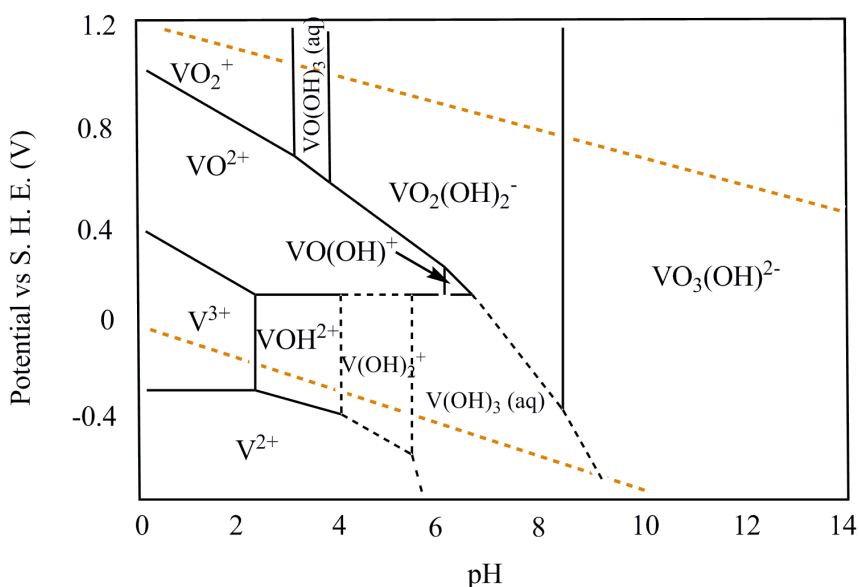
Figure 2.3: Pourbaix diagram illustrating the relationship between vanadium species as a function of pH and reduction potential. Boundaries indicated by dashed lines indicate an uncertainty in literature whereas dashed lines (orange) represent the upper and lower limits of the stability of water.[25]
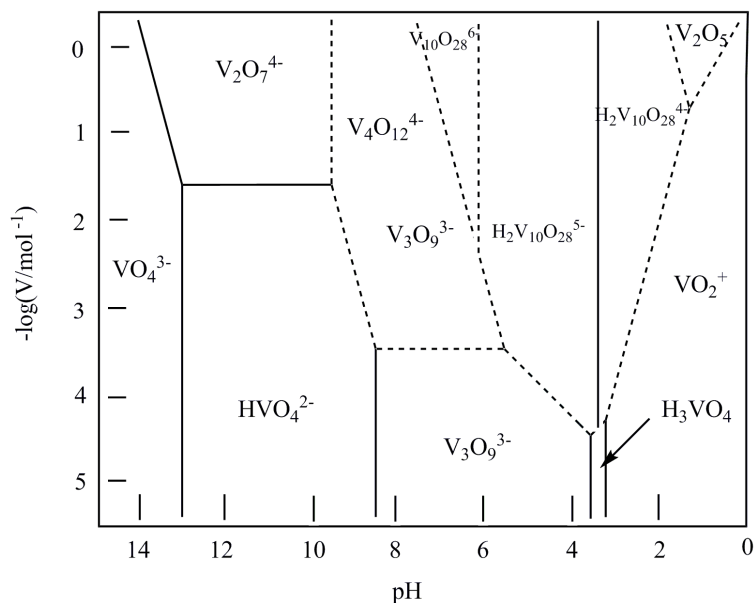
Figure 2.4: Distribution of various vanadate and polyvanadate species in aqueous medium as a function of pH and concentration. Dashed lines indicate uncertainties to which species predominates at a specific pH.

From these two illustrations (Figure 2.3 and 2.4) it is clear how complex the identification of vanadium species becomes once in solution. Three dominant species exist in the pH

---

[25] Baes, C. F., Mesmer, R. E., *The Hydrolysis of Cations*, John Wiley & Sons, **1976**, 193.

region 6-9, namely; $[V_{10}O_{28}]^{6-}$; $[V_4O_{12}]^{4-}$ and $[HV_2O_7]^{3-}$. At a lower concentration the $[V_3O_9]^{3-}$ and $[HVO_4]^{2-}$ species become more prominent.

2.4.1 Vanadium(IV)

The best known vanadium(IV) compound is the water soluble $VOSO_4$. When dissolved in an acidic medium the hydrated vanadyl cation $[VO(H_2O)_5]^{2+}$ is formed. The structure for the hydrated cation can be seen in Figure 2.5. Upon raising the pH this air stable cation will generate oligomeric and polymeric species.[26,27,28] Some of these polymers are highly insoluble and result in precipitates that complicate their study. A solution to this problem is using the affinity of vanadium(IV) for "hard" ligands containing oxygen, nitrogen and sulphur donor groups to prevent the formation of precipitates.
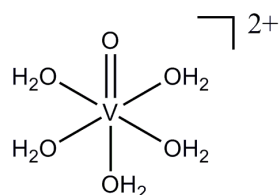
Figure 2.5: Structure of hydrated $VOSO_4$ at low pH, $[VO(H_2O)_5]^{2+}$.

2.4.2 Vanadium(V)

In the solid state vanadate exists in typical four- and five-coordinate systems such as NH_4VO_3, $NaVO_3$, Na_3VO_3 and V_2O_5.[18] In solution, however, all the species will arrange themselves in an oxometallate form based on the $H_2VO_4^-$ anion. These species can exist in monomeric, dimeric, trimeric, tetrameric, pentameric and higher forms. Some of these polymeric forms are illustrated in Figure 2.6. Speciation diagrams such as those illustrated in Figures 2.3 and 2.4 offer more accurate determination of which species exists at specific pH, concentration and temperature conditions.[29,30,31]

[26] Boyd, D. W., Kustin, K., *Adv. Inorg. Biochem.*, **1984**, *6*, 311.
[27] Mustafi, D., Makinen, M. W., *Inorg. Chem.*, **1988**, *6*, 3360.
[28] Francavilla, J., Chasteen, N. D., *Inorg. Chem.*, **1975**, *14*, 2860.
[29] Heath, E., Howarth, O. W., *J. Chem. Soc., Dalton Trans.*, **1981**, 1105.
[30] Pettersson, L., Hedman, B., Andersson, I., Ingri, N., *Chem. Scrip.*, **1983**, *22*, 254.
[31] Pettersson, L., Andersson, I., Hedman, B., *Chem. Scrip.*, **1985**, *25*, 309.
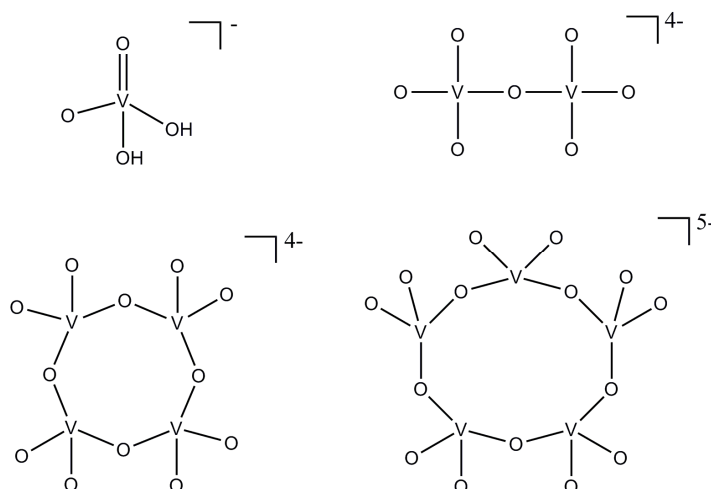
Figure 2.6: Structural illustrations of polymeric forms of the $H_2VO_4^-$ ion as found in solution of V^{5+} species.

At a pH of less than 3, all of the anionic forms convert to the hydrated form of VO_2^+ as observed in Figure 2.3. This is the principal *cis*-dioxovanadium unit found in some vanadium(V) complexes. The $H_2VO_4^-$ ion has often been described as a phosphate analogue as many structural and electronic similarities exist. A comparison of their pK_a values (phosphate = 2.1, 7.2 and 12.7, vanadate = 3.5, 7.8 and 12.5) offers further evidence of their similarity.[32] The two ions also show unique stability with the stable H_3PO_4 comparable to VO_2^+, which is stabilized by the increased coordination offered by the hydrated forms.[33]

At the physiological pH and a low concentration of 1 mM, vanadate mainly exists as the monomeric form of $H_2VO_4^-$.[34] Some of the most important vanadium(V) species in aqueous solution are given in Table 2.5 along with their pK_a and ^{51}V NMR chemical shift values.[33]

---

[32] Chasteen, N. D., *Vanadium in Biological Systems*, Kluwer Academic, **1990**, 25.
[33] Tracey, A. S., *ACS Symposium Series*, **1998**, 2.
[34] Crans, D. C., Mahroof-Tahir, M., Keramidas, A. D*., Mol. Cell. Biochem.*, **1995**, *153*, 17.

Table 2.5: pK_a and ^{51}V NMR chemical shift values for important vanadium(V) species.

Species	pK_a	^{51}V NMR δ (ppm)
VO_4^{3-}	-	-541.2
HVO_4^{2-}	13.4	-538.8
$V_2O_7^{4-}$	-	-561.0
$H_2VO_4^{-}$	7.91	-560.4
$H_2V_{10}O_{28}^{4-}$	3.68	-425, -506, -524
VO_2^{+}	-	-545

The VO_2^{+} ion often exhibits line-broadening in ^{51}V NMR studies that can be attributed to the exchange reaction between the VO_2^{+} cation and a mixed VO_2^{+} -VO^{2+} complex.[35] As the species is redox active, changes in the acidic medium as well as the presence of different reducing agents will affect the rate of the reaction.[36,37]

All of the protonation states have a general formula of $H_nVO_4^{3-n}$. The fully protonated H_3VO_4 only occurs in a narrow pH range and further protonation becomes favourable as structural rearrangement will afford an octahedral geometry with the formula of $[VO_2(H_2O)_4]^{+}$. This species is frequently quoted in literature as the cationic species of vanadium(V), VO_2^{+}.[38,39]

2.5 Importance of Vanadium in Biology

2.5.1 Occurrence of Vanadium in Biological Systems

The discovery of two classes of vanadium enzymes instigated a surge of research into vanadium model compounds during the last few decades. Vanadium-nitrogenases and vanadate-dependent haloperoxidases play vital roles in nature. Vanadium-nitrogenases occurs in a low to medium oxidation state and acts as part of an iron-sulphur unit that is

[35] Okamoto, K., Jung, W. S., Tomiyasu, H., Fukutomi, H., *Inorg. Chem.*, **1995**, *34*, 5680.
[36] Martire, D. O., Feliz, M. R., Capparelli, A. L., *Polyhedron*, **1991**, *10*, 359.
[37] Issa, F. A., Grzeskowiak, K., Halliday, C., Henry, A., Pittenger, S. T., Hicks, K. W., *Inorg. Chim. Acta*, **1987**, *130*, 85.
[38] Cruywagen, J. J., Heyns, J. B. B., Westra, A. N., *Inorg. Chem.*, **1996**, *35*, 1556.
[39] Pettersson, L., Hedman, B., Nenner, A. M., Andersson, I., *Acta Chem. Scand.*, **1985**, *A 39*, 499.

responsible for the activation and reductive protonation of N_2 to form ammonia that can be utilized by plants.[40,41] The haloperoxidases catalyzes the oxidation of halides in the vanadium(V) form. Model compounds that resemble the active centre of these haloperoxidases have been studied for their ability to also catalyze *in vitro* oxidations of substrates such as thioethers.[42] This revelation has fuelled further research for biologically orientated model investigations that can be applied to industrially relevant processes.[43]

As far as living organisms are concerned, vanadium is accumulated mainly in sea squirts and mushrooms. Sea squirts (*Ascidiaceae*) take up vanadium from sea water through tunichromes (pigments that contain a catecholate moiety) and store the vanadium in the +3 oxidation state in their adapted blood cells. The concentration of this stored vanadium has been shown to be more than six times the concentration of vanadium in the surrounding water (150 nM).[44,45] The function of the vanadium in sea squirts remains unknown but it is thought that these sea creatures are the main contributors of vanadium in crude oil and oil shales in the form of vanadyl porphyrins.[46]

The fly agaric toadstool of the genus Amanita, as well as other fungi belonging to this genus, contain a low molecular weight vanadium(IV) compound, named amavadin that contains carboxylate and hydroxylamide functional groups.[47] The structure of amavadin is given in Figure 2.7.

---

[40] Chen, J., Christiansen, J., Tittsworth, Hales, B. J., Coucouvanis, D., Cramer, S. P., *J. Am. Chem. Soc.*, **1993**, *115*, 5509.

[41] Dillworth, M. J., Glenn, A. R., *Biology and Biochemistry of Nitrogen Fixation*, Elsevier, **1991**.

[42] Schmidt, H., Bashipoor, M., Rehder, D., *J. Chem. Soc. Dalton Trans.*, **1996**, 3865.

[43] Rehder, D., *Coord. Chem. Rev.*, **1999**, *182*, 297.

[44] Smith, M. J., *Experientia*, **1989**, *45*, 452.

[45] Taylor, S. W., Kammerer, B., Bayer, E., *Chem. Rev.*, **1997**, *97*, 333.

[46] Dolphin, D., *The Porphyrins vol. 1*, Academic Press, **1978**, 485.

[47] Armstrong, E. M., Beddoes, R. L., Calviou, L. J., *J. Am. Chem. Soc.*, **1993**, *115*, 807.
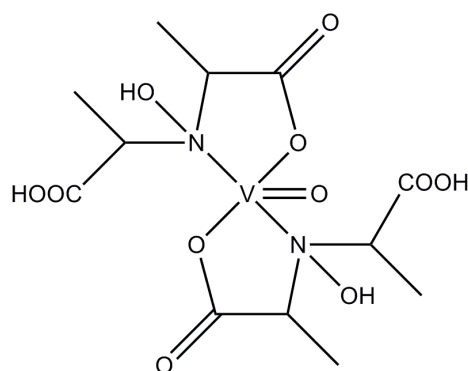
Amavadin

Figure 2.7: The chemical structure of amavadin as found in mushrooms of the genus Amanita.

2.5.2 Vanadium as Essential Element?

At first it may seem that vanadium is not an essential element for life on earth as only low quantities are present in living organisms. However, investigating several properties of vanadium might suggest otherwise, including: availability, low toxicity levels at physiological conditions and functionality that relates to biological processes.

As mentioned in Section 2.2.2, vanadium constitutes 0.0136 % of the earth's crust and is also the second most abundant transition metal in sea water. An average concentration of 30 nM in seawater has been reported and the most general form is vanadate in the form of the contact ion pair, $Na^+H_2VO_4^-$.[48] It has been shown that iron, derived from undersea vents, scavenges vanadium and thus controls the concentration levels as well as assists in the cycling of vanadium in the ocean.[49]

Vanadium can easily be reduced or oxidized between its +4 and +5 oxidation states. One such redox reaction at a pH of 7 is given in Eq. 2.2. The redox potential as shown is -0.341 V and is in the range where VO^{2+} is oxidized under aerobic conditions as well as where vanadate is reduced to the vanadyl ion (VO^{2+}) by cellular components such as glutathione and proteins.[50,51]

$$H_2VO_4^- + 4H^+ + e^- \rightleftarrows VO^{2+} + 3H_2O \qquad E = -0.341V \qquad \text{(Eq. 2.2)}$$
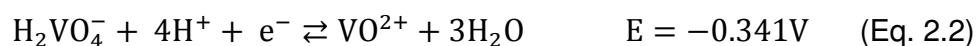
[48] Butler, A., *Science*, **1998**, *281*, 207.
[49] Trefry, J. H., Metz, S., *Nature*, **1989**, *342*, 531.
[50] Rehder, D., *Inorganic Chemistry Communications*, **2003**, *6*, 604.
[51] Degani, H., Gohin, Karlish, S. J. D., Shechter, Y., *Biochemistry*, **1981**, *20*, 5795.

Oxovanadium cations are also strong Lewis acids and as such vanadium has fulfilled two requirements to be regarded as a potential biometal, as its redox activity is of the correct electrochemical potential to be relevant for biochemical processes and it has good susceptibility for nucleophilic substituents.

A case may be made for vanadium's importance when investigating the similarities between vanadate ($H_2VO_4^-$) and phosphate (HPO_4^{2-}) at physiological pH and physiological concentrations (see Section 2.4.2). Various studies have indicated the ability of vanadate to inhibit phosphate-metabolizing enzymes, e.g., phosphatases, kinases and ribonucleases, but an added effect is the stimulation of enzymes such as phosphomutases.[52,53] It is these properties that has led to interest in vanadium as insulin mimicking agent in the fight against diabetes.

Vanadium and its compounds have been studied for their importance as well as their therapeutic effects in humans. It has been suggested that vanadium can act as cofactor for enzymes involved in blood sugar metabolism, lipid and cholesterol metabolism, bone and tooth development, fertility, thyroid function, hormone production and as a neurotransmitter metabolite. Effects of deficiency in humans have never been established but in animals the following effects have been determined: infertility, anaemia, iron metabolism defects as well as poor bone and cartilage formation. As such it has been established that vanadium is an essential trace element and a safe daily dosage of 10-100 µg is prescribed for humans.[54]

The role of vanadium in certain species, although uncertain, cannot be without reason. By evaluating its characteristics with those required for a bio-active metal, the conclusion can be made that research into vanadium for medical application can be motivated quite effectively. In the following sections the role that vanadium plays in current research for medical purposes is discussed with specific focus on diabetes and cancer research.

---

[52] Sekar, N., Li, J., Shechter, Y., *Crit. Rev. Biochem. Mol. Biol.*, **1996**, *31*, 339.
[53] Sigel, H., Sigel. A., *Vanadium and Its Role in Life, Metal Ions in Biological Systems vol. 31*, Marcel Dekker, **1995**, 779.
[54] Roat-Malone, R. M., *Bioinorganic Chemistry*, John Wiley & Sons, **2002**, 274.

2.5.3 Historical Role of Vanadium in Medicine

Vanadium salts have been prescribed by physicians from the 19th century for treating a wide array of ailments ranging from malnutrition, anaemia, tuberculosis and diabetes.[55] The most valuable discovery of that time was made in a study by Lyonnet and Martin in 1899 when they observed that diabetic patients treated with sodium vanadate ($NaVO_3$) excreted lower levels of glucose in their urine.[56] It was their discovery that eventually pioneered the research of vanadium in various applications such as insulin mimetic agents to potential anti-cancer agents.

2.5.4 Desirable Properties of Metallopharmaceuticals

The use of metal compounds for medicinal application has existed for centuries despite dominance by organic drugs. It was the unexpected anti-tumour activity of *cis*-platin that changed the focus of much research at the time.[57] The fields of coordination and organometallic chemistry have provided many possibilities to develop other novel metal-based drugs to target various regions within the body. However, there exist a few general qualities that act as guidance when developing new drugs and they are discussed in the section below.

Desirable properties, such as a neutral charge, low molecular weight, thermodynamic and hydrolytic stability, oral bioavailability and bi-functional capability are some of the qualities necessary for a successful pharmaceutical agent.[58] A candidate therapeutic agent must have the ability to cross membranes for both the initial absorption as well as the intracellular uptake. Only the essential metal ions of copper, zinc and iron have known transport mechanisms and it is assumed that other metals rely on a method of diffusion into the cells.[59] As membranes contain many lipids, complexes that are lipophilic will cross barriers easier and as such will be advantageous in systems designed with pharmaceutical use in mind.

A study by Lipinski in 1997 on metalopharmaceuticals that had been synthesized in the last few decades led to the development of Lipinski's rule of five that can be used as

---

[55] Shechter, Y., Shisheva, A., *Endevour*, **1993**, *17*, 27.

[56] Dabrowiak, J. C., *Metals in Medicine*, John Wiley & Sons, **2010**, 219.

[57] Pasheva, E. A., Ugrinova, I., Spassovska, N., C., Pashev, I., G., *The International Journal of Biochemistry & Cell Biology*, **2002**, *34*, 87.

[58] Thompson, K. K., McNeill, J. H., Orvig, C., *Chem. Rev.*, **1999**, *99*, 2561.

[59] Johnson, L. R., *Physiology of the Gastrointestinal Tract 3rd ed.*, Raven Press, **1944**, 1693.

guidelines when synthesizing new compounds aimed at the pharmaceutical industry. These rules are given as follows:[60]

i. Not more than 5 hydrogen bond donors (nitrogen or oxygen atoms that have one or more hydrogen atoms).

ii. Not more than 10 hydrogen bond acceptors present in the compound eg. oxygen and nitrogen.

iii. The molecular mass less than 500 daltons (1 Da = 1.66 x 10^{-27} kg).

iv. An octanol-water partition coefficient (*log P*) not greater than 5.

v. Notable rotation bonds must be less than 10.

2.5.5 Unique Features of Vanadium

In the physiological pH range of 2 - 8 the oxidation states mostly encountered for vanadium are +4 and +5.[61] These two oxidation states are in equilibrium and are mediated *in vivo* by oxygen, acidity and reducing agents such ascorbate, glutathione and catecholamines.[62]

In the field of coordination chemistry vanadium has shown remarkable flexibility as the +5 oxidation state has non-rigid stereochemical requirements. As is shown in Table 2.3 octahedral, pentagonal bipyramidal and dodecahedral geometries have been found. By the 1980's, vanadium compounds were considered unique due to their potent pharmacological effects and their interconversions between cationic and anionic species.[63,64]

Despite inconclusive tests on whether vanadium is safe to consume on a regular basis, it has been added to many mineral supplements on the market and even more interesting is the addition of vanadyl sulphate ($VOSO_4$) as additive in sport supplements to boost performance.[65]

---

[60] Lipinski, C. A., Lombardo, F., Dominy, B. W., Feeney, P. J., *Advanced Drug Delivery Reviews*, **1997**, *23*, 3.
[61] Nriagu, J. O., *Vanadium in the Environment: Part 1: Chemistry and Biochemistry*, Wiley, **1988**, 131.
[62] Page, E. M., Wass, S. A., *Coord. Chem. Rev.*, **1997**, *164*, 203.
[63] Nechay, B. R., *Ann. Rev. Pharmacol. Toxicol.*, **1984**, *24*, 501.
[64] Harris, W. R., Friedman, S. R., Silberman, D., *J. Inorg. Biochem.*, **1984**, *20*, 157.
[65] Kayne, S. B., *Sport and Exercise Medicine for Pharmacists*, Pharmaceutical Press, **2006**, 70.

2.5.6 Diabetes Mellitus

Diabetes mellitus is a disease affecting a large percentage of the world population and the diagnosis rate has dramatically increased over the last two decades due to lifestyle choices within a career driven age.[66] There are two recognised forms of diabetes, namely Type I and II. Type I is defined as absolute insulin deficiency where no production of the hormone insulin is produced. Type II is diagnosed when insulin is produced but without the sufficient response and secretion on cellular level and accounts for more than 90 % of sufferers world-wide.[67]

Metabolism of glucose in non-diabetic individuals takes place in a series of intracellular reactions known as the insulin signalling cascade.[68] Insulin binds to the extracellular side of the cell membranes at insulin receptor sites that then begins the many phosphorylation/ dephosphorylation steps. Absence of endogenously secreted insulin or cellular resistance to the hormone leads to inadequate disposal of blood glucose.[69]

By 1980, the mechanism by which insulin operated was not well understood and a common research approach for new techniques was to test substrates that mimic the actions of insulin in cells.[70] Conditions that inhibit Na^+, K^+-ATPase allow for the activation of glucose transport and oxidation. It was for this reason that diabetes research was also extended to vanadate salts and initial tests on rats showed the ability of sodium vanadate to mimic insulin on hexose uptake and glucose metabolism. Not only was vanadium in the +5 oxidation state active, but the vanadyl ion (+4) exhibited active chemistries.[71] Subsequent studies showed that the inhibition was the result of the vanadate preventing a de-phosphorylated enzyme conformational change.[72] As discussed earlier, the similarities between vanadate and phosphate are quite remarkable and since vanadate is slightly larger than phosphate, inhibition of the phosphate-dependent enzymes occurs.[73]

The discovery of insulin has been critical for the fight against diabetes. Insulin can unfortunately not be administered orally as it is destroyed in the stomach. Injections on a daily level are an inconvenience and so the need for a substitute has become a point of

[66] King, H., Aubert. R., Herman, W., *Diabetes Care*, **1998**, *21*, 1414.
[67] Zimmet, P., Alberti, K. G. M. M., Shaw, J., *Nature*, **2001**, *414*, 782.
[68] Kahn, C. R., White, M. F., *J. Clin. Invest.*, **1998**, *82*, 1151.
[69] White, M. F., Shaleson, S. E., Keutmann, H., Kahn, C. R., *J. Biol. Chem.*, **1988**, *263*, 2969.
[70] Czech, M. P., *Diabetes*, **1980**, *29*, 399.
[71] Fain, J. N., *Endocrinology*, **1968**, *83*, 540.
[72] Karlish, S. J. D., Beauge, L. A., Glynn, I. M., *Nature*, **1979**, *282*, 333.
[73] Gordon, J. A., *Meth. Enzymol.*, **1991**, *201*, 477.
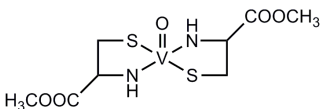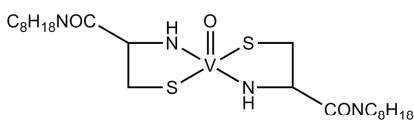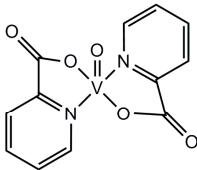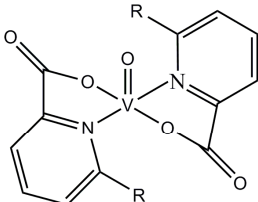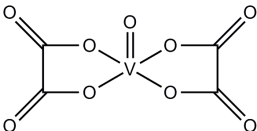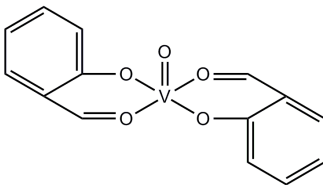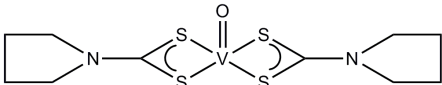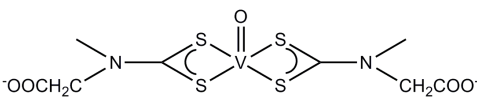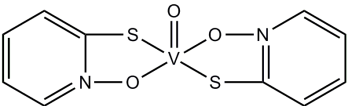
focus for research in diabetes. The ideal substitute should be orally administered and effective.

An advantage of vanadium compounds is their method of administration to patients. $NaVO_3$ was given orally to patients and the hope is that new vanadium insulin mimicking agents can also be administered in such a way in comparison to the current method in treating diabetes with inconvenient daily insulin injections. Novel compounds have been synthesized and tested for activity. Some of these complexes that have tested positive for insulin activity together with their range of binding modes are illustrated in Table 2.6.[74]

Table 2.6: Insulin-mimetic vanadyl complexes.

Mode	Compound
N_2S_2	
N_2O_2	R= CH_3 and C_2H_6
O_4	
S_4	
S_2O_2	

[74] Sakurai, H., Kojima, Y., Yoshikawa, Y., Kawabe, K., Yasui, H., *Coord. Chem. Rev.*, **2002**, *226*, 187.

2.5.7 Vanadium Insulin Enhancing Agents

As this study focuses on *O,O* and *N,O* bidentate ligands, attention will now be given to ligands with these functionalities that have been investigated for diabetic activity as part of vanadium compounds.

2.5.7.1 Vanadium Complexes with O,O Ligands

Vanadium forms neutral complexes with bidentate ligands that posess an ionizable proton. An advantage of using oxygen rich ligands is their general water-solubility and as such the maltolato ligand has received special attention with the pentacoordinated bis(maltolato)oxovanadium(IV) complex testing positive for potential insulin-mimetic properties.[75,76] Maltol is an approved additive in foods in many countries and is known for its bioactivity and low toxicity profile.[77] An illustration of the mentioned compound is given in Figure 2.8.
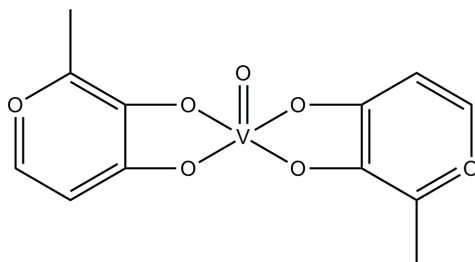
Figure 2.8: Schematical diagram of bis(maltolato)oxovanadium(IV).

The geometry of the compound illustrated in Figure 2.8 is square pyramidal and it has one unpaired electron that is characteristic of the VO^{2+} unit. An infrared stretching frequency of 995 cm^{-1} is assigned for the V=O vibration. This value is slightly high and is an indication that there is either no solvent ligand coordinated in the sixth position or that it is weakly bound.[58]

An interest in maltol and derivatives such as ethylmaltol and kojic acid can also be attributed to their ease at being deprotonated.[78] Maltolato complexes have been the most tested of all the vanadium compounds for insulin activity and the results have been

---

[75] Thompson, K. H., McNeill, J. H., Orvig, C., *Topics in Biological Inorganic Chemistry*; Clarke, M. J., Sadler, P. J., Springer Verlag, **1999**, 139.

[76] McNeill, J. H., Yuen, V. G., Hoveyda, H. R., Orvig, C., *J. Med. Chem.*, **1992**, *35*, 1489.

[77] Comba, P., *Coord. Chem. Rev.*, **1993**, *123*, 1.

[78] Orvig, C., Caravan, P., Gelmini, L., Glover, N., Herring, F. G., Li, H., McNeill, J. H., Rettig, S. R., Setyawati, I. A., *J. Am. Chem. Soc.*, **1995**, *117*, 12759.

largely positive with lowering glucose and lipid levels reported.[79] A delay and prevention of long-term diabetes-induced illnesses has also been reported in studies with rats. The bis(ethylmaltolato)oxovanadium(IV) complex completed phase I trials in 2000.[80]

2.5.7.2 Vanadium Complexes with N,O Ligands

Other bidentate monoprotic ligands that have been proven to influence insulin activity are the picolinato ligand and its derivatives such as methylpicolinato.[81] Vanadyl chelation by amino acids in this coordination mode has also been attempted. When evaluating their effectiveness compared to the maltolato complexes, it was concluded that although good activity was observed, further structural improvement will have to be endeavoured as the complexes had lower solubility and more gastrointestinal irritation.[82]

2.5.7.3 Vanadium Complexes with Acetylacetonates

The β-diketonates deserve a special mention as these ligands are some of the most encountered ligands used in coordination chemistry. [VO(acac)$_2$] was synthesized nearly a century ago but it has only been recently studied for its activity.[83,84] [VO(acac)$_2$] and [VO(Et-acac)$_2$] (Et-acac = 3-ethyl-2,4-pentanedionato) have been structurally characterized and tested against bis(maltolato)oxovanadium(IV) for their respective activity and it was observed that their activity was equally effective in lowering glucose levels.[79] Further research is now being conducted with regard to other β-diketonates in conjunction with vanadium.

2.5.7.4 Peroxovanadium Complexes

Hydrogen peroxide (H_2O_2) acts similarly to vanadate in some of its insulin mimicking effects. By combining these two compounds a new compound with even greater activity could be generated.[85] Peroxovanadium complexes are highly stable and have displayed activity of protein tyrosine phosphotases (PTPs) over 1000 times greater than sodium

---

[79] Reul, B. A., Amin, S. S., Buchet, J. P., Ongemba, L. N., Crans, D. C., Brichard, S. M., *Br. J. Pharmacol.*, **1999**, *126*, 467.

[80] Dikanov, S. A., *J. Am. Chem. Soc.*, **1999**, *121*, 11004.

[81] Sakurai, H., Fujii, K., Watanabe, H., Tamura, H., *Biochem. Biophys. Res. Commun.*, **1995**, *214*, 1095.

[82] Melchior, M., Thompson, K. H., Jong, J. M., Rettig, S. R., Shuter, E., Yuen, V. G., Zhou, Y., McNeill, J. H., Orvig, C., *Inorg. Chem.*, **1999**, *38*, 2288.

[83] Morgan, G. T., Moss, H. W., *J. Chem. Soc.*, **1914**, *103*, 78.

[84] Amin, S. S., Cryer, K., Zhang, B., Dutta, S. K., Eaton, S. S., Anderson, O. P., Miller, S. M., Reul, B. A., Brichard, S. M., Crans, D. C., *Inorg. Chem.*, **2000**, *39*, 406.

[85] Heffetz, D., Bushkin, H., Dror, R., Zick, Y., *J. Biol. Chem.*, **1990**, *265*, 2896.

orthovanadate alone.[86] Two active peroxovanadium complexes have been identified as potassium oxodiperoxo(pyridine-2-carboxylato)vanadium(V) and potassium oxodiperoxo(3-hydroxypyridine-2-carboxylato)vanadium(V).[87]

Studies have suggested that the main explanation for insulin mimesis is the inhibition of PTPs and as a result the increased cellular phosphorylation.[88,89] The mechanism for this inhibition differs for vanadate and peroxovanadium. The two different pathways are illustrated in Figure 2.9.

As mentioned earlier, vanadate can act as a phosphate analogue and as such behaves as a competitive inhibitor of PTPs (**1**) and a weak and reversible bond is created between the thiol and vanadate.[90] Peroxovanadium results in irreversible PTPs inhibition.[88] The differences in pathways results in a difference in interaction with protein serine-threonine phosphotases (PS-TrPs). Vanadates deactivate PS-TrPs whilst peroxovanadium has no inhibition effect.[88]
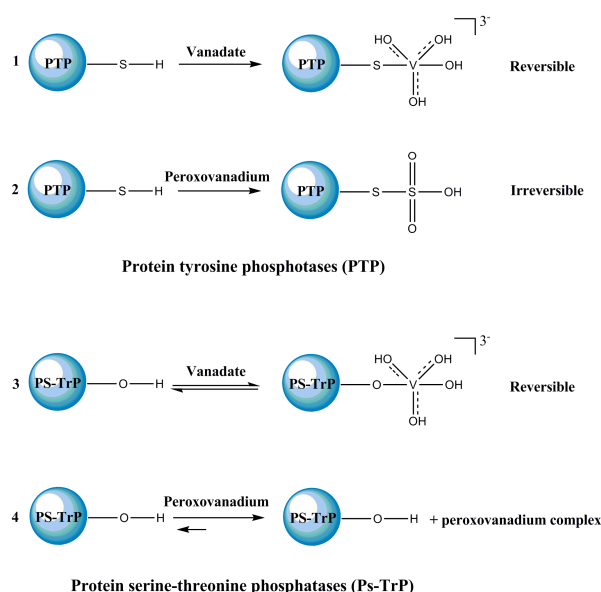
Figure 2.9: Two pathways for the inhibition of PTPs as well as the deactivation of PS-TrPs by vanadate and peroxovanadium complexes.

[86] Bevan, A. P., Burgess, J. W., Yale, J. F., Drake, P. G., Lachance, D., Baquiran, G., Shaver, A., Posner, B. I., *Am. J. Physiol.*, **1995**, *268*, 60.
[87] Shaver, A., Ng, J. B., Hall, D. A., Soo Lum, B., Posner, B. I., *Inorg. Chem.*, **1993**, *32*, 3109.
[88] Posner, B. I., Faure, R., Burgess, J. W., Bevan, A. P., Lachance, D., Zhang-Sun, G., Fantus, I. G., Ng, J. B., Hall, D. A., Lum, B. S., Shaver, A., *J. Biol. Chem.*, **1994**, *269*, 4596.
[89] Fantus, I. G., Deragon, G., Lai, R., Tang, S., *Mol. Cell. Biochem.*, **1995**, *153*, 103.
[90] Huyer, G., Liu, S., Kelly, J., Moffat, J., Payette, P., Kennedy, B., Tsaprailis, G., Gresser, M. J., Ramachandran, C., *J. Biol. Chem.*, **1997**, *272*, 843.

Peroxovanadates can also inhibit glucose-6-phosphotase activity resulting in a glucose-lowering effect. Glucose-6-phosphotase is the metabolite that induces lipogenic enzyme gene expression in a response to glucose. It binds to glycogen synthase and induces a conformational change for the process of dephosphorylation to take place as well as activation of the enzyme.[91] Thus it might not be the inhibition of PTPs that explains the insulinomimetic abilities of peroxovanadates but rather the inhibition of glucose-6-phosphotase. These findings have made peroxovanadium complexes one of the most promising potential drugs.[92] Research is now aimed at improving the stability of these compounds as they are hydrolytically unstable and very redox active, which in turn can result in radical formation.[93]

2.5.8 The Anticancer Activity of Vanadium

As mentioned in Section 2.5.4, the discovery of *cis*-platin instigated the research into metallopharmaceutical agents. A study by Thompson *et al.*[94] showed that the intake of vanadyl sulphate inhibited chemically induced mammary carcinogenesis (breast cancer). Another conclusion from their study was that the compound might be an effective chemo preventive substance and thus started the research into the anticancer activity of vanadium. Peroxovanadates have shown activity in this field being able to induce DNA cleavage chemically and photochemically.[95] Studies to evaluate ligand substitution on $[VO(O_2)_2bpy]$ (bpy= 2,3-bipyridine) and $[VO(O_2)_2phen]$ (phen= 1,10-phenanthroline) contribute to understanding how these DNA cleavage reactions take place.[96]

A few studies are highlighted in the following sections with the effect of vanadium compounds evaluated for different cancers.

---

[91] Foufelle, F., Gouhout, B., Pégorier, J. P., Perdereau, D., Girard, J., Ferré, P., *J. Biol. Chem.*, **1992**, *267*, 20543.
[92] Westergaard, N., Brand, C. L., Lewinsky, R. H., Anderson, H. S., Carr, R. D., Burchell, A., Lungren, K., *Arch. Biochem. Biophys.*, **1999**, *366*, 55.
[93] Krejsa, C. M., Nadler, S. G., Esselstyn, J. M., Kavanagh, J. T., Ledbetter, J. A., Scieven, G. L., *J. Biol. Chem.*, **1997**, *272*, 11541.
[94] Thompson, H. J., Chasteen, N. D., Meeker, L. D., *Carcinogenesis*, **1984**, *5*, 849.
[95] Sakurai, H., Nakai, M., Mika, T., Tsuchiya, K., Takada, J., Matsushita, R., *Biochem. Biophys. Res. Commun.*, **1992**, *189*, 1090.
[96] Hwang, J. H., Larson, R. K., Abu-Omar, M. M., *Inorg. Chem.*, **2003**, *42*, 7967.

2.5.8.1 Central Nervous System

The therapeutic potential of the oxovanadium compound metvan was investigated in a xenagraft model of human glioblastoma. A dose of 10 mg/kg for five days per week showed significant antitumour activity in mice over a period of four weeks.[97]

2.5.8.2 Colon

The antioxidant properties of vanadium has been attributed to the chemopreventive actions of vanadium in colon cancer studies as a study concluded that short-term treatment of 1,2-dimethylhydrazine induced colon cancer with vanadium preventing carcinogenesis by reducing DNA damage and chromosomal aberrations in colon cells. An improvement in glutathione reductase and catalase activities in colon mucosa was also observed.[98]

2.5.8.3 Liver

Several studies have explored vanadium compounds in treatment of primary hepatocellular carcinoma. Supplementation of vanadium (0.5 ppm or 4.27 µmol/L) in drinking water for 4-12 weeks has seen increased glutathione levels and glutathione S-transferase activity in the liver and gastrointestinal systems of rats. This demonstrates the important role that vanadium may play in the detoxification of chemical carcinogens and inhibition of tumorigenesis.[99,100]

2.5.8.4 Haematological System

Although the effect of vanadium on various cancers has been studied, little attention has been given to the haematological diseases. Treatment of xenografted animal models of lymphoid leukaemia and lymphocytic leukaemia with vanadocene dichloride showed a remarkable increase of life-span.[101] Additionally, peroxovanadium compounds have showed up to 20 % increase in life-span and an improved survival rate of 25 %.[102]

[97] Narla, R. K., Chen, C. L., Dong, Y., Uckun, F., *Clin. Cancer Res.*, **2001**, *7*, 2124.
[98] Kanna, P. S., Mahendrakumar, C. B., Indira, B. N., Srivastawa, S., Kalaiselvi, K., Elayaraja, T., Chatterjee, M., *Environ. Mol. Mutagen.*, **2004**, *44*, 113.
[99] Bishayee, A., Chatterjee, M., *Bio. Trace Elem. Res.*, **1995**, *48*, 275.
[100] Bishayee, A., Chatterjee, M., *Anticancer Res.*, **1995,** *15*, 455.
[101] Köpf-Maier, P, Wagner, W., Hesse, B., Köpf, H., *Eur. J. Cancer*, **1981**, *17*, 665.
[102] Djordjevic, C., Wampler, G. L., *J. Inorg. Biochem.*, **1985**, *25*, 51.

2.6 ^{51}V NMR as Research Tool

2.6.1 NMR Properties of ^{51}V

The use of vanadium and its compounds in catalysis as well as its biological and medicinal applications has pioneered extensive studies into the NMR characteristics of vanadium systems. Valuable information regarding the coordination environment of complexes of vanadium in solution, in the solid state and the meso-phase can be gained.[103]

As mentioned in Section 2.3.2, vanadium occupies formal oxidation states of -3 to $+5$. Three of these oxidation states ($-$III, d^8; $-$I, d^6; $+$V, d^0) are diamagnetic and easily susceptible to NMR whilst some of the other oxidation states may be studied by NMR under certain conditions that allow for diamagnetism [$+$I, d^4 (low spin); $+$III, d^2 (low spin); $+$IV, d^1 (dinuclear anti-ferromagnetically coupled)].[103]

Vanadium was one of the first transition metal nuclei to be studied by NMR. This is a result of its advantageous NMR properties that allow for detection at low concentrations and the relative ease at which an experiment might be performed with as much as a ^{13}C probe.[104] The NMR properties of the two isotopes of vanadium are given in Table 2.7. Both isotopes (^{50}V and ^{51}V) are in fact NMR active but due to low natural abundance of ^{50}V and the small gyromagnetic ratio, NMR observations are very limited.[105]

Table 2.7: NMR parameters of vanadium nuclei.

Nucleus	^{50}V	^{51}V
Natural Abundance (%)	0.25	99.75
γ (x 10^7 rad.s^{-1}.t^{-1})	+2.6721	+7.0492
Nuclear Spin	6	7/2
Q (fm^2)	+21	-4.8
r (relative to ^{13}C)	0.76	2170
ν (at 2.35 T) (MHz)	9.988	26.350

γ, gyromagnetic ratio; Q, nuclear electric quadrupole moment; r, receptivity; ν, measuring frequency.

As can be seen from Table 2.7, ^{51}V has a high natural abundance of 99.75 % and its relative sensitivity to carbon is given as 2170. Comparing this to the more often used ^{1}H

---

[103] Rehder, D., Polenova, T., Bühl, M., *Ann. Rep. NMR Spectrosc*, **2007**, *62*, 49.
[104] Rehder, D., *Coord. Chem. Rev.,* **2008**, *252*, 2209.
[105] Lutz, O., Messner, W., Mohn, K. R., *Z. Phys. A,* **1981**, *300*, 111.

nucleus as standard of sensitivity a figure of 0.382 can be assigned.[106] The moderate quadrupole moment (Q) results in signal widths that are sensitive to electric field gradients around the nucleus and reduced signal intensity arising from excessive broadening may result.[107] In the case of ^{51}V NMR, the large spin of the nucleus combats this effect and along with the large shift range, narrow resonance lines are typically observed in ^{51}V NMR spectra.[108] It is thus in principle possible to observe all ^{51}V resonances in solution. As a quadrupolar nucleus the relaxation times in an experiment are short and in the case of ^{51}V NMR over 30 acquisitions per second can be collected.[108]

A large chemical shift range of 5000 ppm is reported for ^{51}V NMR which is unusual for first row metals with the exception of ^{59}Co. The large range reflects part of the complex chemistry of vanadium to accept or donate electrons *via* the *d*-orbitals, depending on its oxidation state.[109] Another aspect that influences the shift is the electronic influences created by the chemical environment surrounding the vanadium nucleus. Small variations in the electronic environment have been shown to have a considerable impact on the spectrum.

2.6.2 ^{51}V NMR Reference Compounds

The reference standard in ^{51}V NMR was formally chosen as $VOCl_3$ with a designated chemical shift at 0 ppm. The major problem associated with this reference however, is its extreme reactivity with water. Its harmful decompositions include HCl and vanadium oxides which are all toxic.[110] An inert atmosphere of the highest quality is needed to handle this compound. Fortunately, over the last few decades secondary standards have been employed such as 1 M orthovanadate which has two active species in solution at pH 12 namely $[VO_4]^{3-}$ (δ= -535.7 relative to $VOCl_3$) and $[V_2O_7]^{4-}$ (δ= -559.0).[111] Other references such as saturated solutions of $NaVO_3$ (δ= -578) and KVO_3 (δ= -576) have also been employed successfully in ^{51}V NMR studies.[112]

[106] Rehder, D., *Bulletin of Magnetic Resonance*,**1982**, 4, 33.
[107] Rehder, D., *Multinuclear NMR*, Plenum Press, New York, **1987**, 488.
[108] Tracey, A., S., *Coord. Chem. Rev.*, **2003**, *237*, 113.
[109] Howarth, O. W., *Progress in NMR Spectroscopy*, **1990**, *22*, 453.
[110] Vanadium(V) oxychloride Material Safety Data Sheet, http://www.sigmaaldrich.com/catalog/DisplayMSDSContent.do, accessed: 20-07-2011.
[111] Rehder, D., Hoch, M., Jameson, C. J*., Magn. Reson. Chem.*, **1990**, *28*, 128.
[112] Han, O. H., Kim, S., Lee, S. G., Kwon, Y., *Journal of Non-Crystalline Solids*, **2005**, *351*, 3365.

2.6.3 Isotropic Systems

Solutions of vanadium complexes in water and organic solvents are termed isotropic as there are no preferred orientations for the molecules due to irregular tumbling. NMR parameters such as chemical shifts (shielding), nuclear spin-spin coupling (scalar coupling constants) and line widths obtained from a spectrum thus reflects averaged conditions. Line widths are related to the electric field gradient found at the nucleus of vanadium and the molecular correlation time. In the case of dynamic systems, this implies the exchange equilibria between two or more species on the sub-millisecond scale.[103]

As mentioned earlier, ^{51}V displays very favourable NMR properties and is susceptible to NMR in almost every environment including slowly tumbling vanadium-containing systems and low local symmetry vanadium systems. Impurities of paramagnetic vanadium species such as V^{IV} in a solution may even be tolerable if no exchange occurs between V^{IV} and V^{V}.[103]

2.6.4 Shielding

Chemical shift is related to shielding and even in the same group of compounds shielding can have a huge impact on the chemical shift of compounds. Figure 2.10 illustrates the shift ranges covered by various groups of vanadium compounds.[103] The chemical shift range indicated in blue is of particular interest as this covers the various inorganic compounds that are of interest to this study.

There exists no direct correlation between the oxidation state of a compound and its shielding range. The range for cyclopentadienylvanadium(III) overlaps with those of V^{-I}, V^{+I} and V^{V} as seen in Figure 2.10.[104]
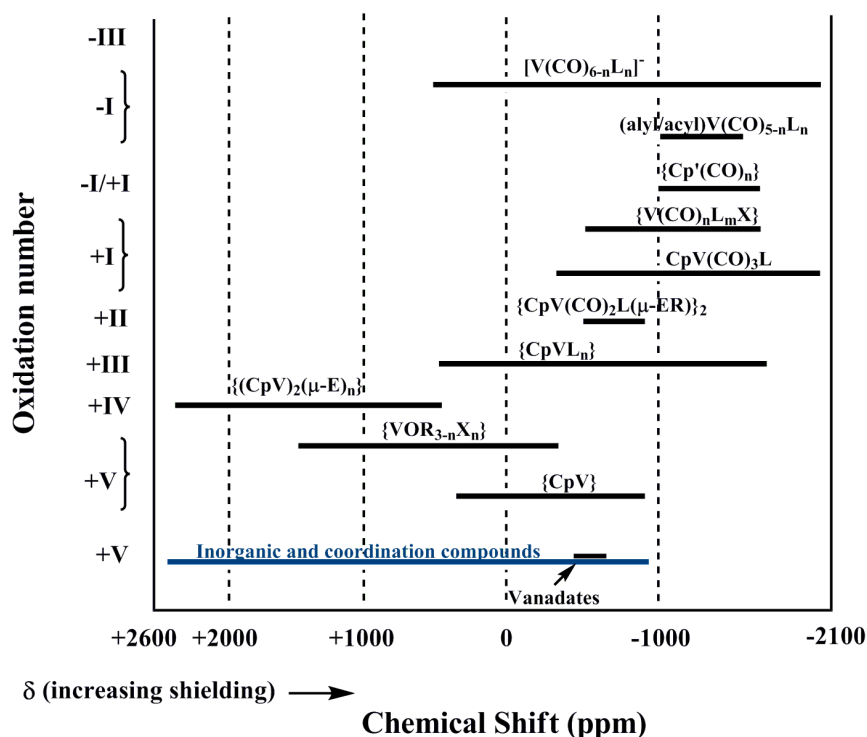
Figure 2.10: Chemical shift ranges of various families of vanadium compounds.
***Abbreviations*: L= ligand (phosphine, isonitrile, amine and others); Cp=η^5-cyclopentadienyl; Cp'= Cp derivative; X= halide, hydride; E= group 16 donor; R= alkyl or aryl. The notation of { } denotes the core of the compound.**

The total nuclear shielding in ^{51}V NMR is attributed to direct diamagnetic shielding (σ_{dia}), indirect diamagnetic shielding (σ_{dia}) and paramagnetic shielding (σ_{para}). These terms can be summarized in the following equation consisting of the mentioned parts:[104]

$$\sigma = \sigma_{local}(dia) + \sigma_{local}(para) + \sigma_{non-local} \qquad \text{(Eq. 2.3)}$$

Where the non-local term refers to the small value consisting of contributions of medium effects such as polarity of solvents or the nature of a counter ion/ ligand and intermolecular interactions. A shift of a few ppm can be observed in the spectrum if these effects are taken into account. Most often this term is ignored in calculations due to the small size of its contribution to the total nuclear shielding.[109]

The local diamagnetic term (σ_{dia}) arises from the shielding effect of the core electrons and although sizable is generally constant and thus also excluded from calculations when

investigating shielding trends. Local diamagnetic values (σ_{dia}) for species such as $[VO_4]^{3-}$ and $[V(CO)_6]^-$ have been determined as 1708 and 1718 ppm respectively.[113,114]

In ^{1}H NMR studies, the shielding arising from the para factor contributes the most to the total shielding effect. In ^{6,7}Li NMR the σ_{dia} and σ_{para} contribute equally to the total shielding parameter. In all the heavier nuclei NMR studies the shielding is mostly determined by the σ_{para} parameter.

The term that thus gives the most insight into the shielding effects present in ^{51}V NMR is the local paramagnetic term. An equation has been developed to represent this term as follows:[104]

$$\sigma_{local}(para) = \frac{-e^2}{2mc^2}(\Delta E^{-1})_{av}\langle r^{-3}\rangle_{3d}c^2 \qquad \text{(Eq. 2.4)}$$

The terms expressed in the above equation are defined as follows: $(\Delta E^{-1})_{av}$ where $(\Delta E)_{av}$ refers to the average HOMO-LUMO splitting where only singlet transitions are allowed; $\langle r^{-3}\rangle_{3d}$ (r= distance of 3d electrons) and c^2 where c= valence d-electron LCAO (linear combination of atomic orbitals) coefficient, m is the mass and e is the mathematical constant 2.718. These terms take into account the ligand field strength, the hardness *vs.* softness of ligands and the covalency of metal-ligand bonds. The local paramagnetic term is a negative term indicating a deshielding effect, thus if the paramagnetic term increases the overall shielding will decrease.

2.6.5 Shielding in Inorganic Vanadium Compounds

As can be seen from Figure 2.10, the chemical shift range of inorganic vanadates(V) has a range from +2570 to -895 ppm. Soft ligands (Se^{2-}, S^{2-}, Br^-, Cl^-) induces a deshielding effect and have thus low-field shifts whilst hard ligands (O^{2-}, OH^-, F^-) will result in high-field shifts. These effects are collectively known as the "inverse electronegativity dependence of shielding" in high valent (d^0) systems. As χ (electronegativity) increases, ΔE will increase, the σ_{para} term will decrease and as a result the total shielding will be increased.[115]

[113] Jameson, C. J., Rehder, D., Hoch, M., *J. Am. Chem. Soc.*, **1987**, *109*, 2589.
[114] Bechthold, H. C., Kececi, A., Rehder, D., Schmidt, H., Siewig, M., *Z. Naturforsch*, **1982**, *B37*, 631.
[115] Kidd, R. G., *Ann. Rep. NMR. Spectrosc.*, **1978**, *10A*, 1.

A study by Rehder *et al.* in 1988 set out to determine the relationship between chelate ring sizes and shielding as observed in ^{51}V NMR.[116] Table 2.8 summarizes their results with the following trends apparent:

i. Open structures with monodentate ligands and 5-membered chelate rings display an increase in shielding as the polarizability of the ligands decreases.

ii. Strained structures due to steric bulk and three- and four-membered chelate rings result in much larger shielding. Bidentate ligands that include the peroxo, hydroxylamido and the carboxylato group are therefore considered as ligands with considerable electronegativities (χ) to impact shielding.

iii. Variation in the coordination number has neglible effects on the shielding as the overall increase in χ is cancelled by the increase of the coordination number.

Table 2.8: ^{51}V δ values for compounds with *O,O* and *N,O* chelate-ring structures for different coordination numbers for the vanadium centre.

Coordina-tion number	Open structures, 5-membered rings		3, 4-membered rings		2, 3-membered rings	
	δ(ppm)	Example	δ(ppm)	Example	δ(ppm)	Example
4	520-580	O_4	-		-	
5	500-520	carboxylate, glycolate	630	O_3(peroxo)	-	
6	440-530	O_2(carboxylate or glycolate)	595	O(dipic, (peroxo)	690-710	$O_2(R_2NO^-)$
7	-		580	O(pic, Ox, edta)	793	O_3(acetate, carbonate, nitrate)

[(**dipic**)= 2,6-dipicolinate, (**pic**)= picolinate, (**Ox**)= 8-Hydroxyquinolinate, (**edta**)= ethylenediaminetetraacetic acid)]

Known as the "inverse chelate effect" of metal shielding in low-valent complexes the above mentioned trends can be explained in the following example: if we assume that the strain in 4-membered chelate ring structures (carboxylato and carbonato) and 3-membered chelate rings give rise to overlapping variations, then a smaller oxygen π donation into the *3d* and *4p* orbitals of vanadium is experienced. This then results in a lower c^2 value in Eq. 2.4. As the *para* term decreases the overall shielding will increase.

---

[116] Rehder, D., Weidemann, C., Duch, A., *Inorg. Chem.*, **1988**, *27*, 584.

Another theory is based on the delocalization of bonding electron density over the ring that results in an increased r value that will lead in turn to a smaller σ_{para} term.[116]

2.6.6 Use of Shielding to Determine pK$_a$

Deprotonation in a compound generally gives rise to shielding and as a result a high field chemical shift is often observed with a change in shift of between -20 and -30 ppm. Larger values of up to -70 ppm have been reported for peroxovandate and can even result in a reverse sign and a shift in a positive direction. This has been evidenced for tetrahedral species such as the vanadate monoanion (+22 ppm).[108] The effect of protonation on chemical shifts is illustrated in Figure 2.11. Similar equations were derived for experimental work done by Roodt *et al.*[117] for cyano complexes.
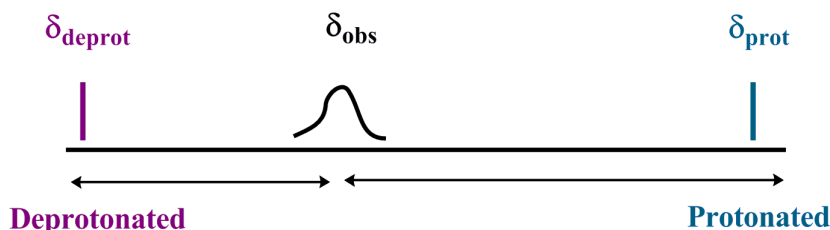
Figure 2.11: The influence of pH on a signal influenced by a protonation/deprotonation reaction. δ_{deprot} is the limiting chemical shift at low pH; δ_{prot} the limiting chemical shift at high pH and δ_{obs} is the observed signal.

From this effect a relationship between signal position, pH and pK$_a$ can be established and is given in Equation 2.5. By determining the y-intercept from a graph of pH against the log of the change in shift, the pK$_a$ can be obtained.

$$pH = pK_a + log\,{\left(\delta_{deprot} - \delta_{obs}\right)}\Big/{\left(\delta_{obs} - \delta_{prot}\right)}$$ (Eq. 2.5)

2.6.7 Isotopic and Temperature Influence

The study of bonding models further gives insight into the chemical shift as a dependence on isotopic substitution. Temperature can also influence the chemical shift. A study by Jameson[113] into the similar vibrational force fields for M(CO)$_6$ (M=Cr, Mo, W)

---

[117] Roodt, A., Leipoldt, J.G., Helm, L., Merbach, A. E., *Inorg. Chem.*, **1992**, *31*, 2864.

along with the vibrational spectroscopy data of $[V(CO)_6]^{-1}$ revealed that Δr_{vc} (the change in V-C bond length) upon substitution of ^{13}C for ^{12}C is -1.27×10^{-4} Å. The change in chemical shift was -0.27 ppm. The paramagnetic contribution to the chemical shift thus decreases as the metal-to-ligand distance decreases.[118] Taking into account the temperature effect, an argument was made on theoretical basis that the main contribution might be to the change in r_{vc} that would influence the ΔE as the temperature increases. An increase in temperature will result in a deshielding effect being observed.[113] This has been verified by the phosphomolybdato- and silicotungstatovanadates(V) where the chemical shift decreased by 3 to 7 ppm as the temperature rose from 300 to 350 K.[119]

The factors that influence shielding are complex as the σ-donor and π-acceptor strengths of the ligands can be influential, as well as the general symmetry of the compound. The influence of symmetry is relevant as the selection rules restricts the excitations to only those molecular orbitals that have transformation properties that are the same as the angular momentum operator.

2.6.8 Trends in High-valent (open shell: d^0 (CpV^{+V}), d^1 (spin coupled dinuclear $(CpV^{IV})_2$

Complexes with vanadium in a high valence state consist of ligands that are effective σ/π-donors i.e. "hard" ligands. These are ligands with high electronegativities. Some of the most notable ligands in this group contain an *O*- or *N*- functional group such as acetylacetonate or 8-hydroxyquinolinate. Both of these functions are of relevance to the current research project. These ligands will induce a high level of shielding as an inverse electronegativity is taken into account. More polarisable and also less electronegative ligands such as the halides, sulphides and selenides result in deshielding as only small HOMO-LUMO separations can occur and thus a large σ_{local} paramagnetic value is reported.[120]

As mentioned in Section 2.6.7, an increase in temperature creates changes in internuclear distances and angles and ultimately decreases shielding. In high valence vanadium complexes this effect is however reduced.

---

[118] Ihmels, K., Rehder, D., Pank, V., *Inorg. Chim. Acta*, **1985**, *96*, L69.
[119] Maksimovskaya, R. I., Fedotov, M. A., Mastikhin, V. M., Kuznetsova, L. I., Matveev, V. M., *Dokl. Akad. Nauk. SSR,* **1978**, *240*, 117.
[120] Harrison, A. T., Howarth, O. W., *J. Chem. Soc. Dalton Trans.*, **1986**, 1405.

2.7 Coordination Chemistry of Vanadium with O,O and N,O Ligands

As mentioned in Chapter 1, a main aim of this study is the synthesis of novel vanadium compounds in the +4 and +5 oxidation states. To achieve this goal, focus was placed on *O,O* and *N,O* ligand systems to be used for coordination to vanadium. β-diketones are of special interest as these versatile ligands have become invaluable in the field of coordination chemistry and their wide applicability in industry and biology has been discussed. This section of the chapter aims to explore some of the systems already synthesised as well as exploring some of the attributes of the ligands to be used in this study.

2.7.1 β-diketones

β-diketones and their derivatives have received special interest in the field of coordination chemistry as their coordination to metal centres often yields interesting interactions. The oxygen atoms easily act as uninegative O_2-chelating donors that can stabilize many mononuclear and polynuclear complexes.[121] Another determining factor of the advantageous chemical properties of β-diketones is their ability to undergo keto-enol tautomersim as illustrated in Scheme 2.1.[122]

Keto

Two Enolic forms   Conjugated form
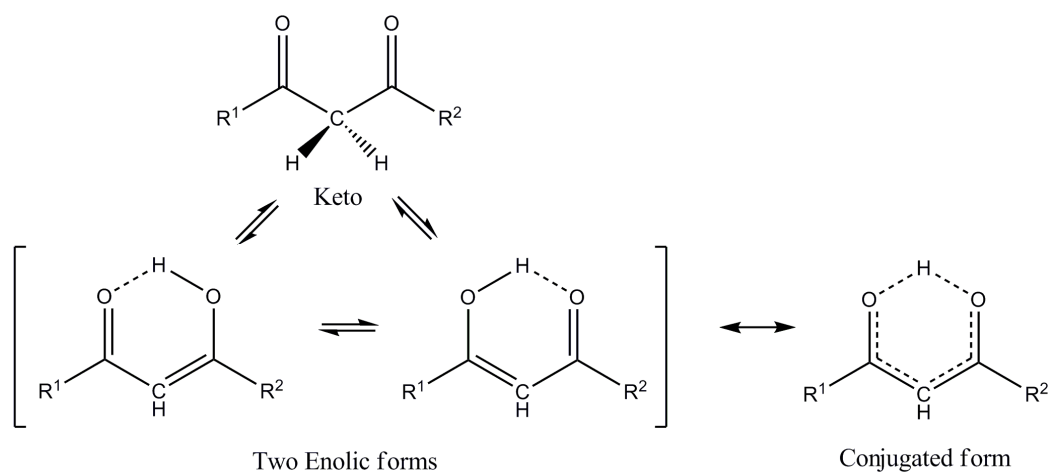
Scheme 2.1: Different enolic forms of asymmetric β-diketones exist in solution.

The total number of possible enol and keto forms is shown in Figure 2.12. β-diketones have different tautomers that can react with metals at different rates as the characteristics

---

[121] Vigato, P. A., Peruzzo, V., Tamburini, S., *Coord. Chem. Rev.*, **2009**, *253*, 1099.
[122] Aromí, G., Gamez, P., Reedijk, J., *Coord. Chem. Rev.*, **2008**, *252*, 964.

of the enol and keto isomers can differ substantially.[123] In solution, mixtures of the two isomers exist that are related by a 1,3 hydrogen shift. Asymmetric β-diketones can exist in two different enolic forms as shown in Scheme 2.1. The enolic forms are stabilized by π-electron conjugation and an intramolecular hydrogen bond.[124]
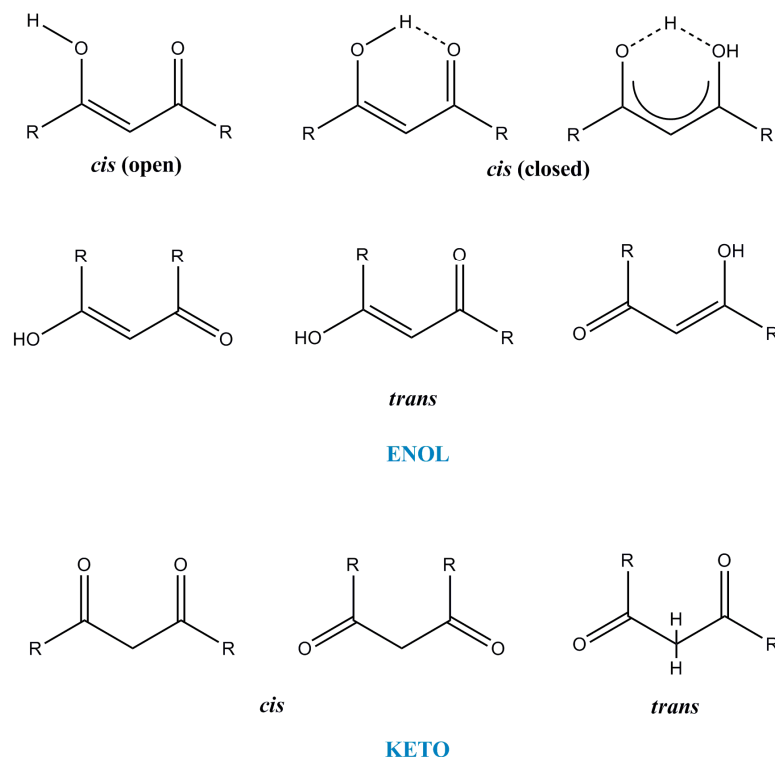
Figure 2.12: Possible enol and keto forms of β-diketones.

Determination of which form will dominate in solution has been studied extensively and it was concluded that the substituents labelled as R_1 and R_2 contribute significantly. By having a substituent attached to one of the carbonyl carbons a stabilization effect towards the enol form is observed. By implication the hydroxyl group of the enol form will be located on the substituted carbon. Aromatic and electron withdrawing groups on the carbonyl carbons tend to favour the enolic tautomers, whilst sterically bulky substituents induce keto-enol tautomerism towards the keto isomer.[125]

---

[123] Jaffe, M. R., Fay, D. P., Cefola, M., Sutin, N., *J. Am. Chem. Soc., Dalton Trans.*, **1983**, 2657.
[124] Han, K. L., Zhao, G. J., *Hydrogen Bonding and Transfer in the Excited State vol. 1*, Wiley & Sons, **2010**, 356.
[125] Gericke, H. J., *MSc Dissertation*, University of the Free State, **2009**.

Acetylacetone (Hacac) is referred to as the best known β-diketone. It exists mainly in its enolic form at ambient conditions.[126] Bonds are formed with metal centres by the two oxygen donor atoms but μ and μ_3 coordination modes have also been found as can be seen in Scheme 2.2.[122]

acetylacetonato   μ-acetylacetonato μ_3-acetylacetonato
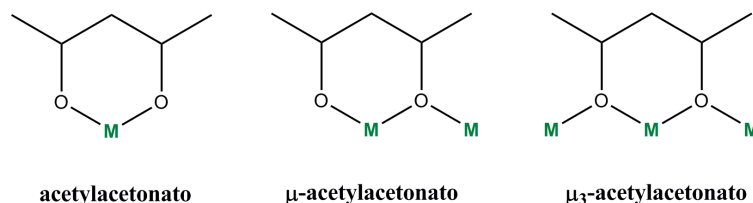
Scheme 2.2: Selected coordination modes of acetylacetone with metal centres.

2.7.2 Bis(acetylacetonato)oxovanadium(IV)

[VO(acac)$_2$] was first synthesised by Jones in 1957 but was only used to prepare other vanadium complexes in the 1990s.[127] It acts as an excellent precursor for further synthesis as the oxygen-metal bonds found in [VO(acac)$_2$] are weak and can be substituted by stronger ligands.[128] This method has been informally named the 'acac' method of synthesis[129] and has been utilized extensively in this research project and will be discussed further in Chapter 4.

If the substitution reaction is performed under anaerobic conditions the product synthesized will be in the +4 oxidation state whilst exposure to aerobic conditions will favour the formation of the stable VO^{2+} ion resulting in a vanadium complex in the +5 oxidation state. Oxidized complexes may also adopt a VO^{3+}, VO_2^+ or $V_2O_3^{4+}$ core although these states are rare.[127]

2.7.3 Complexes with *O,O* and *N,O* ligands

Some of the most studied complexes of vanadium have been those with mono-deprotonated hydroxylamines and hydroxamic acids as these compounds have shown

[126] Lowrey, A. H., George, C., Dantonio, P., Karle, J., *J. Am. Chem. Soc.*, **1971**, *93*, 6399.
[127] Maurya, M. R., *Coord. Chem. Rev.*, **2003**, *237*, 163.
[128] Syamal, A., Maurya, M. R., *Coord. Chem. Rev.*, **1989**, *95*, 183.
[129] Vicente, J., Chicote, M. T., *Coord. Chem. Rev.*, **1999**, *193*, 1143.

great potential as biological inhibitors of protein tyrosine phosphotases (see Figure 2.9).[130]

The *N,O* donor ligand picolinic acid along with quinoline derivatives have been a subject of study for catalytic applications as well as biological activity upon coordination to vanadium as found in a study by Crans and Shin in 1998.[131]

The complexes formed with di-and triethanolamine ligands are synthesized under mild conditions and a study recently established a pH dependent stability owing to the extensive solution chemistry of vanadium (see Section 2.4 with Figures 2.3 and 2.4).[23]

Depending on the different conditions set in the synthesis, different products may be isolated from a reaction. For the 8-hydroxyquinoline ligand the different pathways of reaction are illustrated in Scheme 2.3.[127] The starting reagent in the scheme is the $[(V^VOL_2)_2\mu\text{-}O]$ complex that forms under aerobic conditions with acetone as solvent.
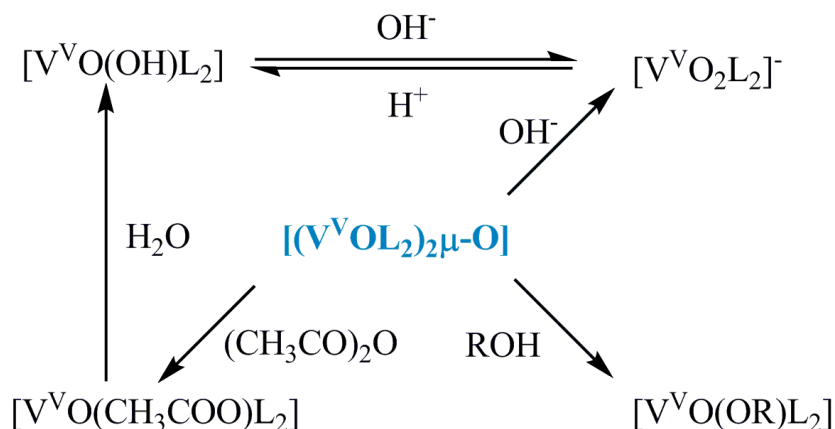
Scheme 2.3: Vanadium complexes formed under different conditions with 8-hydroxyquinoline (LH).

2.8   Conclusion

Various aspects of the rich chemistry of vanadium were discussed with regard to its uses, chemical reactivity, oxides and solution behaviour in this chapter. A short summary was given as to the biological role of vanadium and current studies towards testing novel vanadium compounds for medical applications and the unique characteristics that

[130] Nxumalo, F., Glover, N. R., Tracey, A. S., *J. Biol. Inorg. Chem.*, **1998**, *3*, 534.
[131] Crans, D. C., Shin, P. K., *Inorg. Chem.*, **1998**, *27*, 1797.

vanadium possesses that makes it an ideal biometal. The value of ^{51}V NMR in studies of vanadium compounds was discussed and the large amount of information to be gathered from using this technique was highlighted. Lastly, the chapter was concluded with a brief mentioning of the ligand systems to be investigated in this study, as a lead into the synthesis part of the project.

Chapter 3: Basic Theory of NMR, IR, UV/Vis, XRD and Chemical Kinetics

3.1   Introduction

Characterization of compounds is an essential part of research in the laboratory. The aim of all characterization techniques is to collect qualitative and quantitative information that will identify/ establish the chemical and structural composition of a sample. Many instrumental methods of characterization rely on the principle of matter interacting with electromagnetic radiation by three distinct processes namely transmission, scattering and absorption.[1] The nature of the interaction is defined as a function of the properties of the radiation, such as energy, polarization, and the chemical properties of the matter under investigation. The interaction of the radiation and the sample is then measured accordingly with regard to transmission, scattering or absorption and provides valuable insight concerning chemical composition or structure of the sample. Figure 3.1 provides a guide to the potential absorption spectroscopy available across the electromagnetic spectrum.
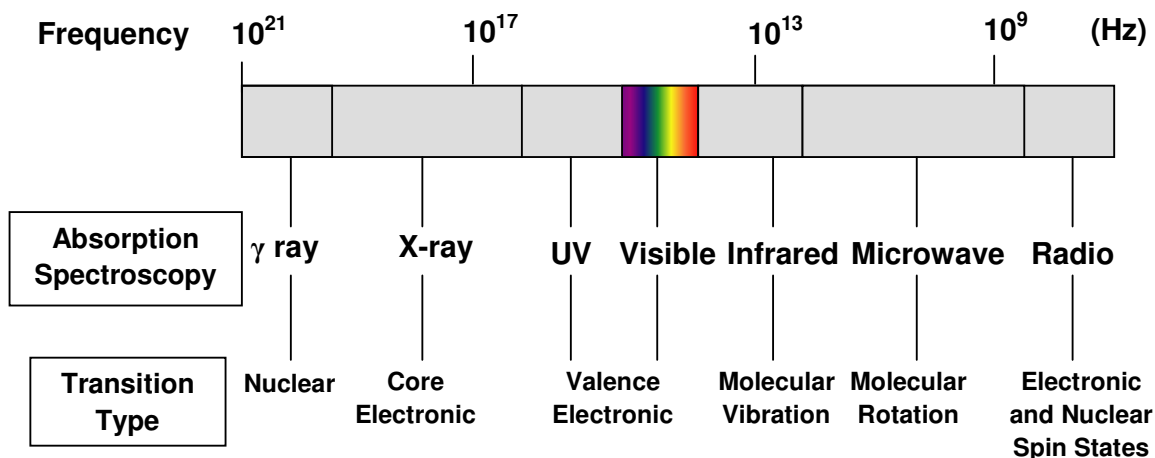
Figure 3.1: Analytical potential for the various absorption spectroscopies across the electromagnetic spectrum.

---

[1] Krull, U. J., Thompson, M., *Encyclopedia of Physical Science and Technology: Analytical Chemistry 3rd edition,* Academic Press, **2001**, 549.

This chapter outlines the basic theory regarding the techniques of Nuclear Magnetic Resonance, Infrared, UV/Vis spectroscopy, single crystal X-ray diffraction and an introduction to chemical kinetics. These techniques were all utilized in this study for accurate identification of synthesized products as well as the study of these compounds under a variety of influences such as temperature and concentration changes.

3.2   Nuclear Magnetic Resonance Spectroscopy

Nuclear Magnetic Resonance (NMR) spectroscopy has become one of the most powerful tools available to chemists in determining the structure of chemical species. In 1924, Pauli postulated that certain nuclei possess properties such as spin and magnetic moments. This postulation was later verified and proved to be the foundation upon which NMR techniques are based. Eventually, F. Bloch and E. Purcell shared the Nobel Prize in Physics for their work demonstrating the effect that electromagnetic radiation has on nuclei placed in an applied magnetic field.[2]

3.2.1 Properties of a Spinning Nucleus

The spin property of nuclei includes a ground state nuclear spin quantum number, I, to be assigned to each isotope of every known element. This value is dependent on atomic and mass numbers of elements and is expressed as $n/2$ with n being an integer. Isotopes having atomic and mass numbers that are both even have $I = 0$ with no NMR spectrum obtainable for e.g. elements such as ^{12}C and ^{56}Fe. $I \neq 0$ indicates an element with angular momentum whilst the group with $I = 1/2$ includes some of the nuclei most commonly studied in NMR such as ^{1}H, ^{13}C and ^{19}F. Since nuclei are positively charged, the spin movement represents the circulation of electric charges similarly to the flow of electrons through a coil. The effect of the spin movement with a resulting magnetic dipole moment being generated is illustrated in Figure 3.2.

---

[2] Skoog, D. A., Holler, F. J., Crouch, S. R., *Principles of Instrumental Analysis 6th edition*, Thomson Brooks/Cole, **2007**, 430.
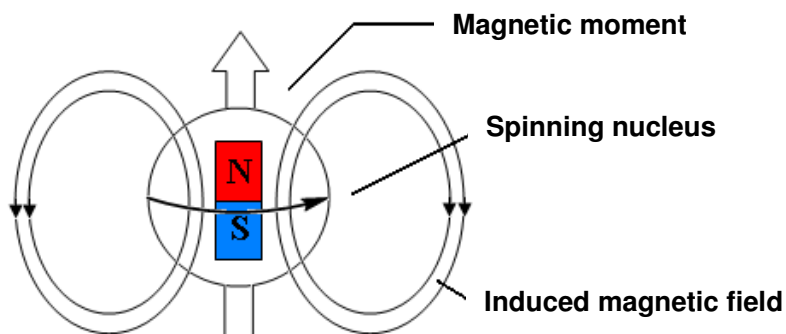
Figure 3.2: Illustration of the magnetic dipole moment generated by the spin movement of the nucleus.

In the absence of an external magnetic field the nuclei will arrange themselves in a random pattern whereas in the presence of an applied magnetic field an arranged orientation will be assumed as shown in Figure 3.3.
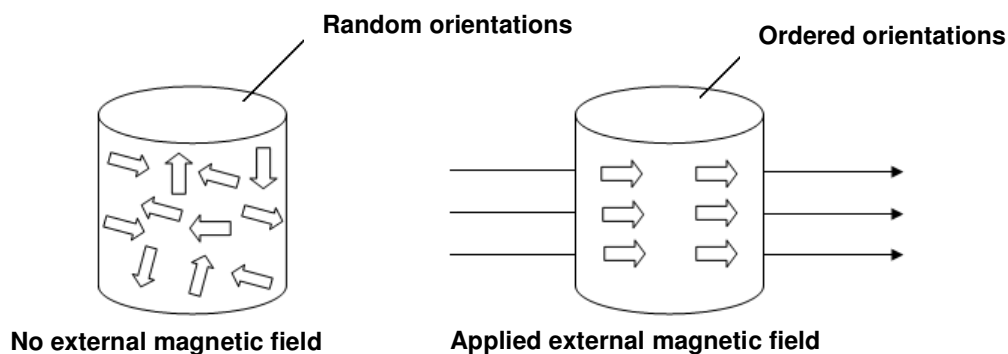
Figure 3.3: Arrangement of nuclei in response to an applied magnetic field.

The number of orientations that nuclei occupy in an applied magnetic field can be calculated by quantum mechanical principles as given by Eq. 3.1.

$$Number\ of\ orientations = 2I + 1 \qquad \text{(Eq. 3.1)}$$

Nuclei such as ^{1}H with I = 1/2 can thus occupy two orientations as well as two different energy levels. The energy states are illustrated in Figure 3.4. The orientation parallel to the field direction indicates the low energy state whereas the anti-parallel orientation results in a high energy state.
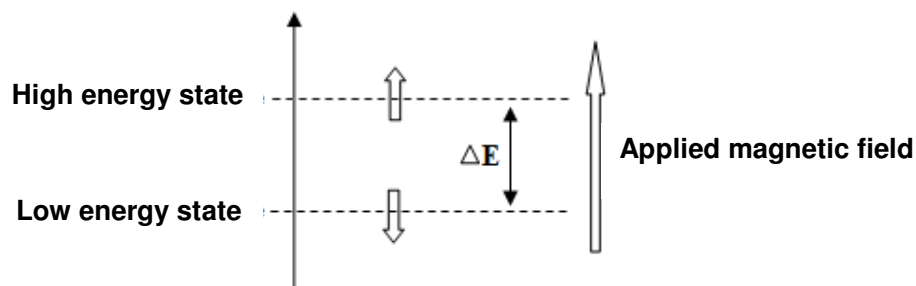
Figure 3.4: High and low energy state occupation of ^{1}H nuclei.

The difference in energy states (*ΔE*) represents the energy needed for the magnetic dipole to be excited from a low energy state to a high energy state. Accordingly, this excitation can be initiated by the radiation of the nuclei with electromagnetic radiation of appropriate frequency, termed as the resonance frequency or the Larmor frequency.

3.2.2 Chemical Shifts

During an NMR experiment, radiation with the Larmor frequency will be absorbed by the nuclei and recorded as absorption signals by the spectrometer. The plot of absorption of energy against frequency represents an NMR spectrum. The Larmor frequency is dependent solely on the magnetic field experienced by the nuclei and as such the effective magnetic field differs from the magnetic field applied during an experiment. The difference is caused by the environment surrounding the nuclei. As nuclei are situated in different positions in a molecule, different Larmor frequencies exist and thus different resonance signals are recorded to give a typical NMR spectrum.

The peaks visible on a spectrum are in actual fact not Larmor frequencies but chemical shifts relative to a standard. The relationship between the chemical shift, Larmor frequency of the sample (v_I) as well as the internal standard (v_0) is given in Eq. 3.2. A factor of 10^6 is brought into the calculation merely to simplify results and chemical shifts are reported as parts per million (ppm).[3]

$$\delta = \frac{(v_I - v_0)}{Instrument\ frequency} \qquad \text{(Eq. 3.2)}$$

---

[3] Ebsworth, E. A. V., Rankin, D. W. H., Cradock, S. *Structural Methods in Inorganic Chemistry*, Blackwell Scientific Publications, **1987**, 28.

3.2.3 Shielding and Spin-spin Coupling

Electrons surrounding a nucleus generate a small local magnetic field that leads to shielding of the nucleus against the externally applied field. This results in lower Larmor frequencies and introduces the concept of shielding and deshielding of nuclei.[4] The spectrum is affected in such a way that chemical shifts move downfield when deshielding occurs with the opposite being true of shielding as illustrated in Figure 3.5.

| Absent electrons shifts signal downfield | | Shielding by electrons shifts the signal upfield |

External magnetic field strength

Downfield   Upfield
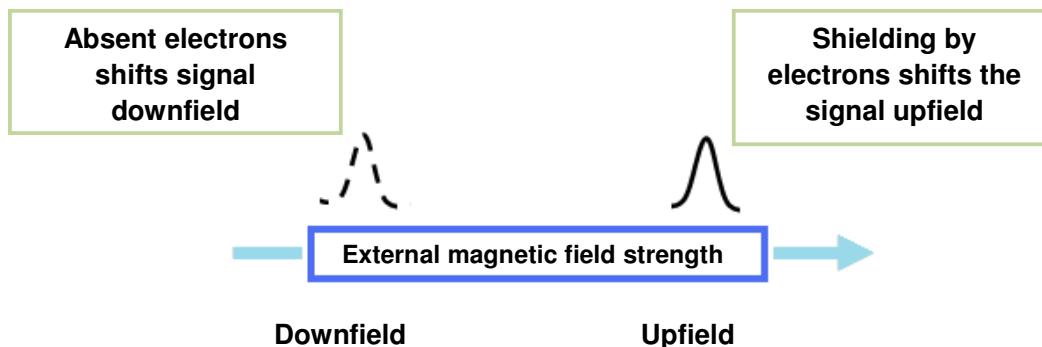
Figure 3.5: Shielding causes absorption to be shifted to a higher magnetic field strength.

Another phenomenon typically seen in NMR studies is that of spin-spin coupling in which an interaction occurs between die magnetic dipole of a proton with the magnetic dipole of another proton in close proximity. This results in a splitting of resonance signals. In ^{1}H NMR no splitting is observed for chemically equivalent (homotopic) protons or protons that are enantiotopic.

NMR spectroscopy has enabled chemists as well as biochemists to elucidate structures of molecules of interest for several decades with research continuing to provide new techniques to enhance the capabilities of this powerful tool even further.

3.3   Infrared Spectroscopy

Infrared (IR) spectroscopy is another important and effective technique in the identification of compounds. One of the many advantages of this technique is the versatility with regard to the sample state to be used. Liquids, solutions, pastes, powders, films, fibres, gasses and surfaces can all be examined by IR spectroscopy.[5]

---

[4] Solomons, G., Fryhle, C. *Organic Chemistry 7th edition*,Wiley & Sons, **2000**, 366.
[5] Staurt, B., *Infrared Spectroscopy: Fundamentals and Application*, Wiley & Sons, **2004**, 1.

As the name implies a sample is irradiated with infrared waves that cause atoms or groups of atoms to vibrate about the covalent bonds that connect them. The infrared spectrum is a result of passing infrared radiation through a sample and plotting the fraction of the incident radiation that is absorbed at a particular energy. The energy at which these peaks appear relates to the frequency of a vibration of a part of the sample molecule.

3.3.1 The Selection Rule

For a molecule to be "infrared active" an electric dipole moment of a molecule must change during the vibration. This constitutes the *selection rule* of infrared spectroscopy. Thus for a homonuclear diatomic molecule such as Br_2, which has no electric dipole moment, stretching of the bond will not be "infrared active".[6]

As functional groups of organic molecules signify a specific arrangement of bonded atoms, absorption of infrared energy will occur in a characteristic manner unique to the types of bonds and atoms present in the specific functional groups of the molecule. This leads to quantization of vibrations as the compound absorbs IR energy in particular regions of the infrared portion of the spectrum.

The location of an IR absorption band is specified in frequency-related units by its wavenumber ($\bar{\nu}$) expressed in reciprocal centimetres (cm^{-1}) or by its wavelength. The wavenumber represents the number of cycles of the wave in each centimetre along the light beam.

3.3.2 Molecular Vibration

Molecules are able to vibrate in a variety of ways. Two atoms joined by a covalent bond can undergo a stretching vibration where the atoms move back and forth as if joined by a spring. The various vibrations are illustrated in Figure 3.6.

---

[6] Lindon, J. C., Tranter, G. E., Holmes, J. L., *Encyclopedia of Spectroscopy and Spectrometry: Volume 1*, Academic Press, **2000**, 1066.
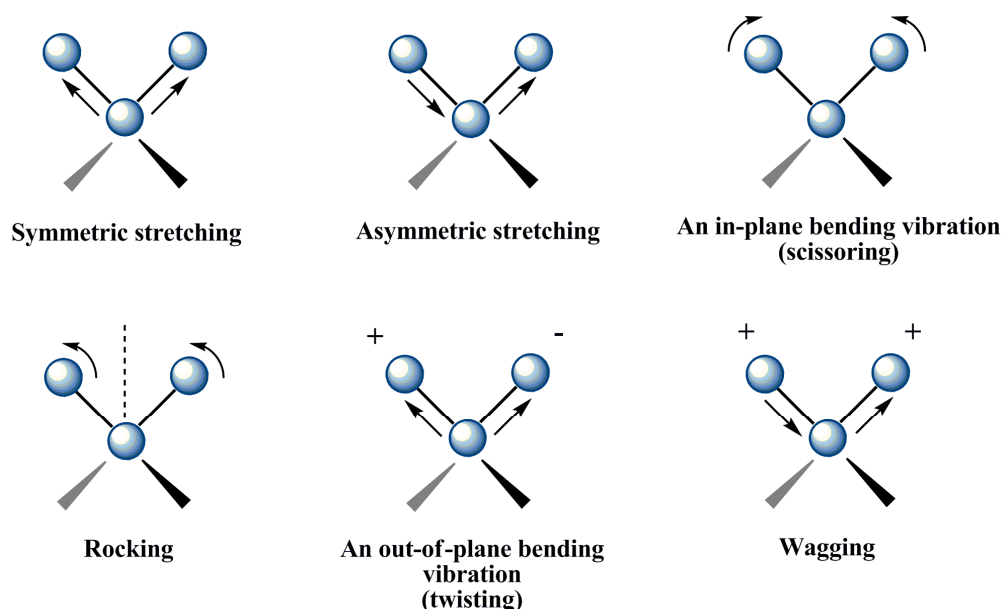
Figure 3.6: Different stretching and bending vibrations bonds/ molecules can undergo.

Frequencies of given stretching vibrations in an IR spectrum can be related to the mass of the bonded atoms as well as the rigidness of the bond. Atoms light of weight vibrate at higher frequencies whilst heavier atoms vibrate at lower frequencies. The rigidness of the bond refers to the strength of the bond, where triple bonds being stronger than double bonds will vibrate at a higher frequency. This clarifies the tendency for all groups involving hydrogen to vibrate at high frequencies such as C-H at (2962 cm^{-1}) and N-H at (3500 cm^{-1}).[5]

As stated in Section 3.3.1, absorption of infrared radiation requires a change in the dipole moment as the vibration occurs. The four hydrogen atoms of methane vibrate symmetrically and is one of the compounds that do not absorb IR energy. The ethene and ethyne double and triple bonds also result in no absorptions.

IR spectroscopy is a useful tool in identifying a compound or functional groups present in a substance and is becoming invaluable to chemists as a quick analysis tool.

3.4   Ultraviolet/ Visible Spectroscopy

Identification of materials based on colour is one of the earliest examples of qualitative molecular absorption spectrophotometry. The conclusion that colour intensity can be related to concentration became the first application of employing molecular absorption spectroscopy for quantitative analysis. Where the naked eye was once used in this

regard it has been replaced by advanced spectrophotometers that employ a wide range of filters, solid-state detectors, digital data acquisition and processing, and double-or single-beam operation.

3.4.1 Uses of UV/Vis Spectroscopy

Industrial application of spectrophotometry ranges wide, from process monitoring to product assay in the pharmaceutical industry. Within the last few decades combination of UV/Vis with separation techniques such as high-performance liquid chromatography (HPLC) has led to it becoming an essential tool in the modern laboratory.

One of the most important uses is perhaps the use of spectrophotometric measurements to study electronic states and with the ability of rapid data acquisition times, UV/Vis techniques such as slower UV/Vis and stopped-flow UV/Vis can be employed for kinetic studies of reactions.[7]

3.4.2 Basic Principals of UV/Vis Spectroscopy

The interaction between matter with radiation leads to a number of processes, including reflection, scattering, absorbance, fluorescence/ phosphorescence (absorption and re-emission), and photochemical reaction (absorbance and bond breaking). In measuring UV/Vis spectra only the process of absorbance is evaluated.

As mentioned in the introduction, light is a form of energy and absorption of light by matter causes changes in the energy content of molecules. The total potential energy of a molecule can be given by Eq. 3.3:

$$E_{total} = E_{electronic} + E_{vibrational} + E_{rotational} \qquad \text{(Eq. 3.3)}$$

The amount of energy each molecule possesses in each form exists in discrete levels or states. The differences in magnitude of these states are in the order:

$$E_{electronic} > E_{vibrational} > E_{rotational}$$

With some molecules and atoms, photons of UV and visible light cause transitions between the different electronic energy levels. The wavelength absorbed is thus the

---

[7] Settle, F. *Handbook of Instrumental Techniques for Analytical Chemistry*, Prentice Hall PTR, **1997**, 481.

amount of energy needed to move an electron from a lower energy level to a higher energy level. This is illustrated in Figure 3.7.
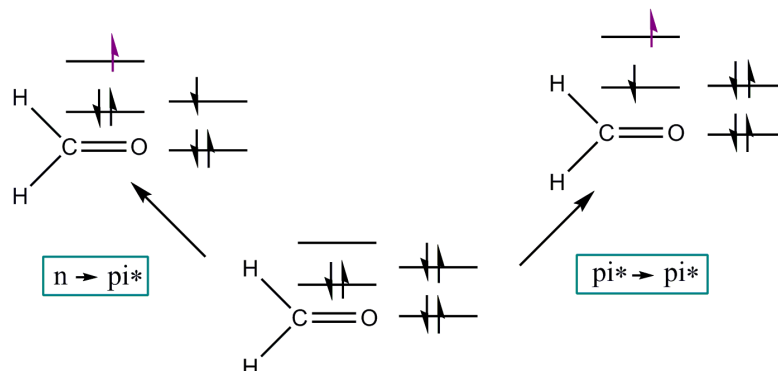
Figure 3.7: Electronic transitions in formaldehyde.

In theory, these transitions result in very narrow absorbance bands at wavelengths that are characteristic of the difference in energy levels of the absorbing species as is shown in Figure 3.8.
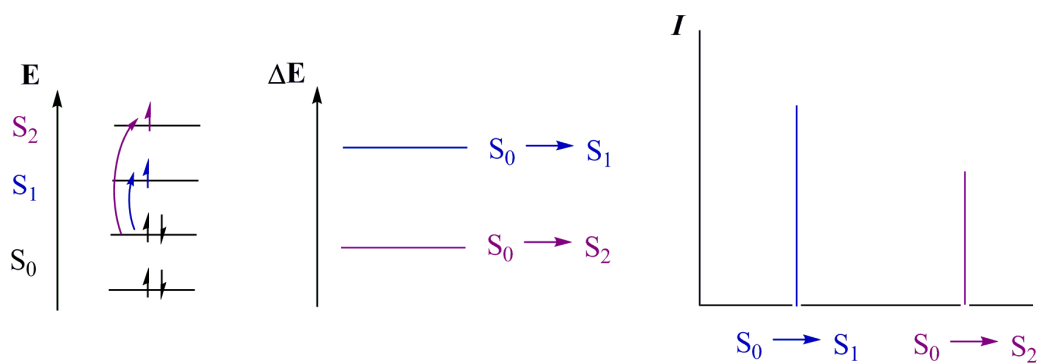
Figure 3.8: Electronic transitions and spectra of atoms.

Molecules, however, display a different absorption pattern. Their vibrational and rotational energy levels are superimposed on the electronic energy levels. A wide range of transitions with different energies can occur and thus the bands are broadened. This is illustrated in Figure 3.9 with broadening even greater when solvent-solute interactions occur to yield a typical UV/Vis spectrum.
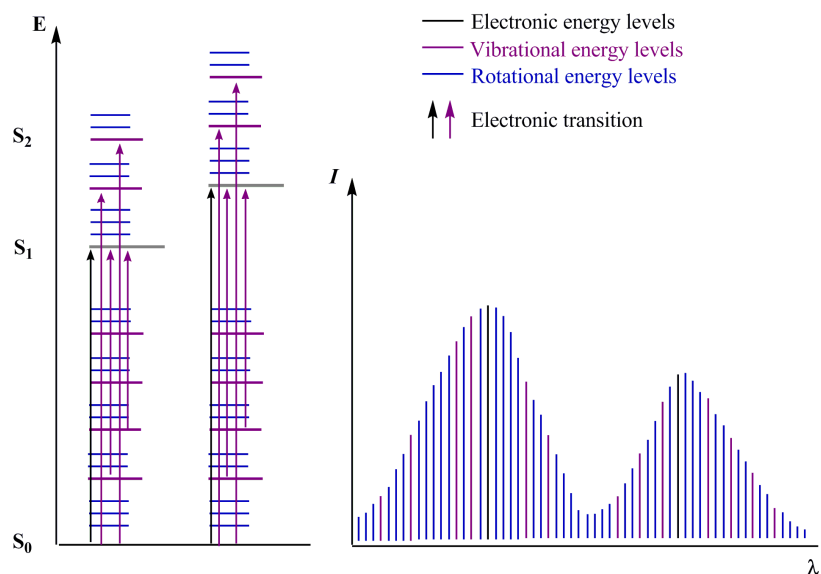
Figure 3.9: Electronic transitions and UV/visible spectrum for molecules.

3.4.3 Quantitative Analysis

The greatest use of UV/Vis spectroscopy has been its application in making quantitative measurements. It has wide application to both organic and inorganic systems with typical detection limits of 10^{-4} to 10^{-5} M. High selectivity and good accuracy limits have made UV/Vis spectroscopy one of the most useful tools available to scientists.[2]

Quantitative analysis is based on the Beer-Lambert-Bouguer law. Beer's law was developed from the relationship between transmission and pathlength described by Pierre Bouguer in 1729 viz:[8]

$$T = {}^{I}\!/_{I_0} = e^{-kb} \qquad \text{(Eq. 3.4)}$$

In Eq. 3.4, I_0 is the incident intensity, I is the transmitted intensity, e is the base of the logarithm, k is a constant and b is the path length. Simplified, the above equation states that if 100 photons of light enters a cell and only 50 emerge on the other side the transmittance is 0.5 or 50 percent. If these 50 photons then pass through another cell then only 25 will emerge. August Beer used this equation to illustrate the relationship of concentration and transmission. The amount of light absorbed can be directly related to the amount of absorbing molecules through which the light passes. The combined two laws are given in Eq. 3.5, with c as the concentration.

---

[8] Owen, T., *Fundamentals of Modern UV/Visible Spectroscopy*, Agilent Technologies, **2000**, 3.

$$T = {I}/{I_0} = e^{-kbc} \qquad \text{(Eq. 3.5)}$$

To obtain a linear relationship, Eq. 3.5 is expressed in logarithms and Beer's law in its most familiar form, in terms of absorbance, A, is obtained.

$$A = -logT = -log\,{I}/{I_0} = log\,{I_0}/{I} = \varepsilon bc \qquad \text{(Eq. 3.6)}$$

In Eq. 3.6, ε is the molar absorptivity that is characteristic for each substance. This simple linear relationship between concentration and absorption of light forms the basis for all quantitative experiments involving UV/Vis spectroscopy. This is done by studying reactions in terms of change in absorbance over time.

UV/Vis spectroscopy has some application as a characterisation method to evaluate structures, however, it is best to use this method in conjunction with NMR or single crystal X-ray diffraction studies to effectively evaluate a product.

3.5   Single Crystal X-Ray Diffraction

The experimental technique which has been of immeasurable value in determining the structure of unknown species is X-ray diffraction (XRD). Where crystals are obtainable, the result of such an experiment is ultimately a three-dimensional representation of the molecular structure of the compound involved, determined from a particular mathematical model. When a crystalline sample is bombarded with X-rays, the X-rays are diffracted by a pair of atoms and the interference pattern produced depends on the wavelength of the X-rays and the distance between the atoms. As the wavelength is known, a direct measurement of distances between atoms can take place.

3.5.1 The Structure of Crystals

Crystals contain atoms, molecules, or ions that are arranged by a repetitive pattern. The term unit cell refers to the smallest arrangement of atoms that can describe the crystal as it is the characteristic part of the crystal that repeats itself. Packed in three dimensions, the unit cells describe the bulk arrangement of atoms in the crystal which is termed the lattice. The unit cell is described by the lengths of its edges along the *a*, *b* and *c* axis, as

well as by the angles α, β and γ that the axis intersect. [9] To describe vectors and atomic planes within a crystal the three-value Miller index notation (*hkl*) was developed.

3.5.2 The Physical Experiment and Bragg's law

X-rays interact with electrons in an atom and scatters. X-rays have this ability as their wavelength is in the order of the distance between atoms and it is this scattered radiation that we use to interpret the internal arrangement of crystals. More electrons in the crystal will lead to better scattering and the term atomic scattering factor relates to the specific scattering power of an atom where scattering increases with an increase in atomic number, *Z*.

The discovery of X-ray diffraction in crystals by Laue and Bragg predates the First World War, with W. L. Bragg envisioning crystals as layers or planes of atoms behaving in effect as reflecting planes.[10] Here the angle of incidence equals the angle of reflection as illustrated in Figure 3.10. Although this does not agree completely with the true physical environment of the crystal, the geometrical aspect is rationally correct and can be given by Eq. 3.7, which can be used for the analysis of a crystal structure. In the equation λ is the wavelength, *n* is the order of reflection, d_{hkl} is the lattice plane spacing and θ is the angle of incidence/ reflection with respect to the plane.

$$n\lambda = 2d_{hkl}sin\theta \qquad \text{(Eq. 3.7)}$$
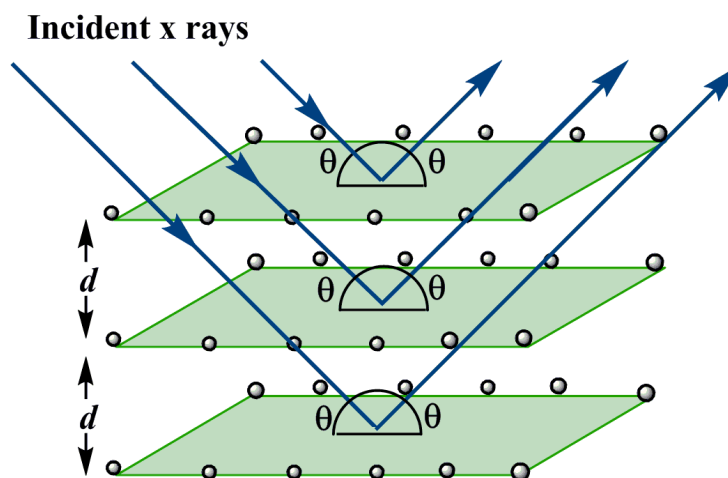
Figure 3.10: Incident X-rays undergo diffraction by the planes with the angle of incidence equal to the angle of diffraction.

[9] Whitten, K. W., Davis, R. E., Peck, M. L., *General Chemistry*, Thompson Brooks/Cole, **2004**, 512.
[10] Hammond, C., *The Basics of Crystallography and Diffraction*, Oxford Science Publications, **1998**, 125.

The object of the crystallographic experiment is to measure intensities accurately for as many reflections as possible. This is followed by the refinement of the coordinates and vibrational parameters for all the atoms, to fit the observed structure amplitudes.

Three essential components are important in the XRD experiment, namely a source, a sample and a detector. The source of X-rays in the laboratory consists of a metal anode (either copper or molybdenum) that emits X-rays when irradiated with high-energy electrons. The monochromator selects radiation of the required wavelength (usually 1.542 Å for copper radiation and 0.711 Å for molybdenum sources). The sample consists of a single crystal with typical dimensions of 0.3 mm in each direction. The crystal is mounted on a goniometer head that ensures movement of the crystal so that all facets of the crystal may be irradiated. The recorder may either be a camera or a detector and counter.[10]

As mentioned above, the location of an atom as obtained from the data of an X-ray diffraction experiment is in actual fact the average of all positions it occupies. The structure is often presented in the form of thermal ellipsoids. These ellipsoids are indicators of the probability where the atoms are most likely to be. From these ellipsoids certain information regarding the atoms may be deduced. An egg-shaped ellipsoid suggests motion of the atom in a back and forth manner. A curling-stone shaped ellipsoid is indicative of a wobbling motion around the bond axis. The more rigid an atom is in place in a molecule, the smaller the thermal ellipsoid appears as is often seen for heavy metal atoms such as platinum.[11]

3.5.3 Structure Factor

The structure factor is a mathematical description of how material scatters incident radiation and is an important tool to interpret interference patterns from X-ray diffraction experiments. Two numerical values are associated with each reflection, namely the amplitude $|F(hkl)|$ and the phase Φ. Scattering from each atom in the unit cell should be added to obtain the resultant beam. The superposition takes the phase and amplitude of each reflection into account. Each *hkl* reflection can then be described by a structure factor; as in Eq. 3.8.[12]

---

[11] Huheey, J. E., Keiter, E. A., Keiter, R. L. *Inorganic Chemistry 4th edition*, Harper Collins College Publishers, **1993**, 233.
[12] Azaroff, L. V., *Elements of X-ray Crystallography*, McGraw-Hill, **1968**, 610.

$$F_{hkl} = |F_{hkl}|exp(i\Phi_{hkl}) = \sum_{j=1}^{N} f_j \, exp\left[i2\pi\left(hx_j + ky_j + lz_j\right)\right] \quad \text{(Eq. 3.8)}$$

N in the above equation reflects the number of atoms in the unit cell; index j is a numerical value from 1 to N; f_j is the atomic scattering factor of atom j at the respective Bragg angle; x_j, y_j and z_j are the fractional coordinates of atom j.

Eq. 3.8 illustrates that the structure factor magnitude depends on the relative disposition of the N atoms and the atomic scattering factors. Each term in the equation represents a wavelet that expresses the path length with amplitude f_j and phase $\Phi = 2\pi\left(hx_j + ky_j + lz_j\right)$. The structure factor becomes the result of wavelets scattered by N atoms in the unit cell. The equation can be rewritten as:

$$F_{hkl} = \sum_{j=1}^{N} f_j \left[cos2\pi\left(hx_j + ky_j + lz_j\right) + isin2\pi\left(hx_j + ky_j + lz_j\right)\right] \quad \text{(Eq. 3.9)}$$

The energy associated with the cosine wave is directly proportional to the square of the amplitude. The term, $I_0(hkl)$, where the subscript 0 denotes an experimentally observed quantity, is used in X-ray diffraction to represent $|F_{hkl}|^2$ as shown in Eq. 3.10. This forms the basis of X-ray structure analysis where the experimental quantities of $I_0(hkl)$ can be related to the structure factor through $|F_{hkl}|^2$.

$$I_0(hkl) \propto |F_{hkl}|^2 \quad \text{(Eq. 3.10)}$$

The aim of X-ray crystallography is to determine crystal structures. The crystal structure is represented by a map of electron density; $[\rho(x, y, z)]$, with the atoms located in these high electron density areas. It is known that the structure factor is related to intensity and as such only the phase is additionally needed to obtain a structure.

3.5.4 Phase Problem

In order to find the electron density at a point in the crystal structure all the individual scattered X-ray waves are added. To determine a structure, the amplitude as well as phase must be known. Methods have been developed to compensate for the missing information with regard to the phase, namely the Patterson function and direct methods. A third method called "Charge Flipping" exists, but is not very commonly used.

3.5.4.1 Patterson Synthesis

The Fourier transform of observed diffracted beam amplitudes $|F_0|$ gives the correct electron density, but the phases are required. By taking the Fourier transform of the squared observed amplitudes F_0^2 with all the phases set to zero gives the Patterson synthesis:[13]

$$P(xyz) = \frac{1}{V}\Sigma_{hkl}|F_0(hkl)|^2 \ exp\big(-2\pi i(hx + ky + lz)\big) \qquad \text{(Eq. 3.11)}$$

The Patterson map looks similar to an electron density map as it has peaks of positive intensity, however they do not represent the position of atoms in the structure. Rather it is a map of vectors between pairs of atoms in the structure. Thus for every peak in the Patterson map, at (u, v, and w) there must be two atoms whose:

- x coordinate differ by u
- y coordinate differ by v
- z coordinate differ by w

The Patterson map can be interpreted by taking the following into account:

i. Every atom forms a pair: There are N^2 vectors in the unit cell, where N are self-vectors (zero length at origin) and the coordinates (0, 0, 0) will be the largest vector on the map.

ii. The vector between atom A and B will be exactly equal and opposite to the vector between atom B and A implying thus that the Patterson map has an inversion centre.

iii. A considerable overlap of peaks often occurs, resulting in not all the peaks being resolved.

The most significant peaks seen on the map are often vectors between 'heavy atoms'. If a structure only has a few heavy atoms, the Patterson map will have a small number of large peaks showed prominently.[14]

---

[13] Rademeyer, M. (oral presentation), *School of Fundamental Crystallography*, Bloemfontein, date: 12-16 April 2010.
[14] Clegg, W., *Crystal Structure Determination*, Oxford University Press, **1998**, 34.

3.5.4.2 Direct Methods

Direct methods aim to obtain approximate reflection phases from the measured intensities by using constraints or statistical correlations between the phases of different Fourier components. In two dimensions it is relatively easy to solve the phase problem but in three dimensions it was the initiative taken by Hauptman and Karle, with the introduction of their general form of the triplet formula first described by Sayre in 1952, that resulted in a practical solution.[15] This formula is given as:

$$s(hkl) \approx \sum_{h'k'l'} s(h'k'l'). s(h - h', k - k', l - l')$$ (Eq. 3.12)

The various forms of direct methods are currently the methods of choice to solve the phase problem in structures containing small atoms. For structures containing heavy atoms such as metals from the transition series, the Patterson synthesis remains the popular choice.

3.5.5 Least-Squares Refinement

The least-squares refinement technique compares calculated diffraction patterns with observed ones. This enables a measurement of how the experimental data fits the calculated structure factor. This is known as a *residual index* or the *R-factor*[16]*:*

$$R = \frac{\sum \left| |F_0| - |F_c| \right|}{\sum |F_0|}$$ (Eq. 3.13)

An R-factor in the range of 0.05 indicates good correlation between the experimental data and the calculated data and the crystal structure solved. Another term, namely a weighting factor is also commonly used and incorporates information on the relative reliability of different measurements. This equation is given as:

$$wR^2 = \frac{\sum w \left(F_0^2 - F_c^2 \right)^2}{\sum w \left(F_0^2 \right)^2}$$ (Eq. 3.14)

3.6   Chemical Kinetics

Chemistry by its nature is concerned with change and kinetics focuses on the change from one substance to another under a specified set of conditions and more importantly

---

[15] Glusker, J. P., Trueblood, K. N., *Crystal Structure Analysis*, Oxford University Press, **2010**, 116.
[16] Stout, G. H., Jensen, L. H., *X-ray Structure Determination: A Practical Guide*, Macmillan Company, **1968**, 467.

the rate at which this change occurs. Chemical kinetics is a very important aspect in research as it has wide application for our modern day lives. It relates to how fast medicine becomes active in the body or the balance between ozone depletion and formation in the atmosphere. In industrial application chemical kinetics is of vital importance as it is used to analyze the effectiveness of catalysts.[17] An introduction to some of the most important terminology in the field of kinetics is discussed in the following text.

3.6.1 The Rate

The rate of a reaction is expressed in terms of either one of the reactants or one of the products. For the reaction given as:

$$aA + bB \ldots \rightarrow mM + nN \ldots \qquad \text{(Eq. 3.15)}$$

the reaction rate is related to the rate of disappearance and the rate of formation by the following:

$$Rate = -\left(\frac{1}{a}\right)\frac{d[A]}{dt} = -\left(\frac{1}{b}\right)\frac{d[B]}{dt} = \frac{1}{m}\frac{d[M]}{dt} = \frac{1}{n}\frac{d[N]}{dt} \qquad \text{(Eq. 3.16)}$$

Where $d[A]$ and $d[B]$ are the changes in concentration of reactants over a period of time and $d[C]$ refers to the increase in concentration of the product formed during the reaction. In practice the rate is often stated in terms of the species of which the concentration is being monitored during the reaction. The stoichiometry of the reaction will also have an effect on the rate as stated in the definition of the rate constant.

3.6.2 The Rate Law

The rate law is an experimentally determined dependence of the reaction on the concentrations of the reagents. A general form is often stated as:

$$Rate = k[A]^m[B]^n \ldots \qquad \text{(Eq. 3.17)}$$

In this equation, *k* represents the proportionality constant called the rate constant and the exponents *m* and *n* are determined experimentally in the kinetic study without having any relation to the stoichiometric coefficients in the balanced chemical reaction. The rate law

---

[17] Brown, T. L., LeMay, H. E., Bursten, B. E., *Chemistry: The Central Science 10th edition*, Prentice Hall, **2006**, 575.

often contains species that do not appear in the balanced equation as it is a sum of several terms for different reaction pathways. Representing the concentrations of the species needed to complete the reaction by the lowest energy pathway, the rate law is an important piece of mechanistic information for the reaction.[18]

3.6.3 Order of the Rate Law

By taking the sum of the exponents m and n, as stated in Eq. 3.17, the order of the rate law can be determined. If $m=1$ and $n=-2$ an overall order of -1 can be described. In simple cases the order can be described with respect to individual reagents stating that the reaction is first order in $[A]$ and inverse second-order in $[B]$.

3.6.4 Pseudo First-order Reactions

The rate constant, k, is unique for each reaction and is independent of the concentrations of the reagents or the products formed in the reaction. However, the order of the reaction is dependent on change in concentration of one or both reactants. As these values are difficult to determine experimentally, conditions to simulate first order conditions are employed. This is called pseudo first-order conditions and typically involves one of the reactants to be in excess of the other reactant in at least a tenfold magnitude. This implies that the concentration of one of the reactants will remain constant whilst the other will vary, thus:

$$[B] \gg [A]$$

The rate equation can now be stated as:

$$Rate = k_{obs}[A]^m \ and \ then \ k_{obs} = k[B]^n \qquad \text{(Eq. 3.18)}$$

where k_{obs} refers to the observed pseudo-first order rate constant observed experimentally. Variation of the concentration of B will lead to the determination of the rate constant, k. A pseudo-first order equilibrium reaction can be given as:

$$a[A] + b[B] \underset{k_2}{\overset{k_1}{\rightleftharpoons}} m[M] \qquad \text{(Eq. 3.19)}$$

---

[18] Jordan, R. B., *Reaction Mechanisms of Inorganic and Organometallic Systems*, Oxford University Press, **1991**, 2.

The new rate law becomes:

$$Rate = k_1[A][B] + k_2[A] \qquad \text{(Eq. 3.20)}$$

For pseudo first-order conditions, k_{obs} can be given as follows:

$$k_{obs} = k_1[B] - k_2 \qquad \text{(Eq. 3.21)}$$

In the above reactions, k_1 represents the forward reaction and k_2 the reverse reaction. The equilibrium constant can now be calculated as:

$$K_{eq} = {k_1}/{k_2} \qquad \text{(Eq. 3.22)}$$

Integration of the initial rate equation from t= 0 to t yields the following:

$$ln\frac{[M]_t}{[M]_0} = -k_{obs}t \quad or \quad [M]_t = [M]_0 e^{-k_{obs}t} \qquad \text{(Eq. 3.23)}$$

The terms $[M]_t$ and $[M]_0$ refer to the concentration of the product at time = t and 0 respectively. As mentioned in Section 3.4 the Beer-Lambert law can be successfully used in chemical kinetic studies as concentration can be related to absorbance. The following equation to relate absorbance and k_{obs} is therefore obtained:

$$A_{obs} = A_\infty - (A_\infty - A_0)e^{-k_{obs}t} \qquad \text{(Eq. 3.24)}$$

In the above equation, A_0 is the initial absorbance and A_∞ is the absorbance at infinite time. This forms the basis for studying chemical kinetics as absorbance data can be collected in the laboratory and by using Eq. 3.24, it can be related to the observed rate constant for a reaction.

Chapter 4: Synthesis of [VO(L,L⁻-Bid)ₙ] Complexes

4.1 Introduction

The synthesis and characterization of vanadium(IV) and vanadium(V) complexes are discussed in this chapter. The characterization performed on the mentioned compounds utilized techniques such as IR, NMR, single crystal X-ray diffraction studies and elemental analysis where applicable. The reader is referred to Chapter 3 for the theory and principles of these techniques.

The ligands chosen for coordination with vanadium contained O,O^- and N,O^- donor functionalities (in general indicated by L,L'-Bid) as the strong Lewis acidity of vanadium favours these donor groups. Additionally, one of the goals of this project was to investigate compounds with these functionalities as they hold potential for biological activity and as industrial catalysts such as the Amavadine catalyst used in methane conversion (see Section 1.2.2 of Chapter 1).

4.2 Chemicals and Apparatus

All reagents used for the synthesis and characterization of vanadium complexes were of analytical grade and obtained from Sigma-Aldrich, South Africa, and used as purchased.

All infrared spectra of synthesized complexes were recorded on a Bruker Tensor 27 Standard System spectrophotometer with a laser range of $4000 - 370$ cm^{-1}. NMR spectroscopic data were obtained on a Bruker Avance II 600 MHz spectrometer. Chemical shifts are reported in ppm and given relative to TMS for ^{1}H NMR spectra. ^{51}V NMR spectra were referenced externally to a saturated solution of sodium orthovanadate which has two active species in solution at pH 12, namely $[VO_4]^{3-}$ (δ= -535.7 relative to $VOCl_3$) and $[V_2O_7]^{4-}$ (δ= -559.0)[1], $NaVO_3$ (δ= -578)[2] or KVO_3 (δ= -576)[2]. All UV/Vis spectra were recorded using a Varian Cary 50 Conc UV-Visible spectrophotometer

[1] Rehder, D., Hoch, M., Jameson, C. J*., Magn. Reson. Chem.*, **1990**, *28*, 128.
[2] Han, O. H., Kim, S., Lee, S. G., Kwon, Y., *Journal of Non-Crystalline Solids*, **2005**, *351*, 3365.

equipped with a Julabo F12-mV temperature cell regulator (accurate within 0.1 °C) in a 1.000 ± 0.001 cm quartz cuvette cell.

4.3 Synthesis of Compounds with *O,O* Functionalities

4.3.1 Synthesis of [VO(acac)$_2$]
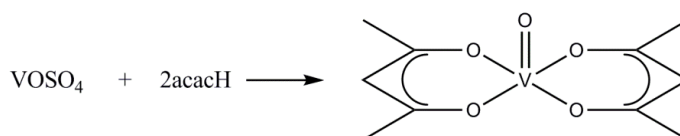
Scheme 4.1: Schematic representation of the synthesis of [VO(acac)$_2$].

A solution of anhydrous Na$_2$CO$_3$ (2.0 g, 19 mmol) and 2 cm^3 of acetylacetone was prepared. A solution of vanadyl sulfate (2.1 g, 12 mmol) was prepared by dissolving the solid in warm water taking care to not heat the mixture above 60 °C as this would lead to decomposition of the VOSO$_4$. The dissolved vanadyl sulfate solution was added to the solution of acetylacetone and stirred for 30 minutes. The formation of a dark green-blue precipitate was observed and the reaction mixture was cooled in an ice bath. The product was filtered and washed with one portion of cold water and two portions of ethanol. The precipitate was recrystallized by dissolving the precipitate in a minimum amount of hot chloroform and adding a layer of diethyl ether. Small blue-green needle-like crystals were collected as product. (**Yield**: 1.9 g, 61 %)

^{1}H and ^{13}C NMR: The vanadium(IV) compound is paramagnetic and could not be analyzed by NMR (see Section 2.6.1 in Chapter 2).

IR (ATR) ν (cm^{-1}): 788, 990 (V=O), 1516.

UV/Vis: λ_{max}= 580 nm, ε= 452 cm^{-1}.M^{-1}; 775 nm, ε= 360 cm^{-1}.M^{-1}

4.3.2 Synthesis of [VO(acac)$_2$L] complexes

Several [VO(acac)$_2$L] complexes have been reported in literature[3] with a nitrogen donor ligand expected to coordinate in an axial position *trans* to the oxo bond in the compound. Scheme 4.2 illustrates the nitrogen ligands chosen to fill the sixth coordinating position of vanadium.
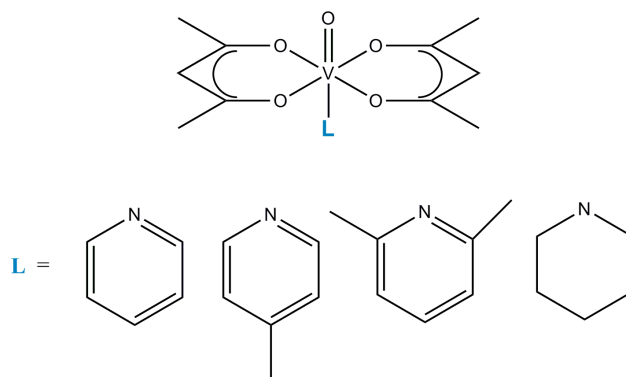
Scheme 4.2: Nitrogen ligands chosen to coordinate axially to the V=O bond in the synthesized [VO(acac)$_2$] complex.

The two methods that were employed for these reactions are given as:

4.3.2.1 Method 1

[VO(acac)$_2$] (20 mg, 0.15 mmol) was mixed with a small portion of the nitrogen ligand (pyridine, 3-methylpyridine, 2,6-lutidine, piperidine) and heated slowly in a watch glass until all the liquid had been evaporated. The product was collected as green solids for all of the tested complexes.

IR (ATR) v (cm^{-1}) for the 2,6-lutidine complex: 788, 991 (V=O), 1517.

From the IR spectra obtained for these products a conclusion was made that this method was not effective and the collected product was merely [VO(acac)$_2$] (990 cm^{-1}) used as starting material.

4.3.2.2 Method 2

The second method employed for these compounds was more time consuming but produced interesting results.

---

[3] Isobe, K., Nakamura, Y., Kawaguchi, S., *J. Inorg. Nucl. Chem.*, **1978**, *40*, 607.

[VO(acac)$_2$] (0.52 g, 1.89 mmol) was dissolved in 20 cm^3 of the different nitrogen ligands and left to evaporate at room temperature as well as 4 °C. A surprising product was isolated from this experiment as the decavanadate compound reported in literature.[4] It was postulated that this product was a decomposition product due to oxidation.

IR (ATR) ν (cm^{-1}): 930 (V=O), 1373, 1515.

In the following procedures various O,O bidentate ligands that resemble the 'acac' backbone were coordinated to vanadium(IV) centres to yield either vanadium(IV) or vanadium(V) compounds.

4.3.3 Synthesis of [VO(thtfac)$_2$] using VOSO$_4$
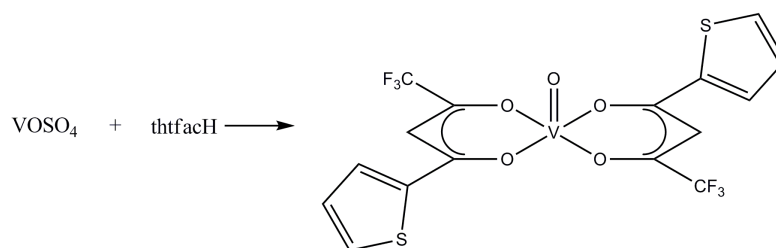
Scheme 4.3: Schematic representation of the synthesis of [VO(thtfac)$_2$] using VOSO$_4$.

VOSO$_4$ (0.22 g, 1.19 mmol) and thenoyltrifluoroacetone (0.35 g, 1.35 mmol) were dissolved in 15 cm^3 of methanol and refluxed for three hours. After the elapsed time the reaction mixture was filtered and the filtrate used for various crystallization attempts. A yellow-brown powder was collected as product. (Yield: 0.27 g, 45 %)

^{1}H and ^{13}C NMR: The vanadium(IV) compound is paramagnetic and could not be analyzed by NMR.

IR (ATR) ν (cm^{-1}): 890 (V=O), 1141, 1293.

UV/Vis: λ_{max}= 503 nm, ε= 512 cm^{-1}.M^{-1}

Elemental analysis: calculated: %C: 37.7, %H: 1.62; found: %C: 38.5, %H: 2.55.

---

[4] Arrieta, J. M., *Polyhedron*, **1992**, *11*, 3045.

4.3.4 Synthesis of [VO(thtfac)₂] using [VO(acac)₂]
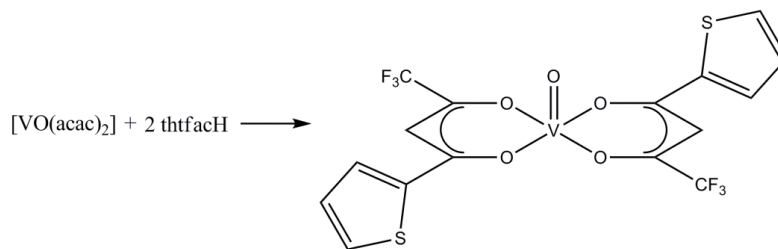
Scheme 4.4: Schematic representation of the synthesis of [VO(thtfac)₂] using [VO(acac)₂].

The same complex as described in Section 4.3.3 was attempted in this synthesis by using [VO(acac)₂] as starting material. As was mentioned in Section 2.7.2 the 'acac' method of synthesis is particularly effective as the oxygen-metal bonds are easily broken and replaced by stronger substituting ligands.

[VO(acac)₂] (0.52 g, 1.89 mmol) was dissolved in 40 cm^3 methanol after which thenoyltrifluoroacetone (0.9 g, 4.0 mmol) was added to the reaction mixture and refluxed for three hours. A yellow-brown precipitate was collected as product and the filtrate was used for crystallization. The combination of methanol and pentane in a diffusion technique yielded crystals suitable for XRD analysis and the final product was identified as a polymeric structure of the predicted product structure. A polymeric chain is formed through the oxido groups with both diketonato ligands coordinated to each vanadium centre in the chain in the equatorial plane. This procedure was performed with the same quantities, using acetone as solvent and yielding the same product as confirmed by IR. (Yield: 0.69 g, 72 %)

^{1}H and ^{13}C NMR: The vanadium(IV) compound is paramagnetic and could not be analyzed by NMR.

IR (ATR) ν (cm^{-1}) reaction in methanol: 1139 (V=O).

IR (ATR) ν (cm^{-1}) reaction in acetone: 1143 (V=O).

UV/Vis: λ_{max}= 503 nm, ε= 512 cm^{-1}.M^{-1}

4.3.5 Synthesis of [VO(dbm)₂] and [VO(dbm)₂L]

$VOSO_4$ + 2 dbmH ⟶
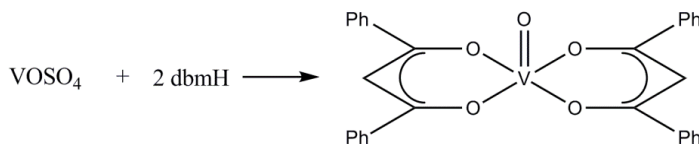
Scheme 4.5: Schematic representation of the synthesis of [VO(dbm)₂].

4.3.5.1 Method 1

The synthesis of Meštrović et al.[5] was followed.

V_2O_5 (1.1 g, 5.5 mmol) was added to a mixture of 5 cm^3 ethanol, 2 cm^3 water and 2 cm^3 sulfuric acid and refluxed for one hour. It was observed that the yellow mixture had turned to a brilliant blue colour after the allocated time. A solution of 1,3-diphenyl-1,3-propanedione (4.93 g, 22 mmol) in ethanol was added to the reaction mixture and stirred. A saturated solution of sodium carbonate (20 cm^3) was added to the mixture and the resulting green precipitate was collected by filtration. Crystals of adequate quality for XRD analysis was obtained by dissolving the precipitate in chloroform and leaving the solution to evaporate at room temperature over a period of three days. (Yield: 2.1 g, 78 %)

When dissolving the precipitate in methanol and left to evaporate the result was the formation of dark red crystals that was analyzed by single crystal X-ray diffraction as [VO(dbm)₂(MeOH)]•2MeOH. (Yield: 0.33 g, 27 %)

Elemental analysis: calculated: %C: 65, %H: 5.62; found: %C: 67, %H: 5.03.

4.3.5.2 Method 2

Another synthetic procedure for this compound has been reported in literature and was additionally tested in an attempt to improve the yield obtained from the previous method. The procedure was suggested by Grdenić *et al.*[6] in 1964. [VO(acac)₂] (0.5 g, 1.89 mmol) was refluxed with 1,3-diphenyl-1,3-propanedione (1.2 g, 5.4 mmol) in 30 cm^3 of toluene

---

[5] Meštrović, E., Bučar, D., K., Halasz, I., Stilinović, V., *Acta Cryst.*, **2004**, *E60*, m1920.
[6] Grdenić, D., Korpar-Čolig, b., *Inorg. Chem.*, **1964**, *3*, 1328.

for 2 hours. The original procedure used benzene as solvent but due to safety hazards[7] it was replaced by toluene for this experiment. The dark green solution was then left to stand for crystallization. Green crystals were observed to have formed after 4 weeks. (Yield: 0.62 g, 70 %)

^{1}H and ^{13}C NMR: The vanadium(IV) compound is paramagnetic and could not be analyzed by NMR.

IR (ATR) ν (cm^{-1}): 943 (V=O), 1069, 1364, 1519.

UV/Vis: λ_{max}= 679 nm, ε= 385 cm^{-1}.M^{-1}

The complex of the title compound, [VO(dbm)$_2$], with pyridine was prepared by dissolving a portion of the green precipitate collected from the synthesis of [VO(dbm)$_2$] in pyridine and allowing the pyridine to evaporate over a period of three weeks. This resulted in the formation of orange crystals, confirmed by XRD analysis to be [VO(dbm)$_2$py].

IR (ATR) ν (cm^{-1}): 949 (V=O), 1369, 1516.

4.3.6 Synthesis of [VO(trop)$_2$]
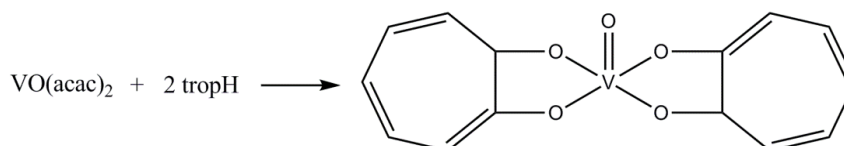
Scheme 4.6: Schematic representation of the synthesis of [VO(trop)$_2$].

The 'acac' method of synthesis was employed in the preparation of this compound. [VO(acac)$_2$] (0.52 g, 1.89 mmol) was dissolved in 40 cm^3 methanol after which tropolone (0.48 g, 3.90 mmol) was added to the reaction mixture and refluxed for a period of three hours. After the elapsed time the mixture was filtered hot and the precipitate dried for analysis (Yield: 0.37 g, 58 %).

The dark-red coloured filtrate was used in combination with various solvents for crystallization purposes. Although crystals were successfully obtained from combinations of the methanol filtrate with chloroform and octane, no high angle reflections could be observed in a single crystal X-ray diffraction study. For that reason the reaction was

---

[7] Benzene Material Safety Data Sheet, http://www.sigmaaldrich.com/catalog/DisplayMSDSContent.do, accessed: 29-11-2011.

repeated in acetone, water and DMF. The reaction in acetone yielded the same product as confirmed by IR and NMR. For this species to be NMR active it would have to be in the +5 oxidation state. Therefore it was postulated that a methoxy group coordinated to the vanadium centre and the presence of such a group was confirmed by NMR analysis.

^{1}H (600 MHz, CDCl$_3$) δ 7.57 (t, 2H, J = 12 Hz), 7.36 (d, 2H, J = 9 Hz), 7.17 (t, 1H, J = 9.7 Hz), 1.5 (s, 3H).

^{51}V NMR (158 MHz, DMSO-d$_6$) δ -460.

IR (ATR) ν (cm^{-1}) reaction in methanol: 717, 944 (V=O), 1313, 1412.

UV/Vis: λ$_{max}$= 683 nm, ε= 373 cm^{-1}.M^{-1}

As with the previous compounds synthesized, nitrogen ligands were chosen to coordinate to the synthesized compound. Pyridine and 3-methylpyridine were chosen in this case. [VO(trop)$_2$] (0.21 g, 0.97 mmol) was dissolved in either pyridine or 3-methylpyridine and left at room temperature for a period of 4 weeks. No pure product could be isolated from the oily residue that had formed.

4.3.7 Synthesis of [VO(cupf)$_2$]
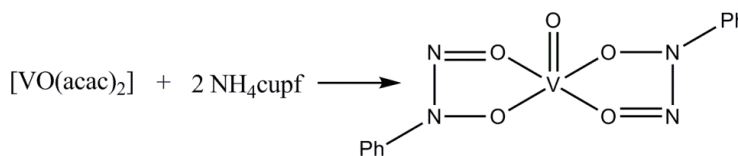
Scheme 4.7: Schematic representation of the synthesis of [VO(cupf)$_2$].

Again, the 'acac' method of synthesis was employed successfully to yield a new compound. [VO(acac)$_2$] (0.52 g, 1.89 mmol) was dissolved in 40 cm^3 of acetone after which cupferron (0.58 g, 3.70 mmol) was added. The reaction mixture was then stirred for a period of 24 hours. A yellow-green precipitate was filtered and dried. Dissolving the precipitate in methanol yielded a deep orange coloured solution and after keeping the solution at 4 °C for a period of two weeks, orange needle-like crystals suitable for XRD analysis were observed to have formed. (Yield: 0.51 g, 52 %)

^{1}H (600 MHz, DMSO-d$_6$) δ 7.85 (s, 3H), 7.55 (s, 5H), 3.42 (s, 12H), 2.08 (s, 1H), 1.39 (s, 10H).

^{13}C (151 MHz, DMSO-d$_6$) δ 204.9, 139.1, 129.7, 129.6, 118.8, 58.6, 49.9, 30.87, 27.7.

^{51}V NMR (158 MHz, DMSO-d$_6$) δ -478.

IR (ATR) ν (cm^{-1}): 750, 850, 941 (V=O), 901 (V=O), 1285.

UV/Vis: λ_{max}= 691 nm, ε= 375 cm^{-1}.M^{-1}

Elemental analysis: calculated: %C: 49.1, %H: 5.29, %N: 10.89; found: %C: 49.1, %H: 5.62, %N: 13.3.

From the crystal structure it was established that the product was in fact an anionic vanadium compound with a novel organic counter-ion formed during the reaction. The formed product is illustrated in Scheme 4.8.
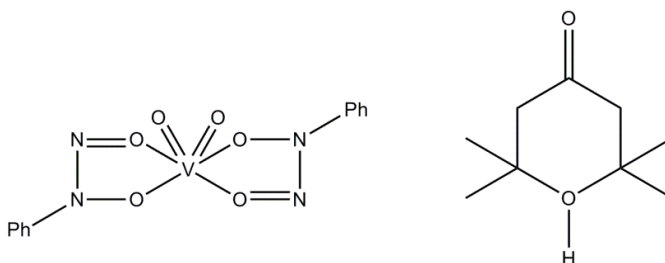
Scheme 4.8: Anionic vanadium(V) compound with novel organic cation isolated as product.

4.3.8 Synthesis of K$_4$[V$_2$O$_2$(C$_6$H$_4$O$_7$)$_2$]•6H$_2$O
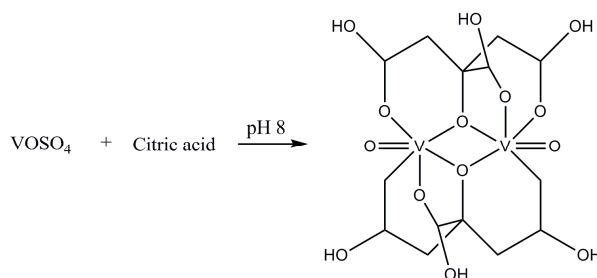
Scheme 4.9: Schematic representation of the synthesis of K$_4$[V$_2$O$_2$(C$_6$H$_4$O$_7$)$_2$]•6H$_2$O.

The procedure used in this synthesis was adapted from the procedure by Tsaramyrsi *et al*.[8] for the synthesis of K$_4$[V$_2$O$_2$(C$_6$H$_4$O$_7$)$_2$]•6H$_2$O. VOSO$_4$ (0.10 g, 0.58 mmol) was dissolved in 5 cm^3 water with citric acid (0.11 g, 0.58 mmol). The pH was subsequently adjusted to pH 10 with 0.4 M NaOH. The blue-purple reaction mixture was stirred for 24 hours after which the solvent was evaporated and the blue residue redissolved in 2 x distilled water and 2-propanol. The solution was kept at 4 °C and after five days a blue crystalline product was observed to have formed. (Yield: ca.0.15 g, 50 %)

---

[8] Tsaramyrsi, M., Kaliva, M., Salifoglou, A., *Inorg. Chem.*, **2001**, *40*, 5772.

¹H and ¹³C NMR: The vanadium(IV) compound is paramagnetic and could not be analyzed by NMR.

IR (ATR) ν (cm⁻¹): 958 (V=O), 1375, 1582, 3420 (O-H).

UV/Vis: λ_{max}= 567 nm, ε= 360 cm⁻¹.M⁻¹

4.4   Synthesis of Compounds with *N,O* Functionalities

4.4.1   Synthesis of [VO(Ox)₂]
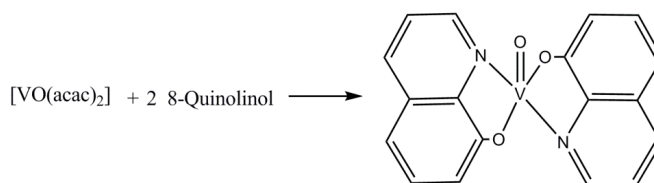
Scheme 4.10: Schematic representation of the synthesis of [VO(Ox)₂].

[VO(acac)₂] (0.52 g, 1.89 mmol) was refluxed with 8-hydroxyquinoline (0.60 g, 3.80 mmol) in 40 cm³ methanol for five hours. The hot reaction mixture was then filtered and the precipitate used for crystallization to obtain the title compound in a pure form. Crystallization from chloroform yielded crystals of adequate quality to be collected on the XRD for structural analysis. This, together with NMR and IR analysis led to positive identification of the title compound with the added sixth coordinating ligand showed to be a methoxy group thought to originate from the methanol solvent used during the experimental procedure. (Yield: 0.52 g, 68 %)

¹H (600 MHz, CDCl₃) δ 8.52 (d, 1H, *J* = 5.1 Hz), 8.36 (d, 1H, *J* = 4.3), 8.16 (d, 1H, *J* = 8.6), 8.12 – 8.05 (m, 1H), 7.61 (dt, 1H, *J* = 13.1, 8.8), 7.46 (d, 1H, *J* = 7.3), 7.30 (dd, 1H, *J* = 8.7, 4.6), 5.55 (s, 1H), 3.47 (s, 1H), 2.15 (s, 1H), 1.54 (s, 3H).

¹³C (151 MHz, CDCl₃) δ 147.7, 146.9, 139.9, 137.8, 133.2, 131.1, 128.2, 124.1, 123.2, 122.5, 115.9, 112.6, 112.5, 109.6, 31.2, 31.1.

⁵¹V NMR (158 MHz, DMSO-d₆) δ -504.

IR (ATR) ν (cm⁻¹): 739, 959 (V=O), 1103.

UV/Vis: λ_{max}= 493 nm, ε= 523 cm⁻¹.M⁻¹

4.4.2 Synthesis of [VO(acac)(pic)]
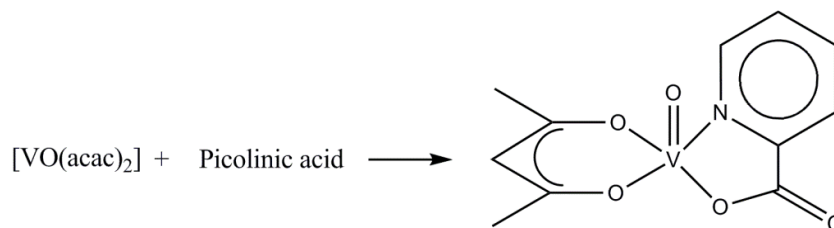
Scheme 4.11: Schematic representation of the synthesis of [VO(acac)(pic)].

[VO(acac)$_2$] (0.52 g, 1.89 mmol) was added to a solution of picolinic acid (0.27 g, 2.2 mmol) in 40 cm^3 of acetone and refluxed for 3 hours, after which the reaction mixture was kept at -20 °C. No crystalline product could be produced from the dark blue solution, but a light green precipitate was isolated. (Yield = 0.14 g, 26 %)

^{1}H and ^{13}C NMR: The vanadium(IV) compound is paramagnetic and could not be analyzed by NMR.

IR (ATR) ν (cm^{-1}): 691, 760, 962 (V=O), 1411, 1589.

4.4.3 Synthesis of [VO(acac)(2,3-dipic)]
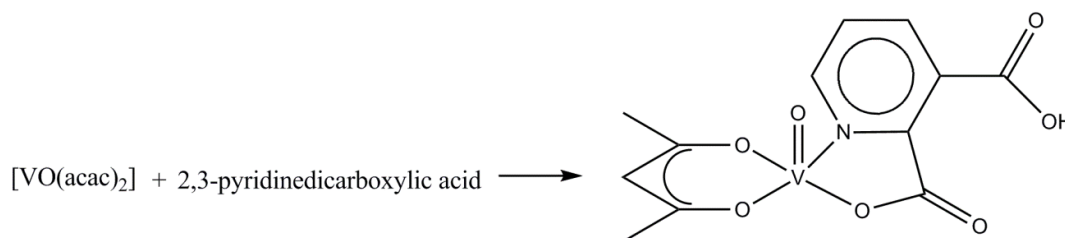
Scheme 4.12: Schematic representation of the synthesis of [VO(acac)(2,3-dipic)].

[VO(acac)$_2$] (0.52 g, 1.89 mmol) was refluxed with 2,3-pyridinedicarboxylic acid (0.35, 2.1 mmol) in 30 cm^3 of methanol for three hours. The solution was cooled and then kept at -20 °C. After a period of two weeks unstable blue-green crystals were observed to have formed and were suitable to be analyzed by XRD. (Yield = 0.19 g, 30 %)

^{1}H and ^{13}C NMR: The vanadium(IV) compound is paramagnetic and could not be analyzed by NMR.

IR (ATR) ν (cm^{-1}): 744, 897 (V=O), 1350, 1601.

The XRD results indicated a compound in which one acetylacetonato ligand and one 2,3-pyridinedicarboxylato ligand had coordinated to the vanadium centre with a *N,O* coordination as shown in Scheme 4.12.

4.4.4 Attempted Synthesis of a 2-aminophenol Complex with Vanadium

[VO(acac)$_2$]   +   2-Aminophenol   ⟶
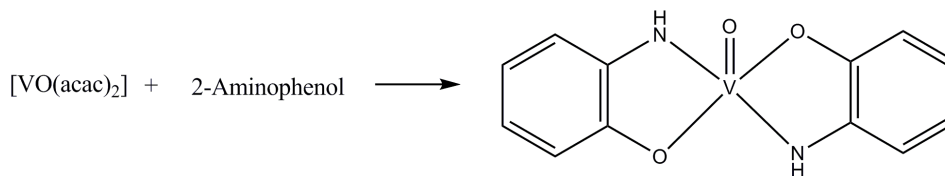
Scheme 4.13: Schematic representation of the synthesis of a vanadium complex with 2-aminophenol.

[VO(acac)$_2$] (0.52 g, 1.89 mmol) was refluxed with 2-aminophenol (0.25 g, 2.30 mmol) in 40 cm^3 of methanol for five hours. A sparingly soluble black product was isolated from the reaction mixture. The reaction was then repeated using acetone as solvent yielding the same black solid as product. No crystals could be obtained for this product.

^{1}H and ^{13}C NMR: The vanadium(IV) compound is paramagnetic and could not be analyzed by NMR.

IR (ATR) ν (cm^{-1}): 958 (V=O), 1587, 3412.

UV/Vis: λ_{max}= 428 nm, ε= 583 cm^{-1}.M^{-1}

4.5 Discussion

The synthesis of different vanadium compounds in the +4 and +5 oxidation states with O,O^- and N,O^- donor ligands were relatively simple. The use of [VO(acac)$_2$] as starting material was preferred over the use of VOSO$_4$ as more organic solvents such as methanol, acetone and chloroform could be utilized. Additionally, VOSO$_4$ was noted to decompose at temperatures above 60 °C and as such refluxing conditions could not easily be used for the procedures if VOSO$_4$ was used as starting material.

Much debate exists within literature with regard to the synthesis of vanadium(IV) compounds under aerobic conditions as lower oxidation states of vanadium tend to undergo air-oxidation to vanadium(V).[9] During this project a range of vanadium(IV) compounds were successfully synthesized in the presence of oxygen.

---

[9] Cornelis, R., Caruso, J., Crews, H., Heumann, K., *Handbook of Elemental Speciation II- Species in the Environment, Food, Medicine and Occupational Health*, Wiley & Sons, **2005**, 466.

It is known from literature that a simple inter-conversion between vanadium (IV) and (V) oxidation states exists.[10] Vanadate (+5), under some conditions, acts as oxidizing agent and is readily reduced to vanadium(IV) or (III) with production of an oxidized product. In neutral and basic pH ranges, air oxidation will quickly regenerate vanadate unless the vanadium(IV) is strongly bound to good stabilizing ligands. The appropriate reducing agents could maintain the vanadium(IV) oxidation state and extend stability to these complexes. It has been shown that free aqueous vanadium(IV) in the form of vanadyl is stable to air oxidation only under acidic conditions.[10] Thus, manipulation of conditions could assist in yielding products of a chosen oxidation state.

For the synthesized $(C_9H_{17}O_2)[VO_2(cupf)_2]$ complex it was mentioned that a novel organic counter ion was determined in the structure by single crystal X-ray diffraction. As the reaction was performed in acetone it was suggested that this compound was formed from the acetone present in excess during the reaction. It is postulated that an acid catalyzed self-condensation of three acetone molecules results in the formation of 2,2,6,6-tetramethyldihydropyran-4-onium. The mechanism proposed for this reaction is given in Scheme 4.14. In support of this mechanism is the compound isophorone that is commercially sold as solvent with a similar structure as 2,2,6,6-tetramethyldihydropyran-4-onium. It is known that isophorone is produced by the base catalyzed self-condensation of acetone.[11] Alternatively, the vanadium could assist in facilitating the reaction as vanadium is well known as catalyst in condensation reactions.[12]

---

[10] Crans, D. C., Tracey, A. S., *ACS Symposium Series*, **1998**, *711*, 2.

[11] Teissier, R., Kervennal, J., *Production of Isophorone and Related Products*, **US Patent nr: US2399976**, filed January 28, 1943, and issued May 7, 1946.

[12] Sabitha, G., Reddy, G. S. K. K., Reddy, K. B., Yadav, J. S., *Tetrahedron Lett.*, **2003**, *44*, 6497.
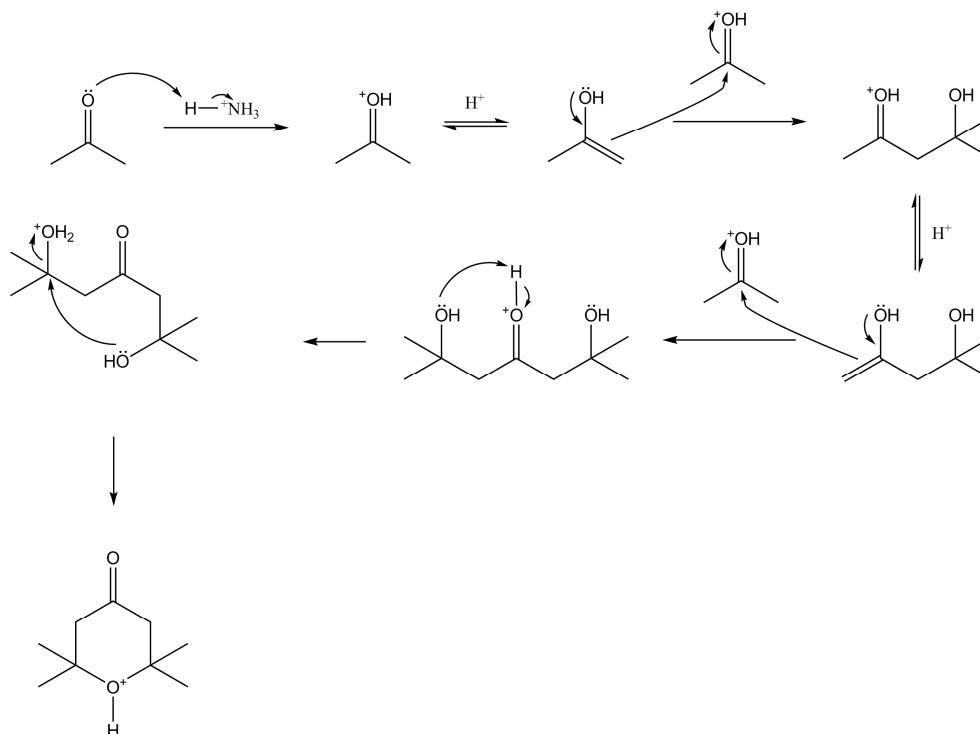
Scheme 4.14: Proposed mechanism for the formation of 2,2,6,6-tetramethyldihydropyran-4-onium *via* acid catalyzed self-condensation of acetone.

The IR spectra recorded for the synthesized products provided valuable insight into the coordination of the ligands to the vanadium metal centre. The very well known V=O bond has a characterisitc IR stretching frequency in the region of ~ 900 cm⁻¹.[13] As this bond was present in all the synthesized products, evaluating these V=O stretching frequencies were of significant importance as this would shed light on the strength of the other ligands coordinated to the vanadium centre.

The oxido bond (V=O) in the complexes is classified as a multiple covalent bond formed by the donation of p_π electrons of oxygen to the d_π orbitals of vanadium, superimposed upon the sigma bond. The amount of $p_\pi - d_\pi$ donation is dependent upon the tendency of oxygen to donate and the ability of vanadium to accept electrons. The donor capacity of oxygen is not expected to change appreciably by coordination of different ligands to the vanadium centre. However, the acceptor ability of vanadium with a lone *d*-electron in the case of vanadium(IV) compounds should be grealty affected. The coordinated ligands, which donate their electron pairs will increase the electron density in the metal *d*-orbitals

---

[13] Barnwell, C. N., *Fundamentals of Molecular Spectroscopy 3ʳᵈ edition*, McGraw Hill Book Company, **1983**, 72.

and consequently the $p_\pi - d_\pi$ donation from the oxygen to vanadium will be reduced depending upon the donor ability of the ligands. As a result the V=O bond order will be lowered and as such the V=O stretching frequency.

Table 4.1 gives the V=O bond stretching frequencies of the vanadium compounds synthesized for this study and of selected compounds from literature.

Additionally, a comparison may be made between the different V=O stretching frequencies of 5-coordinated complexes, 6-coordinated complexes and lastly the three compounds containing dioxido bonds. This is illustrated in Figures 4.1, 4.2 and 4.3. It is clear from these graphs that not only does the number of coordinated ligands have an effect on the V=O stretching frequency but also the type of ligand chosen.

As an example from Figure 4.1 a comparison may be made between the ligands of acetylacetonato (acac) and 1,3-diphenylpropane-1,3-dionato (dbm). The 1,3-diphenylpropane-1,3-dionato ligand is less electron-donating than the acetylacetonato ligand and consequently the V=O bond is stronger with acetylacetonato ligands coordinated to the vanadium centre. This implies a higher stretching frequency for the V=O bond within the [VO(acac)$_2$] complex (990 cm^{-1}) than the reported band for [VO(dbm)$_2$] (943 cm^{-1}).

Table 4.1: $\nu_{v=o}$ frequencies of vanadium(IV) and vanadium(V) compounds synthesized in this study as well as comparable complexes found in literature (py = pyridine,   MeOH = methanol, OMe = methoxy).

Compound	$\nu_{(V=O)}$ (cm^{-1})	Reference
O,O donor ligands		
[VO(acac)$_2$]	990	*a*
[VO(acac)$_2$py]	930	*a*
[VO(thtfac)$_2$]$_x$	890	*a*
[VO(dbm)$_2$]	943	*a*
[VO(dbm)$_2$py]	949	*a*
[VO(trop)$_2$(OMe)]	944	*a*
(C$_9$H$_{17}$O$_2$)[VO$_2$(cupf)$_2$]	901, 941	*a*
[VO(ox)(H$_2$O)$_2$]	986	*b*
[VO(malon)(H$_2$O)$_2$]·2H$_2$O	990	*b*
[VO(ttfacac)$_2$]	995	*c*
[VO(bza)$_2$]	995	*c*
N,O donor ligands		
[VO(Ox)$_2$(OMe)]	959	*a*
[VO(acac)(pic)]	962	*a*
[VO(acac)(quin)(OMe)]	897	*a*
[VO$_2$(pca)$_2$]⁻	862, 873	*d*
[VO$_2$(ana)$_2$]⁻	825, 875	*d*

a Compounds synthesized in this MSc study ; *b* synthesized by Sathyanarayana and Patel[14] ;
c synthesized by Aliyu and Mustapha[15] ; *d* synthesized by Süss-Fink *et al.*[16]

[**(acac)** = acetylacetonato, **(thtfac)** = thenoyltrifluoroacetonato, **(dbm)** = dibenzoylmethanato, **(trop)** = tropolonato, **(cupf)** = cupferrato, **(ox)** = oxalate, **(malon)** = malonate,
(ttfacac) = 2-thinoyltrifluoroacetonato, **(bza)** = benzoylacetonato, **(Ox)** = 8-hydroxyquinolinato,
(pic) = 2-pyridinecarboxylato, **(quin)** = 2,4-quinolinedicarboxylato, **(pca)** = pyrazine-2-carboxylato, **(ana)** = 2-aminobenzonato]

[14] Sathyanarayana, D. N., Patel, C. C., *J. Inorg. Nucl. Chem.*, **1968**, *30*, 207.
[15] Aliyu, H. N., Mustapha, A., *African Scientist*, **2009**, *10*, 123.
[16] Süss-Fink, G., Stanislas, S., Shul'pin, G. B., Nizova, G. V., Stoeckli-Evans, H., Neels, A., Bobillier, C., Claude, S., *J. Chem. Soc., Dalton Trans.*, **1999**, 3169.
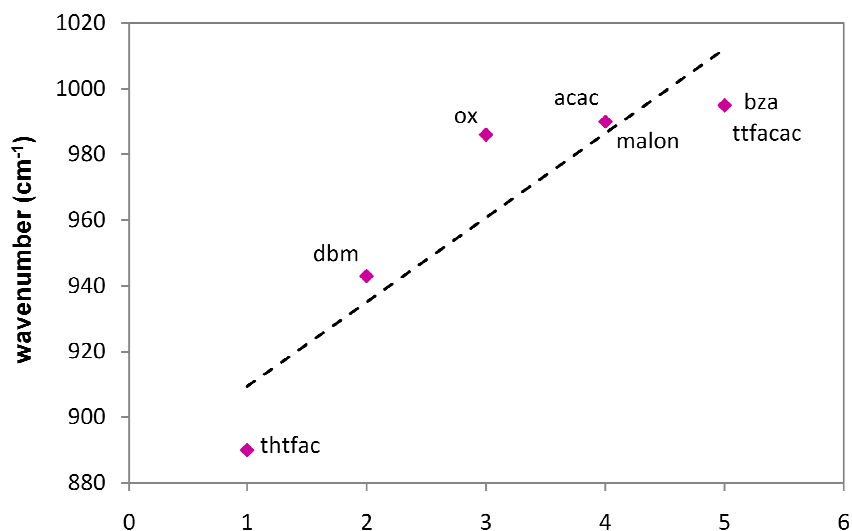
Figure 4.1: Illustration of the effect that ligand choice exhibits in V=O stretching frequencies observed for all the 5-coordinated species listed in Table 4.1.
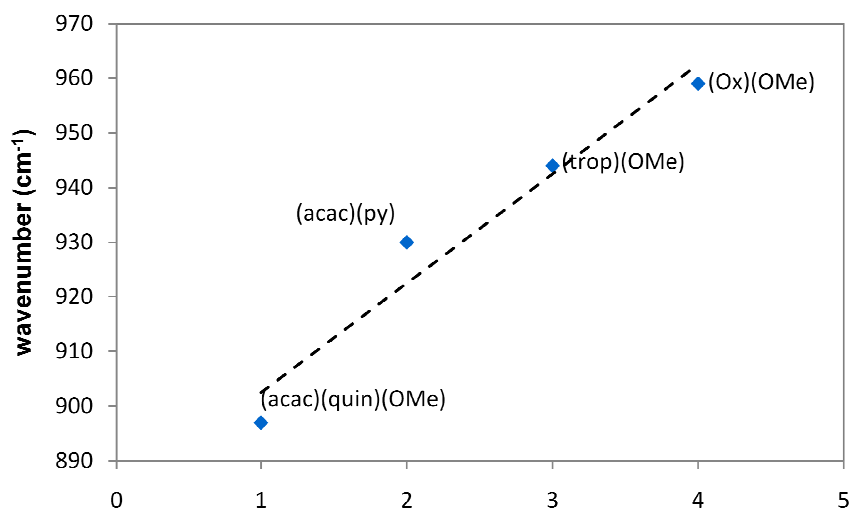
Figure 4.2: Illustration of the effect that ligand choice exhibits in V=O stretching frequencies observed for all the 6-coordinated species listed in Table 4.1.
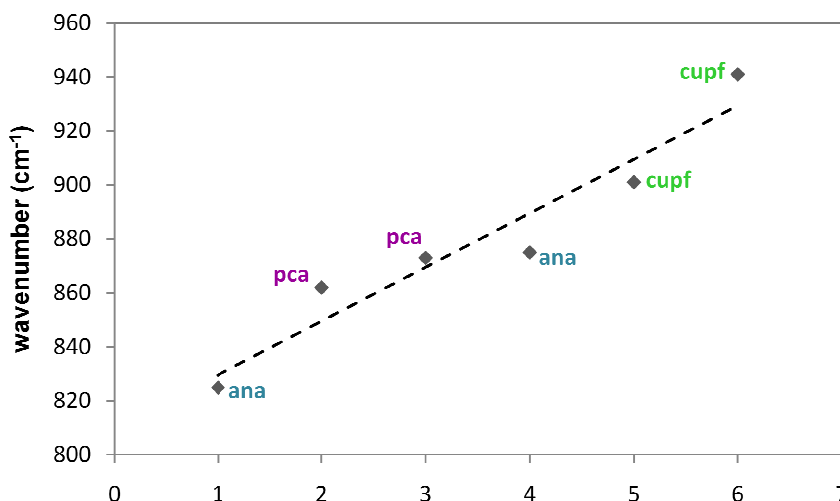
Figure 4.3: Illustration of the effect that ligand choice exhibits in V=O stretching frequencies observed for all the dioxido containing compounds.

From IR spectra it could also be observed that the various β-diketonates chosen in this study had indeed coordinated to the vanadium centre. The free ligands typically show a band in the region 1750 – 1600 cm^{-1} that is assigned as the tautomer of the C=O bond *via* enolization.[17] In all the compounds synthesized with β-diketonates as coordinating ligands, peaks at ~1500 cm^{-1} were noted ([VO(acac)$_2$] = 1516 cm^{-1}, [VO(dbm)$_2$] = 1519 cm^{-1}, [VO(trop)$_2$] = 1412 cm^{-1}) and could be attributed to the newly formed C-O group.[15]

The synthesized complex of [VO(dbm)$_2$] with pyridine showed an IR stretching frequency for the V=O bond of 949 cm^{-1}. Two values have been quoted for this compound by Ikeda *et al.*[18], namely 947 and 955 cm^{-1}. It has been postulated that two pyridine molecules can coordinate to the [VO(dbm)$_2$] complex, but this seems unlikely due to steric bulk. A more reasonable assumption might be that [VO(dbm)$_2$py] could perhaps exist in two different steric forms. As was confirmed by single crystal X-ray diffraction in this study, there does indeed exist two different forms of the compound mentioned (see Section 5.6 of Chapter 5).

[51]V NMR was also utilized in this study extensively and the results of the compounds synthesized and analyzed by [51]V NMR compared to similar 5-membered chelate rings with vanadium is given in Table 4.2.

---

[17] Kushekar, B. A., Khanolkar, D. D., *Ind. J. Chem.*, **1983**, *22A*, 881.
[18] Ikeda, S., Yamamoto, A., Kurita, S., Takahashi, K., Watanabe, T., *Inorg. Chem.*, **1966**, *5*, 611.

Table 4.2: [51]V chemical shift values for compounds with *O,O* and *N,O* chelate-ring structures reported for this study and selected examples from literature.

Compound	[51]V NMR Chemical shift (ppm)	Reference
[VO(trop)$_2$(OMe)]	-460	*a*
(C$_9$H$_{17}$O$_2$)[VO$_2$(cupf)$_2$]	-478	*a*
[VO(Ox)$_2$(OMe)]	-504	*a*
[VO(OEt)(Me-oxin)$_2$]	-466	*b*
[VO(O$_2$)(2,6-dipic)]⁻	-595	*b*

a Compounds synthesized in this MSc study; *b* Reported by Rehder *et al.*[19]

[**(trop)** = tropolonato, **(cupf)** = cupferrato, **(Ox)** = 8-hydroxyquinolinato, **(Me-oxin)** = 2-methylquinolinato, **(dipic)** = 2,6-dipicolinato, **(OMe)** = methoxy, **(OEt)** = ethoxy]

For all the compounds listed in Table 4.2, the chemical shifts reported are well in the range expected for inorganic and coordination compounds (see Figure 2.10 in Chapter 2). The chemical shifts differ in relation to the shielding experienced by the vanadium centre in each complex. The [VO(Ox)$_2$(OMe)] (δ = -504 ppm) and [VO(O$_2$)(dipic)]⁻ (δ = -595 ppm) complexes exhibits the largest amount of shielding.

In Section 2.6.5 of Chapter 2 reference was made to the shielding experienced in inorganic vanadium compounds. An "inverse electronegativity dependence of shielding" exists in high valent (d^0) systems. As the electronegativity increases the total shielding will increase.

Additionally Rehder *et al.*[19] suggested from his studies that increased steric strain could result in larger shielding effects. When comparing the strain between the [VO(trop)$_2$(OMe)] complex and the (C$_9$H$_{17}$O$_2$)[VO$_2$(cupf)$_2$] complex the bite angles for the complexes can be taken into account. The bite angle for metal tropolonato complexes[20] are typically ~79 ° where as cupferrato complexes[21] exhibit bite angles of ~73 °. The (C$_9$H$_{17}$O$_2$)[VO$_2$(cupf)$_2$] (δ = -478 ppm) complex thus experiences the greatest strain and as a result higher shielding than the [VO(trop)$_2$(OMe)] (δ = -460 ppm) complex. In addition, the [VO(Ox)$_2$(OMe)] complex with 8-hydroxyquinolinato ligands has a bite angle of ~76 °. It would thus be expected that the order of chemical shifts from least shielding to highest shielding is: [VO(trop)$_2$(OMe)] < [VO(Ox)$_2$(OMe)] < (C$_9$H$_{17}$O$_2$)[VO$_2$(cupf)$_2$]. The

---

[19] Rehder, D., Weidemann, C., Duch, A., *Inorg. Chem.*, **1988**, *27*, 584.
[20] Steyl, G., *PhD Thesis*, University of Johannesburg, **2004**, 44.
[21] Venter, J. A., Purcell, W., Visser, H. G., *Acta Cryst.*, **2009**, *E65*, 1528.

[VO(Ox)$_2$(OMe)] complex however experiences the most shielding as the chemical shift was observed at -504 ppm.

It may be that the 8-hydroxyquinolinato ligands induce an efficient ligand-to-metal electron density transfer that results in higher shielding. This has been observed for hydroxalmato and catecholato ligands.[22]

The ^{1}H NMR and ^{13}C NMR spectra provided further confirmation of the structures of all the compounds synthesized. Most of the vanadium(IV) compounds were found to be relatively unstable out of solution whilst the vanadium(V) compounds can be stored for months without signs of decomposition.

4.6   Conclusion

The various synthetic procedures utilized in the preparation of novel vanadium(IV) and vanadium(V) compounds were outlined in this chapter. The various characterization methods of IR, NMR and elemental analysis were used for the identification of the compounds synthesized. The results obtained from the IR and ^{51}V NMR studies were compared with literature examples and general conclusions were made with regard to the coordination of various ligands to vanadium. With some of the compounds synthesized, single crystals suitable for single crystal X-ray diffraction studies could be collected. Four of these complexes will be discussed in Chapter 5.

---

[22] Rehder, D., Polenova, T., Bühl, M., *A Survey of ^{51}V NMR Spectroscopy*, Bulletin of Magnetic Resonance,**2007**, 4, 63.

Chapter 5: Crystallographic Study of Selected [VO(L,L⁻-Bid)ₙ] Complexes

5.1 Introduction

One of the main aims of this research project was to synthesize and characterize vanadium(IV) and vanadium(V) complexes (see Chapter 1) containing different L,L'-Bid ligands (L,L'-Bid= bidentate ligands with L,L' donor atoms). Various O,O and N,O ligands were used to achieve this aim as was discussed in Chapter 4, and four complexes that were characterized by single crystal X-ray crystallography are reported in this chapter. Focus will be placed on basic coordination of O,O'-Bid ligands at the vanadium metal centre and on important interactions that occur within the compounds. These compounds are: [VO(dbm)$_2$], [VO(dbm)$_2$(MeOH)]•2MeOH, [VO(dbm)$_2$py] and (C$_9$H$_{17}$O$_2$)[VO$_2$(cupf)$_2$].

5.2 Importance of Hydrogen Bonding

The hydrogen bond is defined as the attractive interaction between a hydrogen atom and an electronegative atom occurring on both intra and intermolecular scale.[1] Contributing greatly to the stability of crystal systems these bonds are manipulated in forming networks that can be used for channelling of smaller molecules or production of materials like nylon which relies on hydrogen bonding for its strength.[2]

According to Grabowski there exist three groups of hydrogen bonding namely strong, moderate and weak.[3] The requirements for the three types of hydrogen bonding are given in Table 5.1. For weak interactions the requirements are that the D-H distance be much smaller than the H⋯A distance. The D⋯A distance must be between 3 and 4.5 Å and the angle DHA must be larger than 90 °.

[1] Arunan, E., Desiraju, G. R., Klein, R. A., Sadlej, J., Scheiner, S., Alkorta, I., Clary, D. C., Crabtree, R. H., Dannenberg, J. J., Hobza, P., Kjaergaard, H. G., Legon, A. C., Mennucci, B., Nesbitt, D. J., *Pure Appl. Chem.*, **2011**, *83*, 1637.

[2] Green, M. M., Wittcoff, H. A. *Organic Chemistry Principles and Industrial Practice*, Wiley & Sons, **2003**, 112.

[3] Grabowski, S. J., *Hydrogen Bonding-New Insights*, Springer, Netherlands, **2006**, 3.

Table 5.1: Classification of hydrogen bonds and their properties.

H-bond parameters	Strong	Moderate	Weak
Interaction type	Strongly covalent	Mostly electrostatic	Electrostatic/ dispersed
Examples	$[F{\cdots}H{\cdots}F]+$ $[N{\cdots}H{\cdots}N]+$	$N\text{-}H{\cdots}O{=}C$	$C\text{-}H{\cdots}O$ $N\text{-}H{\cdots}F\text{-}C$ $O\text{-}H{\cdots}\pi$
Bond energy (kcal.mol-1)	15 - 40	4 - 15	<4
D-H vs. H⋯A	D-H ≈ H⋯A	D-H < H⋯A	D-H << H⋯A
Lengthening of D-H (Å)	0.05 - 0.2	0.01 - 0.05	≤0.01
D⋯A range (Å)	2.2 - 2.5	2.5 - 3.0	3.0 - 4.5
H⋯A range (Å)	1.2 - 1.5	1.5 - 2.2	>2.2
D-H⋯A angles range (°)	170 - 180	>130	>90
Effect on crystal packing	Strong	Distinctive	Variable
Covalency	Pronounced	Weak	Vanishing
Electrostatic contribution	Significant	Dominant	Moderate

By use of the data presented in Table 5.1 the strength and influence of hydrogen bonds in crystal systems may be evaluated in this study and provide insight into how crystal systems are stabilized through these interactions.

5.3   Experimental

The reflection data for the structure determinations of the above mentioned compounds were collected on a Bruker X8 Apex II 4K Kappa CCD diffractometer using graphite monochromated Mo Kα radiation (λ= 0.70926 Å) with ω- and φ-scans at 100(2) K. The Apex II software package[4] was utilized along with the optimum measurement method to collect more than a hemisphere of reciprocal space predicted by COSMO.[5] The SAINT-Plus and XPREP software packages were utilized for frame integration and data reductions whilst SADABS was utilized for the multi-scan absorption correction.[6] Structures were solved by direct methods package SIR97[7] and refinement using the WinGX software package[8] that incorporates SHELXL[9]. All atoms with the exception of

---

[4] Bruker, *Apex2 (version 1.0-27)*, Bruker AXS Inc.,Madison, Wisconsin, USA, **2005**.
[5] Bruker, *COSMO (version 1.48)*, Bruker AXS Inc., Madison, Wisconsin, USA, **2003**.
[6] Bruker, *SAINT-Plus (version 7.12 including XPREP)*, Bruker AXS Inc., Madison, Wisconsin, USA, **2004**.
[7] Altomare, A., Burla, M. C., Camalli, M., Cascarano, G. L., Giacovazzo, C., Guagliardi, A., Moliterni, A. G. G., Polidori, G., Spagna, R., *J. Appl. Cryst.*, **1999**, *32*, 115.
[8] Farrugia, L. J., WinGX, *J. Appl. Cryst.*, **1999**, *32*, 837.
[9] Sheldrick, G. M., *Acta Cryst.*, **2008**, *A64*, 112.

hydrogen atoms were refined anisotropically and were positioned geometrically and refined utilizing a riding model with fixed C-H distances of 0.95 Å (CH) [U_{iso}(H)= 1.2 Ueq] for aromatic hydrogens. Methyl H-atoms were fixed at 0.98 Å (CH) [U_{iso}(H)= 1.2 Ueq]. Molecular diagrams were drawn with the Mercury software package[10] with a 50 % thermal envelope probability for all non-hydrogen atoms. General crystal data and refinement parameters are represented in Table 5.2. The complete list of atomic coordinates, equivalent isotropic parameters and hydrogen coordinates of each data set is given in the Appendix.

[10] Macrae, C. F., Bruno, I. J., Chisholm, J. A., Edgington, P. R., McCabe, P., Pidcock, E., Rodriquez-Monge, L., Taylor, R., van de Streek, J., Wood, P. A., *J. Appl. Cryst.*, **2008**, 41, 466.

Table 5.2: General crystal data for [VO(dbm)$_2$], [VO(dbm)$_2$(MeOH)]·2MeOH, [VO(dbm)$_2$py] and (C$_9$H$_{17}$O$_2$)[VO$_2$(cupf)$_2$].

Crystallographic Data	[VO(dbm)$_2$]	[VO(dbm)$_2$ (MeOH)]·2MeOH	[VO(dbm)$_2$py]	(C$_9$H$_{17}$O$_2$)[VO$_2$(cupf)$_2$]
Empirical Formula	C$_{30}$H$_{22}$O$_5$V	C$_{33}$H$_{34}$O$_8$V	C$_{35}$H$_{27}$NO$_5$V	C$_{19}$H$_{27}$N$_4$O$_8$V
Molecular weight (g/mol)	513.42	609.54	592.52	514.41
Crystal system, space group	Orthorhombic, *Pbca*	Monoclinic, *P2$_1$/c*	Monoclinic, *P2$_1$/c*	Monoclinic, *P2$_1$/c*
a (Å)	14.6295(4)	16.1406(11)	6.3022(5)	12.2758(5)
b (Å)	16.4605(4)	10.7450(6)	18.3396(18)	13.4950(5)
c (Å)	19.9538(5)	18.5378(13)	23.7959(24)	14.0520(6)
α (°)	90.0	90.0	90.0	90.0
β (°)	90.0	113.5789(21)	92.5408(36)	96.0212(18)
γ (°)	90.0	90.0	90.0	90.0
Volume (Å^3)	4805.1(3)	2946.7(2)	2748.6(7)	2315.0(2)
Z	8	4	4	4
Density calculated (g/cm^3)	1.419	1.374	1.432	1.476
Absorption coefficient (mm^{-1})	0.453	0.388	0.408	0.483
F (000)	2120	1276	1228	1072
Crystal size (mm^3)	0.26 x 0.18 x 0.11	0.47 x 0.07 x 0.05	0.33 x 0.04 x 0.03	0.45 x 0.12 x 0.10
Morphology, colour	Cuboid, green	Needle, red	Needle, orange	Needle, yellow
Θ range for data collection	2.7 to 28.3	1.4 to 28.3	2.2 to 25.2	2.1 to 18.3
Completeness for collection (%)	99.8	99.9	99.4	99.8
Index ranges	-18≤ h ≥19 -20≤ k ≥21 -26≤ l ≥21	-21≤ h ≥21 -14≤ k ≥8 -24≤ l ≥24	-5≤ h ≥8 -24≤ k ≥24 -31≤ l ≥31	-16≤ h ≥16 -18≤ k ≥18 -17≤ l ≥17
Reflections collected	56562	38622	49283	46713
Independent reflections	5985	7318	6836	5737
Observed reflections	4896 (R$_{int}$= 0.049)	5545 (R$_{int}$= 0.046)	4725 (R$_{int}$= 0.094)	4593 (R$_{int}$= 0.056)
Max. and min. transmission	0.891 and 0.952	0.839 and 0.981	0.8772 and 0.9879	0.812 and 0.953
Data/ restraints/ parameters	5985/ 0/ 333	7318/ 0/ 423	6836/ 0/ 387	5737/ 0/ 316
Goodness-of-fit on F^2	1.04	1.029	1.18	1.07
Final R indices	R1= 0.0351 wR2= 0.0892	R1= 0.0401 wR2= 0.0913	R1= 0.0774 wR2= 0.1781	R1= 0.0489 wR2= 0.1346
R indices	R1= 0.0462 wR2= 0.0959	R1= 0.0627 wR2= 0.1029	R1= 0.1154 wR2= 0.1920	R1= 0.0609 wR2= 0.1463
Largest diff. Peak and hole (e.Å^{-3})	0.41 and -0.28	0.45 and -0.43	1.17 and -0.71	1.10 and -0.85

5.4 Crystal Structure of [VO(dbm)₂]

The crystal structure of [VO(dbm)$_2$] was first reported by Schilde *et al.*[11] in 1995. The complex was synthesized and X-ray data recollected at a lower temperature as to yield more accurate data compared to the previous collection. The redetermination was done and although no significant deviations were found in terms of bond lengths and angles, a better R_{int} value (0.0351) was achieved in comparison to the previous collection (R_{int}=0.0591).

Bis(1,3-diphenyl-1,3-propanedionato)oxidovanadium(IV), [VO(dbm)$_2$], crystallized in the orthorhombic space group *Pbca* with eight molecules in the unit cell and only one molecule in the asymmetric unit. The structure and subsequent atom numbering scheme is illustrated in Figure 5.1, while the general crystal data of the structure is given in Table 5.2. Some of the important bond distances and angles are listed in Table 5.3 along with the data reported by Schilde *et al.*[11]
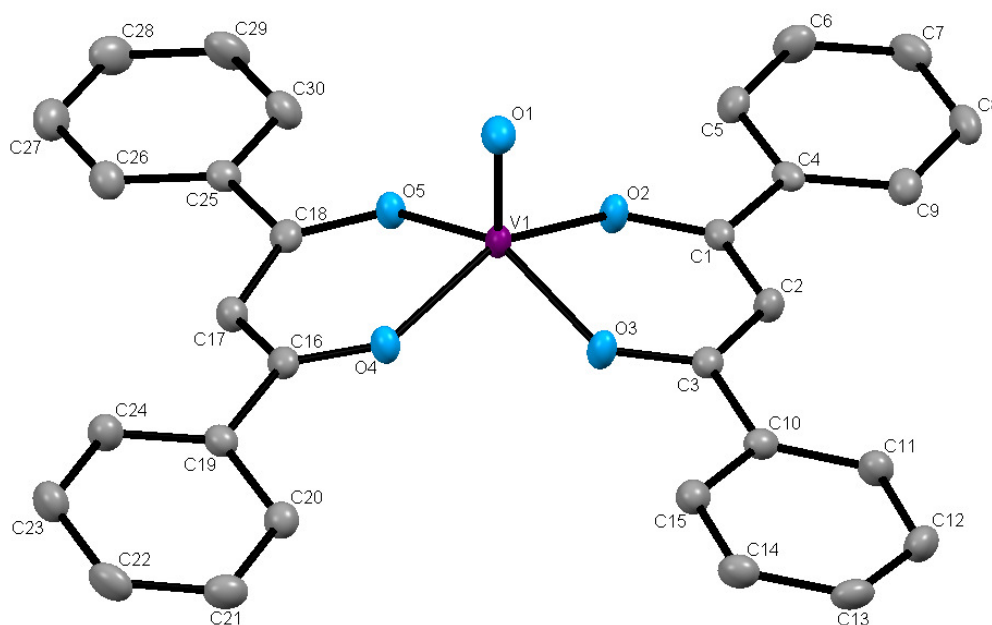
Figure 5.1: Structural representation of [VO(dbm)₂]. Hydrogen atoms have been omitted for clarity. The atom numbering scheme is shown (thermal ellipsoid probability = 50 %).

[11] Schilde, U., Bannse, W., Ludwig, E., Uhlemann, E., *Z. Kristallogr.*, **1995**, *210*, 627.

Table 5.3: Selected bond lengths and angles for [VO(dbm)$_2$].

Atoms	Bond Lengths (Å)	Bond Lengths (Å) Schilde *et al.*[11]	Atoms	Angle (°)	Angle (°) Schilde *et al.*[11]
O1-V1	1.5922(4)	1.578(6)	O3-V1-O2	86.78(5)	87.0(2)
O2-V1	1.9566(5)	1.957(5)	O4-V1-O5	86.48(5)	87.6(2)
O3-V1	1.9515(4)	1.944(5)	O1-V1-O2	106.57(6)	106.7(3)
O4-V1	1.9616(4)	1.941(4)	O1-V1-O3	106.27(5)	106.1(3)
O5-V1	1.9728(3)	1.941(5)	O1-V1-O4	106.14(6)	107.4(3)
O2-C1	1.2849(3)	1.252(9)	O1-V1-O5	107.54(6)	106.6(3)
C1-C2	1.3935(3)	1.417(9)	O2-V1-O4	147.24(5)	145.9(2)
C2-C3	1.3973(4)	1.420(1)	O3-V1-O5	146.15(5)	147.2(2)
C3-O3	1.2787(3)	1.262(9)			
O5-C18	1.2817(3)	1.258(9)			
C18-C17	1.3957(3)	1.420(1)			
C17-C16	1.3990(4)	1.420(9)			
C16-O4	1.2877(3)	1.255(9)			

The vanadium metal centre is surrounded by two 1,3-diphenyl-1,3-propanedionate (dbm) ligands in the equatorial plane and one oxido group in the axial position. The V=O bond is typically found in many vanadium complexes and has been labelled the most stable diatomic ion, remaining intact for many reactions (see Section 2.3.2 of Chapter 2).[12] The V1-O1 bond length in this complex is 1.5922(4) Å and is in the range reported for related vanadyl complexes, including [VO(bzac)$_2$] (1.612(10) Å)[13] (bzac= 1-phenyl-1,3-butanedionato) and [VO(acen)] (1.585(7) Å)[14] (acen= N,N'- ethylenebis(acetylaceto-neiminato)). If the bond were considered to be a V-OH bond, the V1-O1 distance would have been in the range of 1.8 Å.[15] The length of the bond (1.5922 Å) is considerably longer than the V=O bond length for [VO(acac)$_2$] (1.561(10) Å) and can suggest a decrease in electron-donating ability of the 1,3-diphenylpropane-1,3-dione ligand

---

[12] Selbin, J., *Chem. Rev.*, **1965**, *65*, 153.
[13] Hon, P. K., Belford, R. L., Pfluger, C. E., *J. Chem. Phys.*, **1965**, *43*, 1323.
[14] Bruins, D., Weaver, D. L., *Inorg. Chem.*, **1970**, *9*, 130.
[15] Triantafillou, G. D., Tolis, E. I., Terzis, A., Deligiannakis, Y., Raptopoulou, C. P., Sigalas, M. P., Kabanos, T. A., *Inorg. Chem.*, **2004**, *43*, 79.

compared to acetylacetonate. A similar conclusion was made by Amin *et al.*[16] in his comparison of Et-acacH (Et-acac= 3-ethyl-2,4-pentanedionato) and Me-acacH (Me-acac= 3-methyl-2,4-pentanedionato) ligands to Hacac in coordination to vanadium.

It is clear from Figure 5.2, that the complex exhibits a distorted square pyramidal geometry with the vanadium atom situated above the basal equatorial plane. The vanadium atom lies 0.561(2) Å above the best least-squares plane through O2, O3, O4 and O5. This is a similar value in comparison to the reported complexes of [VO(acac)$_2$] (0.55 Å)[17], [VO(Et-acac)$_2$] (0.56 Å)[16], [VO(Me-acac)$_2$] (0.55 Å)[16] and [VO(acen)] (0.58 Å)[14]. The similar values indicate that changes in the substituents on the diketonato functionality have little effect on the value.

The central atom in the diketonato backbone of the dbm ligand has a C17-plane distance of -0.571 Å, while the phenyl rings show the greatest deviation with C21 and C22 having distances of 1.052 Å and 0.897 Å from the plane respectively. The average C-C bond distance of 1.387 Å in the phenyl rings and bond angles of 120 ° are in good agreement with reported data by Lamprecht *et al.*[18] Figure 5.3 (a) shows the bisecting of planes constructed through the phenyl rings of one dbm ligand coordinated to the vanadium centre. The dihedral angle between the two planes was measured as 4.70 °. The planes constructed through the other two phenyl rings of the second coordinated dbm ligand have a dihedral angle of 15.60 °.
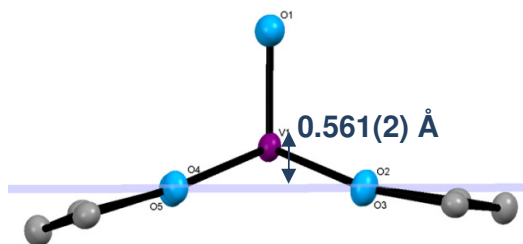
Figure 5.2: Partial structure of [VO(dbm)$_2$] with a plane through O2, O3, O4 and O5 showing the distorted square pyramidal geometry and bent dbm backbone.

[16] Amin, S.S., Cryer, K., Zhang, B., Dutta, S. K., Eaton, S. S., Anderson, O. P., Miller, S. M., Reul, B. A., Brichard, S. M., Crans, D. C., *Inorg. Chem.*, **2000**, *39*, 406.
[17] Dodge, R. P., Templeton, D. H., Zalkin, A., *J. Chem. Phys.*, **1961**, *35*, 55.
[18] Lamprecht, G. J., Leipoldt, J. G., van Biljon, C. P., *Inorg. Chim. Acta*, **1984**, *88*, 55.

a

b
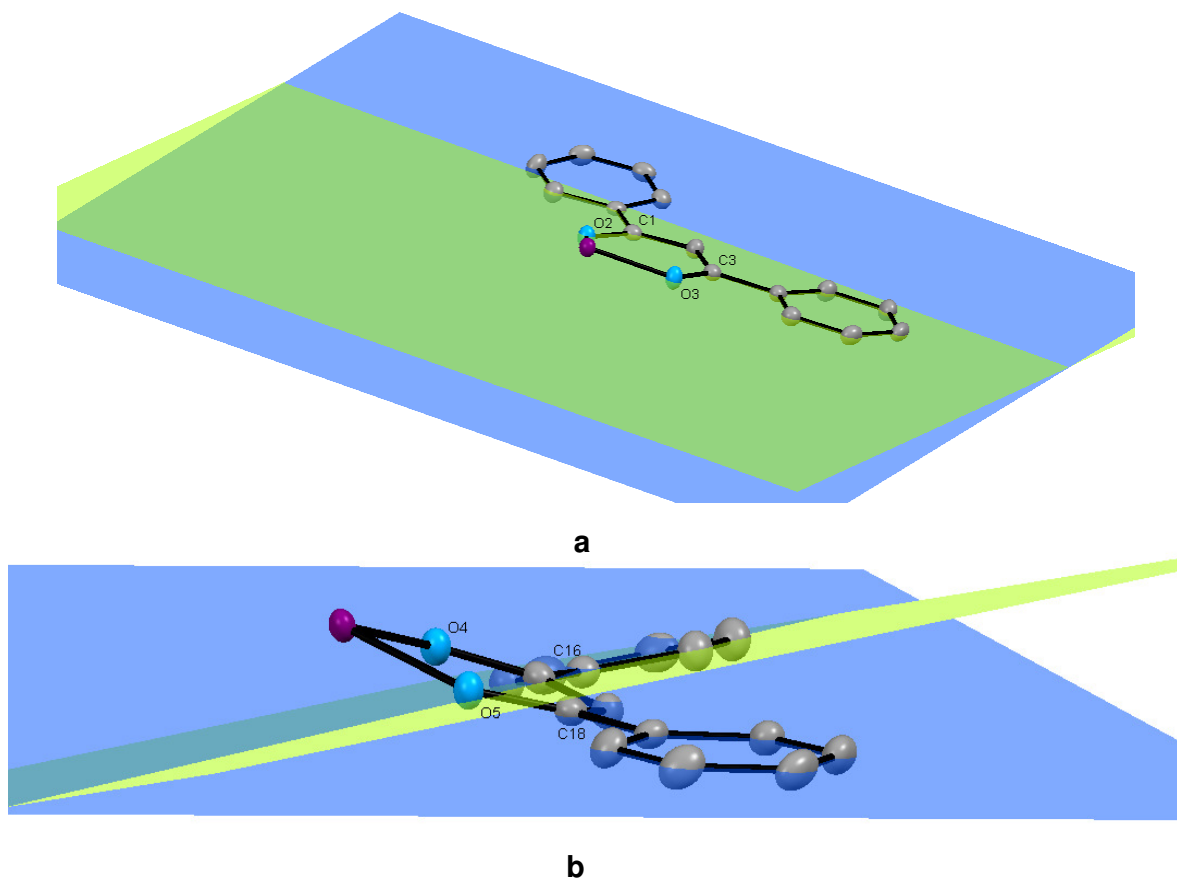
Figure 5.3: Partial structure of [VO(dbm)$_2$] with planes constructed through the phenyl rings of the dbm ligands. a) The dihedral angle between Plane C1 (blue) and Plane C3 (green) is 4.70 °. b) The dihedral angle between Plane C16 (green) and C18 (blue) was measured as 15.60 °.

The torsion angle of O2-C1-C3-O3 has a value of -2.68 ° with the O1 atom slightly more elevated above the equatorial plane and the C3 carbon (0.241 Å) further from the plane than C1 (0.171 Å). The torsion angle of O4-C16-C18-O5 has a value of 3.39 ° with the C16 atom (0.369 Å) further away from the equatorial plane than the C18 atom (0.322 Å).

The interactions governing the manner in which the molecules pack in the unit cell are dominated by two groups of interactions. Intermolecular bonding exists between H13 and O1 of the [VO(dbm)$_2$] molecule (x, 1/2-y, -1/2+z; D-A = 3.3263 Å). These interactions are illustrated in Figure 5.4. The complete list of H-bond interactions is given in Table 5.4. Similar values have been reported by Mandal *et al.*[19] (2.624 Å) and Beddoes *et al.*[20] (2.588 Å) for the distances between the hydrogen atom and the acceptor atom (D(H···A)).

---

[19] Mandal, D. Chatterjee, P. B., Ganguly, R., Tiekink, E. R. T., Clérac, R., Chaudhury, M., *Inorg. Chem.*, **2008**, *47*, 584.
[20] Beddoes, R. L., Eardley, D. R., Mabbs, F. E., Moorcroft, D., Passand, M. A., *Acta Cryst.*, **1993**, *C49*, 1923.

H13 has two interactions with O1 and O5 and such interactions may be labelled bifurcation.[21]

According to the classification set out by Grabowski[3] (see Section 5.2) the length of the hydrogen bonds indicate that the weak hydrogen bonds are electrostatic / dispersed in nature and their contribution to the packing can be varied.
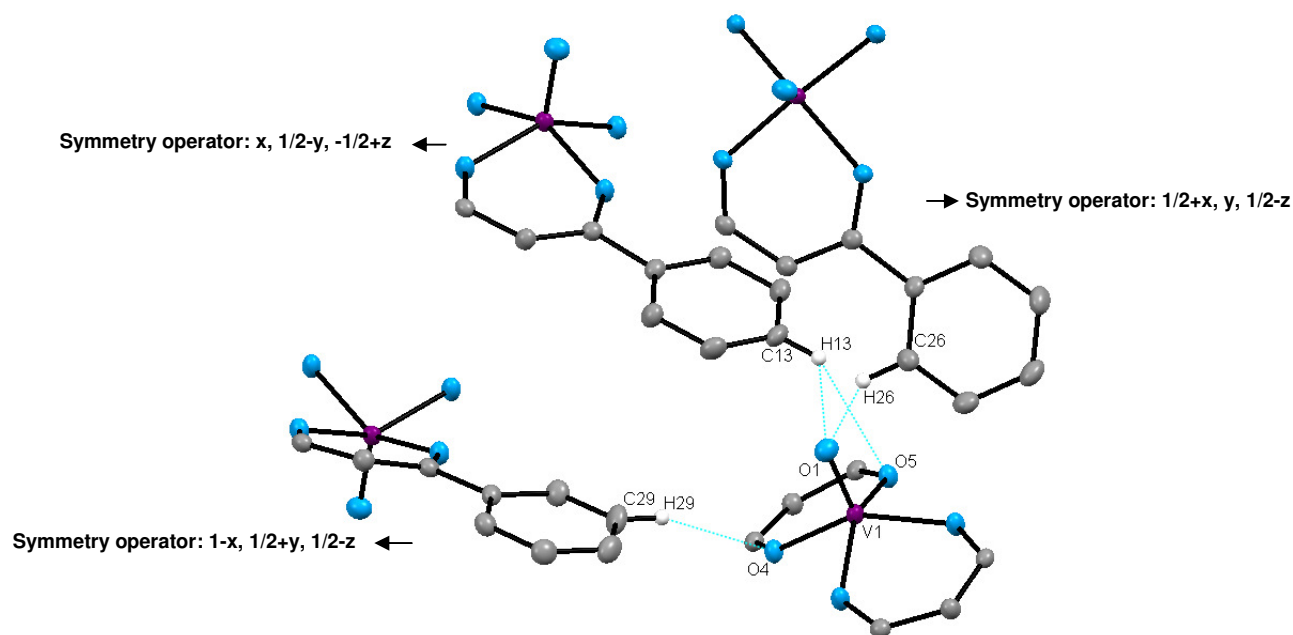
Figure 5.4: O···H interactions (indicated in blue) between the oxido group of [VO(dbm)$_2$] and two other molecules with some fragments omitted for clarity.

Table 5.4: Hydrogen bonding in [VO(dbm)$_2$].

D-H···A	D(D-H) (Å)	D(H···A) (Å)	D(D···A) (Å)	<(DHA) (°)
C29-H29···O4	0.950	2.558	3.4749(9)	162.15
C13-H13···O1	0.950	2.640	3.2888(8)	125.97
C13-H13···O5	0.950	2.680	3.4141(6)	134.57
C26-H26···O1	0.950	2.601	3.2438(9)	125.28

The second group of interactions predominating in this structure is $\pi\cdots\pi$ interactions between two molecules, as illustrated in Figure 5.5 and reported in Table 5.5. One of these interactions occurs between carbon atoms of the dbm backbone (C1 to C1).

[21] Francl, M. M., Petro, W. J., Hehre, W. J., Brinkley, J. S., Gordon, M. S., DeFrees, D. J., Pople, J. A., *J. Chem. Phys.*, **1982**, *77*, 3654.

Soldatov *et al.*[22] in their study of different metal compounds with 1,3-diphenyl-1,3-propanedionate as ligand, reported similar distances (3.426 Å) for interactions between the β-diketonato backbones in nickel complexes. The values found were also in good comparison to those found in the published structure by Schilde *et al.*[11] (3.453 Å). An angle of 0 ° was measured between the two planes that were constructed through the two ligand moieties of the two molecules. The interaction is classified as $\pi\cdots\pi$ interactions rather than $\pi\cdots$C interactions due to the delocalization of electrons from the C=O bonds in the dbm backbone rendering a π-character to the backbone.
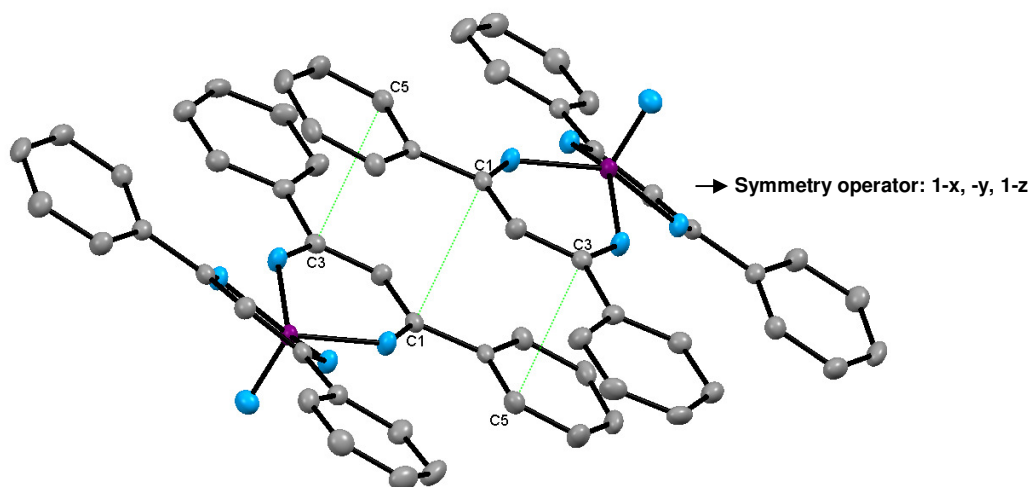
Figure 5.5: $\pi\cdots\pi$ **interactions (indicated in green) between two of the carbons of the β-diketonato backbone and one carbon of the aromatic ring between two molecules.**

Table 5.5: $\pi\cdots\pi$ **interactions between [VO(dbm)₂] molecules.**

Atoms	Distance (Å)
C3-C5	3.333(1)
C1-C1	3.314(1)
C5-C3	3.333(1)

The second coordinated dbm ligand in the compound has C···C soft contacts between C20 and C29 atoms between two molecules. C···H intermolecular interactions occur between C25, C26 and C27 atoms and H23 of another molecule. These interactions are illustrated in Figure 5.6 and the distances for contacts are summarized in Table 5.6.

---

[22] Soldatov, D. V., Henegouwen, A. T., Enright, G. D., Ratcliffe, C. I., Ripmeester, J. A., *Inorg. Chem.*, **2001**, *40*, 1626.
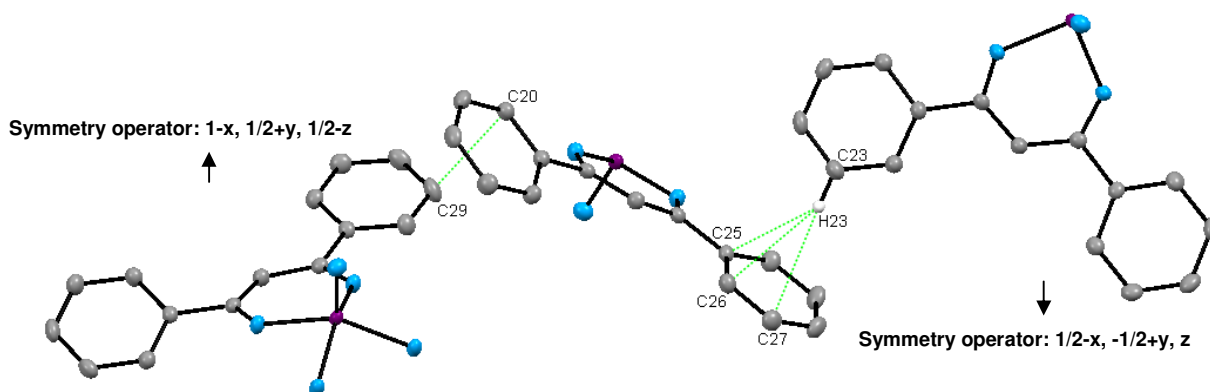
Figure 5.6: C⋯C and C⋯H intermolecular interactions (indicated in green) between the second coordinated dbm ligand in [VO(dbm)₂]. Some fragments have been omitted for clarity.

Table 5.6: C⋯C and C⋯H interactions between [VO(dbm)₂] molecules.

Atoms	Distance (Å)
H23-C25	2.8961(8)
H23-C26	2.8146(6)
H23-C27	2.8743(5)
C20-C29	3.389(1)

The $\pi\cdots\pi$ interactions between the C1-C1 and C5-C3 carbons of two dbm backbones in two molecules result in a planar arrangement of these dbm backbones in terms of their phenyl rings (see Figure 5.3 (a)). A small dihedral angle between planes through the phenyl rings of this dbm ligand was reported (4.70 °). The slight distortion of one of these phenyl rings (C3) can be attributed to the O⋯H intermolecular interactions between O1 and H13. Such interactions are absent in the other coordinated dbm ligand and thus a larger dihedral angle between planes of the phenyl rings is reported (15.60 °).

The packing for [VO(dbm)₂] is illustrated in Figure 5.7 with the pattern in which the molecules are arranged as shown on the right-hand side of Figure 5.7. The packing illustrates a sheet-like structure with alternating positions for the molecules in a two-fold rotation. No significant π-stacking was observed in the structure.
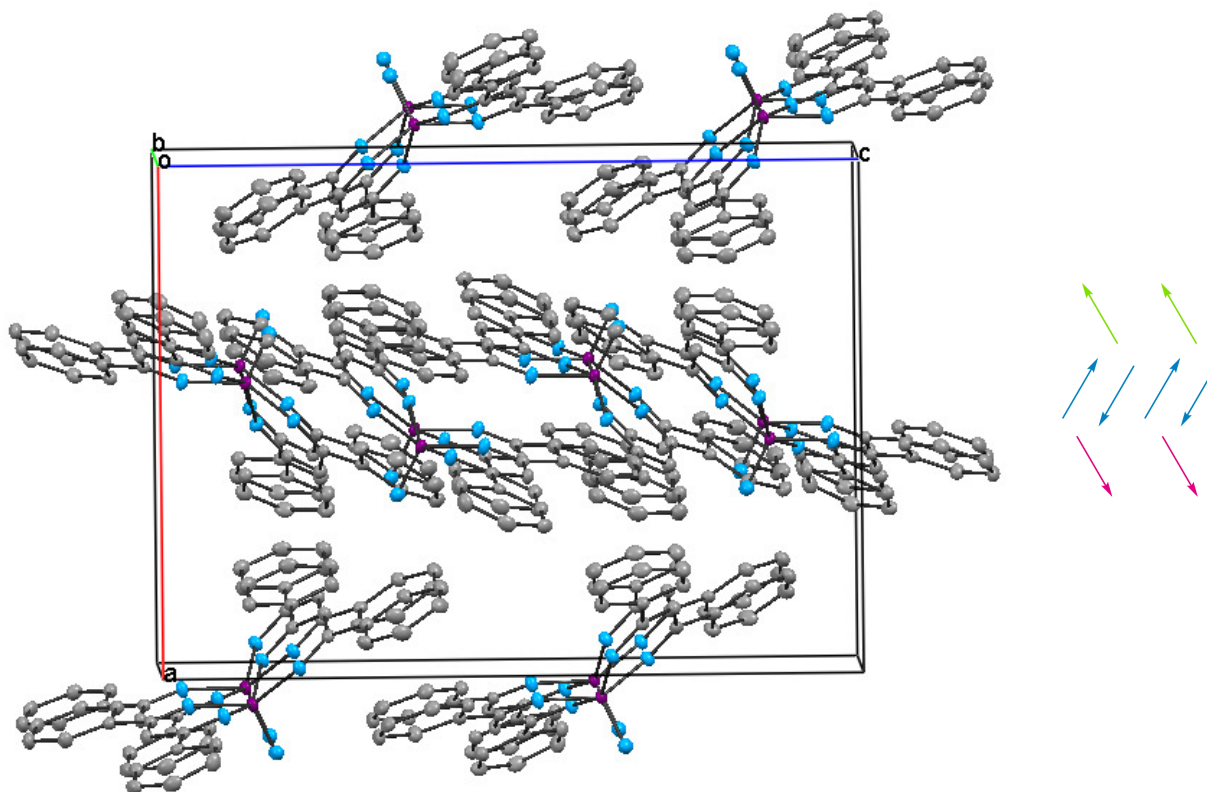
Figure 5.7: Packing of [VO(dbm)₂] viewed along the *b*-axis showing the sheet-like stacking of molecules.

5.5 Crystal Structure of [VO(dbm)₂(MeOH)]·2MeOH

The complex bis(1,3-diphenyl-1,3-propanedionato)methanolato-oxidovanadium(IV), [VO(dbm)₂(MeOH)], crystallized in the monoclinic space group $P2_1/c$ with four formula units in the unit cell. Within the asymmetric unit, one complex molecule along with two solvent molecules (MeOH) is found. The structure with atom numbering scheme is represented in Figure 5.8. Important bond distances and angles for the compound are listed in Table 5.7.
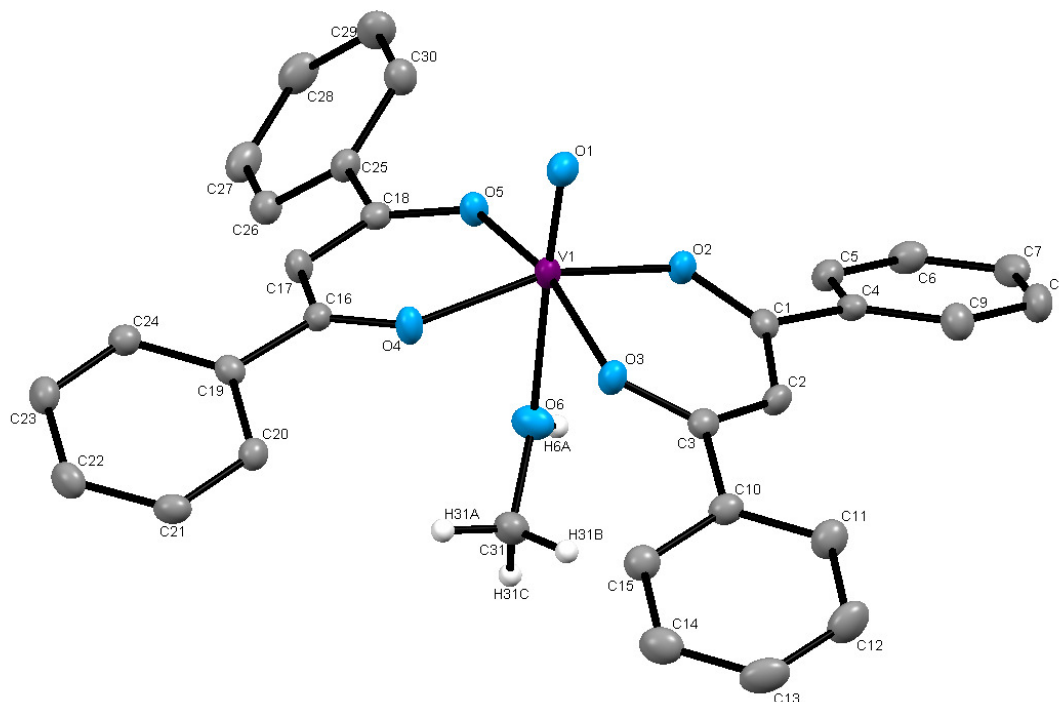
Figure 5.8: Structural representation of [VO(dbm)$_2$(MeOH)]·2MeOH. Hydrogen atoms as well as solvent molecules have been omitted for clarity (thermal ellipsoid probability = 50 %).

The complex has two coordinated 1,3-diphenylpropane-1,3-dione ligands in the equatorial plane, the same as in the [VO(dbm)$_2$] structure discussed in Section 5.4. The oxido group is again found in the axial position and no significant change in bond length is reported for the O1-V1 bond of 1.5964(3) Ǎ as compared to the previous structure (1.5922(4) Å). The sixth coordination position of the vanadium centre is occupied by a methanol molecule. The rather long bond length of 2.3022(5) Ǎ is indicative of methanol coordination as structures by Gao *et al.*[23] (2.346 Å), Chen *et al.*[24] (2.333 Å) and Tasiopoulos *et al.*[25] (2.301 Å) reported similar bond lengths for this type of coordination. A methoxy group bonded to a vanadium metal centre would have a V-OMe bond length of approximately 1.755 Å.[26] Moreover; an additional cation would also have been required.

---

[23] Gao, S., Weng, Z., Liu, S., *Polyhedron*, **1998**, *17*, 3595.
[24] Chen, C. T., Lin, J. S., Kuo, J. H., Weng, S. S., Cuo, T. S., Lin, Y. W., Cheng, C. C., Huang, Y. C., Yu, J. K., Chou, P. T., *Organic Letters*, **2004**, *6*, 4471.
[25] Tasiopoulos, A. J., Troganis, A. N., Evangelou, A., Raptopoulou, C. P., Terzis, A., Deligiannakis, Y., Kabanos, T. A., *J. Eur. Chem.*, **1999**, *5*, 910.
[26] Bansse, W., *Z. Anorg. Allg. Chem.*, **1992**, *613*, 36.

Table 5.7: Selected bond distances and angles for [VO(dbm)$_2$(MeOH)]·2MeOH.

Atoms	Bond Lengths (Å)	Atoms	Angle (°)
O1-V1	1.5964(3)	O3-V1-O2	89.93(5)
O2-V1	1.9973(7)	O4-V1-O5	89.14(5)
O3-V1	2.0045(5)	O1-V1-O2	99.25(6)
O4-V1	1.9847(8)	O1-V1-O3	98.18(6)
O5-V1	1.9940(2)	O1-V1-O5	99.44(6)
O6-V1	2.3022(5)	O1-V1-O4	101.25(6)
C2-C3	1.3900(5)		
C3-O3	1.2763(3)		
O4-C16	1.2705(3)		
C16-C17	1.4006(6)		
C17-C18	1.3825(6)		
C18-O5	1.2836(3)		

The bond lengths between the chelating oxygen donor ligands and vanadium centre are in the range of ~2 Å. This is slightly longer than those reported for the previous structure (~1.96 Å). Bond lengths of ~2 Å imply that an enolate type delocalization occurs within the dbm bidentate ring as the average C=O bond distance of 1.23 Å is much shorter than the reported bond lengths in this structure (~1.28 Å)[27]. Single C-O bond distances are also unlikely in this structure as the average length for these bonds are in the range of 1.43 Å.[28] Additionally, the carbon atoms of the dbm backbone have longer bond lengths of ~1.4 Å than that reported for carbon-carbon double bonds (1.32 Å)[29] but are also shorter than single C-C bonds (1.53 Å).[30]

As with the [VO(dbm)$_2$] structure, this complex also exhibits a distorted geometry. With the methanol coordinated in the axial position the vanadium complex exhibits a distorted octahedral geometry. The vanadium atom is distorted above the basal plane with a distance of 0.330(3) Å as illustrated in Figure 5.9.

---

[27] Brink, A., *MSc Dissertation*, University of the Free State, **2007**, 69.
[28] Ishida, T., Inoue, M., Nasu, K., Kurihara, T., *Acta Cryst.*, **1983**, *C39*, 470.
[29] Pauling, L., *The Nature of the Chemical Bond and Structure of Molecules and Crystals*, Cornell University Press, **1960**, 237.
[30] March, J., *Advanced Organic Chemistry: Reactions, Mechanisms and Structures 6th edition*, Wiley & Sons, **2007**, 23.
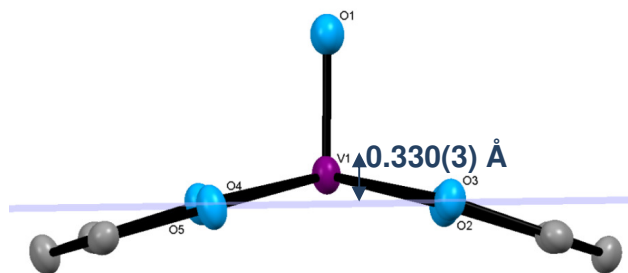
Figure 5.9: The plane (blue) shown illustrates the lifting of the vanadium centre out of the equatorial plane to yield a distorted octahedral geometry.

The phenyl rings of the β-diketonato ligands are twisted out of plane as shown in Figure 5.10. Planes constructed through the carbon atoms of the phenyl rings connected to C1 and C3 illustrate bisecting of the planes with a dihedral angle between Plane C1 (green) and Plane C3 (blue) of 32.9(3) °. For the phenyl rings of the coordinated dbm ligand through C16 and C18, the dihedral angle between Plane C16 (blue) and Plane C18 (green) is 47.9(6) °.
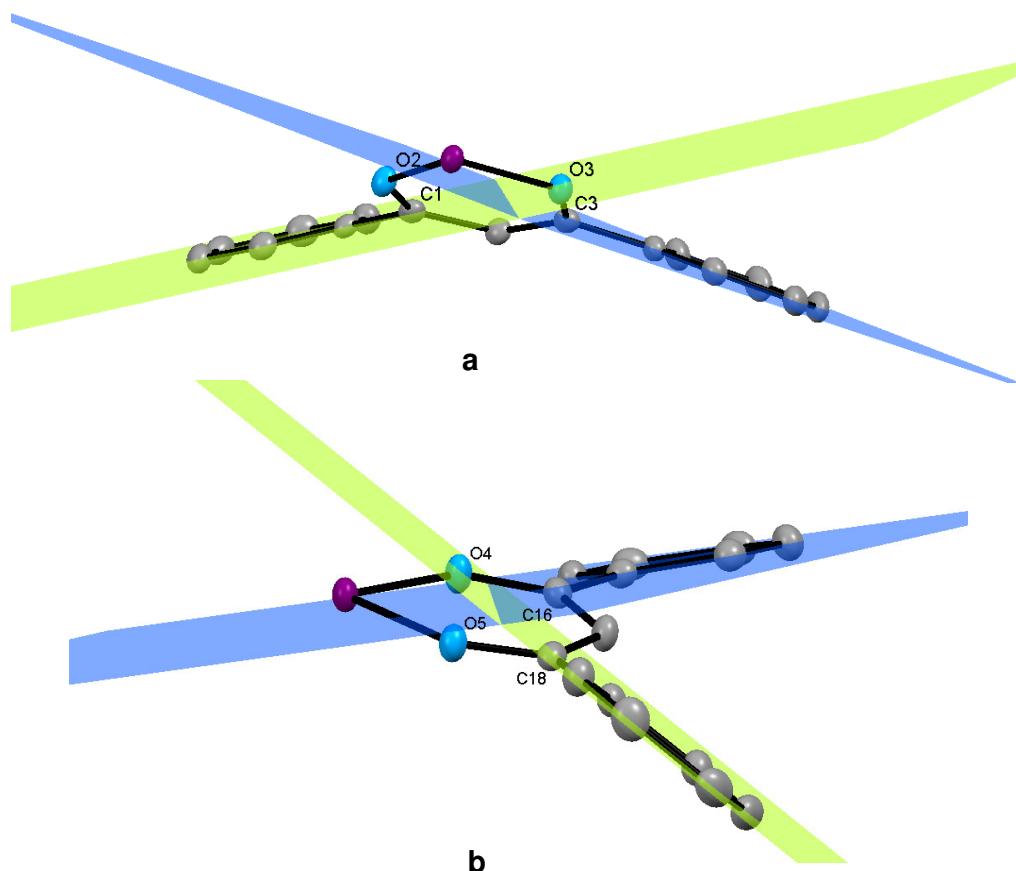
Figure 5.10: Partial structure of [VO(dbm)₂MeOH]·2MeOH. a) Planes bisecting the phenyl rings of the C1-C2-C3 backbone. b) Planes constructed through the phenyl rings of the other coordinated dbm ligand.

Hydrogen bonding occurs in the structure between a methanol molecule interacting with a hydrogen on the coordinated methanol of the complex as shown in Figure 5.11. The methanol solvate has a second hydrogen bond with a neighbouring methanol. A third interaction then occurs with an oxygen atom of the chelating ligand in the complex.

The complete list of hydrogen bonding interactions is given in Table 5.8. The distances for these bonds are well in accordance with reported literature values for similar interactions (1.954 Å and 2.004 Å) for H···A distances.[31,32] These values additionally indicate that the bonds in the present structure may be classified as moderate hydrogen bonds that are mostly electrostatic in nature and contributes distinctively to the packing of molecules within the crystal.[3]
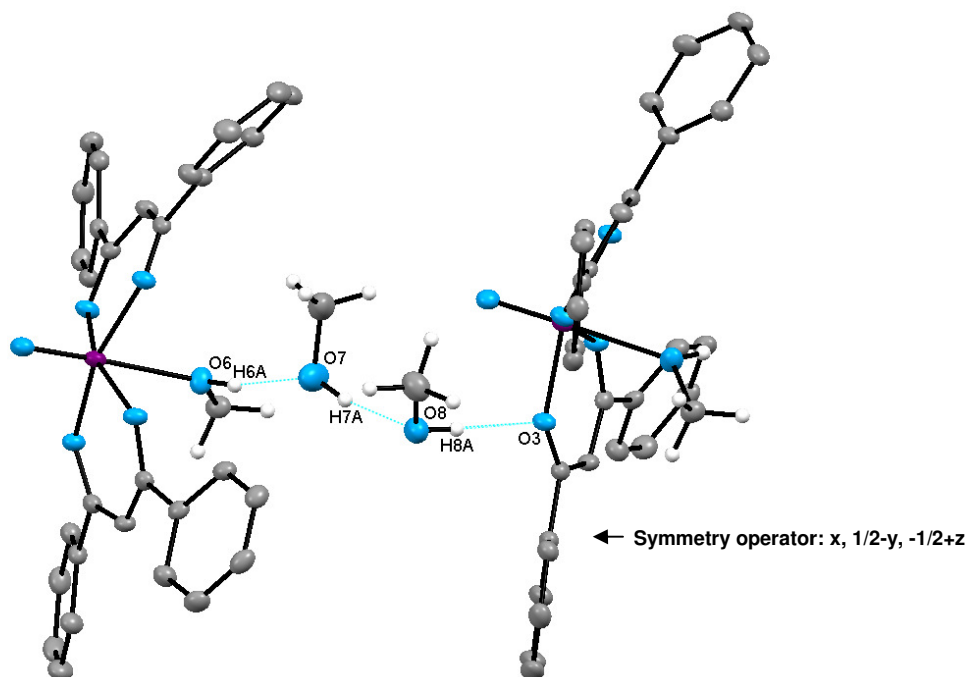
Figure 5.11: Hydrogen bonds (indicated in blue) linking between one of the compound molecules and a solvent molecule before linking again to another solvent molecule that has hydrogen bonding with a second complex molecule.

[31] Aromi, G., Boldron, C., Gamez, P., Roubeau, O., Kooijman, H., Spek, A. L., Stoeckli-Evans, H., Ribas, J., Reedijk, J., *Dalton Trans.*, **2004**, 3586.
[32] Shiga, T., Nakanishi, T., Ohba, M., Okawa, H., *Polyhedron*, **2005**, *24*, 2732.

Table 5.8: Hydrogen bonds for [VO(dbm)₂(MeOH)]•2MeOH.

D-H···A	D(D-H) (Å)	D(H···A) (Å)	D(D···A) (Å)	<(DHA) (°)
O6-H6A···O7	0.82(3)	1.84(3)	2.644(3)	168.32
O7-H7A···O8	0.87(3)	1.90(3)	2.749(3)	166.44
O8-H8A···O3	0.90(4)	1.96(4)	2.853(2)	177.07

These interactions eventually lead to the formation of polymeric chains of the complex along the *b*-axis, as illustrated in Figure 5.12. The packing of the complex within the unit cell is dependent upon the polymer chain formation that occurs (see Figure 5.14).
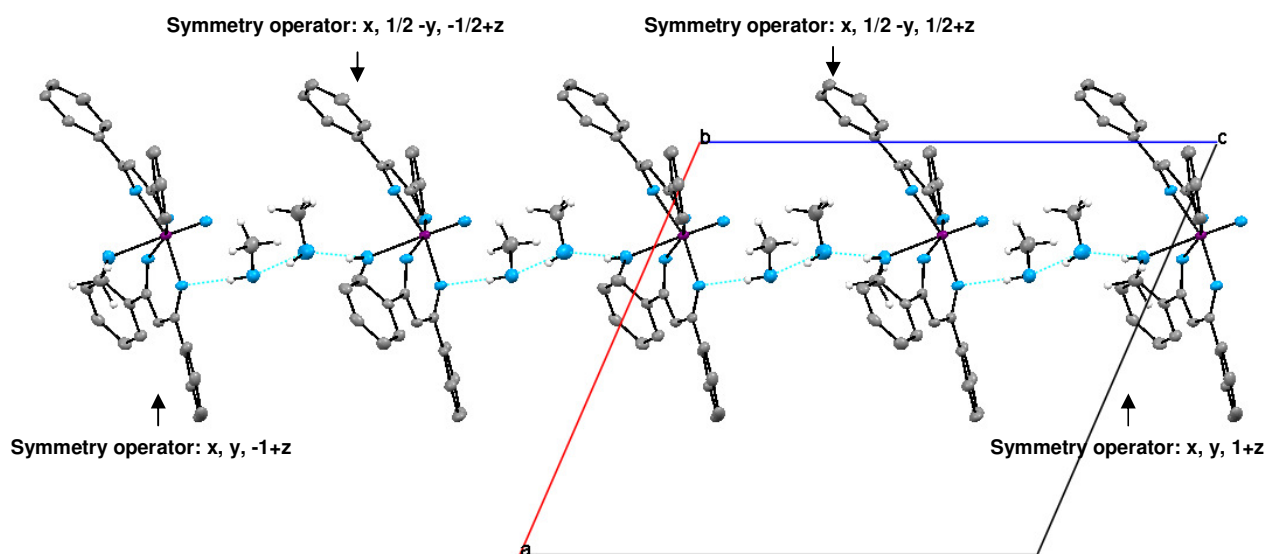
Figure 5.12: The hydrogen bonding (indicated in blue) leads to the formation of polymeric chains of the complex along the *b*-axis.

Another type of intermolecular interaction found in the crystal structure is those depicted in Figure 5.13. The C···H interactions occur between two molecules through the methine carbon (C2) on the dbm backbone along with the bonded hydrogen (H2) to C7 of the phenyl ring of another molecule. The distance between the C2 carbon and C7 carbon of the phenyl ring is 3.315(2) Å. The H2···C7 interaction has a measured length of 2.870 Å.
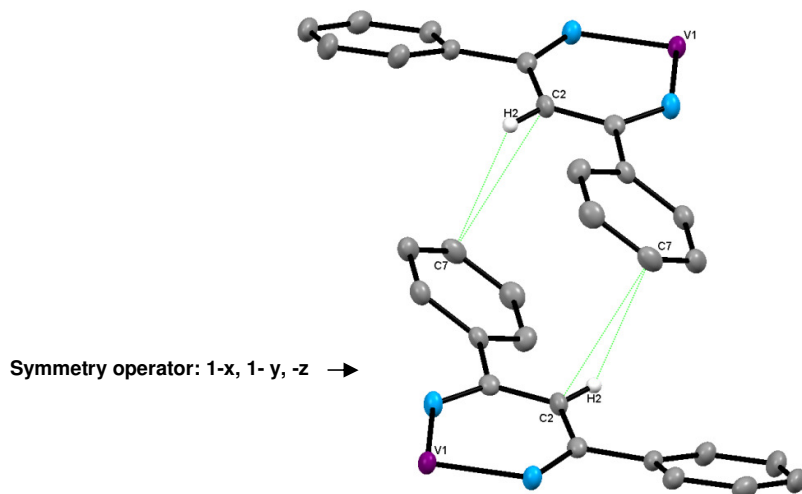
Figure 5.13: C⋯H soft contacts between the methine carbon and H2 of the dbm ligand and C7 of the phenyl ring on another molecule.

The sheet-like packing for the compound is represented in Figure 5.14 with a packing motif illustrating a typical head-to-tail arrangement.
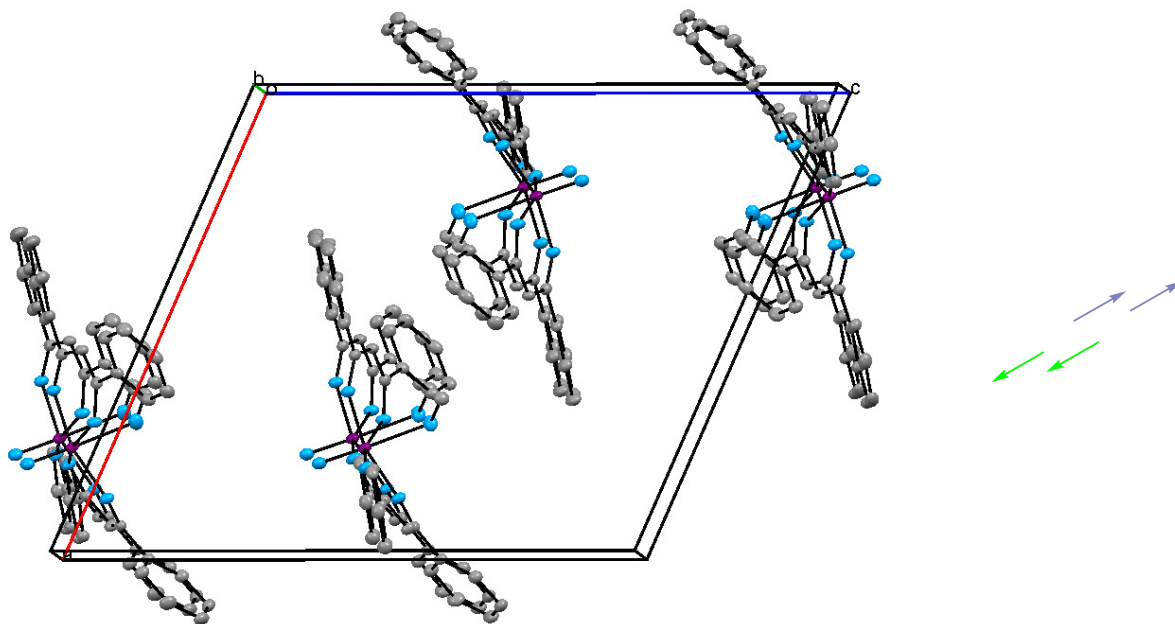
Figure 5.14: Packing of [VO(dbm)$_2$(MeOH)]·2MeOH as viewed along the *b*-axis, illustrating sheet-like packing.

5.6   Crystal Structure of [VO(dbm)₂py]

Bis(1,3-diphenyl-1,3-propanedionato)oxidopyridinevanadium(IV), [VO(dbm)₂py], crystallized in the monoclinic space group $P2_1/c$ with four molecules in the unit cell. The structure is represented with assigned numbering in Figure 5.15 with important bond distances and angles for the complex listed in Table 5.9.

The vanadium metal centre is surrounded by two coordinated 1,3-diphenyl-1,3-propanedionate ligands and one pyridine ligand. The expected oxido bond is also present and situated in an axial position whilst the pyridine ligand adopts a *cis* configuration with the oxido group as can be seen in Figure 5.15. The *cis* configuration of the pyridine ligand opposed to the expected axial position with regard to the oxido bond could possibly be attributed to steric constraint within the structure.
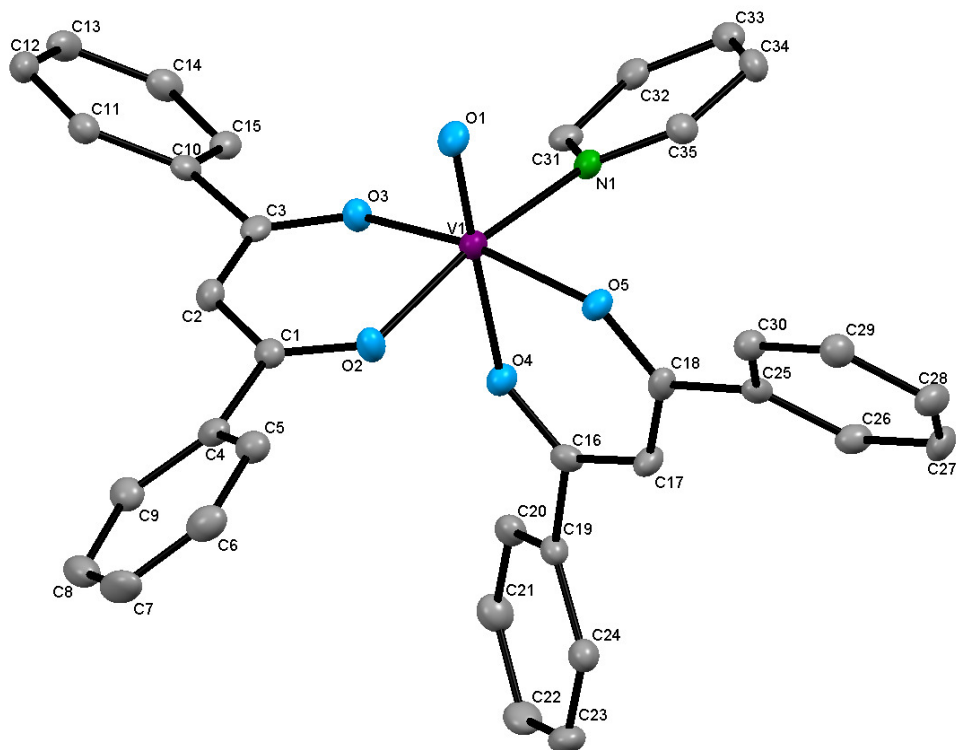
Figure 5.15: Structural representation of [VO(dbm)₂py] and numbering scheme. Hydrogen atoms have been omitted for clarity (thermal ellipsoid probability = 50 %).

Table 5.9: Selected bond distances and angles for [VO(dbm)$_2$py].

Atoms	Bond Lengths (Å)	Bond Lengths (Å) Meštrović *et al.*[34]	Atoms	Angle (°)	Angle (°) Meštrović *et al.*[34]
O1-V1	1.612(3)	1.598(2)	O3-V1-O2	88.31(1)	88.52(6)
O2-V1	2.004(3)	1.986(2)	O4-V1-O5	83.69(1)	81.91(6)
O3-V1	1.994(3)	1.973(2)	O1-V1-O2	98.4(2)	98.62(7)
O4-V1	2.138(3)	2.143(2)	O1-V1-O3	96.6(2)	97.67(7)
O5-V1	1.994(3)	1.983(1)	O1-V1-O4	176.9(2)	176.64(7)
N1-V1	2.154(4)	2.147(2)	O1-V1-O5	97.6(2)	95.44(7)
O2-C1	1.2717(3)	1.272(2)	O2-V1-O4	84.4(1)	83.48(6)
C1-C2	1.4024(5)	1.395(3)	O3-V1-O5	165.8(1)	166.88(6)
C2-C3	1.3900(5)	1.394(3)	O1-V1-N1	93.1(2)	94.23(8)
C3-O3	1.2763(3)	1.281(2)	O2-V1-N1	168.5(1)	166.93(7)
O4-C16	1.2705(3)	1.274(3)			
C16-C17	1.4006(6)	1.394(3)			
C17-C18	1.3825(6)	1.389(3)			
C18-O5	1.2836(3)	1.276(3)			

The V=O bond length for this structure (1.612(3) Å) is within the range for other reported V=O bond distances as a Mogul geometry search yielded values of 1.5 – 1.6 Å for this type of bond.[33] The reported bond is slightly longer than the V=O bond distances in the [VO(dbm)$_2$] and [VO(dbm)$_2$(MeOH)] compounds (see Tables 5.3 and 5.7). This may be interpreted in terms of electron donation from the *trans* situated ligand, thereby making the vanadium atom less able to accept charge from the oxygen and so reducing the strength of the oxido bond.

The V-O$_{dbm}$ bond distances are longer than those found in the [VO(dbm)$_2$] and [VO(dbm)$_2$(MeOH)] compounds and thus a conclusion may be made that the V-O$_{dbm}$ distances are influenced by the sixth coordinating ligand. A weak coordinating ligand of methanol will have a slight effect on bond distances and a strong coordinating ligand such as pyridine induces a much greater effect in terms of the vanadium centre being able to accept charge.

---

[33] Bruno, I. J., Cole, J. C., Kessler, M., Luo, J., Motherwell, W. D. S., Purkis, L. H., Smith, B. R., Taylor, R., Cooper, R. I., Harris, S. E., Orpen, A. G., *J. Chem. Inf. Comput. Sci.*, **2004**, *44*, 2133.

[VO(dbm)$_2$py] has previously been reported by Meštrović *et al.*[34] in 2004. The crystal structure however was reported with different cell dimensions than for the structure reported here. A comparison of the cell dimensions for the two crystal structures are given in Table 5.10 in the same space group of *P*2$_1$/*c*. The bond lengths found in the published structure of Meštrović *et al.*[34] is summarized in Table 5.9 along with the distances reported for the structure under investigation.

Table 5.10: Comparison of cell dimensions for the structure reported here and the published structure by Meštrović *et al.*[34]

Cell dimension	Found	Published
a (Å)	6.3022(5)	15.291(4)
b (Å)	18.3396(18)	18.973(4)
c (Å)	23.7959(24)	9.831(2)
α (°)	90.0	90.0
β (°)	92.5408(36)	97.920(18)
γ (°)	90.0	90.0

From the comparison it can be concluded that the structure reported here is a polymorph of the published structure. An overlay of the two crystal structures gives further insight into the differences between the two structures. Figure 5.16 represents the overlay of the two crystal structures with clearly visible differences in the twisting of the phenyl rings as well as the pyridine ligand orientation.

---

[34] Meštrović, E., *Acta Cryst.*, **2004**, *E60*, m1920.
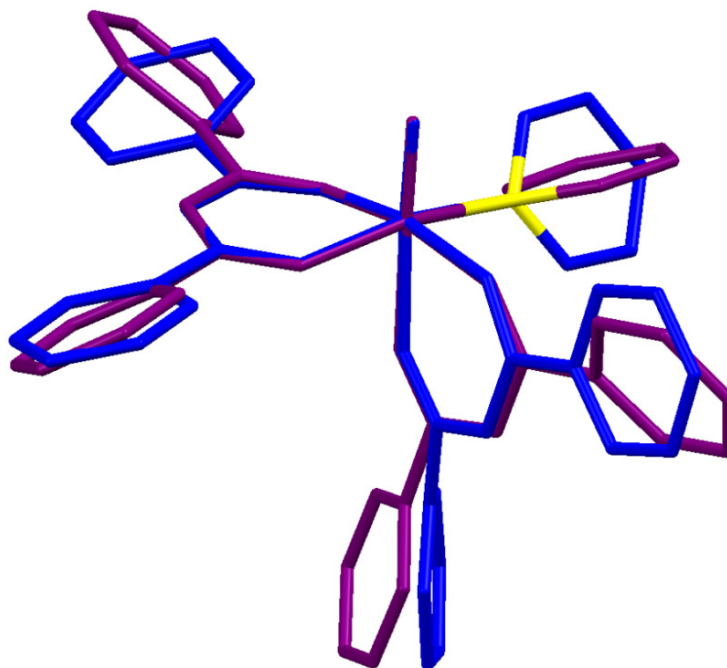
Figure 5.16: Overlay of the structure reported here (purple) with the published structure for [VO(dbm)₂py] (blue) and nitrogen indicated in yellow. RMS = 1.25 Å.

The reported structure by Meštrović *et al.*[34] displayed dimer formation of the [VO(dbm)₂py] complex connected by an intermolecular C-H···O contact as seen in Figure 5.17. For the complex reported here no such interactions could be found to indicate dimer formation.

Symmetry operator: -x, 2-y, 1-z
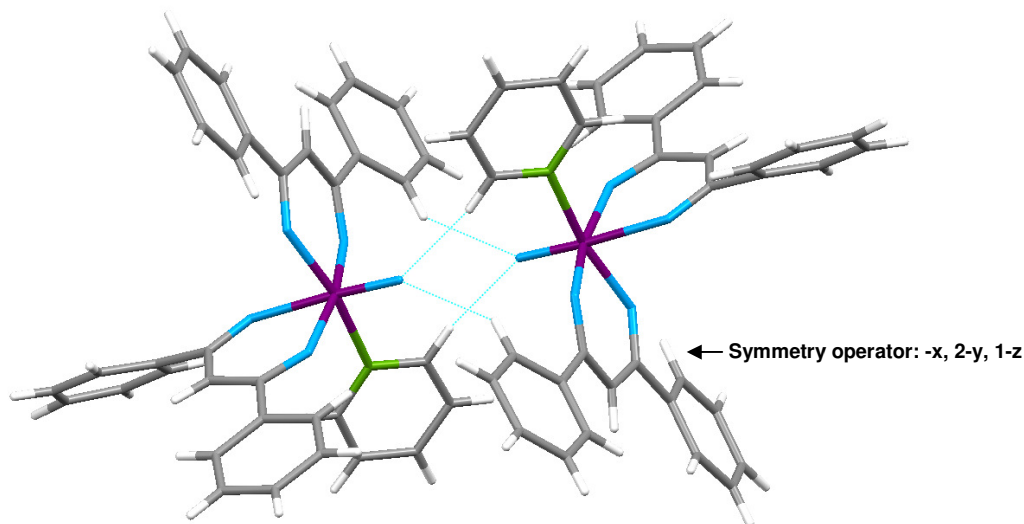
Figure 5.17: The dimer formation in the [VO(dbm)₂py] structure by Meštrović *et al.*[34]

As with the structure reported in Section 5.5, a distorted octahedral geometry exists for the complex with a distance of 0.227(2) Å between the vanadium atom and the best least-squares plane through atoms O2, O3, N1 and O5. The out of plane vanadium centre can be seen in Figure 5.18.
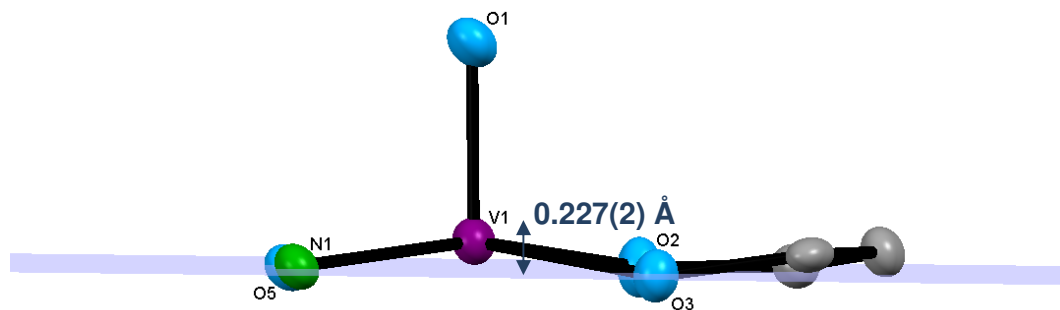
Figure 5.18: The plane (blue) shown illustrates the vanadium centre out of plane to yield a distorted octahedral geometry.

The structure reported here shows the greatest deviation of the phenyl rings with respect to each other as is illustrated in Figure 5.19. A dihedral angle of 65.47 ° was measured between the two phenyl rings C1 and C3 (Figure 5.19 (a)). For the two phenyl rings of the other coordinated dbm ligand a dihedral angle of 55.69 ° was determined (Figure 5.19(b)).

a

b
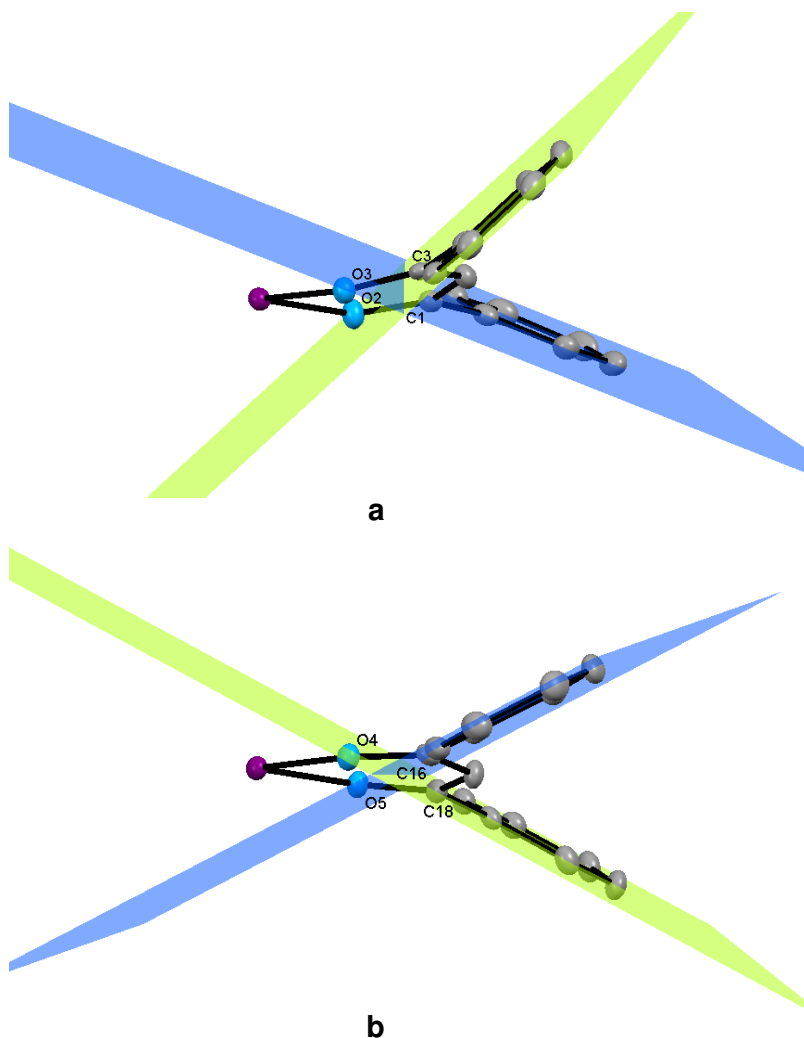
Figure 5.19: Partial structure of [VO(dbm)₂py]. a) Planes dissecting the phenyl rings of the C1-C2-C3 backbone. b) Planes through the phenyl rings of the other coordinated dbm ligand.

As with the [VO(dbm)₂] structure, interactions occur between the oxido group on the vanadium and other atoms of a second molecule. These three hydrogen bonds are shown in Figure 5.20 with accompanying distances of the contacts given in Table 5.11.
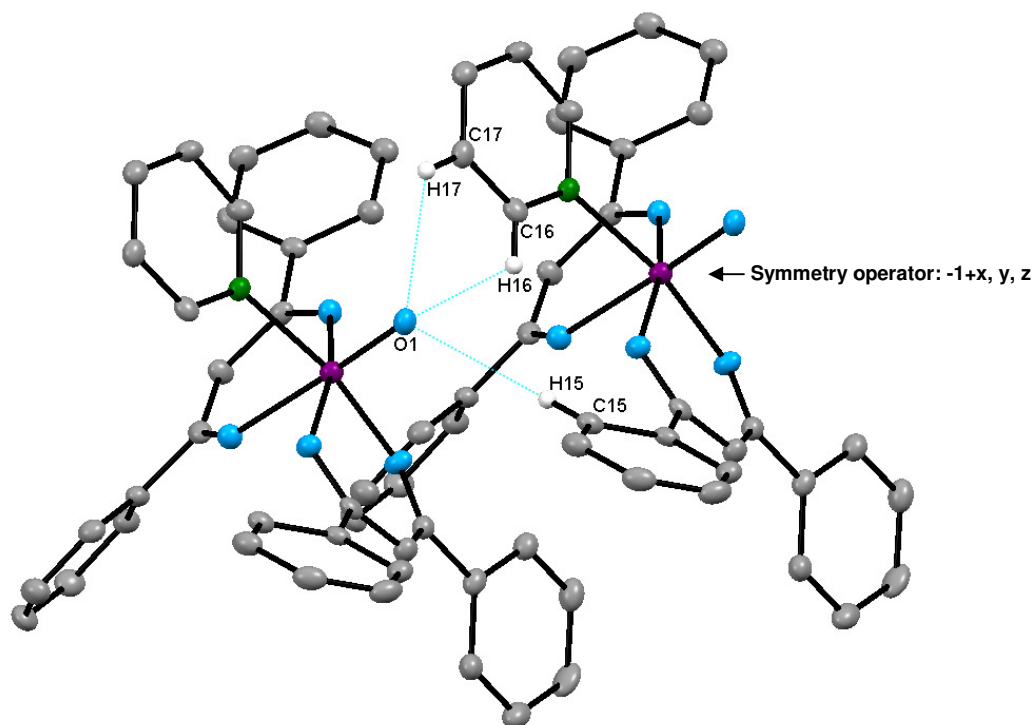
Figure 5.20: O···H interactions between the oxido group on one complex molecule interacting with a second molecule through the pyridine molecule primarily. Only hydrogens involved in the interactions are shown.

Table 5.11: Hydrogen bonds for [VO(dbm)$_2$py].

D-H···A	D(D-H) (Å)	D(H···A) (Å)	D(D···A) (Å)	<(DHA) (°)
C15-H15···O1	0.950(5)	2.6560(9)	3.469(1)	143.90
C16-H16···O1	0.950(5)	2.554(2)	3.181(2)	123.74
C17-H17···O1	0.950(5)	2.5634(6)	3.170(1)	121.94

The interactions between the oxido group and hydrogens of the pyridine molecule have distances in good agreement with structures published by Xiao *et al.*[35] (2.614 Å) and Bernalte *et al.*[36] (2.448 Å) for H···A distances.

Some π-stacking interactions are observed in the crystal packing between the pyridine rings of the two molecules as illustrated in Figure 5.21. These interactions are found between C16 and C18 in a "head-to-tail" mode and a centroid to centroid distance of 3.571 Å was determined with an angle of 93.37 °. This distance is well in accordance with

---

[35] Xiao, D., Wang, E., An, H., Xu, L., Hu, C., *J. Mol. Struct.*, **2004**, *707*, 77.
[36] Bernalte, A., Barros, F. J. G., Cavaco, I., Costa Pessoa, J., Gillard, R. D., Higes, F. J., Tomaz, I., *Polyhedron*, **1998**, *17*, 3269.

literature values (3.64 Å).[37] This type of π-stacking is denoted as the "sandwich type" due to the position of the aromatic systems lying almost directly atop one another.[38]
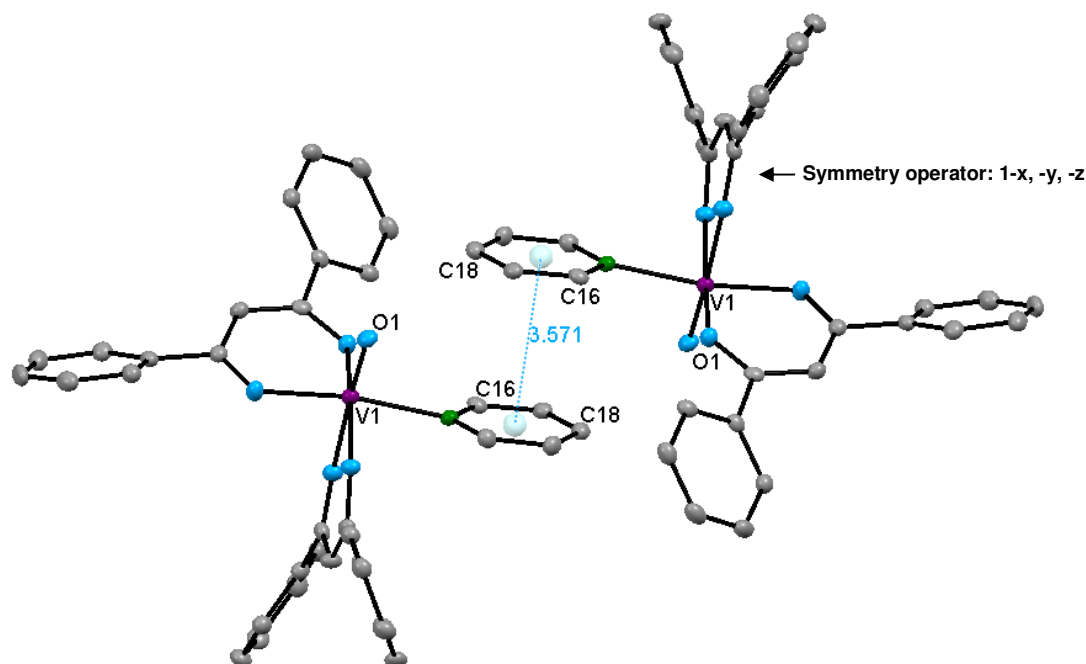
Figure 5.21: An illustration of the π-stacking found between two pyridine rings of two adjacent molecules.

Figure 5.22 demonstrates how the π-stacking influences the packing within the crystal. No π-π stacking was found in the structure published by Meštrović *et al.*[34] This can be explained in terms of the geometry of the pyridine ligands as can be seen in Figure 5.17.

[37] Broomhead, J. A., Greenwood, R., Pienkowski, W., Sterns, M., *Aust. J. Chem.*, **1986**, *39*, 1895.
[38] Bloom. J. W. G., Wheeler, S. E., *Angew. Chem. Int. Ed.*, **2001**, *50*, 7847.
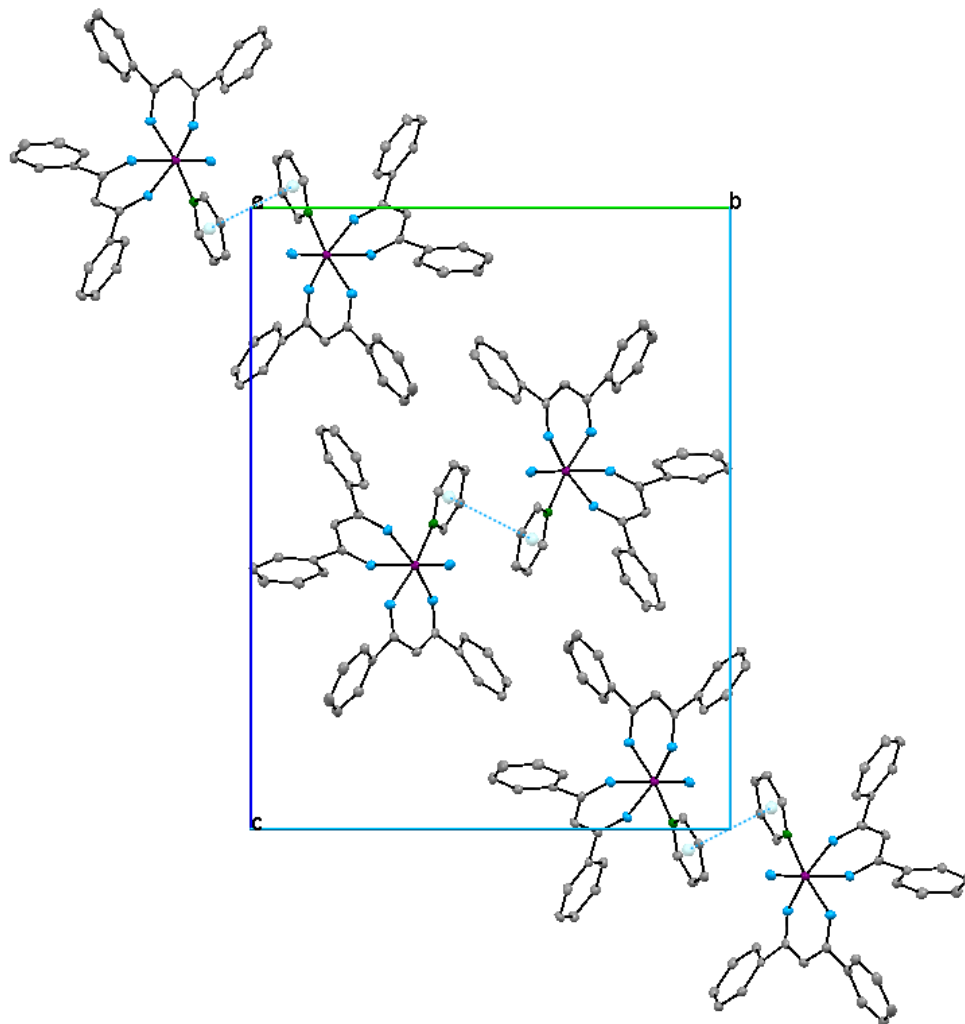
Figure 5.22: An illustration of how the π-stacking found between the molecules influences the packing along the *a*-axis.

The packing within the crystal structure between the molecules is illustrated in Figure 5.23 and the packing motif represents a classic head-to-head arrangement.
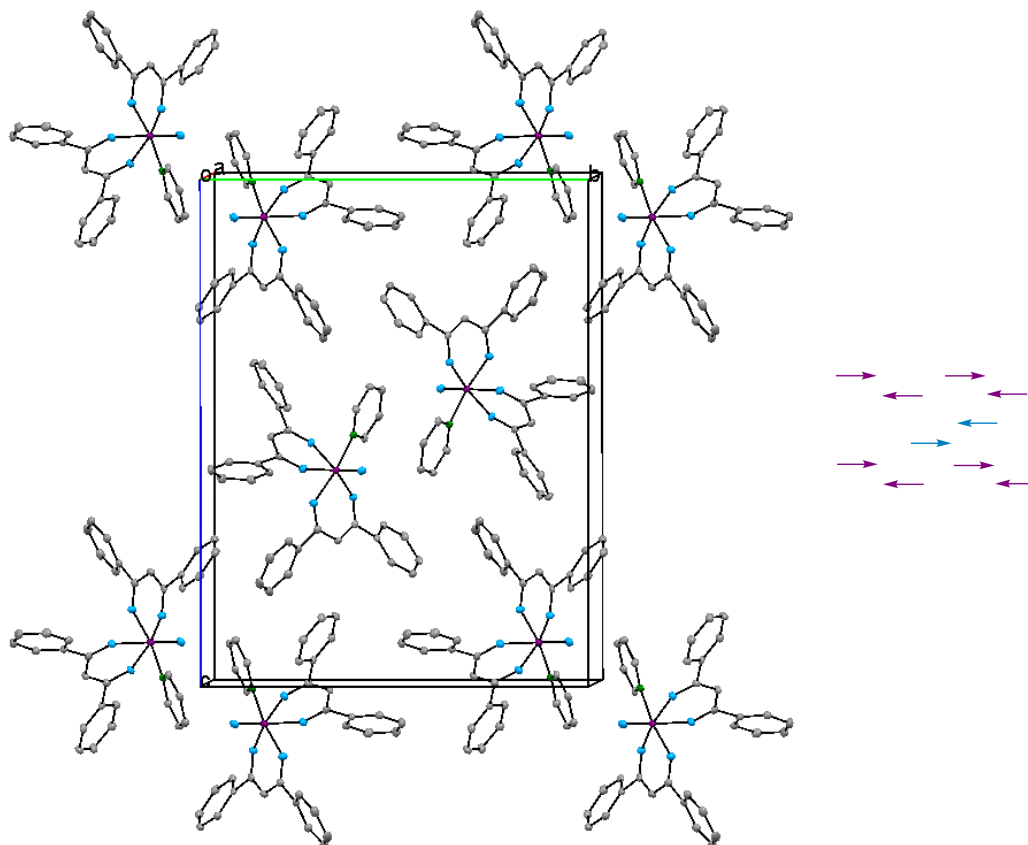
Figure 5.23: Packing of [VO(dbm)₂py] as viewed along the *a*-axis with accompanying packing motif. Hydrogens omitted for clarity.

5.7 Crystal Structure of *cis*-(C₉H₁₇O₂)[VO₂(cupf)₂]

The novel complex 2,2,6,6-tetramethyldihydropyran-4-onium bis-(N-nitroso-N-phenylhydroxylaminato-O,O')dioxidovanadium(V), (C₉H₁₇O₂)[VO₂(cupf)₂], crystallized in the monoclinic space group $P2_1/c$ with one cation and one [VO₂(cupf)₂]⁻ in the asymmetric unit. The vanadium complex is anionic with an overall -1 charge and crystallized with a novel organic counter-ion. The structure is represented with assigned numbering in Figure 5.24. Important bond distances and angles for the complex are listed in Table 5.12.

The vanadium metal centre is surrounded by two N-nitroso-N-phenylhydroxylamine ligands and two oxido bonds resulting in the -1 charge of the complex. The vanadium metal centre is situated on a glide plane along the *c*-axis. One of the bidentate ligands is situated in the equatorial plane whilst the other has the V1-O3 bond in the equatorial plane and the V1-O4 bond in the axial position. The V1-O1 bond lies in the equatorial plane whilst the V1-O2 bond is in the favoured axial position.
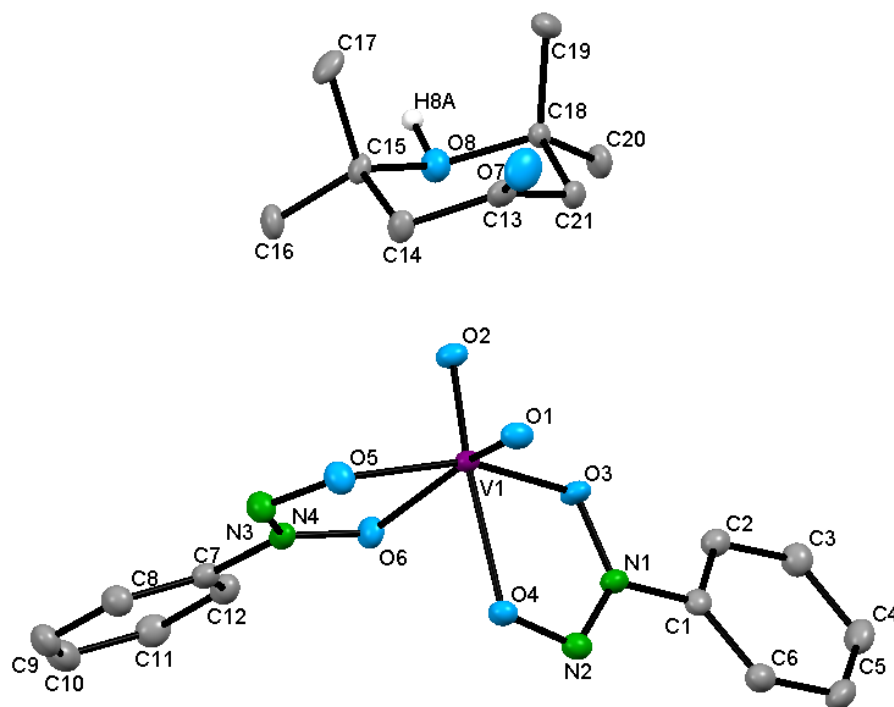
Figure 5.24: Structural representation of *cis*-(C₉H₁₇O₂)[VO₂(cupf)₂]. Hydrogen atoms have been omitted for clarity (thermal ellipsoid probability = 50 %).

Table 5.12: Important bond lengths and angles for $(C_9H_{17}O_2)[VO_2(cupf)_2]$.

Atoms	Bond Lengths (Å)	Atoms	Angle (°)
O1-V1	1.6561(6)	O4-V1-O3	73.16(5)
O2-V1	1.6353(6)	O5-V1-O6	72.61(6)
O3-V1	1.9661(6)	O1-V1-O2	104.78(7)
O4-V1	2.1757(7)	O1-V1-O3	106.01(7)
O5-V1	2.0053(7)	O2-V1-O3	91.37(6)
O6-V1	2.1455(7)	O1-V1-O4	88.47(7)
O3-N1	1.336(2)	O2-V1-O4	162.11(7)
O5-N3	1.324(2)	O1-V1-O5	88.51(7)
O4-N2	1.292(2)		
O6-N4	1.298(2)		
N1-N2	1.289(2)		
C13-C21	1.5074(4)		
C21-C18	1.5382(5)		
C18-O8	1.5212(4)		
O8-C15	1.5243(4)		
C15-C14	1.5391(5)		
C14-C13	1.5076(4)		

The V1-O1 and V1-O2 bond lengths are 1.6561(6) Å and 1.6353(6) Å respectively indicating that both these bonds are oxido bonds to the vanadium centre. There are only approximately 400 structures of vanadium known in the Cambridge Structural Database[39] with more than one oxido bond present.

The V1-O3, V1-O4, V1-O5 and V1-O6 bond lengths are ~2 Å indicating the single bond character of these bonds as with the previous structures reported in Sections 5.4, 5.5 and 5.6. The angle V1-O6-N4 was measured as 111.68 ° with the oxygen atoms displaying sp^3 hybridization being close to the idealized 109 °.[40]

The angles between O3-V1-O4 (73.16 °) and for O5-V1-O6 (72.61 °) are well in accordance with the bite angles found for other transition metal complexes with the

[39] Allen, F. H., *Acta Cryst.*, **2002**, *B58*, 380.
[40] Zumdahl, S. S., *Chemical Principles 6ᵗʰ edition*, Houghton Mifflin Company, USA, **2009**, A55.

cupferrate ligand such as the copper structure published by Charalambous *et al.*[41] that contained only one cupferrate ligand (75.08 °) and the rhodium structure by Venter *et al.*[42] (78.74 °).

The novel organic counter ion with a +1 charge that crystallized with the title compound (Figure 5.25 (a)) exhibits a chair conformation (Figure 5.25 (b)). It is postulated that 2,2,6,6-tetramethyldihydropyran-4-onium is formed by the acid catalyzed aldol condensation of three acetone molecules. The mechanism which is postulated for this reaction is given in Section 4.5. As mentioned in Section 5.5 the average C=O bond distance is 1.23 Å. This is in good agreement for the C13-O7 bond length of 1.2141(5) Å and indicates the double bond character of this bond. The C13-C21, C21-C18, C14-C13, C14-C15 bond lengths are approximately 1.5 Å indicating single bonds within the cyclic organic structure. The oxygen atom O8 was found to be protonated due to the presence of electron density at a suitable distance from this atom (1.0354(3) Å). This results in the organic compound yielding a +1 charge in contrast to the -1 charge of the vanadium complex.

a   **b**
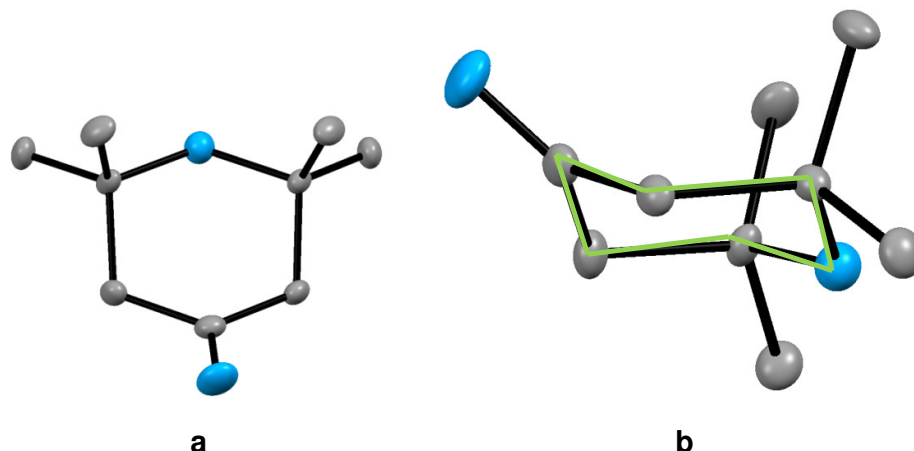
Figure 5.25: a) Illustration of 2,2,6,6-tetramethyldihydropyran-4-onium b) chair conformation of the cation. Hydrogen atoms omitted for clarity.

The vanadium complex exhibits a distorted octahedral geometry with the V(IV) atom lying above the basal equatorial plane as can be seen in Figure 5.26. The vanadium atom is situated 0.235(3) Å above the equatorial plane and is comparable to the reported value of 0.227 Å for the [VO(dbm)₂py] complex discussed in Section 5.6.

---

[41] Charalambous, J., Haines, L. I. B., Harris, N. J., Henrick, K., Taylor, F. B., *J. Chem. Res.*, **1984**, *220*, 2101.
[42] Venter, J. A., Purcell, W., Visser, H. G., *Acta Cryst.*, **2009**, *E65*, 1528.
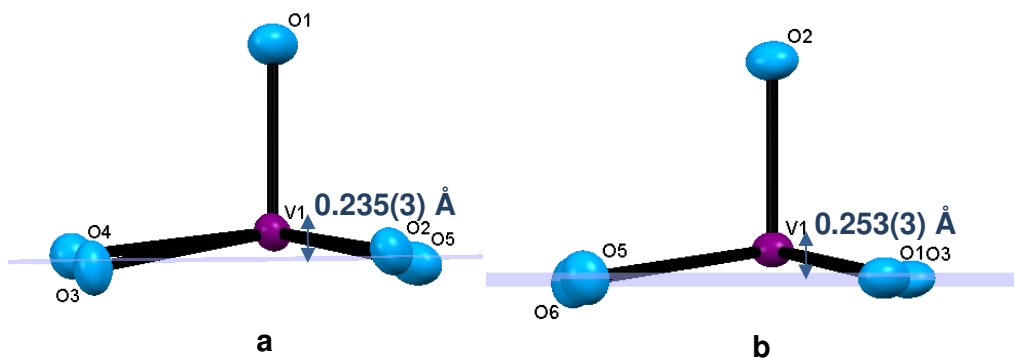
Figure 5.26: a) Plane intersecting the oxygen atoms in the equatorial plane with O1 as axial atom showing the distorted geometry with the vanadium lifted out of plane b) O2 as axial atom with a greater distortion of the vanadium atom.

To help understand why the two out of plane distances varies in the structure, the oxido bond distances as well as the distance between vanadium and the *trans* situated ligand need to be taken into account. These values are given in Table 5.13. The V1-O2 bond distance is much shorter (1.6353(6) Å) than the V1-O1 bond length (1.6561(6) Å). This implies that the V1-O2 bond is slightly stronger than the V1-O1 bond. This can be verified in terms of the *trans* situated atom distance to the vanadium centre. The V1-O4 bond length is 2.1757(7) Å whilst the V1-O6 bond distance is 2.1455(7) Å showing that the O4 atom is not as strongly bonded to the vanadium centre as the O6 atom. In Section 5.6 it was discussed how a stronger V=O bond implies a larger degree of distortion of the vanadium centre out of the equatorial plane. Thus, depending on which atoms are chosen for the equatorial plane, the V1-basal plane distance will differ as the two V=O bonds differ in strength within the structure.

Table 5.13: Different bond lengths influencing distortion within $(C_9H_{17}O_2)[VO_2(cupf)_2]$.

Atom in axial position	Bond	Bond length (Å)
O1	V1-O1	1.6561(6)
	V1-O6	2.1455(7)
O2	V1-O2	1.6353(6)
	V1-O4	2.1757(7)

Planes constructed through the two coordinated cupferrate ligands illustrate a near perfect arrangement in octahedral complexes (Figure 5.27). The measured dihedral angle between the plane O3, O4, N1, N2 (green) and the plane O5, O6, N3, N4 (pink) of 87.45 ° is close to the idealized 90 °.
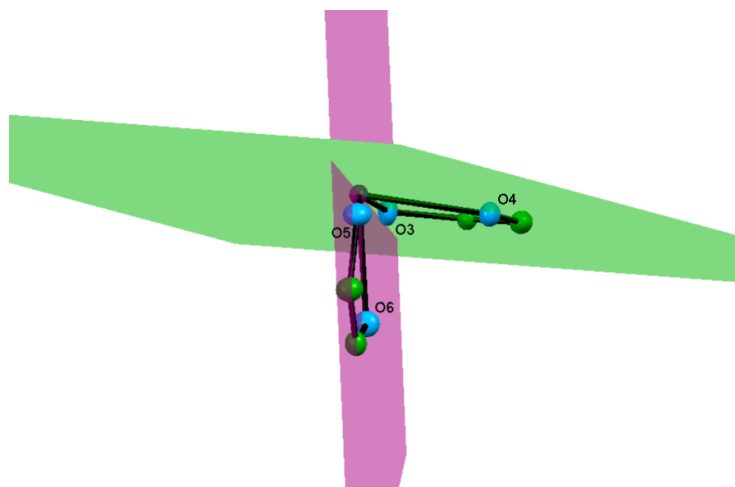
Figure 5.27: Planes constructed through the two cupferrato moieties coordinated to the vanadium centre illustrate a dihedral angle of 87.45 °.

As with the structures in Sections 5.4, 5.5 and 5.6, hydrogen bonding is present in the structure. Intermolecular interactions occur between the oxido groups bonded to the vanadium centre and various hydrogens of the cationic species present in the crystal structure. The four interactions are illustrated in Figure 5.28 and accompanying distances and angles of the contacts is given in Table 5.14. As with the [VO(dbm)₂] and the [VO(dbm)₂py] structures, the hydrogen bonding can be classified as weak hydrogen bonding and the influence in terms of packing within the crystal structure is limited by these interactions.
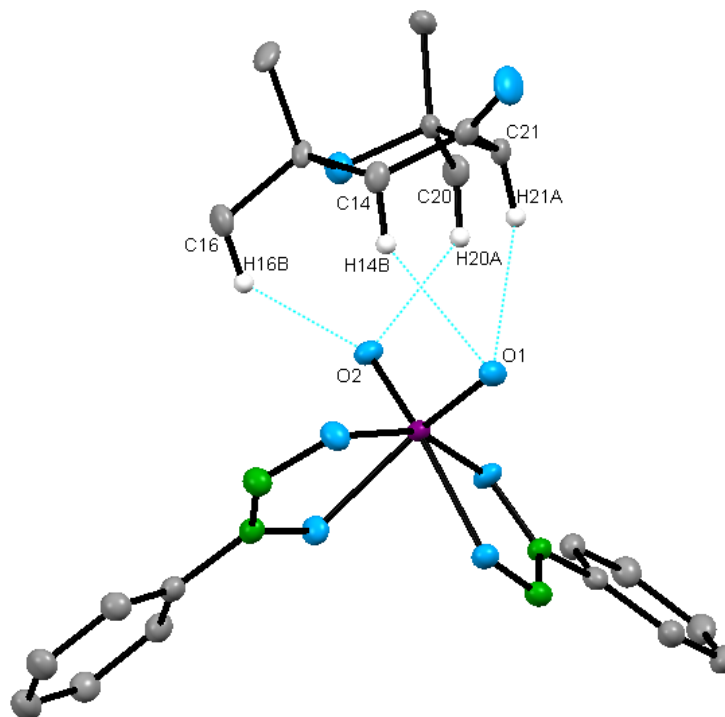
Figure 5.28: O···H interactions between the anionic vanadium compound and 2,2,6,6-tetramethyldihydropyran-4-onium. Hydrogens have been omitted unless involved in interactions.

Table 5.14: Hydrogen bonding for [VO$_2$(cupf)$_2$]⁻ and cation.

D-H···A	D(D-H) (Å)	D(H···A) (Å)	D(D···A) (Å)	<(DHA) (°)
C14-H14B···O1	0.9900(3)	2.5622(6)	3.4112(8)	143.75
C21-H21A···O1	0.9900(3)	2.5586(6)	3.4099(9)	144.05
C16-H16B···O2	0.9800(3)	2.5789(7)	3.3396(8)	134.48
C20-H20A···O2	0.9800(3)	2.6101(7)	3.3559(8)	133.0

Two other hydrogen bonding interactions are observed within the structure and are illustrated in Figure 5.29. The distances of the H-bond interactions are given in Table 5.15. The C19···N3 distance of 3.4763(9) Å is well in accordance with literature values reported by Kotzé[43] (3.253 Å) for hydrogen bonding involving nitrogen atoms.

---

[43] Kotzé, P. D. R., *PhD Thesis*, University of the Free State, **2010**, 171.
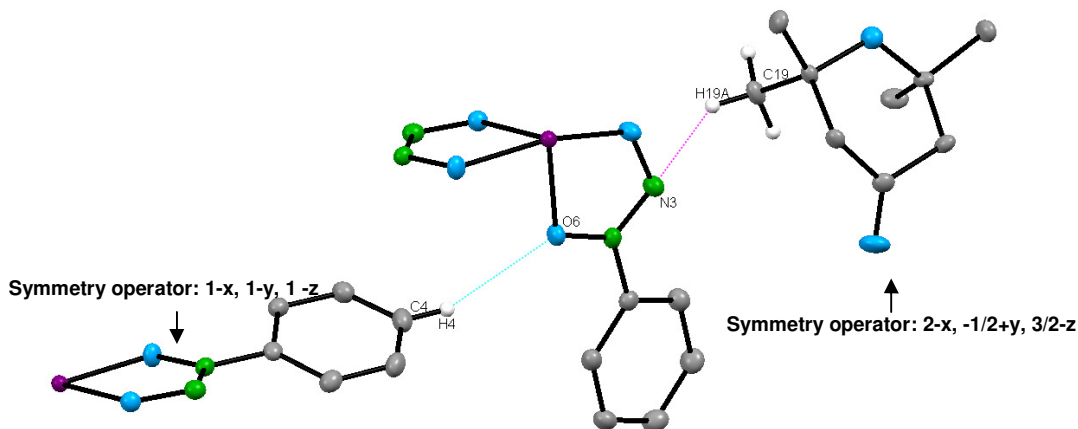
Figure 5.29: Illustration of the O···H and N···H interactions between two molecules. Some fragments have been omitted for clarity.

Table 5.15: Hydrogen bonding data from Figure 5.29.

D-H···A	D(D-H) (Å)	D(H···A) (Å)	D(D···A) (Å)	<(DHA) (°)
C19-H19A···N3	0.9800(3)	2.6240(6)	3.4763(9)	145.51
C4-H4···O6	0.9500(3)	2.6636(8)	3.4270(9)	137.77

Some π-stacking interactions are observed in the crystal structure between the two phenyl rings of two complex molecules as illustrated in Figure 5.30. These interactions are found between C1, C2 and C3 in a "tail-to-tail" mode and a centroid-to-centroid distance of 3.616 Å was determined.
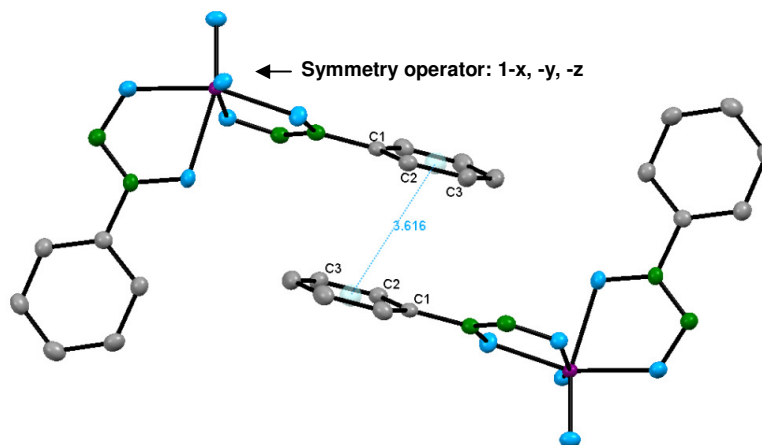
Figure 5.30: An illustration of the π-stacking found between phenyl rings of two molecules.

The packing of molecules within the unit cell is illustrated in Figure 5.31 with the packing motif illustrating a tail-to-tail arrangement of molecules due to the strong influence of π-π stacking of the phenyl rings.
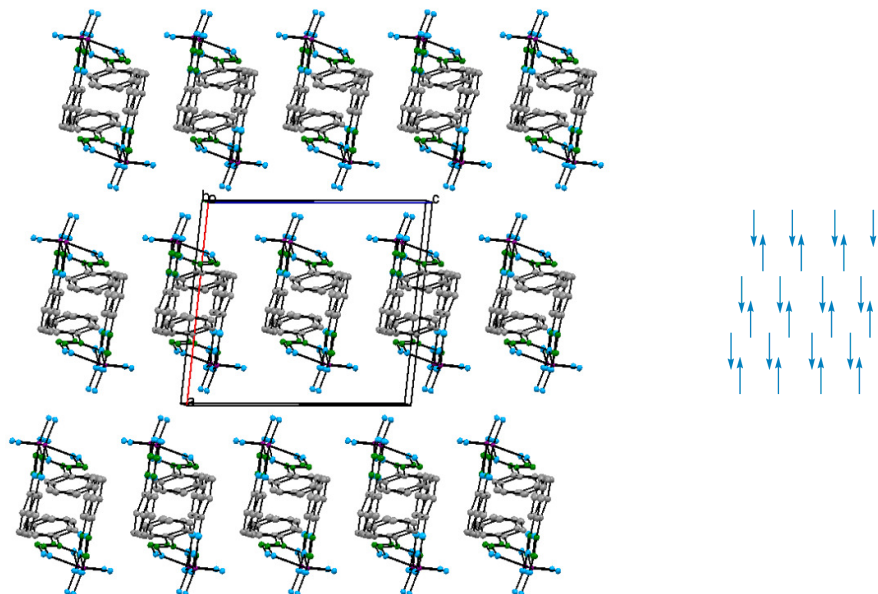
Figure 5.31: Packing for *cis*-(C$_9$H$_{17}$O$_2$) [VO$_2$(cupf)$_2$] with packing motif. A sheet-like packing along the *b*-axis is observed with a tail-to-tail arrangement of molecules. Cations have been omitted for clarity.

5.8 Comparison of [VO(dbm)$_2$], [VO(dbm)$_2$(MeOH)]•2MeOH, [VO(dbm)$_2$py] and (C$_9$H$_{17}$O$_2$)[VO$_2$(cupf)$_2$]

As stated in the introduction this study focused on different *O,O* and *N,O* ligands and that four of the successfully synthesized compounds were analysed by single crystal X-ray diffraction. In all the mentioned complexes an oxido bond was present as well as two coordinated bidentate ligands, In [VO(dbm)$_2$(MeOH)]•2MeOH and [VO(dbm)$_2$py] an additional ligand was coordinated. To compare these different structures the most important bond lengths and angles are summarized in Table 5.16 and labelled according to Figure 5.32.
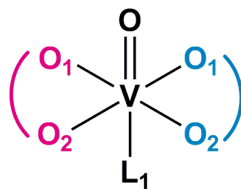
Figure 5.32: Labelling system for bond length and angle comparison in Table 5.16.

Table 5.16: Comparison of reported crystal structures for this chapter.

Compound	V=O (Å)	V-O_1	V-O_2	V-O_1	V-O_2	V-L_1
[VO(dbm)$_2$]	1.5922(4)	1.9566(5)	1.9515(4)	1.9616(4)	1.9728(3)	-
[VO(dbm)$_2$(MeOH)]	1.5964(3)	1.9973(7)	2.0045(5)	1.9847(8)	1.9940(2)	2.3022(5)
cis-[VO(dbm)$_2$py]	1.612(3)	2.004(3)	1.994(3)	2.138(3)	1.994(3)	2.154(4)
cis-[VO$_2$(cupf)$_2$]⁻	1.6561(6), 1.6353(6)	1.9661(6)	2.1757(7)	2.0053(7)	2.1455(7)	-

In all of the complexes the V=O bond lengths are within range for this type of bond.[44] As a *trans* coordinating moeity is added the V=O bond distance is increased indicating a loss in bond strength. Depending on the strength of the coordinating ligand the V-L1 bond length may be long, as for [VO(dbm)$_2$(MeOH)]•2MeOH, and thus the effect on the oxido bond is less pronounced and *vice versa*. As in the case of *cis*-(C$_9$H$_{17}$O$_2$)[VO$_2$(cupf)$_2$], the *trans* situated atom is part of the coordinating cupferrate ligand. This *trans* influence is further evident by the lengthening of the V-O bond lengths from ~2 Å to ~2.2 Å.

All of the complexes displayed distorted geometries where the five coordinated [VO(dbm)$_2$] displayed square pyramidal geometries and the six coordinated complexes yielding a typical octahedral geometry. The distortion distances of the vanadium centre from the equatorial planes are given in Table 5.17. From this table it can be seen that addition of a sixth ligand to fill the coordination sphere of the vanadium has a dramatic effect on the distortion of the geometry. In the absence of a ligand, such as in the [VO(dbm)$_2$] compound, the vanadium is merely influenced by the oxido group situated in the axial position. This has a 'pull' effect on the vanadium centre lifting the metal out of the least-squares equatorial plane. The addition of a ligand in the axial position *trans* to the oxido group decreases this effect and the vanadium is less distorted out of plane. A

---

[44] Rehder, D., *Bioinorganic Vanadium Chemistry*, Wiley & Sons, **2008**, 36.

weak coordinating ligand such as methanol influences the effect of the oxido group on the vanadium centre. It is however strongly coordinating ligands or *trans* situated atoms that have the largest impact on this value with distances almost a third (0.227 Å) in value when compared with the [VO(dbm)$_2$] structure (0.561 Å).

Table 5.17: Distances between vanadium and the basal plane in the complexes.

Compound	Distance of vanadium centre from the equatorial plane (Å)
[VO(dbm)$_2$]	0.57
[VO(dbm)$_2$(MeOH)]•2MeOH	0.33
***cis*-[VO(dbm)$_2$py]**	0.23
***cis*-(C$_9$H$_{17}$O$_2$)VO$_2$(cupf)$_2$]**	0.24, 0.25

Intrachelate O···O distances between the three dbm containing structures reported can also now be compared to the free ligand, 1,3-diphenyl-1,3-propanedionate. The intrachelate distances for the three related compounds reported in Sections 5.4, 5.5 and 5.6 are given in Table 5.18. For the three known polymorphs of the non-coordinated 1,3-diphenylpropane-1,3-dione, the O···O distances have been reported as 2.452 Å, 2.461 Å and 2.459 Å.[45,46,47] The shorter distance in the uncoordinated ligand could be attributed to the intramolecular hydrogen bond (O-H···O) found in the structure. Comparison between the compounds leads to the conclusion that the addition of a strongly coordinating sixth ligand such as pyridine to the complexes leads to an increase in these O···O distances between the oxygen donor atoms of the coordinated ligand.

[45] Etter, M. C., Jahn, D. A., Urbanczyk-Lipkowska, Z., *Acta Cryst.*, **1987**, *C43*, 260.
[46] Kaitner, B., Meštrović, E., *Acta Cryst.*, **1993**, *C49*, 1523.
[47] Ozturk, S., Akkurt, M., Ide, S., *Z. Kristallogr.*, **1997**, *210*, 627.

Table 5.18: Intrachelate O···O distances between the free dbmH ligand and in the compounds reported in Sections 5.3, 5.4 and 5.5.

dbmH	
Atoms	**Distance (Å)**
O1-O2	2.452, 2.461, 2.459

[VO(dbm)$_2$]	
Atoms	**Distance (Å)**
O2-O3	2.6847(7)
O5-O4	2.6953(7)

[VO(dbm)$_2$(MeOH)]	
Atoms	**Distance (Å)**
O2-O3	2.828(1)
O6-O5	2.7919(9)

[VO(dbm)$_2$py]	
Atoms	**Distance (Å)**
O2-O3	2.784(5)
O5-O4	2.759(5)

5.9   Conclusion

The aim of the research described in this chapter was to successfully characterize the complexes by single crystal X-ray diffraction which has clearly been achieved. The chosen complexes of [VO(dbm)$_2$], [VO(dbm)$_2$(MeOH)]•2MeOH, [VO(dbm)$_2$py] and *cis*-(C$_9$H$_{17}$O$_2$)[VO$_2$(cupf)$_2$] were discussed and important structural information highlighted. Additionally, interactions that play an essential role in the crystal structure were illustrated and discussed. Important differences were discussed between the crystal structures reported and further insight was gained with regard to key aspects of vanadium coordination chemistry. In the following chapter the substitution reaction of [VO(O$_2$)$_2$bpy]⁻ will be investigated to meet aim three of the objectives set for this project.

Chapter 6: Kinetic Study on Substitution Reactions of the [VO(O$_2$)$_2$bpy]$^-$ Complex

6.1   Introduction

Kinetic investigations provide insight into the mechanism by which a reaction occurs by taking into account the various factors which might affect the rate such as concentration, temperature, pressure variations, etc. Moreover, time-resolved progress of reactions is obtained. The properties of an organometallic complex further complicate kinetic investigations with the different metal centres as well as steric and electronic demands of the coordinated ligand playing a role in studies. As was mentioned in Chapter 1 and 2, peroxovanadates offers a wide and diverse chemistry. Peroxovanadates are known for their stability and their varied reactivity with kinetic investigations only recently being pursued.[1] By investigating substitution reactions, valuable insight might be gained with regard to coordination chemistry of vanadium and can find application for industrial uses where the interactions of catalysts and their stability are crucially researched. In the pharmacological field kinetics provide information regarding the lability of ligands and is used in design of future pharmaceutical agents. In particular, peroxovanadates hold application as insulin-mimicking agents and this necessitates further kinetic investigations regarding these complexes.

The kinetics and mechanism of the ligand substitution reaction of oxidobisperoxobipyridinevanadium(V) [VO(O$_2$)$_2$(bpy)]$^-$ with an entering ligand 2,3-pyridinedicarboxylic acid (2,3-dipic) has therefore been investigated as model reaction to illustrate the complexity of a seemingly 'simple' vanadium peroxo complex in this study and is reported in this chapter. The general reaction that was investigated is illustrated in Scheme 6.1. The study of this specific substitution reaction was chosen for comparison with related substitution studies by Hwang, Larson and Abu-Omar[2] concerning picolinic acid (pic) and 2,6-pyridinedicarboxylic acid (2,6-dipic) with the same vanadium complex. The comparison would yield valuable information with regards to mechanistic pathways

[1] Butler, A., Clague, M. J., Meister, G. E., *Chem. Rev.*, **1994**, *94*, 625.
[2] Hwang, J. H., Larson, R. K., Abu-Omar, M. M., *Inorg. Chem.*, **2003**, *42*, 7967.

for substitution with similar ligands as well as bring to light the influence of electronic factors with regard to entering ligand and other factors influencing the reaction.

bpVbpy

B-B = 2,3 bipyridine

L-L = 2,3 pyridinedicarboxylic acid, = O,N⌣OH
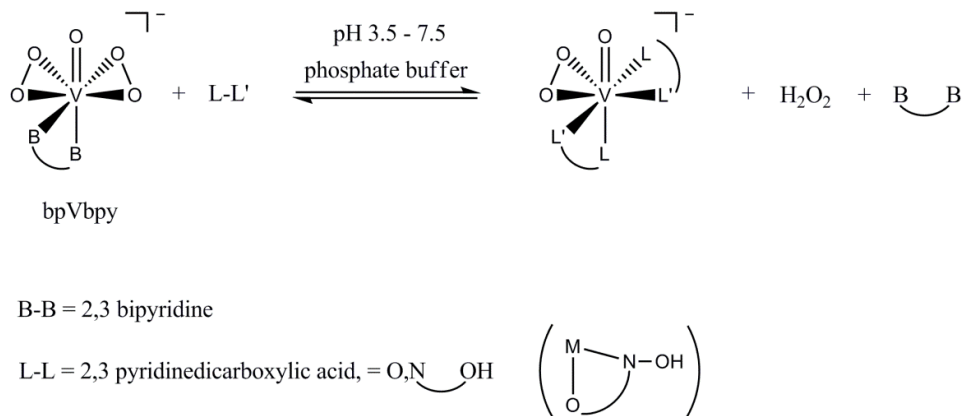
Scheme 6.1: General overview of the substitution reaction under investigation for [VO(O$_2$)$_2$(bpy)]$^-$.

6.2   Experimental Procedures

6.2.1 General Procedure

All reagents and chemicals were of analytical grade and purchased from Sigma-Aldrich South Africa. The synthesis of (NH$_4$)[VO(O$_2$)$_2$(bpy)] was performed according to the procedure given by Vuletic and Djordjevic.[3] Kinetic measurements were performed on a Varian Cary 50 Conc UV/Visible spectrophotometer. Temperature control of the reaction solutions was maintained to within ± 0.1 °C by means of a circulating water bath system. NMR spectroscopic data were obtained on a Bruker Avance II 600 MHz spectrometer at 158 MHz. ^{51}V NMR spectra were referenced externally to a saturated solution of sodium orthovanadate which has two active species in solution at pH 12, namely [VO$_4$]$^{3-}$ (δ= -535.7 relative to VOCl$_3$) and [V$_2$O$_7$]$^{4-}$ (δ= -559.0).[4] The Scientist Micromath, version 2.01[5] program and Microsoft Office Excel 2007[6] were used to fit the data to selected functions. All kinetic runs were performed under pseudo first-order conditions with the ligand concentration in excess in each case. A 0.10 M phosphate buffer solution ([NaH$_2$PO$_4$]/[Na$_2$HPO$_4$]) was used for all solutions and a constant ionic strength of µ =

[3] Vuletic, N., Djordjevic, C., *J. Chem. Soc., Dalton Trans.*, **1973**, 1137.
[4] Rehder, D., Hoch, M., Jameson, C. J*., Magn. Reson. Chem.*, **1990**, *28*, 128.
[5] Micromath Scientist for Windows, Version 2.01, Copyright © **1986 – 1995**, MicroMath, Inc.
[6] Microsoft Office Professional Edition 2007, Copyright © **2007**, Microsoft Corporation.

1.00 M was maintained by use of excess ammonium chloride in all experiments performed. The solid lines in the figures represent computer least-squares fits of data, while experimental values are represented as individual points, denoted by selected symbols. All the experimental data is given in the Appendix.

6.2.1 Treatment of Data

By using the Beer-Lambert law (see Chapter 3) followed by integration, an equation may be constructed for evaluation of absorbance change *vs* time in simple first-order reactions. This equation is given below in Eq. 6.1.

$$A_t = A_\infty - (A_\infty - A_0)e^{k_{obs}t}$$
(Eq. 6.1)

The pseudo first-order rate constant, k_{obs}, is obtained by a least squares fit of absorbance *vs* time for this first-order reaction. All the kinetic reactions performed in this study were fitted to this equation. Individual observed rate constants are reported in the Appendix (see A5).

6.3   Results and Discussion

6.3.1 Proposed Mechanism

A proposed reaction mechanism for the substitution reaction is presented in Scheme 6.2 as derived from experimental work that will be presented further in this chapter. In the first step of the proposed reaction mechanism the metal complex (Mb) can undergo a protonation step in solution (MbH$^+$) which is followed by the dissociation of the bpyH$^+$ ligand to yield the reactive bis-aqua species (M). The metal species can now undergo mono-substitution (MLH) with one 2,3-dipic ligand before a second ligand is coordinated (M(LH)$_2$). Finally, the kinetic product of a monoperoxo vanadium compound can also undergo a deprotonation step (MLLH) dependent on pH. Scheme 6.3 illustrates the different vanadium species in solution during the substitution reaction.

$$Mb + H^+ \underset{1/K_{av}}{\rightleftharpoons} MbH^+ \underset{-bH^+}{\overset{K_{dv}}{\rightleftharpoons}} M \underset{+LH}{\overset{K_2}{\rightleftharpoons}} MLH \underset{k_{3b}}{\overset{k_{3a} \ +LH}{\rightleftharpoons}} M(LH)_2$$

with pK_{aL} leading to MLLH.
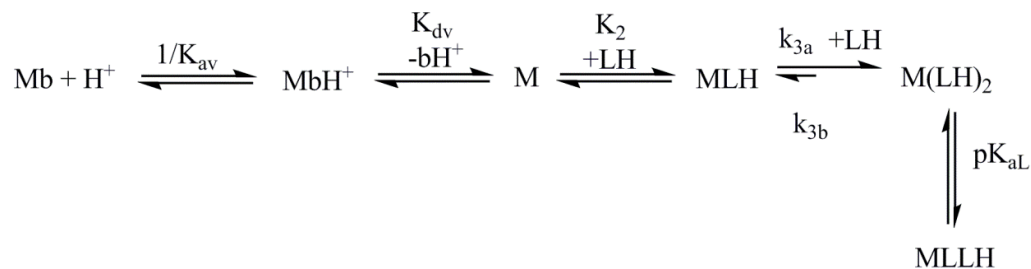
Scheme 6.2: Predicted mechanism of the ligand substitution reaction of $[VO(O_2)_2(bpy)]^-$ with 2,3-dipic.
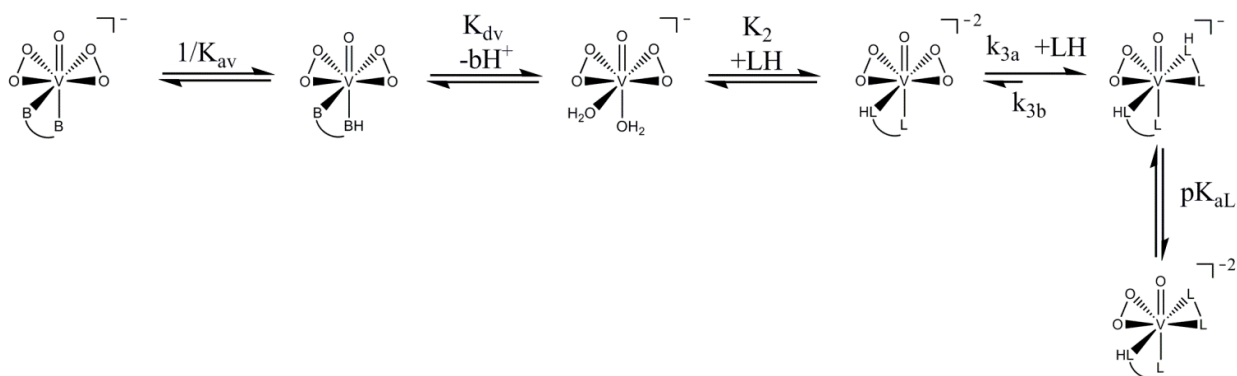
Scheme 6.3: Representation of the various vanadium species in solution during the substitution reaction according to the reaction mechanism given in Scheme 6.2.

The results from experimental studies to confirm the several steps associated with the substitution reaction will be discussed in the following paragraphs.

6.3.2 Detailed Analysis of Reaction Mechanism

In the following paragraphs different experiments are described that evaluate important aspects of the total reaction mechanism in a stepwise manner.

i.   The $[VO(O_2)_2(bpy)]^-$ complex was well characterized by IR, UV/Vis, single crystal X-ray diffraction and ^{51}V NMR.[2,3] A summary of the spectropscopic detail of $[VO(O_2)_2(bpy)]^-$ is given in Table 6.1.

Table 6.1: IR stretching frequencies, UV/Vis extinction coefficents, and ^{51}V NMR chemical shifts for the ammonium oxidobisperoxobipyridinevanadium complex.

	IR, cm^{-1}				UV/vis		^{51}V NMR
	ν (V=O)	ν (O-O)	ν (MO$_2$)	ν (MO$_2$)	λ, nm	ε, M^{-1}.cm^{-1}	δ, ppm
(NH$_4$)[VO(O$_2$)$_2$(bpy)]	929	858, 879	623	587	350	604	-748

ii. The entering ligand favours *N,O* coordination rather than *O,O* through both the carboxyl moieties. This was confirmed by a single crystal structure obtained in this study with the second free carboxylic acid group present (at the 3-position of the pyridine ring) in its protonated form (see Chapter 4). This has been confirmed to be the case also in other literature sources[7] and can be explained in terms of the more stable 5-membered chelate system compared to the 7-membered ring system for *O,O* coordination (see Figure 6.1).

More stable 5-membered chelate ring   Less stable 7-membered chelate ring
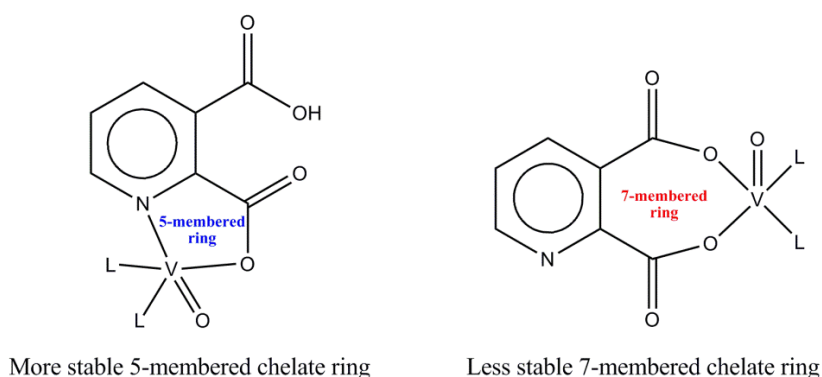
Figure 6.1: Ring strain comparison for the two binding modes of the 2,3-dipic ligand.

iii. The metal complex without addition of any ligand showed a reversible pH dependence as illustrated in Figure 6.2. Represented in the figure are the UV/Vis spectra recorded for the 0.9 mM [VO(O$_2$)$_2$(bpy)]$^-$ complex in aqueous solution at different pH values ranging from pH 6.5 to 3.5. Spectrum 1 is for the [VO(O$_2$)$_2$(bpy)]$^-$ solution at pH 6.5 and subsequent spectra represents a decrease in 0.5 pH units. The spectrum labelled as 8 represents a spectrum obtained after the solution at pH 3.5 had been re-adjusted to pH 6.5 indicating a small dilution effect. This showed that the process of protonation of the metal complex in solution was reversible.

---

[7] Shaver, A., Ng, J. B., Hall, D. A., Posner, B. I., *Mol. Cell. Biochem.*, **1995**, *153*, 5.
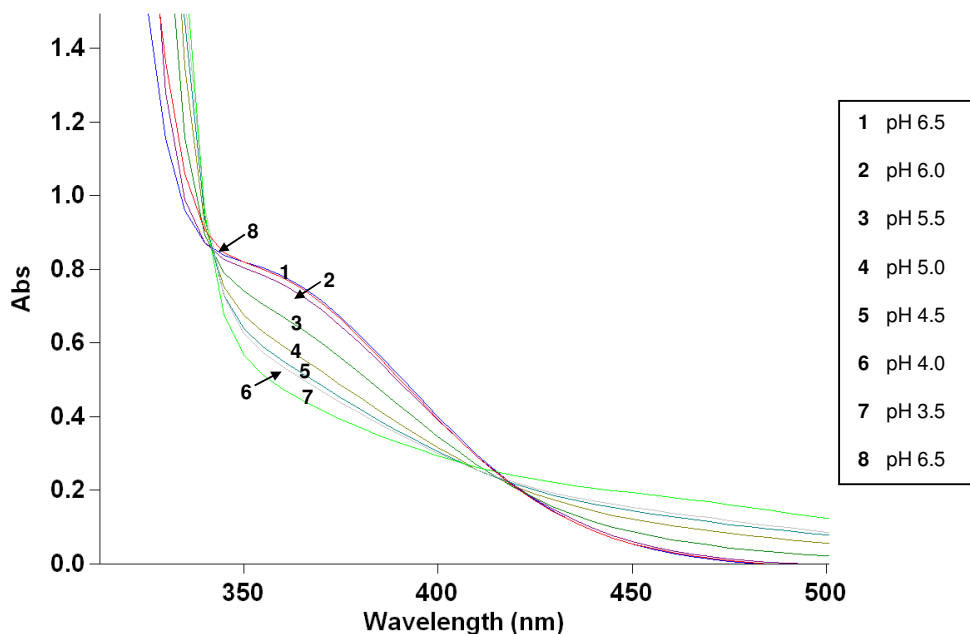
Figure 6.2: UV/Vis spectra of changes as a function of pH for a 0.90 mM [VO(O$_2$)$_2$(bpy)]⁻ complex in 0.10 M sodium phosphate buffer solution, μ = 1.00 M.

iv.   An absorbance *vs* pH plot fitted to Eq. 6.2 for the [VO(O$_2$)$_2$(bpy)]⁻ complex in solution revealed a pK$_a$ curve with a pK$_a$ value of 4.9(1) as shown in Figure 6.3.

$$A = \left(A_h + A_0 \left(\frac{10^{-pK_a}}{10^{-pH}} \right) \right) \Bigg/ \left(1 + \left(\frac{10^{-pK_a}}{10^{-pH}} \right) \right) \qquad \text{(Eq. 6.2)}$$

Where *A* is absorbance measured at a specific pH; *A$_h$*= absorbance of the protonated form; *A$_0$*= absorbance of deprotonated form.
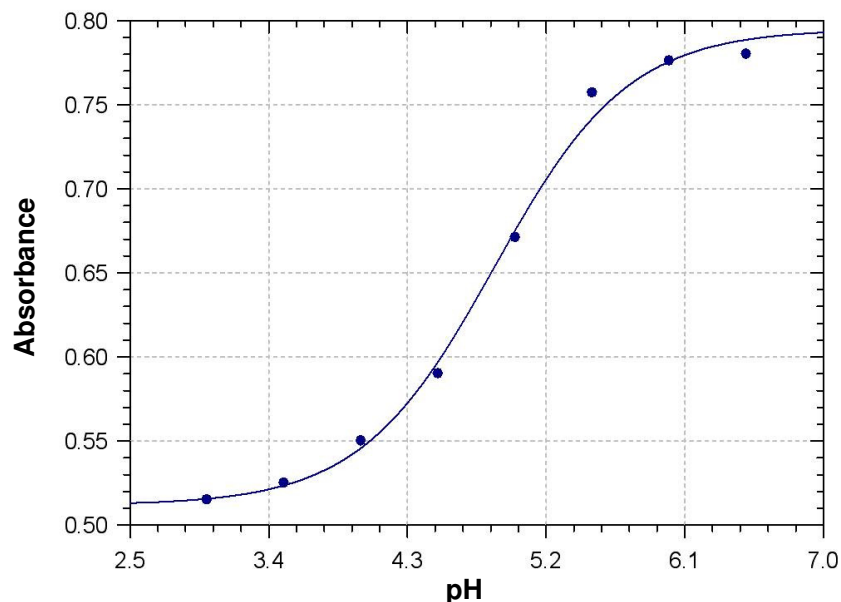
Figure 6.3: Absorbance for different pH values of 0.90 mM [VO(O$_2$)$_2$(bpy)]$^-$ at 360 nm in 0.10 M sodium phosphate buffer, μ = 1.00 M, pK$_a$ = 4.9(1).

v.   Following this information a series of concentrations of the entering ligand, 2,3-dipic was evaluated with the metal complex in a kinetic study *via* UV/Vis spectroscopy. A typical change in absorption spectra can be seen in Figure 6.4 with the change in absorbance against time shown in the insert, which in turn shows how the data was fitted for a one-step reaction (Eq. 6.1). In all kinetic experiments, the absorbance change was monitored at 350 nm since the absorption at this wavelength exhibited the maximum change upon ligand substitution. An isosbestic point at ~406 nm was observed for the reaction indicating that a single set of reactants yielded a single set of products in constant proportions.[8]

---

[8] Moore, J. W., Pearson, R. G., *Kinetics and Mechanisms 3rd edition*, Wiley-Interscience, **1981**, 49.
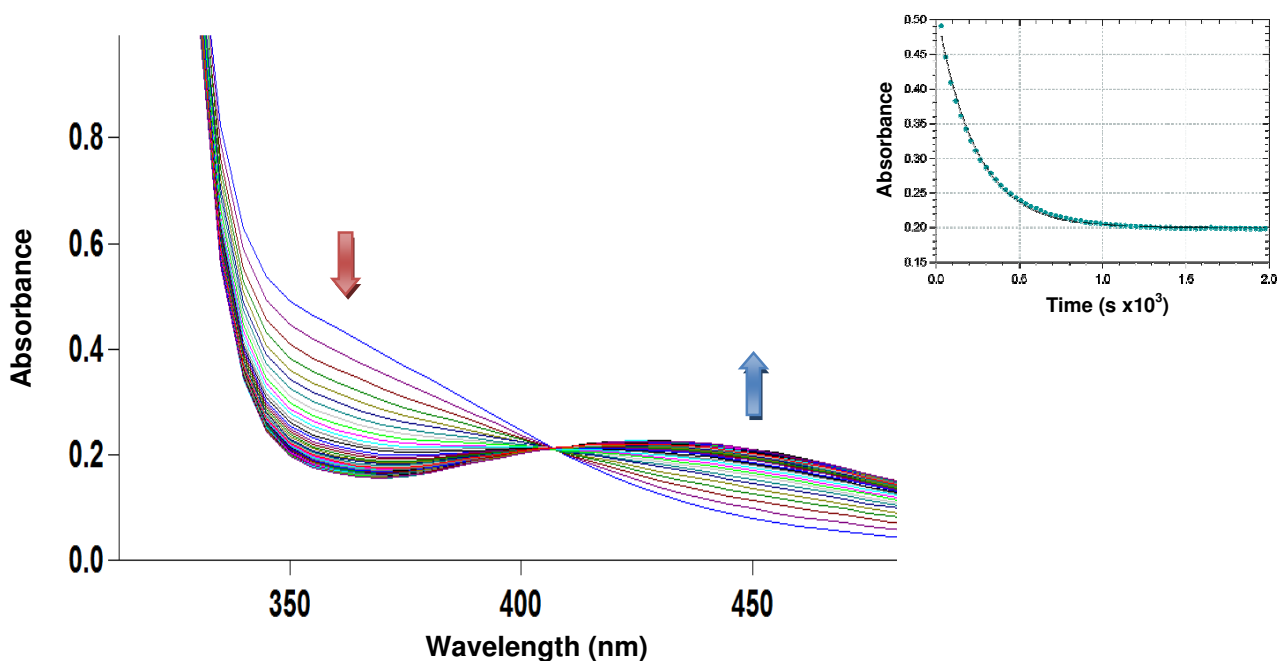
Figure 6.4: Absorption spectra of [VO(O$_2$)$_2$(bpy)]$^-$ (0.90 mM) at pH 5.0 in 0.10 M sodium phosphate buffer, μ = 1.00 M in the presence of 0.25 M 2,3-dipic, 25 °C, total time= 60 min. The insert represents the fitting of the experimental data at 350 nm for a one-step reaction.

vi.   To test whether the metal complex was in equilibrium with a deprotonated and protonated species a simple inhibition reaction was conducted by adding excess (10 times) hydrogen peroxide and 2,2-bipyridine to the reaction solutions, respectively, and comparing the rates of reaction with those obtained without such additions. Free 2,2-bipyridine inhibited the reaction as expected (see Figure 6.5 for the bpy addition) and was thus incorporated into the final rate law to be found at the end of this chapter. Excess hydrogen peroxide was less significant and was incorporated in reverse steps in the reaction mechanism although not directly introduced.
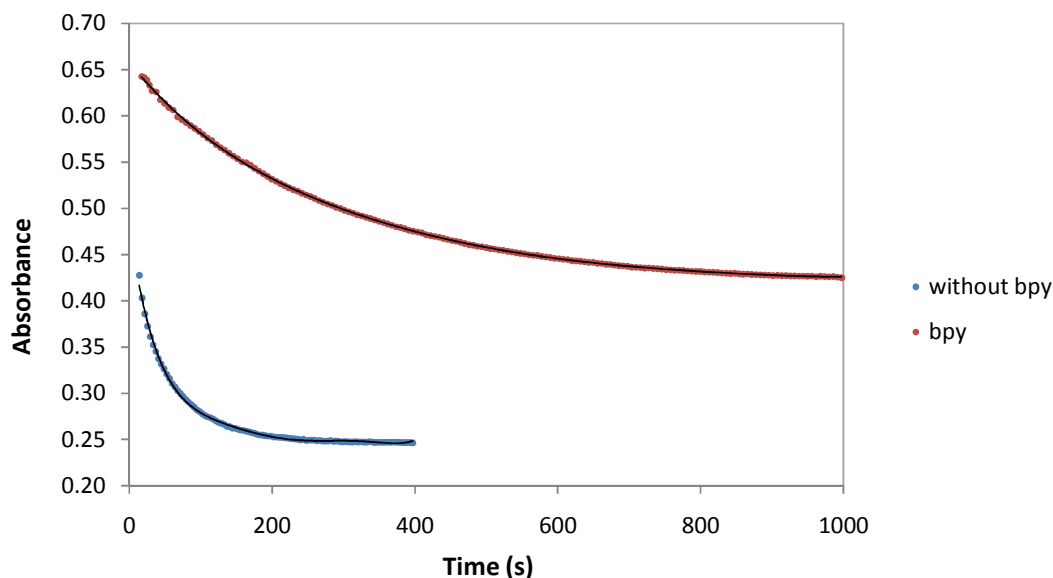
Figure 6.5: Plot of absorbance *vs* time for reaction of 0.90 mM [VO(O$_2$)$_2$(bpy)]$^-$ and 0.25 M 2,3-dipic in the absence (blue) and presence of 0.10 M 2,2 bipyridine (red) at λ = 350 nm, pH 4.5 and 25 °C in a 0.10 M sodium phosphate buffer solution, μ = 1.00 M.

vii. A temperature study was completed at pH 5 and the k_{obs} *vs* ligand concentration plots are shown in Figure 6.6. The linear trends indicated a first-order dependence on ligand concentration. Unfortunately, larger concentrations of the entering ligand ([2,3-dipic] > 0.3 M) was governed by solubility problems and could not be increased. The k_{obs} values nevertheless obtained from the temperature series may be compared to those obtained by Hwang *et al.*[2] and are given in Table 6.2. From the data given in Table 6.2 it can be seen that the rates obtained from this study are in good agreement with those given for substitution by picolinic acid.
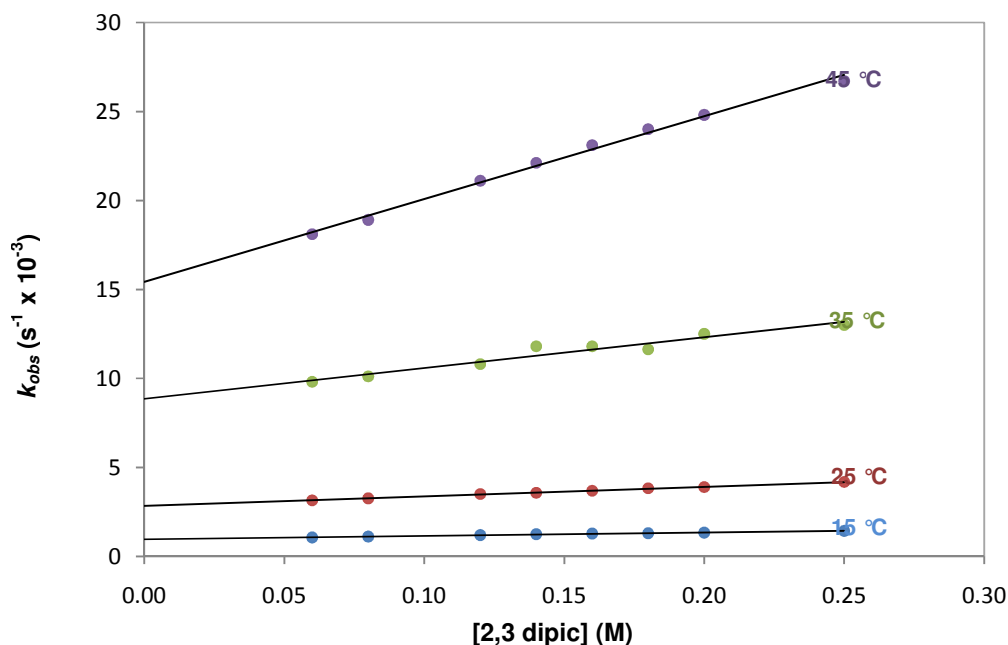
Figure 6.6: Plot of k_{obs} vs [2,3-dipic] for the reaction between [VO(O₂)₂(bpy)]⁻ and 2,3- dipic at different temperatures, [VO(O₂)₂(bpy)]⁻ = 0.90 mM, λ = 350 nm in a 0.10 M sodium phosphate buffer solution, μ = 1.00 M at pH 5.0.

Table 6.2: Rate constants for ligand substitution of [VO(O₂)₂(bpy)]⁻.

	Rate constants (k), L mol. s⁻¹			
T, K	2,3-dipic[a]	T, K	pic[b]	2,6-dipic[b]
288	$1.9(1) \times 10^{-3}$	283	1.38×10^{-3}	5.62×10^{-3}
298	$5.4(1) \times 10^{-3}$	293	4.35×10^{-3}	1.46×10^{-2}
308	$1.7(2) \times 10^{-2}$	303	1.20×10^{-2}	5.28×10^{-2}
318	$3.5(1) \times 10^{-2}$	313	3.11×10^{-2}	1.30×10^{-1}

[a] Results from this study; [b] Results published by Hwang, Larson and Abu-Omar[2]

viii.   The electronic nature of entering ligands plays an important role in the rates of reactions. When comparing 2,6-dipic with 2,3-dipic it can be seen how similar the structures are for these dicarboxylic acids (Scheme 6.4). Electronically, however, they are not the same. The 2,6-dipic has carboxylic groups attached to the pyridine moiety in a *ortho* position whilst 2,3-dipic is *ortho* and *meta* coupled. Electron withdrawing groups affects the *meta* position much more than the *ortho* positioned groups. It would thus be expected that the 2,3-dipic ligand act as a better nucleophile. However, the nitrogen atom located between two carboxylic acid groups in 2,6-dipic is more electron poor than the nitrogen atom of 2,3-dipic. This results in a faster reaction rate for 2,6-dipic as entering ligand as the proton is more easily removed. Additionally, 2,6-dipic binds in a tridentate fashion[7] to the metal centre where as 2,3-dipic has been established to coordinate in a bidentate manner (see Chapter 4). The difference in

bonding could also influence the rate of reaction. The pK_a of 2,3-dipic is reported in literature as 4[9] where as the pK_a for 2,6-dipic is given as 5.1[10]. This results in the deprotonation of 2,3-dipic occurring at a lower pH than 2,6-dipic as suggested.

picolinic acid
(pic)

2,6 pyridinedicarboxylic acid
(2,6-dipic)

2,3 pyridinedicarboxylic acid
(2,3-dipic)
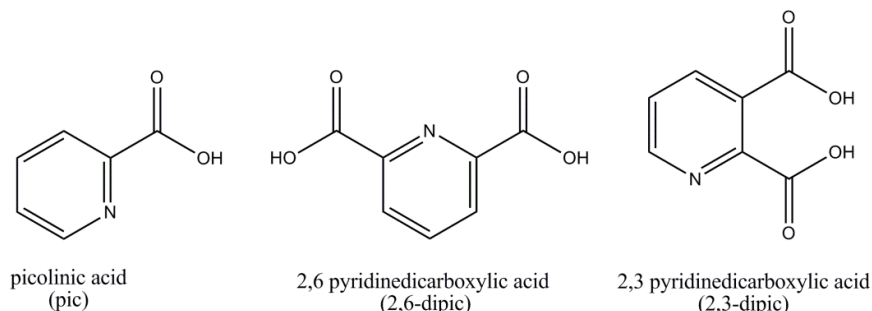
Scheme 6.4: Structural representations of the three ligands involved in substitution.

ix. To investigate what effect pH might have on the k_{obs} *vs* concentration plots a range of kinetic runs were performed with a range of ligand concentrations as well as varying the pH. The results of these experiments are represented in Figure 6.7. A linear trend was noted at each pH value and an increase in the rate of the reaction was observed as the pH was lowered at 25 °C. The reaction is thus clearly pH and concentration dependent. Figure 6.7 also explains the difference in rate constants given in Table 6.2. As Hwang *et al.*[2] had worked at pH 6.8 it would be expected that their rates would be lower than those reported for at pH 5 as is the case.

[9] Van der Westhuizen, H. J., Meijboom, R., Schutte, M., Roodt, A., *Inorg. Chem.*, **2010**, *49*, 9599.
[10] Dey, G. R., Kishore, K., Moorthy, P. N., *Radiat. Phys. Chem.*, **1997**, *49*, 9.
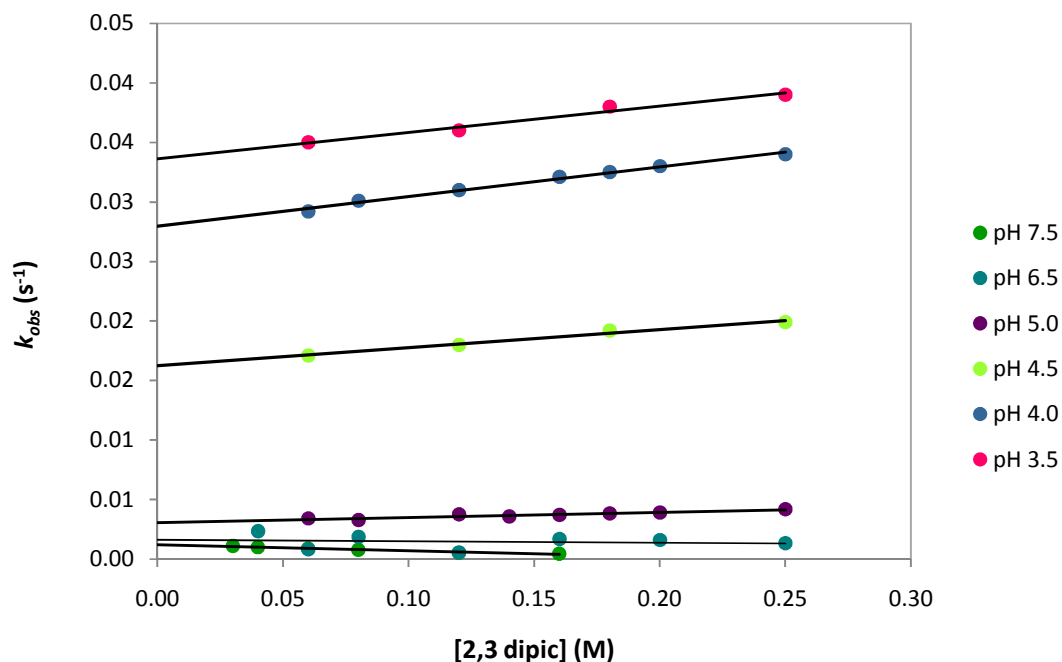
Figure 6.7: k_{obs} **vs concentration plots for 0.90 mM [VO(O₂)₂(bpy)]⁻ at different pH values in a 0.10 M sodium phosphate buffer solution, μ = 1.00 M at 25 °C .**

x. The k_{obs} vs pH plot for a constant ligand concentration (2,3-dipic = 0.12 M) is given in Figure 6.8, which illustrates the pH dependence of the reaction. The pK_a value was determined to be 4.44(2). This correlates fairly well with the pK_a value obtained for the metal complex in solution (4.9(1)).
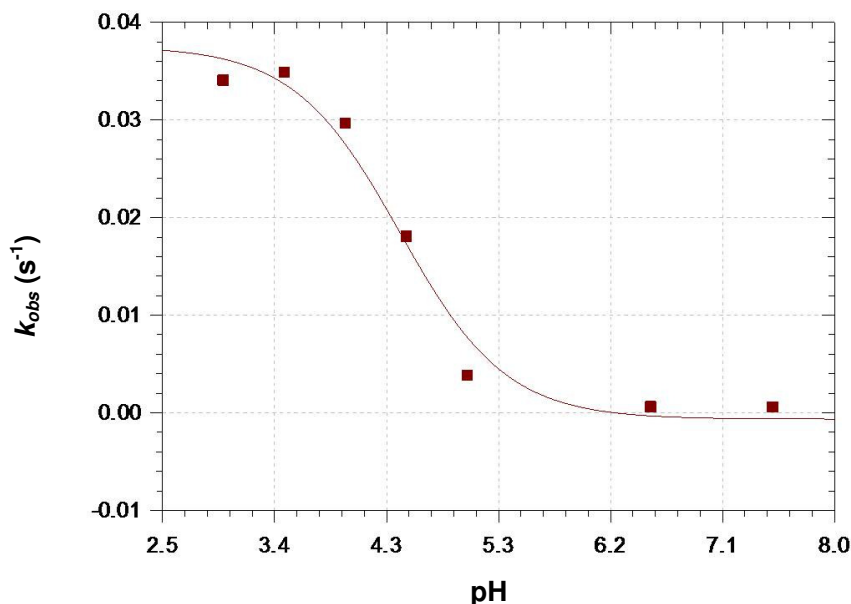
Figure 6.8: k_{obs} **vs pH plot for 0.90 mM [VO(O₂)₂(bpy)]⁻ at fixed ligand concentration of 0.12 M 2,3-dipic at 25 ° in a 0.10 M sodium phosphate buffer, μ = 1.00 M, pK$_a$ = 4.44(2).**

xi.   To gain further insight into how the reaction proceeds [51]V NMR studies were conducted. The metal complex was as with UV/Vis experiments tested for pH dependence and at pH 6.5 to 5 only one vanadium species was present in solution. The peak at ~-746 ppm was attributed to the [VO(O₂)₂(bpy)]⁻ complex as outlined in Table 6.1. At pH 4.5 it was found that a second vanadium species was present in increasing amounts in solution as the pH was lowered. This peak at ~-690 ppm was assigned as the bisperoxo-aqua species [VO(O₂)₂(H₂O)₂]⁻.[11] In Figure 6.9 the two vanadium species in solution at pH 4.5 are shown at -746 and -690 ppm. The bpy ligand thus dissociates upon protonation producing the bisperoxo-aqua species. This species was also acknowledged by Hwang *et al.*[2] in their studies, however at pH 6.8 they reported only observing the species appearing after 6 hours after preparing solutions. A very important point to note is the fact that the process is not simple protonation (then, only one V-species, with a pH dependent chemical shift would have been observed) but represents a protonation and dissociation. The complication of this is that both K$_{dv}$ and K$_{av}$ are small, and K$_{dv}$, K$_{av}$ ≤ 0.001, with pK$_{av}$ ≈ 4(from Figures 6.2 and 6.8).

---

[11] Conte, V., Di Furia, F., Stefano, M., *Inorg. Chim. Acta*, **1998**, *272*, 62.
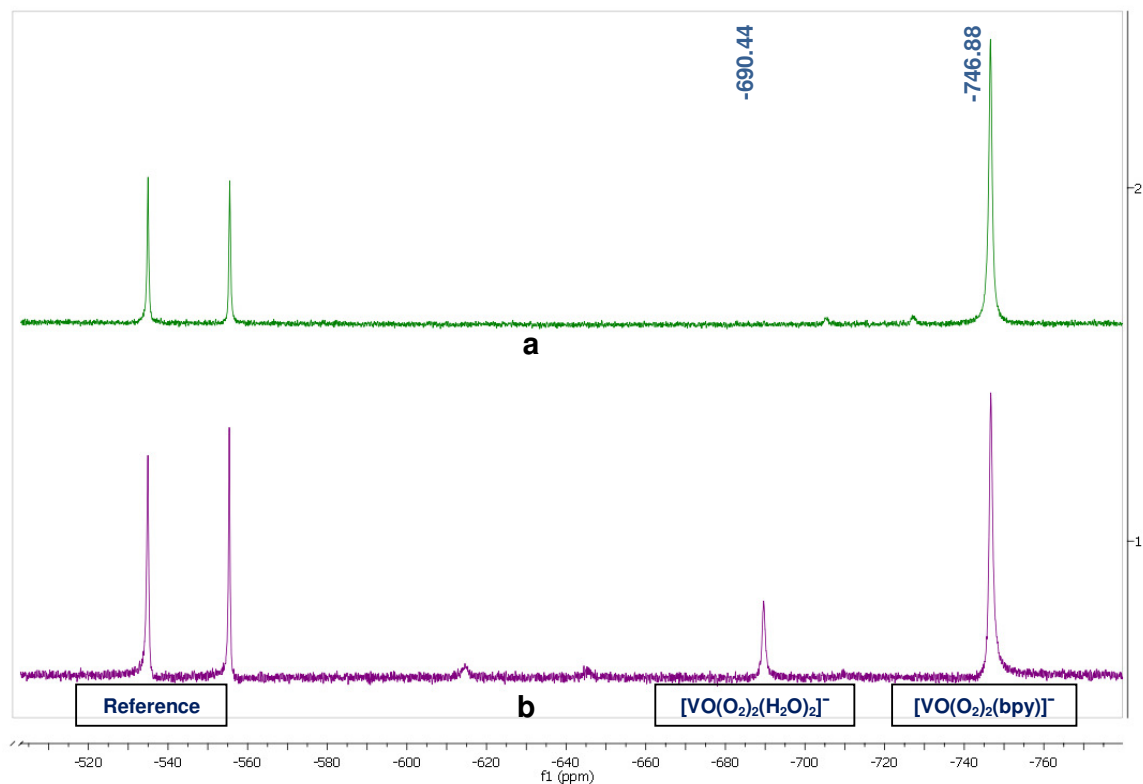
Figure 6.9: ^{51}V NMR spectrum of 0.90 mM [VO(O$_2$)$_2$(bpy)]$^-$ in a 0.10 M sodium phosphate solution (10 % D$_2$O), μ = 1.00 M at 20 °C with a) pH 6.5 and b) pH 4.5.

xii.   Following a kinetic study on ^{51}V NMR the following stacked plot provides information regarding the reaction mechanism.
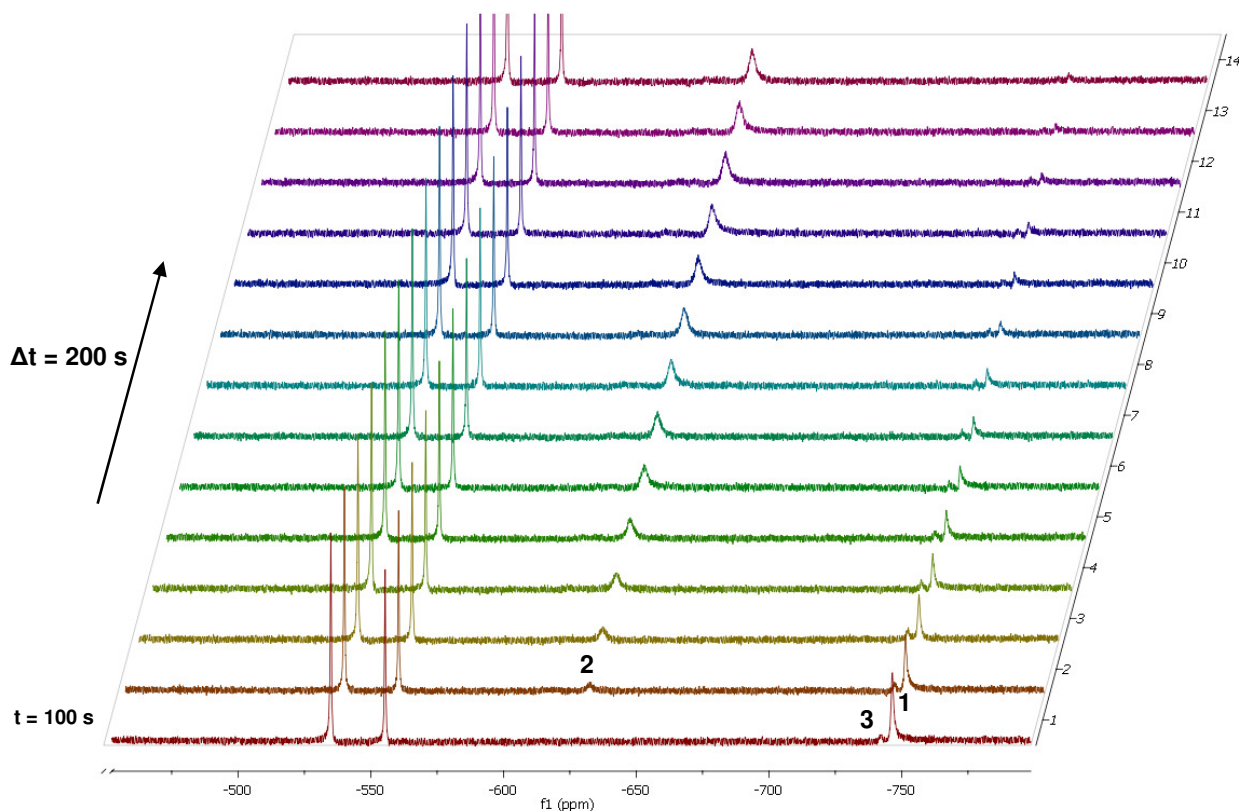
Figure 6.10: Representation of the resulting spectra after the addition of 0.25 M 2,3-dipic to 0.025 M [VO(O$_2$)$_2$(bpy)]$^-$ in a sodium phosphate buffer solution (10 % D$_2$O), μ = 1.0 M at pH 5.0 at 20 °C, followed over a period of 45 minutes.

The peak at -747 ppm (**1**) slowly disappears over time as the intensity of the peak at -627 ppm (**2**) increases with time. A plot can also be constructed of change in peak height *vs* time as shown Figure 6.11 for the disappearance of the [VO(O$_2$)$_2$(bpy)]$^-$ peak (**1**). The rate of disappearance of the [VO(O$_2$)$_2$(bpy)]$^-$ species and the consequent formation of the [VO(O$_2$)$_2$(2,3-dipic)$_2$]$^{2-}$ species (**2**) is in good agreement with that obtained from the UV/Vis kinetic study described earlier in this paragraph. The peak at -747 ppm has been established as the [VO(O$_2$)$_2$(bpy)]$^-$ complex in solution from characterization mentioned in Table 6.1. The peak at -627 ppm could also be identified and is assigned as a bis-picolinato complex and the product of the reaction.[12] It is however important to note that the mono-substituted complex (**3**) is always present in small amounts. This indicates that K$_1$ is fairly small, in the order of K ≤ 0.01.

---

[12] Rehder, D., Polenova, T., Bühl, M., *Ann. Rep. NMR Spectrosc*, **2007**, *62*, 33.
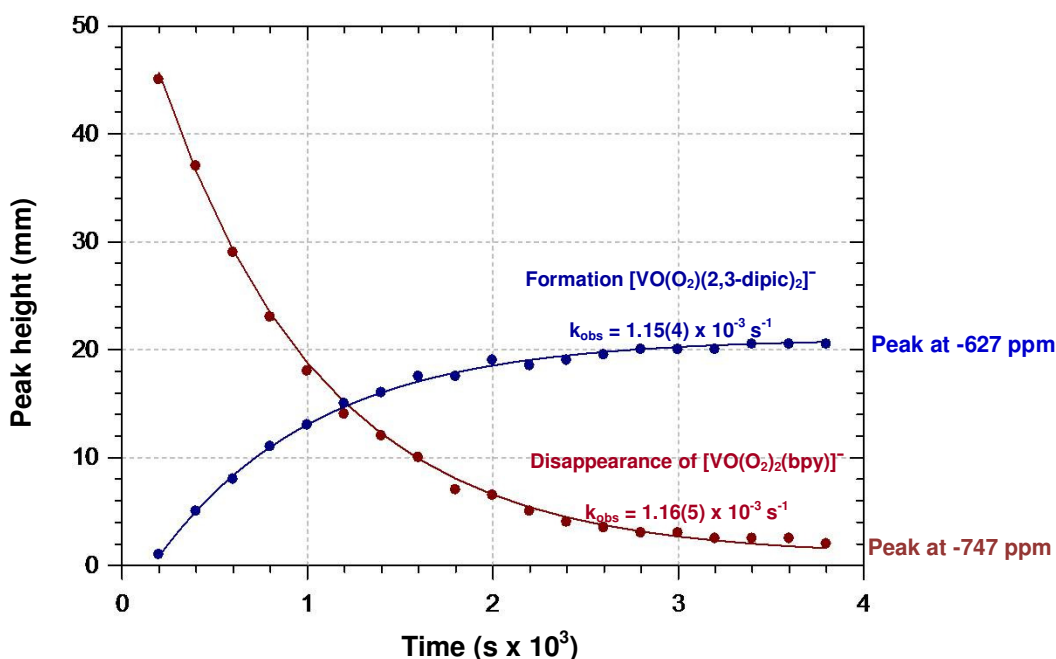
Figure 6.11: Plot of change in peak height *vs* time for the reaction between 0.025 M [VO(O₂)₂(bpy)]⁻ and 0.25 M 2,3-dipic in a 0.10 M sodium phosphate buffer solution (10 % D₂O), μ = 1.00 M, pH 5.0 at 20 °C.

xiii. Upon closer inspection a small peak next to the bulk [VO(O₂)₂(bpy)]⁻ peak at -747 ppm can be identified at -743 ppm (**3**) in Figure 6.10. This peak is known from literature as the mono-substituted pic system belonging thus to [VO(O₂)₂(2,3-dipic)]²⁻.[10] It can be concluded that due to the fact that this peak is present and then grows smaller as the reaction proceeds that the mono-substituted 2,3-dipic complex is an intermediate in the reaction mechanism. This thus confirms the formation of a mono-substituted complex described in the reaction mechanism given in Scheme 6.2.

6.4   Derivation of Rate Law

Based on the different detailed experiments and controlled experiments described in paragraph 6.3 it is concluded that the suggested reaction mechanism is a good representation of the overall process and the experimental data confirms all the separate steps outlined in Scheme 6.5. The derivation of the rate law can thus be given as follows:

$$Mb + H^+ \xrightleftharpoons{1/K_{av}} MbH^+ \xrightleftharpoons[\text{-bH}^+]{K_{dv}} M \xrightleftharpoons[\text{+LH}]{K_2} MLH \xrightleftharpoons[k_{3b}]{k_{3a} \quad \text{+LH}} M(LH)_2$$

$$\text{I} \qquad\qquad \text{II} \qquad\qquad \text{III} \qquad\qquad \text{IV}$$

$$\Updownarrow pK_{aL}\textbf{V}$$

$$MLLH$$
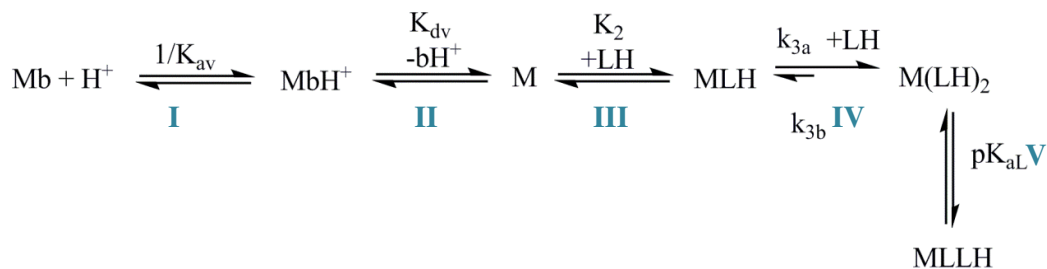
Scheme 6.5: Predicted mechanism of the ligand substitution reaction of $[VO(O_2)_2(bpy)]^-$ with 2,3-dipic.

Formation rate of $[M(LH)_2]$ (step IV) is given by:

$$\text{Rate} = k_{3a}[MLH][LH] - k_{3b}[M(LH)_2] \dots \textbf{0}$$

$$= \text{Rate}^f + \text{Rate}^r$$

Where the superscripts f and r represents the forward and reverse rates respectively.

The different Equilibrium constants associated with steps I – III are given by:

$$K_{av} = \frac{[Mb][H^+]}{[MbH^+]} \dots \textbf{1}$$

$$\therefore [Mb] = \frac{[MbH^+]K_{av}}{[H^+]} \dots \textbf{1a}$$

$$K_{dv} = \frac{[M][bH^+]}{[MbH^+]} \dots \textbf{2}$$

$$\therefore [MbH^+] = \frac{[M][bH^+]}{K_{dv}} \dots \textbf{2a}$$

$$K_2 = \frac{[MLH]}{[M][LH]} \dots \textbf{3}$$

$$\therefore [M] = \frac{[MLH]}{K_2[LH]} \dots \textbf{3a}$$

Just before step IV commences, the total concentration of vanadium species associated with the forward reaction (denoted by superscript 'f') is given by:

$$[M]_{tot}^f = [Mb] + [MbH^+] + [M] + [MLH] \dots \textbf{4}$$

137

$[M]_{tot}$ may be written in terms of 1a, 2a and 3a:

$$[M]_{tot} = \frac{K_{av}}{[H^+]} \cdot \frac{[bH^+]}{K_{dv}} \cdot \frac{[MLH]}{K_2[LH]} + \frac{[bH^+][MLH]}{K_{dv}[LH]} + \frac{[MLH]}{K_2[LH]} + [MLH] \quad x \quad \frac{K_2[LH]}{K_2[LH]}$$

$$[MLH] = \frac{[M]_{tot} \cdot K_2[LH]}{\frac{K_{av}}{[H^+]} \cdot \frac{[bH^+]}{K_{dv}} + \frac{[bH^+]}{K_{dv}} + 1 + K_2[LH]}$$

$$\therefore [MLH] = \frac{[M]_{tot} \cdot K_2[LH]}{1 + \frac{[bH^+]}{K_{dv}}\left(1 + \frac{K_{av}}{[H^+]}\right) + K_2[LH]} \quad \ldots \textbf{4a}$$

By considering Eq. 4a and Eq. 0 the forward rate therefore is represented by:

$$Rate^f = \frac{k_{3a}K_2[LH]^2[M]_{tot}^f}{1 + \frac{[bH^+]}{K_{dv}}\left(1 + \frac{K_{av}}{[H^+]}\right) + K_2[LH]} \quad \ldots \textbf{4b}$$

It is clear from Scheme 6.2 that the reverse rate also shows a pH dependence, for which the following equilibrium holds:

$$K_{aL} = \frac{[MLLH][H^+]}{[M(LH)_2]} \quad \ldots \textbf{5}$$

$$\therefore [MLLH] = \frac{[M(LH)_2]K_{aL}}{[H^+]} \quad \ldots \textbf{5a}$$

The total metal concentration for the reverse step may be written as:

$$[ML]_{tot}^r = [M(LH)_2] + [MLLH] \quad \ldots \textbf{6}$$

Substitute 5a in 6:

$$[M(LH)_2] = \frac{[ML]_{tot}^r}{1 + \frac{K_{aL}}{[H^+]}} \quad \ldots \textbf{6a}$$

This is consolidated into Eq.0 to give the reverse rate:

$$Rate^r = \frac{k_{3b}}{1 + K_{aL}} [ML]_{tot}^r \quad \ldots \textbf{7}$$

By combining Eq. 4b and 7, and utilizing pseudo first-order conditions ([L] >> [M]) the overall pseudo first-order rate constant is given by Eq. 6.3:

$$k_{obs} = \frac{k_{3a}K_2[LH]^2}{1 + \frac{[bH^+]}{K_{dv}}\left(1 + \frac{K_{av}}{[H^+]}\right) + K_2[LH]} + \frac{k_{3b}}{1 + \frac{K_{aL}}{[H^+]}} \qquad (Eq.\,6.3)$$

Eq. 6.3 is a sound representation taking all the experimental results into account.

However, using the complete rate law as given by Eq. 6.3 a very good simulation of the experimentally observed rate constants may be obtained. Figure 6.12 represents the simulation of the total kinetic behaviour of the system studied and clearly confirms the suggested overall mechanism and rate law with data fitted to the simulated trends. This illustrates the k_{obs} dependence on pH as well as [2,3-dipic].
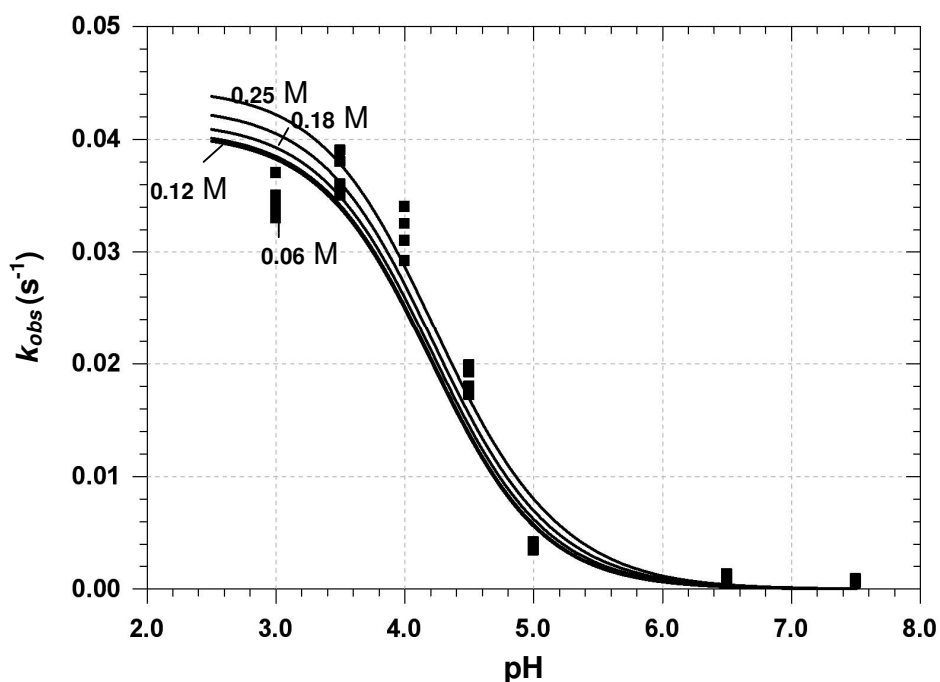
Figure 6.12: Simulated (solid lines) plots of the change in k_{obs} vs pH for constant [2,3-dipic] according to the rate law given in Eq. 6.3 with experimental data (■) fitted to the same equation.

Simplification of Eq. 6.3 is possible by utilizing the stepwise experiments described in paragraph 6.3.2. These include:

1) pK$_{av}$ ~ 4.5 from Figures 6.2 and 6.8 (par. 6.3.2 (iii) and (xi))
2) K$_{dv}$ ≤ 0.001 from Figure 6.8 (par. 6.3.2 (xi))
3) K$_1$ ≤ 0.01 from Figure 6.8 and par. 6.3.2 (xi)

Under these conditions, where the pH is varied between ca. 3 and 7 ([H+] ~ 10^{-3} to 10^{-7}), and in a range [2,3-dipic]= 0 – 0.3 M, the denominator in the first term of Eq. 6.3 (pseudo forward rate constant) simplifies to:

$$1 + \frac{[bH^+]}{K_{dv}}\left(1 + \frac{K_{av}}{[H^+]}\right) + K_2[LH] \approx K_2[LH] \dots \textbf{Eq. 8}$$

Thus, Eq. 6.3 simplifies to:

$$k_{obs} = \frac{k_{3a}K_2[LH]^2}{K_2[LH]} + \frac{k_{3b}}{1 + \frac{K_{aL}}{[H^+]}} \dots \textbf{Eq. 9}$$

$$k_{obs} = k_{3a}[LH] + \frac{k_{3b}}{1 + \frac{K_{aL}}{[H^+]}} \qquad (Eq. 6.4)$$

It is clear that under carefully preselected conditions, a linear reaction plot between k_{obs} and [2,3-dipic] may be obtained, as is illustrated in Figures 6.6 and 6.7 respectively.

Figure 6.13 illustrates the dependence from a different angle with k_{obs} vs [2,3-dipic]. Solid lines represent the simulated trends expected from the rate law stated in Eq. 6.3. Data obtained from this study is plotted against the simulated trends with good correlation visible taking into account the pH values for which the data is fitted were not truly representative of the actual pH the kinetic runs were performed at. This plot is comparable with Figure 6.7 showing good correlation between the predicted trends and the data obtained. The slight curvature of the simulated lines is clearly visible but the variation in [2,3-dipic] was too small to confirm this. However, the pseudo linearity is also clear. An interesting observation is the fact that the pseudo first-order rate constants is much more different (atleast in the pH and [2,3-dipic] range studied), on the intercept i.e. the reverse rate, which is underlined by Eq. 6.4.
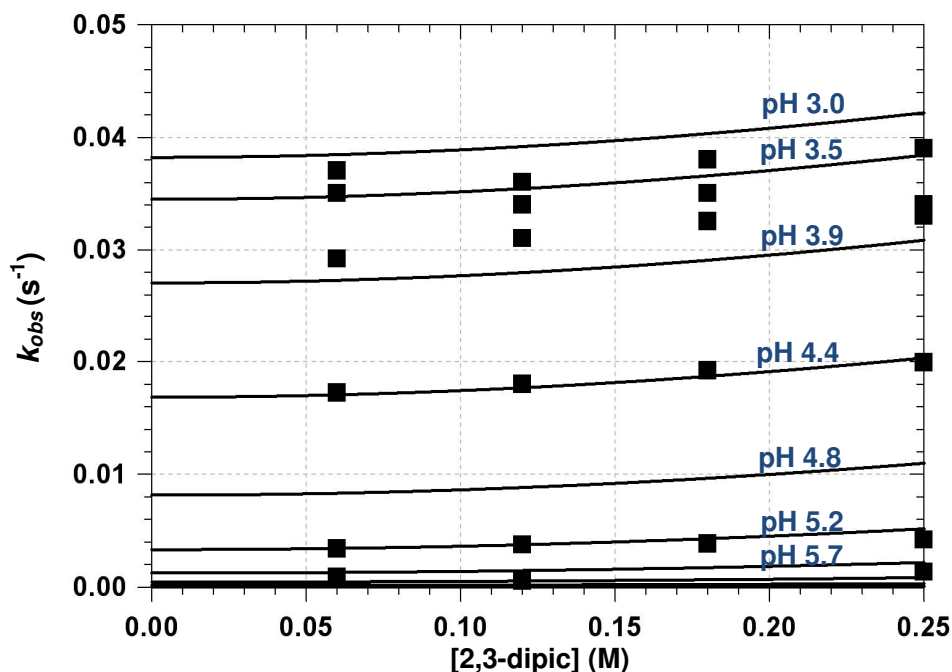
Figure 6.13: Simulated (solid lines) plots of the change in k_{obs} vs concentration 2,3-dipic at different pH according to the rate law given in Eq. 6.3 with experimental data (■) fitted to the same equation.

It is clear from the above discussion and illustrations that the derived rate law adequately describes the kinetic behavior of the overall reaction as presented in Scheme 6.2. A three-dimensional plot may be constructed to illustrate this dependence. Figure 6.14 shows how k_{obs} at high concentration 2,3-dipic and low pH will have larger values in contrast to high pH values where almost no increase in k_{obs} values is experienced, irrespective of ligand concentration. The three-dimensional plot also accurately describes the pH dependence as for example predicted and observed in Figure 6.12.
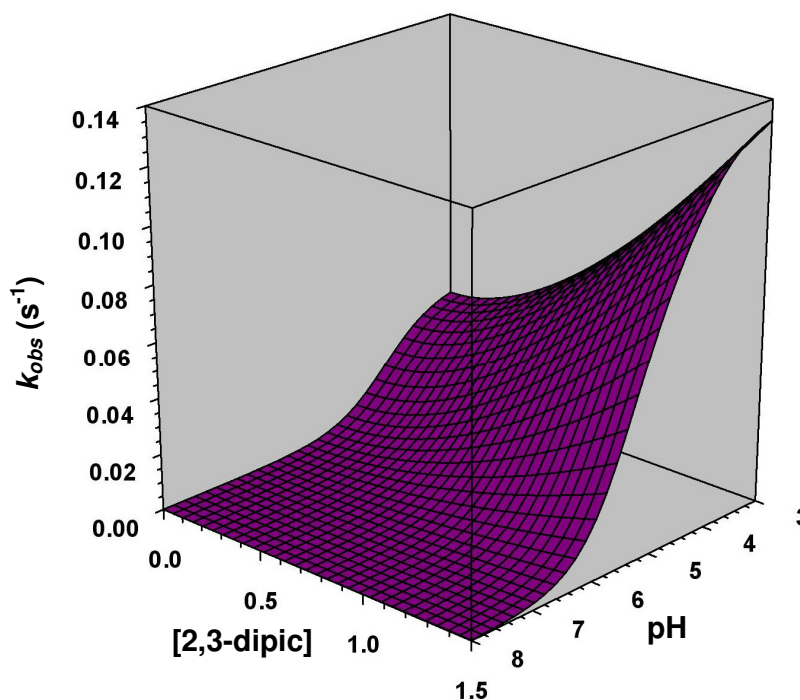
Figure 6.14: Three-dimensional plot to illustrate the dependence of the pseudo first-order rate constant on pH and [2,3-dipic] in a 0.1 M sodium phosphate buffer solution, μ= 1.0 M at 25 °C and [VO(O$_2$)$_2$(bpy)]$^-$= 0.9 mM.

6.5   Conclusion

A detailed investigation of the substitution reaction of [VO(O$_2$)$_2$(bpy)]$^-$ was included as part of this MSc study and the work thereof presented in this chapter. The entering ligand 2,3-dipic was chosen for its similarity to pic and 2,6-dipic but with different electronic properties. Work published with pic and 2,6-dipic could be used for comparison to build a knowledge base of the reaction mechanisms involved for substitution reactions for peroxovanadates. The result of the experimental work was the conclusion of a reaction mechanism involving multiple equilibrium steps with a pH dependence. All experimental work done on UV/Vis and ^{51}V NMR confirmed these equilibrium steps and the pH dependence involved. The substitution reaction illustrated the complexity of studying vanadium solution kinetics but was successfully completed to meet the main aims of this project. The potential complexity of seemingly 'simple' reactions should never be underestimated as clearly highlighted by this study.

Thus, kinetic studies are without doubt extremely vital in the evaluation of potential candidate pharmaceuticals as the lability of ligands must be determined at physiological pH. Several of the complexes synthesized for this study were evaluated in *in vitro* cancer screening tests. The results of these studies are discussed in the next chapter. Similarly, in complex catalytic processes, similar dynamic equilibria and substitution processes, as highlighted by this study, may always be present.

Proper understanding and corresponding management of a system such as this is clearly of significant importance where processes are to be applied in the most effective manner.

Chapter 7: *In Vitro* Cancer Screening of [VO(L,L¯-Bid)$_n$] Complexes

7.1 Introduction

The use of highly active drugs in cancer therapy has ensured that mortality rates from various tumour types have reduced. This is true, especially for platinum-based drugs with activity towards testicular, ovarian and bladder cancers. Platinum compounds have been applied successfully for over 25 years in cancer chemotherapy since the introduction of the parent compound *cis*-diamminedichloroplatinum(II), commonly called *cis*-platin[1]. This has sparked research into other metal complexes and their activity in a pharmaceutical sense.

As mentioned in Section 2.5.4 in Chapter 2, various vanadium compounds are being tested as metallopharmaceutical agents. A study by Thompson *et al.*[2] showed that the intake of vanadyl sulphate inhibited chemically induced mammary carcinogenesis (breast cancer) whilst various other studies are currently being conducted with inorganic vanadium compounds.[3,4,5]

The growth inhibitory effects of three vanadium(IV) and vanadium(V) complexes synthesized from this study were investigated and are reported in this chapter. Three cell lines were tested, consisting of TK-10 (human kidney carcinoma), UACC-62 (human melanoma) and MCF-7 (human mammary adenocarcinoma) cancer cells, using a Sulforhodamine B (SRB) assay.

---

[1] Rosenberg, B., *Cisplatin, Chemistry and Biochemistry of a leading Anticancer Drug*; Lippert, B., Ed.; Helvetica Chimica Acta: Zürich, **1999**, *4*, 3.
[2] Thompson, H. J. et al., *Carcinogenesis*, **1984**, *5*, 849.
[3] Narla, R. K., Chen, C. L., Dong, Y., Uckun, F., *Clin. Cancer Res.*, **2001**, *7*, 2124.
[4] Kanna, P. S., Mahendrakumar, C. B., Indira, B. N., Srivastawa, S., Kalaiselvi, K., Elayaraja, T., Chatterjee, M., *Environ. Mol. Mutagen.*, **2004**, *44*, 113.
[5] Bishayee, A., Chatterjee, M., *Bio. Trace Elem. Res.*, **1995**, *48*, 275.

7.2   SRB Assay

The SRB assay was developed by Skehan and co-workers[6] in 1990 to measure drug-induced cytotoxicity and cell proliferation. As a protein dye, sulforhodamine B is able to bind electrostatically to protein basic amino acid residues of trichloroacetic acid fixed cells. Binding to fixed cellular protein under mild acidic conditions, it can be extracted from cells and solubilized for measurement under mild basic conditions.

The SRB assay for this study was performed by the Council for Scientific and Industrial Research (CSIR), South Africa in accordance with the protocol of the Drug Evaluation Branch, NCI (National Cancer Institute).

7.3   Experimental

The effects of complexes on the growth of human cancer cell lines were evaluated according to the procedure adopted in the NCI's *in vitro* anticancer drug screening that uses the SRB assay[6] to assess growth inhibition.

The human cell lines TK-10, UACC-62 and MCF-7 were obtained from the National Cancer Institute (NCI) in line for collaboration with the CSIR. Cell lines were routinely maintained as monolayer cell cultures in RPMI-1640 containing 5 % heat-inactivated fetal bovine serum, 2 mM L-glutamine and 50 µg/ml gentamicin. For the screening experiment, the cells (3-19 passages) were inoculated in 96-well microtiter plates at plating densities of 7-10 000 cells/well and were able to attach during an incubation period of 24 hours. After 24 hours one plate was fixed with thrichloroacetic acid (TCA) to represent a measurement of the cell population for each cell line at the time of drug addition (T_0). The other plates with cells were treated with the experimental complexes which were previously dissolved in DMSO as 10 mM stock solutions and diluted in medium to a final concentration of 10 µM. Cells without complexes served as control standards, while blank wells contained complete medium without cells. Emetine (10 µM) was used as a reference standard as this compound is known for inhibitory growth effects.[7] The plates were incubated for 48 hours after the addition of the complexes. At the end of the incubation period, the cells were fixed to the bottom of each well with cold 50 % TCA,

---

[6] Skehan, P., Storeng, R., Scudiero, D., Monks, A., McHahon, J., Vistica, D., Warren, J. T., Bokesch, H., Kenney, S., Boyd, M. R., *J. Natl. Cancer Inst.*, **1990**, *82*, 1107.
[7] Grollman, A. P., *Journal of Biological Chemistry*, **1968**, *243*, 4089.

washed, dried and dyed with SRB. Unbound dye was removed and protein-bound dye was extracted with 10 mM Tris base (2-amino-2-hydroxymethyl-propane-1,3-diol) for optical density determination at a wavelength of 540 nm using a multiwall spectrophotometer. Optical density measurements were used to calculate the net percentage cell growth.

The percentage cell growth was calculated according to the following equations:

$$\% \text{ Growth} = \left[(T_i - T_0) \middle/ (C - T_0) \right] x\ 100 \quad for\ concentrations\ at\ which\ T_i \geq T_0 \quad \text{(Eq. 7.1)}$$

$$= \left[(T_i - T_0) \middle/ T_0 \right] x\ 100 \quad for\ concentrations\ at\ which\ T_i < T_0 \quad \text{(Eq. 7.2)}$$

The optical density of the test wells after the 48 hours of exposure to the test compounds is T_i, the optical density is given at time zero as T_0, and the control optical density as C.

7.4   Results

The growth inhibitory effects of three novel complexes of this study are listed in Table 7.1 along with five salicylaldehyde semicarbazone complexes with their activity as reported by Noblía *et al.*[8] The structures are shown in Scheme 7.1, and graphical representations of the results are given in Figures 7.1, 7.2 and 7.3.

The % growth indicates the total growth of cells in treated wells compared to untreated controls over the 48 hour period. A 100 % growth thus indicates the same count of cells in treated wells compared to untreated wells. 0 % Growth would indicate that no change in cell count occurred and -100 % implies no cells remained after the allocated time period.

---

[8] Noblía, P., Vieites, M., Parajón-Costa, B. S., Baran, E. J., Cerecetto, H., Draper, P., González, M., Piro, O. E., Castellano, E. E., Azqueta, A., López de Ceráin, A., Monga-Vega, A., Gambino, D., *J. Inorg. Biochem.*, **2005**, *99*, 443.

[VO(trop)$_2$(OMe)]   [VO(dbm)$_2$]

(C$_9$H$_{17}$O$_2$)[VO$_2$(cupf)$_2$]

L^1: R$_1$ = H,   R$_2$ = H   VO$_2$L^1
L^2: R$_1$ = n-butyl,   R$_2$ = H   VO$_2$L^2
L^3: R$_1$ = 2-naphtyl,   R$_2$ = H   VO$_2$L^3
L^4: R$_1$ = H,   R$_2$ = Br   VO$_2$L^4
L^5: R$_1$ = H   VO$_2$L^5

[VO$_2$L]
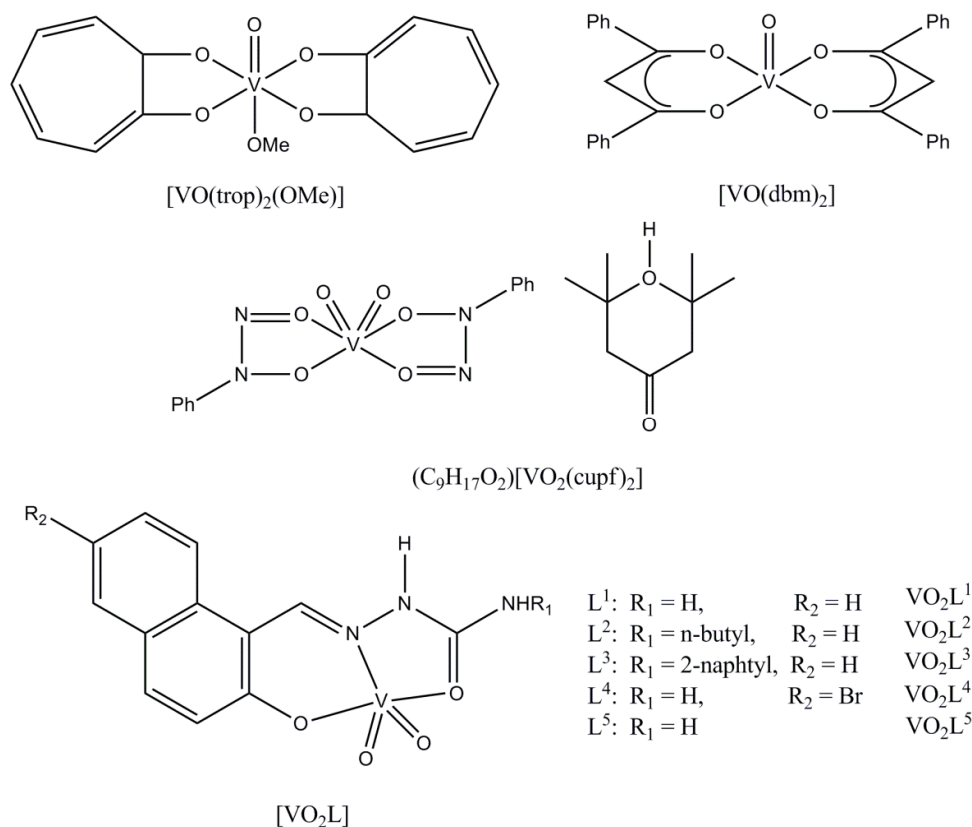
Scheme 7.1: Complexes studied for activity in three cancer lines.

Table 7.1: Net growth results of vanadium complexes against renal, melanoma and skin cancer lines.

Nr.	Compound	Concentration (µM)	Reference	TK-10 (%)	UACC-62 (%)	MCF-7 (%)
1	[VO(trop)$_2$(OMe)]	10	a	-4.41(2)	-21.7(2)	15.14(1)
2	[VO(dbm)$_2$]	10	a	25.69(3)	15.68(8)	36.72(1)
3	[VO$_2$(cupf)$_2$]$^-$	10	a	37.99(1)	34.5(1)	75.62(6)
4	[VO$_2$L^1]	100	b	-60(4)	-	10(1)
5	[VO$_2$L^2]	100	b	-55(3)	-	57(5)
6	[VO$_2$L^3]	100	b	-83(5)	-	68(5)
7	[VO$_2$L^4]	100	b	-34(2)	-	-
8	[VO$_2$L^5]	100	b	-7.0(5)	-	-
9	**Emetine**	**10**	**a**	**-61.980(2)**	**-94.230(5)**	**-47.24(1)**

[a] results from this MSc study, [b] results by Noblía *et al.*[1]
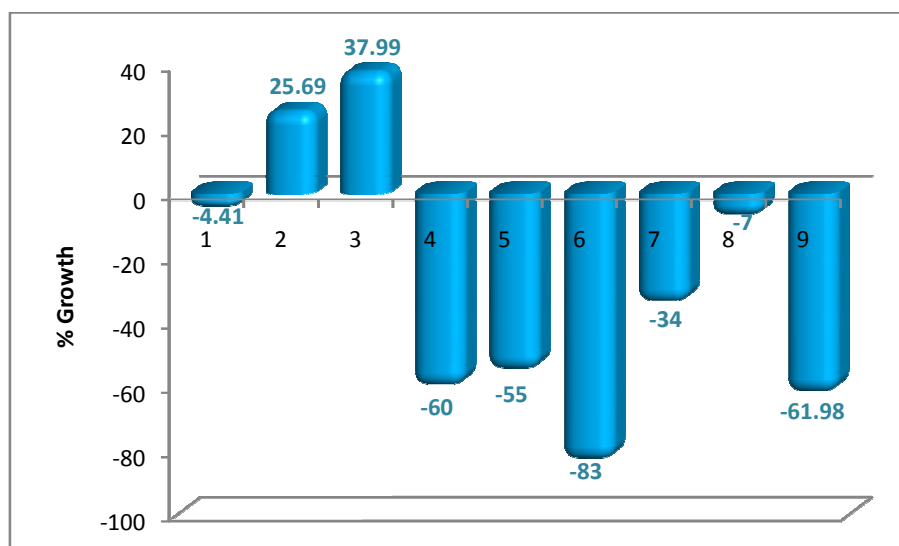
Figure 7.1: % Growth observed for compounds in renal cancer cells (TK-10).
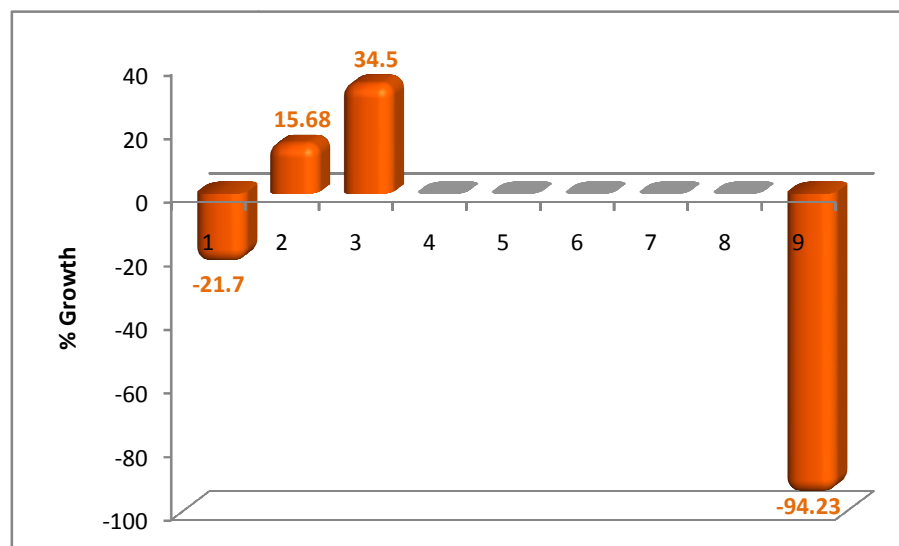
Figure 7.2: % Growth observed for compounds in melanoma cancer cells (UACC-62).
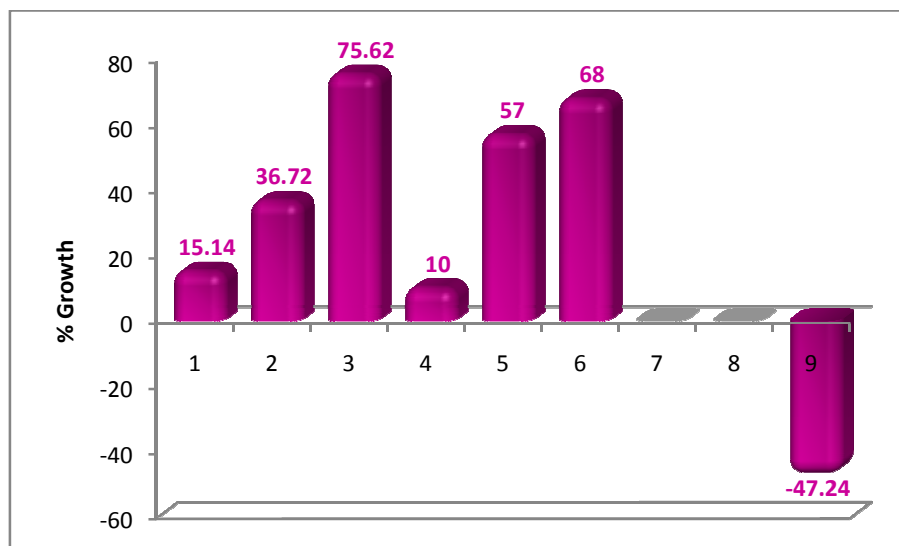
Figure 7.3: % Growth observed for compounds in breast cancer cells (MCF-7).

7.5 Discussion

The results in Table 7.1 illustrate the complexes reported by Noblía *et al.*[7] exhibit high activity against the TK-10 cancer line whilst only one complex of the three tested from this study showed some activity. [VO(dbm)$_2$] and (C$_9$H$_{17}$O$_2$)[VO$_2$(cupf)$_2$] suppress cancer cell growth. Only complex **1** showed cytotoxic activity in the tests conducted with melanoma cancer cells whilst complexes **2** and **3** induced growth. In the test against breast cancer all the complexes tested exhibited growth of cancer cells without any cytotoxic activity. Complex **4** showed the largest inhibition of growth whereas (C$_9$H$_{17}$O$_2$) [VO$_2$(cupf)$_2$] (complex **3)** induced the largest amount of growth.

To illustrate the importance of even negative results, a comparison is made between [VO(trop)$_2$(OMe)] and a free tropolone derivative, theaflavin-3-gallate.[9] The relationship between the activities exhibited by these two compounds is illustrated in Figure 7.4. Theaflavins are tropolone derived compounds with benzotropolone skeletons, found in tea. It can be seen from Figure 7.4 that the theaflavin compound has high cytotoxic activity against the MCF-7 cell line whereas the tested complex from this study, [VO(trop)$_2$(OMe)], induced growth. From comparisons like these between free ligands and coordinated metal complexes a conclusion may be made on whether the metal has

---

[9] Friedman, M., Mackey, B. E., Kim, H., Lee, I., Lee, K., Lee, S., Kozukue, E., Kozukue, N., *J. Agric. Food. Chem.*, **2007**, *55*, 243.

an inhibiting effect on the activity of a ligand or an enhancing effect. It may be suggested from Figure 7.4 preliminarily that the coordination to vanadium has an inhibiting effect on the activity of tropolone derived ligands.
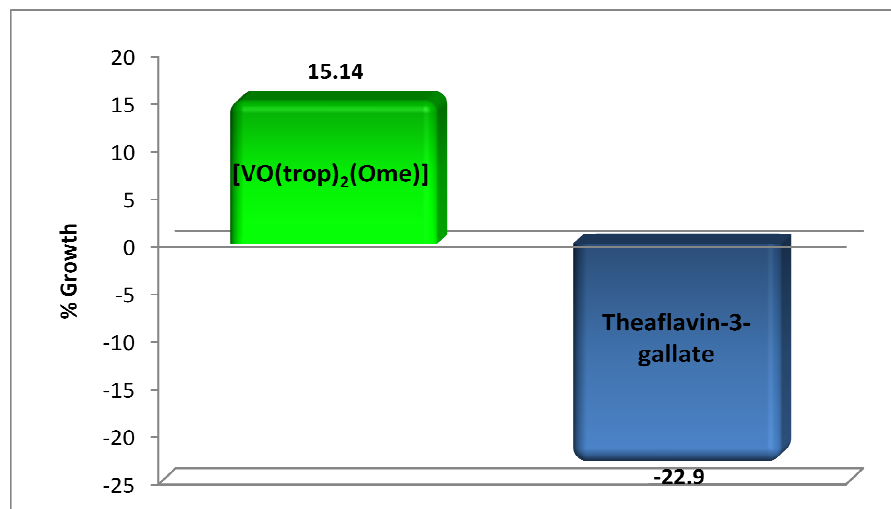
Figure 7.4: % Growth observed of 10 µM [VO(trop)$_2$(OMe)] and 14 µM theaflavin-3-gallate[8]
(tropolone derivative) in MCF-7.

It was expected that the dibenzoylmethane derived complex of vanadium would show more positive activity results as the ligand is a derivative of curcumin. The structures of dibenzoylemethane and curcumin are given in Figure 7.5. Curcumin has been shown to have significant cytotoxic acitivity against a wide range of cancers.[10,11,12] Additionally, dibenzoylmethane has been shown to be effective as an antitumor drug. In a study by Singletary *et al.*[13] rat mammary tumorigenesis was inhibited by 82 % when included as 1 % of a daily diet. This has suggested that β-diketone analogues of curcumin may serve as potential breast cancer chemopreventives. The salicylic vanadium complexes of Noblía *et al.*[7] showed in contrast that the known effects of salicylic acid can be enhanced in combination with metal coordination.

---

[10] Shishodia, S., Sethi, G., Aggarwal, B. B., *Ann. NY Acad. Sci.*, **2005**, *1056*, 206.
[11] Aggarwal, B. B., Kumar, A., Bharti, A. C., *Anticancer res.*, **2003**, *23*, 363.
[12] Duvoix, A., Blasius, R., Delhalle, S., Schnekenburger, M., Morceau, F., Henry, E., Dicato, M., Diederich, M., *Cancer Lett.*, **2005**, *223*, 181.
[13] Singletary, K., MacDonald, C., *Cancer Lett.*, **2000**, *155*, 47.

dibenzoylmethane

(1E,6E)-1,7-bis(4-hydroxy-3-methoxyphenyl)-1,6-heptadiene-3,5-dione
(Curcumin)
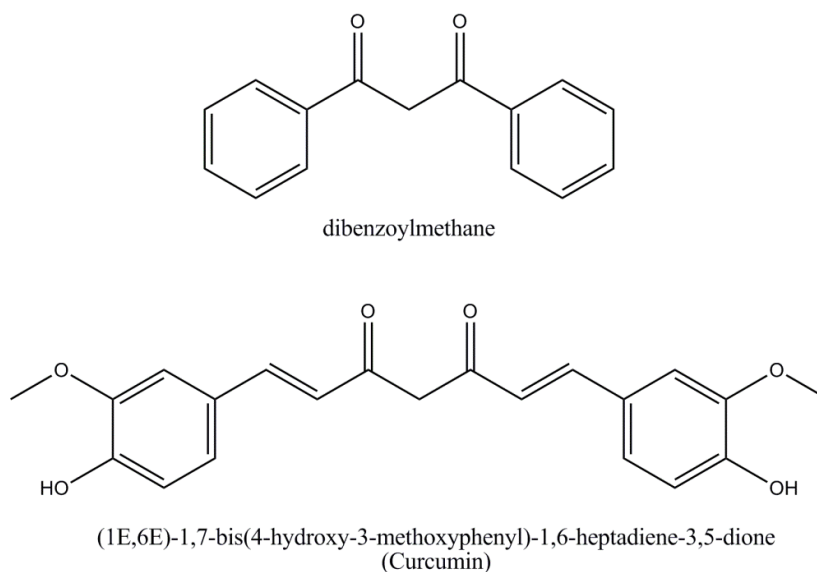
Figure 7.5: Structural representations of dibenzoylmethane and curcumin.

7.6   Conclusion

Three synthesized complexes were tested for cytotoxic activity against TK-10 (human kidney carcinoma), UACC-62 (human melanoma) and MCF-7 (human mammary adenocarcinoma) cells. The results of these tests were presented in this chapter alongside five vanadium complexes chosen from literature. Although results were mostly negative the insight gained by such studies paves the way for future studies. Comparisons between free ligand activity and metal complexes provides further knowledge with regard to understanding the role that metal coordination plays as potential metallopharmaceuticals.

Chapter 8: Evaluation of Study

8.1   Introduction

The successes and failures of this MSc study are discussed in the following sections, in terms of the aims described in Chapter 1, which is followed by some aspects which might be investigated in future.

8.2   Evaluation

8.2.1 Synthesis and Characterization of Vanadium(IV) and Vanadium(V) Compounds

One of the central aims in this study involved the synthesis of various vanadium(IV) and vanadium(V) compounds with ligands containing *O,O'* and *N,O* donor functionalities. The choice of ligands were based upon applications in the biological fields as well as industrial use. A range of complexes were obtained as a result and were successfully characterized by IR and NMR spectroscopy (see Chapter 4).

Some interesting results were obtained from this section of the project. Important structural information was gained, showing that vanadium often fills its coordination sphere with methanol molecules or other ligands to ensure further stability in the +5 oxidation state. Additionally, many vanadium(IV) compounds are labelled as unstable in open air whereas many vanadium(IV) complexes were successfully synthesized during this study in the presence of air, proving that many vanadium(IV) compounds are relatively stable under atmospheric conditions.

A compound to be highlighted of this study was the $(C_9H_{17}O_2)[VO_2(cupf)_2]$ complex that crystallized with a novel cation. This cation is thought to originate from the *in situ* cyclization of acetone in the reaction mixture (see Chapter 4). Alternatively, the vanadium complex itself could participate in the reaction and would be an interesting study for future work.

Single crystal X-ray diffraction studies provided valuable structural information, shedding light on the intriguing coordination chemistry of vanadium. The three β-diketonato

containing compounds discussed were relatable to each other in each case with only one differing ligand in the [VO(dbm)$_2$(MeOH)]•2MeOH and the [VO(dbm)$_2$py] complexes. Systematic electro-steric changes were thus introduced to the vanadium centre. This influenced the strength of coordinating ligands and the degree of distortion out of ideal geometry due to the *trans* influence of the oxido bond on the vanadium centre. Also, the [VO(dbm)$_2$py] complex was obtained as a polymorph of a published structure. Differences in the two structures could successfully be attributed to packing effects rather than being energy related. The dioxido complex of (C$_9$H$_{17}$O$_2$)[VO$_2$(cupf)$_2$] containing two oxido bonds, which are not commonly found in literature was also discussed. Finally, a comparison could be made between the four complexes to illustrate the effects of ligand choice on structural aspects of vanadium coordination chemistry.

Another successfully employed technique used extensively in this study was ^{51}V NMR that provided information with regard to the electronic environment surrounding the vanadium centre in solution. A comparison between shielding and steric strain could be established (see Chapter 4) for chosen vanadium(V) compounds synthesized in this study. In addition, important intermediates and products could be identified utilizing ^{51}V NMR during the substitution kinetic study in this project, which enabled direct correlation with the results obtained from the more detailed UV/Vis study.

8.2.2 Kinetic Study

The kinetic substitution study undertaken for this project involved complex equilibrium studies at different pH values. The results from this study provided information regarding the complex reaction mechanism. It was concluded that the reaction is significantly influenced by pH changes and concentration of entering ligand as well as pK$_a$ values for the different substituted and entering ligands. In general it could be classified as a 'proton catalytic process'. The equilibrium steps proposed for this reaction fit all experimental data that was obtained during this study. The study provided valuable knowledge with regard to the solution behavior of vanadium at different pH values and contributes to this knowledge base of vanadium substitution kinetics. UV/Vis techniques were successfully utilized to reach these conclusions along with ^{51}V NMR.

8.3 Future Work

The substitution kinetic study followed in this work should be expanded to a much broader study involving more picolinic acid derivatives and analogues as well as employing several other experimental techniques to yield more information with regard to this complex reaction mechanism. Low temperature NMR experiments could follow the formation and conversion of intermediates in the reaction at several pH values. An entire range of ligand concentration series at different pH values could be attempted to provide the full spectrum of k_{obs} *vs* pH plots. Stopped-flow techniques could be employed to monitor the reaction of the bis-aqua species with 2,3-dipic. Finally, crystal structure determinations of the kinetic products would affirm the reaction mechanism proposed. 2D ^{51}V NMR studies could also provide a better understanding of the exchanges taking place in solution as the broad peaks observed could suggest dynamic interchange reactions. Experiments such as EXSY (Exchange Spectroscopy) would shed light on such interactions.

In terms of synthesis, the vast scope of the coordination chemistry of vanadium lends itself for several ligand families to be explored in future studies. The choice would depend on the researcher and the interests at hand. Biological fields are concerned with biologically active ligands such as salicylidene. From an industrial viewpoint vanadium catalysts would require certain steric and electronic properties to be tailored by ligand choice. In this regard various new vanadium compounds could be synthesized with an array of ligands to suit the needs at hand.

The testing of compounds synthesized in this study for cancer screening were mostly negative, but provided important information for evaluating the effect the vanadium centre had on already active ligands. Testing of more compounds would perhaps reveal an active compound that could be developed eventually into a successful pharmacological drug.

This work provided a basis for researching vanadium chemistry and much scope exists to expand upon the current project. Structural studies provided undoubtedly some of the most significant contributions to this project and can be expanded to some of the other compounds synthesized. Powder diffraction studies could provide valuable information with regard to solid state structures and ^{51}V NMR studies could be utilized more in future work.

Appendix

A 1. Supplementary Data for [VO(dbm)$_2$]

Table A 1.1: Atomic coordinates and equivalent isotropic displacement parameters ($\mathring{A}^2$) for [VO(dbm)$_2$]. U(eq) is defined as one third of the trace of the orthogonalized U^{ij} tensor.

Atom	x	y	z	U_{eq}
C1	0.60513 (10)	0.01602 (9)	0.47210 (7)	0.0148 (3)
C2	0.61379 (11)	0.07234 (9)	0.52384 (8)	0.0172 (3)
C3	0.58713 (10)	0.15350 (9)	0.51763 (7)	0.0157 (3)
C4	0.63343 (10)	–0.07049 (9)	0.48135 (7)	0.0146 (3)
C5	0.62496 (11)	–0.12302 (9)	0.42677 (8)	0.0194 (3)
C6	0.65505 (12)	–0.20270 (10)	0.43163 (8)	0.0244 (3)
C7	0.69515 (11)	–0.23047 (10)	0.49040 (9)	0.0238 (4)
C8	0.70258 (11)	–0.17929 (10)	0.54490 (8)	0.0209 (3)
C9	0.67161 (11)	–0.09996 (9)	0.54084 (8)	0.0188 (3)
C10	0.59060 (10)	0.21074 (9)	0.57522 (8)	0.0168 (3)
C11	0.62135 (11)	0.18823 (10)	0.63888 (8)	0.0211 (3)
C12	0.62464 (11)	0.24540 (11)	0.69032 (8)	0.0230 (3)
C13	0.59790 (11)	0.32477 (10)	0.67825 (8)	0.0217 (3)
C14	0.56661 (11)	0.34732 (10)	0.61535 (8)	0.0216 (3)
C15	0.56288 (11)	0.29094 (10)	0.56422 (8)	0.0198 (3)
C16	0.40870 (10)	0.24127 (9)	0.31286 (7)	0.0163 (3)
C17	0.38041 (11)	0.18198 (9)	0.26736 (8)	0.0180 (3)
C18	0.42164 (10)	0.10546 (9)	0.26329 (7)	0.0162 (3)
C19	0.36656 (10)	0.32379 (9)	0.31321 (8)	0.0168 (3)
C20	0.36756 (11)	0.36854 (9)	0.37265 (8)	0.0193 (3)
C21	0.33137 (11)	0.44658 (10)	0.37390 (8)	0.0230 (3)
C22	0.29681 (11)	0.48100 (10)	0.31564 (9)	0.0239 (3)
C23	0.29730 (11)	0.43725 (10)	0.25635 (9)	0.0242 (3)
C24	0.33058 (12)	0.35833 (9)	0.25535 (8)	0.0210 (3)
C25	0.39724 (10)	0.04774 (9)	0.20840 (8)	0.0163 (3)
C26	0.34477 (11)	0.07143 (10)	0.15345 (8)	0.0200 (3)
C27	0.32656 (11)	0.01767 (10)	0.10205 (8)	0.0238 (3)

Atom				
C28	0.35904 (12)	–0.06126 (11)	0.10518 (9)	0.0258 (4)
C29	0.41076 (12)	–0.08622 (10)	0.15959 (9)	0.0264 (4)
C30	0.43090 (11)	–0.03150 (10)	0.21106 (9)	0.0223 (3)
O1	0.64965 (8)	0.16450 (7)	0.33840 (6)	0.0218 (2)
O2	0.57376 (8)	0.03350 (6)	0.41371 (5)	0.0182 (2)
O3	0.55799 (8)	0.18463 (6)	0.46294 (5)	0.0181 (2)
O4	0.47175 (7)	0.23138 (6)	0.35670 (5)	0.0172 (2)
O5	0.48277 (7)	0.08048 (6)	0.30490 (5)	0.0173 (2)
V1	0.555110 (17)	0.139998 (15)	0.372363 (12)	0.01412 (8)

Table A 1.2: Hydrogen coordinates and isotropic displacement parameters (Å^2) for [VO(dbm)$_2$].

Atom	x	y	z	U_{eq}
H5	0.5985	–0.1041	0.3862	0.023
H6	0.6482	–0.2384	0.3946	0.029
H7	0.7174	–0.2846	0.4931	0.029
H8	0.7290	–0.1986	0.5854	0.025
H9	0.6763	–0.0653	0.5787	0.023
H11	0.6400	0.1339	0.6471	0.025
H12	0.6452	0.2299	0.7336	0.028
H13	0.6010	0.3639	0.7132	0.026
H14	0.5477	0.4017	0.6074	0.026
H15	0.5413	0.3067	0.5212	0.024
H20	0.3930	0.3457	0.4122	0.023
H21	0.3303	0.4764	0.4146	0.028
H22	0.2728	0.5346	0.3165	0.029
H23	0.2748	0.4613	0.2163	0.029
H24	0.3288	0.3278	0.2150	0.025
H26	0.3213	0.1252	0.1514	0.024
H27	0.2917	0.0349	0.0645	0.029
H28	0.3459	–0.0983	0.0700	0.031
H29	0.4325	–0.1405	0.1619	0.032
H30	0.4675	–0.0483	0.2479	0.027
H2	0.6342 (12)	0.0545 (11)	0.5665 (9)	0.020 (5)
H17	0.3285 (14)	0.1950 (12)	0.2371 (10)	0.030 (5)

Table A 1.3: Anisotropic displacement parameters ($\mathring{A}^2$) for [VO(dbm)$_2$]. The anisotropic displacement factor exponent takes the form: $-2\pi^2[h^2a^{*2}U^{11} + \ldots + 2hka^*b^*U^{23}]$.

Atom	U^{11}	U^{22}	U^{33}	U^{12}	U^{13}	U^{23}
C1	0.0136 (7)	0.0149 (7)	0.0160 (7)	−0.0005 (5)	0.0006 (5)	0.0024 (5)
C2	0.0203 (8)	0.0171 (7)	0.0144 (7)	0.0020 (6)	−0.0013 (6)	0.0002 (5)
C3	0.0141 (7)	0.0174 (7)	0.0155 (7)	−0.0007 (6)	0.0002 (5)	0.0002 (5)
C4	0.0117 (7)	0.0136 (7)	0.0183 (7)	−0.0002 (5)	0.0023 (5)	0.0027 (5)
C5	0.0231 (8)	0.0195 (7)	0.0157 (7)	0.0004 (6)	0.0002 (6)	0.0029 (6)
C6	0.0331 (9)	0.0185 (8)	0.0214 (8)	0.0010 (7)	0.0030 (7)	−0.0037 (6)
C7	0.0241 (9)	0.0153 (8)	0.0319 (9)	0.0044 (6)	0.0050 (7)	0.0054 (6)
C8	0.0184 (8)	0.0207 (8)	0.0235 (8)	0.0012 (6)	−0.0011 (6)	0.0085 (6)
C9	0.0182 (7)	0.0191 (7)	0.0190 (7)	−0.0025 (6)	−0.0008 (6)	0.0017 (6)
C10	0.0144 (7)	0.0185 (7)	0.0176 (7)	−0.0005 (6)	0.0003 (6)	−0.0029 (6)
C11	0.0236 (8)	0.0196 (8)	0.0201 (8)	0.0046 (6)	−0.0004 (6)	−0.0014 (6)
C12	0.0240 (8)	0.0298 (9)	0.0152 (7)	0.0020 (7)	−0.0007 (6)	−0.0019 (6)
C13	0.0213 (8)	0.0235 (8)	0.0204 (8)	−0.0010 (6)	0.0048 (6)	−0.0080 (6)
C14	0.0223 (8)	0.0181 (7)	0.0245 (8)	0.0022 (6)	0.0033 (6)	−0.0025 (6)
C15	0.0190 (8)	0.0221 (8)	0.0183 (7)	0.0013 (6)	−0.0002 (6)	−0.0002 (6)
C16	0.0168 (7)	0.0160 (7)	0.0161 (7)	0.0005 (6)	0.0015 (6)	0.0029 (5)
C17	0.0185 (7)	0.0179 (7)	0.0175 (7)	0.0010 (6)	−0.0018 (6)	0.0006 (6)
C18	0.0158 (7)	0.0168 (7)	0.0162 (7)	−0.0023 (6)	0.0006 (6)	0.0018 (5)
C19	0.0155 (7)	0.0159 (7)	0.0191 (7)	0.0006 (6)	0.0008 (6)	0.0005 (6)
C20	0.0206 (8)	0.0181 (7)	0.0193 (8)	−0.0005 (6)	−0.0004 (6)	0.0011 (6)
C21	0.0231 (8)	0.0203 (8)	0.0256 (8)	−0.0005 (6)	0.0036 (7)	−0.0062 (6)
C22	0.0215 (8)	0.0148 (7)	0.0354 (9)	0.0039 (6)	0.0017 (7)	0.0006 (6)
C23	0.0248 (9)	0.0225 (8)	0.0254 (8)	0.0047 (7)	−0.0028 (7)	0.0027 (6)
C24	0.0231 (8)	0.0199 (7)	0.0200 (8)	0.0024 (6)	−0.0016 (6)	−0.0014 (6)
C25	0.0138 (7)	0.0161 (7)	0.0189 (7)	−0.0020 (5)	0.0003 (6)	−0.0014 (5)
C26	0.0188 (8)	0.0184 (7)	0.0228 (8)	−0.0017 (6)	−0.0018 (6)	0.0015 (6)
C27	0.0211 (8)	0.0281 (8)	0.0224 (8)	−0.0032 (7)	−0.0046 (6)	−0.0011 (7)
C28	0.0216 (8)	0.0283 (9)	0.0273 (9)	−0.0030 (7)	−0.0020 (7)	−0.0103 (7)
C29	0.0230 (8)	0.0200 (8)	0.0362 (10)	0.0045 (7)	−0.0013 (7)	−0.0073 (7)
C30	0.0182 (8)	0.0227 (8)	0.0261 (8)	0.0031 (6)	−0.0036 (6)	−0.0009 (6)
O1	0.0209 (6)	0.0245 (6)	0.0199 (6)	0.0008 (5)	−0.0007 (5)	0.0036 (4)
O2	0.0258 (6)	0.0141 (5)	0.0146 (5)	0.0023 (4)	−0.0039 (4)	0.0010 (4)
O3	0.0263 (6)	0.0136 (5)	0.0143 (5)	0.0015 (4)	−0.0037 (4)	0.0001 (4)

O4	0.0200 (5)	0.0139 (5)	0.0176 (5)	0.0014 (4)	−0.0038 (4)	0.0015 (4)
O5	0.0204 (6)	0.0147 (5)	0.0167 (5)	0.0014 (4)	−0.0040 (4)	0.0004 (4)
V1	0.01716 (14)	0.01287 (13)	0.01233 (13)	0.00082 (9)	−0.00201 (9)	0.00161 (9)

Table A 1.4: Complete listing of bond lengths (Å) for [VO(dbm)$_2$].

Bond	Distance	Bond	Distance
C1—O2	1.2849 (18)	C17—C18	1.399 (2)
C1—C2	1.393 (2)	C17—H17	0.99 (2)
C1—C4	1.494 (2)	C18—O5	1.2877 (18)
C2—C3	1.397 (2)	C18—C25	1.493 (2)
C2—H2	0.949 (18)	C19—C24	1.390 (2)
C3—O3	1.2787 (18)	C19—C20	1.396 (2)
C3—C10	1.487 (2)	C20—C21	1.390 (2)
C4—C5	1.396 (2)	C20—H20	0.9500
C4—C9	1.399 (2)	C21—C22	1.389 (2)
C5—C6	1.387 (2)	C21—H21	0.9500
C5—H5	0.9500	C22—C23	1.385 (2)
C6—C7	1.388 (2)	C22—H22	0.9500
C6—H6	0.9500	C23—C24	1.387 (2)
C7—C8	1.380 (2)	C23—H23	0.9500
C7—H7	0.9500	C24—H24	0.9500
C8—C9	1.385 (2)	C25—C26	1.394 (2)
C8—H8	0.9500	C25—C30	1.395 (2)
C9—H9	0.9500	C26—C27	1.381 (2)
C10—C11	1.398 (2)	C26—H26	0.9500
C10—C15	1.398 (2)	C27—C28	1.385 (2)
C11—C12	1.393 (2)	C27—H27	0.9500
C11—H11	0.9500	C28—C29	1.386 (3)
C12—C13	1.385 (2)	C28—H28	0.9500
C12—H12	0.9500	C29—C30	1.397 (2)
C13—C14	1.387 (2)	C29—H29	0.9500
C13—H13	0.9500	C30—H30	0.9500
C14—C15	1.380 (2)	O1—V1	1.5922 (12)
C14—H14	0.9500	O2—V1	1.9566 (12)
C15—H15	0.9500	O3—V1	1.9515 (12)

C16—O4	1.2817 (18)	O4—V1	1.9616 (11)
C16—C17	1.396 (2)	O5—V1	1.9728 (11)
C16—C19	1.492 (2)		

Table A 1.5: Complete listing of bond angles (°) for [VO(dbm)₂].

Angle	Value	Angle	Value
O2—C1—C2	123.74 (14)	O5—C18—C25	115.84 (13)
O2—C1—C4	115.11 (13)	C17—C18—C25	120.82 (13)
C2—C1—C4	121.14 (13)	C24—C19—C20	119.58 (14)
C1—C2—C3	123.02 (14)	C24—C19—C16	121.66 (14)
C1—C2—H2	119.2 (11)	C20—C19—C16	118.69 (13)
C3—C2—H2	117.6 (11)	C21—C20—C19	119.92 (15)
O3—C3—C2	123.51 (14)	C21—C20—H20	120.0
O3—C3—C10	114.64 (13)	C19—C20—H20	120.0
C2—C3—C10	121.86 (13)	C22—C21—C20	120.06 (15)
C5—C4—C9	118.86 (14)	C22—C21—H21	120.0
C5—C4—C1	117.98 (13)	C20—C21—H21	120.0
C9—C4—C1	123.09 (13)	C23—C22—C21	120.07 (15)
C6—C5—C4	120.19 (15)	C23—C22—H22	120.0
C6—C5—H5	119.9	C21—C22—H22	120.0
C4—C5—H5	119.9	C22—C23—C24	120.06 (15)
C5—C6—C7	120.30 (15)	C22—C23—H23	120.0
C5—C6—H6	119.8	C24—C23—H23	120.0
C7—C6—H6	119.8	C23—C24—C19	120.25 (15)
C8—C7—C6	119.86 (15)	C23—C24—H24	119.9
C8—C7—H7	120.1	C19—C24—H24	119.9
C6—C7—H7	120.1	C26—C25—C30	119.07 (14)
C7—C8—C9	120.26 (15)	C26—C25—C18	122.05 (14)
C7—C8—H8	119.9	C30—C25—C18	118.84 (14)
C9—C8—H8	119.9	C27—C26—C25	120.75 (15)
C8—C9—C4	120.49 (15)	C27—C26—H26	119.6
C8—C9—H9	119.8	C25—C26—H26	119.6
C4—C9—H9	119.8	C26—C27—C28	120.10 (16)
C11—C10—C15	119.09 (14)	C26—C27—H27	119.9
C11—C10—C3	123.05 (14)	C28—C27—H27	119.9

C15—C10—C3	117.85 (14)	C27—C28—C29	120.06 (15)
C12—C11—C10	120.10 (15)	C27—C28—H28	120.0
C12—C11—H11	119.9	C29—C28—H28	120.0
C10—C11—H11	119.9	C28—C29—C30	119.99 (16)
C13—C12—C11	119.96 (15)	C28—C29—H29	120.0
C13—C12—H12	120.0	C30—C29—H29	120.0
C11—C12—H12	120.0	C25—C30—C29	120.01 (15)
C12—C13—C14	120.21 (15)	C25—C30—H30	120.0
C12—C13—H13	119.9	C29—C30—H30	120.0
C14—C13—H13	119.9	C1—O2—V1	129.26 (10)
C15—C14—C13	120.14 (15)	C3—O3—V1	130.29 (10)
C15—C14—H14	119.9	C16—O4—V1	130.81 (10)
C13—C14—H14	119.9	C18—O5—V1	130.84 (10)
C14—C15—C10	120.49 (15)	O1—V1—O3	106.27 (5)
C14—C15—H15	119.8	O1—V1—O2	106.57 (6)
C10—C15—H15	119.8	O3—V1—O2	86.78 (5)
O4—C16—C17	124.66 (14)	O1—V1—O4	106.14 (6)
O4—C16—C19	114.19 (13)	O3—V1—O4	82.66 (5)
C17—C16—C19	121.15 (14)	O2—V1—O4	147.24 (5)
C16—C17—C18	122.65 (14)	O1—V1—O5	107.54 (6)
C16—C17—H17	118.1 (12)	O3—V1—O5	146.15 (5)
C18—C17—H17	119.2 (12)	O2—V1—O5	85.27 (5)
O5—C18—C17	123.34 (14)	O4—V1—O5	86.48 (5)

A 2. Supplementary Data for [VO(dbm)$_2$(MeOH)]·2MeOH

Table A 2.1: Atomic coordinates and equivalent isotropic displacement parameters (Å^2) for [VO(dbm)$_2$(MeOH)]·2MeOH. U(eq) is defined as one third of the trace of the orthogonalized U^{ij} tensor.

Atom	x	y	z	U_{eq}
C1	0.36767 (12)	0.39961 (16)	0.05771 (10)	0.0162 (4)
C2	0.43709 (12)	0.32030 (17)	0.10548 (11)	0.0173 (4)
C3	0.42560 (12)	0.20490 (16)	0.13328 (10)	0.0169 (4)
C4	0.39169 (12)	0.52183 (16)	0.03351 (11)	0.0168 (4)
C5	0.33516 (12)	0.57289 (17)	−0.03830 (11)	0.0200 (4)

C6	0.35512 (13)	0.68761 (17)	−0.06166 (12)	0.0226 (4)
C7	0.43108 (13)	0.75209 (17)	−0.01302 (12)	0.0234 (4)
C8	0.48821 (14)	0.70229 (17)	0.05841 (12)	0.0246 (4)
C9	0.46898 (13)	0.58668 (17)	0.08204 (11)	0.0218 (4)
C10	0.50604 (12)	0.12914 (17)	0.18099 (10)	0.0177 (4)
C11	0.58989 (13)	0.18430 (19)	0.22356 (11)	0.0226 (4)
C12	0.66473 (13)	0.1110 (2)	0.26513 (12)	0.0274 (5)
C13	0.65714 (14)	−0.0174 (2)	0.26528 (12)	0.0278 (5)
C14	0.57376 (14)	−0.07298 (19)	0.22354 (12)	0.0252 (4)
C15	0.49862 (13)	−0.00044 (17)	0.18183 (11)	0.0205 (4)
C16	0.11817 (12)	−0.00936 (16)	−0.01968 (11)	0.0161 (4)
C17	0.05537 (12)	0.05557 (17)	−0.08338 (11)	0.0179 (4)
C18	0.05764 (12)	0.18349 (16)	−0.09553 (10)	0.0159 (4)
C19	0.11005 (12)	−0.14650 (16)	−0.01373 (10)	0.0157 (4)
C20	0.18788 (12)	−0.21569 (16)	0.02781 (10)	0.0172 (4)
C21	0.18348 (13)	−0.34458 (17)	0.03111 (11)	0.0191 (4)
C22	0.10191 (13)	−0.40532 (17)	−0.00637 (11)	0.0209 (4)
C23	0.02358 (13)	−0.33711 (17)	−0.04628 (11)	0.0213 (4)
C24	0.02755 (12)	−0.20826 (16)	−0.04995 (11)	0.0178 (4)
C25	−0.01309 (12)	0.24140 (16)	−0.16673 (11)	0.0173 (4)
C26	−0.05067 (12)	0.17799 (18)	−0.23828 (11)	0.0200 (4)
C27	−0.11258 (13)	0.23700 (19)	−0.30453 (11)	0.0237 (4)
C28	−0.13890 (13)	0.35817 (19)	−0.29932 (12)	0.0253 (4)
C29	−0.10318 (13)	0.42113 (18)	−0.22825 (12)	0.0255 (4)
C30	−0.03948 (12)	0.36339 (17)	−0.16255 (11)	0.0211 (4)
C31	0.33540 (13)	0.05155 (17)	−0.04291 (12)	0.0227 (4)
C32	0.17160 (18)	0.2844 (3)	−0.21686 (16)	0.0405 (6)
C33	0.24949 (17)	−0.0442 (2)	0.22020 (15)	0.0350 (5)
O1	0.19198 (8)	0.26454 (12)	0.11199 (8)	0.0212 (3)
O2	0.28327 (8)	0.37464 (11)	0.03142 (7)	0.0186 (3)
O3	0.34776 (8)	0.15408 (11)	0.11931 (7)	0.0182 (3)
O4	0.18705 (8)	0.04098 (11)	0.03499 (7)	0.0188 (3)
O5	0.11722 (8)	0.25860 (11)	−0.04988 (7)	0.0181 (3)
O6	0.27967 (9)	0.15603 (13)	−0.04550 (9)	0.0239 (3)
O7	0.26612 (12)	0.29179 (17)	−0.16869 (10)	0.0416 (4)
O8	0.32366 (10)	0.04114 (15)	0.24889 (9)	0.0311 (3)

V1	0.22609 (2)	0.21767 (3)	0.046822 (18)	0.01557 (9)

Table A 2.2: Hydrogen coordinates and isotropic displacement parameters (Å^2) for [VO(dbm)$_2$(MeOH)]·2MeOH.

Atom	x	y	z	U_{eq}
H5	0.2826	0.5290	−0.0715	0.024
H6	0.3167	0.7219	−0.1110	0.027
H7	0.4441	0.8312	−0.0288	0.028
H8	0.5405	0.7469	0.0913	0.030
H9	0.5083	0.5520	0.1309	0.026
H11	0.5958	0.2723	0.2241	0.027
H12	0.7216	0.1492	0.2937	0.033
H13	0.7086	−0.0672	0.2937	0.033
H14	0.5682	−0.1610	0.2236	0.030
H15	0.4418	−0.0391	0.1537	0.025
H20	0.2441	−0.1745	0.0539	0.021
H21	0.2367	−0.3911	0.0592	0.023
H22	0.0994	−0.4936	−0.0049	0.025
H23	−0.0327	−0.3787	−0.0711	0.026
H24	−0.0261	−0.1620	−0.0772	0.021
H26	−0.0338	0.0942	−0.2417	0.024
H27	−0.1369	0.1943	−0.3534	0.028
H28	−0.1816	0.3982	−0.3446	0.030
H29	−0.1222	0.5036	−0.2245	0.031
H30	−0.0136	0.4076	−0.1143	0.025
H31A	0.3045	−0.0252	−0.0393	0.034
H31B	0.3928	0.0585	0.0032	0.034
H31C	0.3471	0.0497	−0.0908	0.034
H2	0.4934 (14)	0.3449 (18)	0.1178 (11)	0.016 (5)
H4A	0.2820 (17)	0.203 (2)	−0.0795 (15)	0.040 (7)
H5A	0.2930 (18)	0.340 (3)	−0.1901 (16)	0.052 (8)
H6A	0.333 (2)	0.078 (3)	0.2093 (18)	0.066 (10)
H17	0.0097 (13)	0.0100 (18)	−0.1199 (12)	0.018 (5)
H32A	0.1468 (18)	0.210 (2)	−0.1984 (16)	0.049 (8)
H32B	0.161 (2)	0.273 (3)	−0.2723 (19)	0.067 (9)

H32C	0.1394 (17)	0.364 (2)	−0.2113 (15)	0.044 (7)	
H33A	0.2636 (19)	−0.112 (3)	0.1881 (17)	0.067 (9)	
H33B	0.1935 (18)	−0.005 (2)	0.1797 (15)	0.048 (7)	
H33C	0.2409 (16)	−0.079 (2)	0.2672 (16)	0.047 (7)	

Table A 2.3: Anisotropic displacement parameters ($\mathring{A}^2$) for [VO(dbm)$_2$(MeOH)]·2MeOH. The anisotropic displacement factor exponent takes the form: -2π^2[h^{2}a^{*2}U^{11} + … + 2hka*b*U^{23}].

Atom	U^{11}	U^{22}	U^{33}	U^{12}	U^{13}	U^{23}
C1	0.0170 (9)	0.0157 (8)	0.0158 (9)	−0.0014 (7)	0.0065 (7)	−0.0038 (7)
C2	0.0116 (9)	0.0199 (9)	0.0188 (9)	−0.0003 (7)	0.0044 (7)	−0.0003 (7)
C3	0.0156 (9)	0.0194 (9)	0.0145 (9)	0.0002 (7)	0.0049 (7)	−0.0023 (7)
C4	0.0149 (9)	0.0147 (8)	0.0223 (10)	0.0013 (7)	0.0091 (8)	−0.0006 (7)
C5	0.0154 (9)	0.0204 (9)	0.0239 (10)	−0.0005 (7)	0.0074 (8)	−0.0007 (8)
C6	0.0203 (10)	0.0221 (9)	0.0267 (10)	0.0050 (8)	0.0107 (8)	0.0063 (8)
C7	0.0243 (10)	0.0170 (9)	0.0342 (11)	0.0005 (8)	0.0172 (9)	0.0025 (8)
C8	0.0222 (10)	0.0212 (9)	0.0301 (11)	−0.0057 (8)	0.0101 (9)	−0.0044 (8)
C9	0.0216 (10)	0.0208 (9)	0.0204 (10)	−0.0014 (8)	0.0056 (8)	−0.0010 (8)
C10	0.0161 (9)	0.0209 (9)	0.0156 (9)	0.0028 (7)	0.0057 (7)	0.0029 (7)
C11	0.0198 (10)	0.0251 (9)	0.0197 (10)	0.0005 (8)	0.0046 (8)	0.0050 (8)
C12	0.0173 (10)	0.0373 (12)	0.0226 (10)	0.0020 (9)	0.0027 (8)	0.0071 (9)
C13	0.0238 (10)	0.0364 (11)	0.0226 (10)	0.0136 (9)	0.0086 (9)	0.0113 (9)
C14	0.0306 (11)	0.0234 (10)	0.0227 (10)	0.0067 (8)	0.0119 (9)	0.0065 (8)
C15	0.0201 (9)	0.0225 (9)	0.0172 (9)	0.0015 (8)	0.0057 (8)	0.0021 (7)
C16	0.0137 (8)	0.0160 (8)	0.0189 (9)	−0.0005 (7)	0.0069 (7)	−0.0018 (7)
C17	0.0162 (9)	0.0159 (8)	0.0178 (9)	−0.0018 (7)	0.0028 (8)	−0.0024 (7)
C18	0.0136 (8)	0.0189 (8)	0.0149 (9)	0.0012 (7)	0.0053 (7)	−0.0016 (7)
C19	0.0180 (9)	0.0144 (8)	0.0148 (9)	0.0004 (7)	0.0067 (7)	0.0000 (7)
C20	0.0156 (9)	0.0186 (8)	0.0161 (9)	−0.0013 (7)	0.0050 (7)	−0.0009 (7)
C21	0.0200 (9)	0.0187 (9)	0.0199 (9)	0.0055 (7)	0.0091 (8)	0.0037 (7)
C22	0.0270 (10)	0.0147 (8)	0.0223 (10)	−0.0008 (8)	0.0112 (8)	0.0015 (7)
C23	0.0209 (9)	0.0192 (9)	0.0238 (10)	−0.0042 (8)	0.0090 (8)	−0.0009 (8)
C24	0.0167 (9)	0.0182 (8)	0.0180 (9)	0.0016 (7)	0.0065 (7)	0.0005 (7)
C25	0.0142 (9)	0.0178 (8)	0.0176 (9)	−0.0004 (7)	0.0040 (7)	0.0016 (7)
C26	0.0178 (9)	0.0194 (9)	0.0212 (10)	−0.0010 (7)	0.0064 (8)	−0.0011 (7)
C27	0.0181 (10)	0.0332 (11)	0.0166 (9)	−0.0029 (8)	0.0037 (8)	0.0004 (8)

C28	0.0179 (9)	0.0318 (11)	0.0222 (10)	0.0022 (8)	0.0038 (8)	0.0095 (8)
C29	0.0223 (10)	0.0201 (9)	0.0296 (11)	0.0048 (8)	0.0057 (9)	0.0061 (8)
C30	0.0192 (9)	0.0196 (9)	0.0203 (10)	0.0002 (7)	0.0036 (8)	0.0001 (7)
C31	0.0214 (10)	0.0191 (9)	0.0273 (10)	0.0018 (8)	0.0095 (8)	–0.0016 (8)
C32	0.0375 (14)	0.0534 (16)	0.0321 (13)	–0.0118 (12)	0.0155 (11)	–0.0011 (12)
C33	0.0393 (14)	0.0317 (12)	0.0305 (13)	–0.0020 (10)	0.0102 (11)	0.0021 (10)
O1	0.0164 (7)	0.0228 (7)	0.0219 (7)	–0.0014 (5)	0.0050 (6)	–0.0022 (5)
O2	0.0136 (6)	0.0157 (6)	0.0228 (7)	–0.0008 (5)	0.0035 (5)	–0.0003 (5)
O3	0.0140 (6)	0.0173 (6)	0.0200 (7)	–0.0010 (5)	0.0034 (5)	0.0016 (5)
O4	0.0170 (6)	0.0152 (6)	0.0185 (7)	–0.0024 (5)	0.0010 (5)	0.0010 (5)
O5	0.0153 (6)	0.0155 (6)	0.0188 (7)	–0.0003 (5)	0.0019 (5)	–0.0004 (5)
O6	0.0289 (8)	0.0198 (7)	0.0250 (7)	0.0063 (6)	0.0130 (6)	0.0057 (6)
O7	0.0354 (9)	0.0487 (10)	0.0377 (10)	–0.0031 (8)	0.0115 (8)	0.0180 (8)
O8	0.0287 (8)	0.0390 (9)	0.0259 (8)	0.0001 (7)	0.0114 (7)	0.0018 (7)
V1	0.01260 (15)	0.01394 (14)	0.01701 (16)	–0.00090 (12)	0.00260 (12)	–0.00023 (12)

Table A 2.4: Complete listing of bond lengths (Å) for [VO(dbm)$_2$(MeOH)]·2MeOH.

Bond	Distance	Bond	Distance
C1—O2	1.278 (2)	C21—C22	1.382 (3)
C1—C2	1.404 (3)	C21—H21	0.9500
C1—C4	1.488 (2)	C22—C23	1.391 (3)
C2—C3	1.383 (3)	C22—H22	0.9500
C2—H2	0.88 (2)	C23—C24	1.389 (3)
C3—O3	1.298 (2)	C23—H23	0.9500
C3—C10	1.487 (2)	C24—H24	0.9500
C4—C5	1.391 (3)	C25—C30	1.390 (3)
C4—C9	1.398 (3)	C25—C26	1.396 (3)
C5—C6	1.387 (3)	C26—C27	1.388 (3)
C5—H5	0.9500	C26—H26	0.9500
C6—C7	1.383 (3)	C27—C28	1.385 (3)
C6—H6	0.9500	C27—H27	0.9500
C7—C8	1.383 (3)	C28—C29	1.385 (3)
C7—H7	0.9500	C28—H28	0.9500
C8—C9	1.393 (3)	C29—C30	1.387 (3)
C8—H8	0.9500	C29—H29	0.9500
C9—H9	0.9500	C30—H30	0.9500

C10—C11	1.397 (3)	C31—O6	1.427 (2)
C10—C15	1.398 (3)	C31—H31A	0.9800
C11—C12	1.389 (3)	C31—H31B	0.9800
C11—H11	0.9500	C31—H31C	0.9800
C12—C13	1.385 (3)	C32—O7	1.429 (3)
C12—H12	0.9500	C32—H32A	1.01 (3)
C13—C14	1.391 (3)	C32—H32B	0.98 (3)
C13—H13	0.9500	C32—H32C	1.03 (3)
C14—C15	1.388 (3)	C33—O8	1.431 (3)
C14—H14	0.9500	C33—H33A	1.02 (3)
C15—H15	0.9500	C33—H33B	1.01 (3)
C16—O4	1.286 (2)	C33—H33C	1.01 (3)
C16—C17	1.397 (3)	O1—V1	1.5964 (14)
C16—C19	1.487 (2)	O2—V1	1.9972 (14)
C17—C18	1.396 (3)	O3—V1	2.0045 (13)
C17—H17	0.92 (2)	O4—V1	1.9847 (15)
C18—O5	1.281 (2)	O5—V1	1.9936 (13)
C18—C25	1.492 (2)	O6—V1	2.3022 (15)
C19—C24	1.396 (2)	O6—H4A	0.82 (3)
C19—C20	1.396 (2)	O7—H5A	0.87 (3)
C20—C21	1.389 (3)	O8—H6A	0.90 (3)
C20—H20	0.9500		

Table A 2.5: Complete listing of bond angles (°) for [VO(dbm)$_2$(MeOH)] •2MeOH.

Angle	Value	Angle	Value
O2—C1—C2	124.95 (17)	C24—C23—C22	120.09 (17)
O2—C1—C4	115.89 (15)	C24—C23—H23	120.0
C2—C1—C4	119.16 (16)	C22—C23—H23	120.0
C3—C2—C1	125.93 (17)	C23—C24—C19	120.27 (17)
C3—C2—H2	116.6 (13)	C23—C24—H24	119.9
C1—C2—H2	117.4 (13)	C19—C24—H24	119.9
O3—C3—C2	124.49 (16)	C30—C25—C26	119.14 (17)
O3—C3—C10	115.70 (16)	C30—C25—C18	119.14 (16)
C2—C3—C10	119.79 (16)	C26—C25—C18	121.66 (16)
C5—C4—C9	119.63 (17)	C27—C26—C25	120.21 (18)

C5—C4—C1	119.10 (16)	C27—C26—H26	119.9
C9—C4—C1	121.26 (17)	C25—C26—H26	119.9
C6—C5—C4	120.29 (17)	C28—C27—C26	120.01 (18)
C6—C5—H5	119.9	C28—C27—H27	120.0
C4—C5—H5	119.9	C26—C27—H27	120.0
C7—C6—C5	119.86 (18)	C27—C28—C29	120.20 (18)
C7—C6—H6	120.1	C27—C28—H28	119.9
C5—C6—H6	120.1	C29—C28—H28	119.9
C6—C7—C8	120.54 (18)	C28—C29—C30	119.81 (18)
C6—C7—H7	119.7	C28—C29—H29	120.1
C8—C7—H7	119.7	C30—C29—H29	120.1
C7—C8—C9	119.93 (18)	C29—C30—C25	120.59 (18)
C7—C8—H8	120.0	C29—C30—H30	119.7
C9—C8—H8	120.0	C25—C30—H30	119.7
C8—C9—C4	119.74 (18)	O6—C31—H31A	109.5
C8—C9—H9	120.1	O6—C31—H31B	109.5
C4—C9—H9	120.1	H31A—C31—H31B	109.5
C11—C10—C15	118.96 (17)	O6—C31—H31C	109.5
C11—C10—C3	121.46 (17)	H31A—C31—H31C	109.5
C15—C10—C3	119.56 (16)	H31B—C31—H31C	109.5
C12—C11—C10	120.26 (19)	O7—C32—H32A	107.4 (15)
C12—C11—H11	119.9	O7—C32—H32B	110.7 (17)
C10—C11—H11	119.9	H32A—C32—H32B	109 (2)
C13—C12—C11	120.53 (19)	O7—C32—H32C	110.3 (14)
C13—C12—H12	119.7	H32A—C32—H32C	110 (2)
C11—C12—H12	119.7	H32B—C32—H32C	109 (2)
C12—C13—C14	119.56 (18)	O8—C33—H33A	109.0 (16)
C12—C13—H13	120.2	O8—C33—H33B	112.1 (15)
C14—C13—H13	120.2	H33A—C33—H33B	102 (2)
C15—C14—C13	120.30 (19)	O8—C33—H33C	107.5 (14)
C15—C14—H14	119.8	H33A—C33—H33C	112 (2)
C13—C14—H14	119.8	H33B—C33—H33C	114 (2)
C14—C15—C10	120.38 (18)	C1—O2—V1	127.28 (11)
C14—C15—H15	119.8	C3—O3—V1	126.95 (11)
C10—C15—H15	119.8	C16—O4—V1	128.72 (11)
O4—C16—C17	124.22 (16)	C18—O5—V1	127.86 (12)

O4—C16—C19	115.61 (15)	C31—O6—V1	128.35 (12)
C17—C16—C19	120.12 (16)	C31—O6—H4A	106.8 (18)
C18—C17—C16	124.84 (17)	V1—O6—H4A	122.6 (18)
C18—C17—H17	118.2 (12)	C32—O7—H5A	110.6 (18)
C16—C17—H17	117.0 (12)	C33—O8—H6A	111.7 (19)
O5—C18—C17	125.10 (17)	O1—V1—O4	101.25 (6)
O5—C18—C25	115.35 (15)	O1—V1—O5	99.44 (6)
C17—C18—C25	119.55 (16)	O4—V1—O5	89.14 (5)
C24—C19—C20	119.12 (16)	O1—V1—O2	99.25 (6)
C24—C19—C16	122.05 (16)	O4—V1—O2	159.47 (6)
C20—C19—C16	118.81 (16)	O5—V1—O2	88.66 (5)
C21—C20—C19	120.30 (17)	O1—V1—O3	98.18 (6)
C21—C20—H20	119.9	O4—V1—O3	86.02 (5)
C19—C20—H20	119.9	O5—V1—O3	162.32 (5)
C22—C21—C20	120.25 (17)	O2—V1—O3	89.93 (5)
C22—C21—H21	119.9	O1—V1—O6	177.73 (6)
C20—C21—H21	119.9	O4—V1—O6	80.78 (6)
C21—C22—C23	119.93 (17)	O5—V1—O6	81.56 (6)
C21—C22—H22	120.0	O2—V1—O6	78.71 (6)
C23—C22—H22	120.0	O3—V1—O6	80.89 (6)

A 3. Supplementary Data for [VO(dbm)$_2$py]

Table A 3.1: Atomic coordinates and equivalent isotropic displacement parameters (Å^2) for [VO(dbm)$_2$py]. U(eq) is defined as one third of the trace of the orthogonalized U^{ij} tensor.

Atom	x	y	z	U_{eq}
C1	0.0938 (7)	0.2017 (2)	0.19142 (18)	0.0158 (9)
C2	0.2470 (7)	0.1543 (3)	0.21547 (18)	0.0169 (9)
C3	0.3938 (7)	0.1161 (2)	0.18503 (18)	0.0148 (8)
C4	–0.0386 (7)	0.2468 (2)	0.22829 (18)	0.0173 (9)
C5	–0.2465 (7)	0.2629 (2)	0.21025 (19)	0.0197 (9)
C6	–0.3727 (8)	0.3075 (3)	0.2419 (2)	0.0237 (10)
C7	–0.2902 (8)	0.3371 (3)	0.2923 (2)	0.0265 (11)

C8	−0.0835 (8)	0.3207 (3)	0.3106 (2)	0.0242 (10)
C9	0.0426 (7)	0.2753 (3)	0.27926 (19)	0.0197 (9)
C10	0.5490 (7)	0.0654 (2)	0.21427 (18)	0.0147 (8)
C11	0.4982 (7)	0.0255 (2)	0.26209 (18)	0.0179 (9)
C12	0.6417 (8)	−0.0239 (3)	0.28591 (19)	0.0222 (10)
C13	0.8382 (8)	−0.0332 (3)	0.26323 (19)	0.0215 (10)
C14	0.8910 (7)	0.0063 (3)	0.21616 (19)	0.0201 (9)
C15	0.7481 (7)	0.0552 (2)	0.19162 (18)	0.0168 (9)
C16	0.3745 (7)	0.3107 (2)	0.05094 (18)	0.0161 (9)
C17	0.2143 (7)	0.3248 (2)	0.00968 (18)	0.0175 (9)
C18	0.0541 (7)	0.2762 (2)	−0.00548 (18)	0.0160 (9)
C19	0.5330 (7)	0.3692 (2)	0.06715 (18)	0.0159 (9)
C20	0.7333 (7)	0.3490 (3)	0.08720 (18)	0.0186 (9)
C21	0.8808 (8)	0.4008 (3)	0.1038 (2)	0.0229 (10)
C22	0.8284 (8)	0.4743 (3)	0.1011 (2)	0.0230 (10)
C23	0.6278 (8)	0.4953 (3)	0.0808 (2)	0.0226 (10)
C24	0.4786 (7)	0.4431 (2)	0.06338 (18)	0.0192 (9)
C25	−0.0983 (7)	0.2943 (2)	−0.05319 (17)	0.0145 (8)
C26	−0.0420 (7)	0.3395 (2)	−0.09724 (19)	0.0186 (9)
C27	−0.1866 (8)	0.3553 (3)	−0.14135 (19)	0.0211 (10)
C28	−0.3883 (7)	0.3261 (2)	−0.14121 (19)	0.0210 (10)
C29	−0.4475 (7)	0.2807 (3)	−0.09820 (19)	0.0193 (9)
C30	−0.3014 (7)	0.2644 (2)	−0.05437 (18)	0.0171 (9)
C31	0.5825 (7)	0.0978 (2)	0.01721 (19)	0.0168 (9)
C32	0.6975 (7)	0.0645 (2)	−0.02403 (19)	0.0181 (9)
C33	0.6001 (7)	0.0535 (2)	−0.07663 (19)	0.0186 (9)
C34	0.3919 (7)	0.0767 (2)	−0.08623 (18)	0.0189 (9)
C35	0.2884 (7)	0.1091 (2)	−0.04296 (18)	0.0180 (9)
N1	0.3816 (6)	0.1193 (2)	0.00882 (15)	0.0150 (7)
O1	0.0464 (5)	0.08538 (17)	0.07478 (13)	0.0185 (7)
O2	0.0566 (5)	0.21017 (17)	0.13886 (12)	0.0183 (7)
O3	0.4119 (5)	0.12093 (17)	0.13196 (12)	0.0165 (6)
O4	0.3997 (5)	0.24982 (17)	0.07579 (12)	0.0171 (6)
O5	0.0218 (5)	0.21516 (17)	0.01910 (12)	0.0163 (6)
V1	0.19239 (12)	0.15756 (4)	0.07601 (3)	0.01457 (18)

Table A 3.2: Hydrogen coordinates and isotropic displacement parameters (Å^2) for [VO(dbm)$_2$py].

Atom	x	y	z	U_{eq}
H5	−0.3026	0.2430	0.1758	0.024
H6	−0.5147	0.3179	0.2294	0.028
H7	−0.3750	0.3683	0.3140	0.032
H8	−0.0275	0.3407	0.3450	0.029
H9	0.1831	0.2638	0.2924	0.024
H11	0.3645	0.0325	0.2782	0.021
H12	0.6052	−0.0515	0.3179	0.027
H13	0.9371	−0.0668	0.2799	0.026
H14	1.0261	−0.0003	0.2007	0.024
H15	0.7851	0.0819	0.1593	0.020
H20	0.7696	0.2988	0.0895	0.022
H21	1.0187	0.3862	0.1172	0.028
H22	0.9296	0.5100	0.1131	0.028
H23	0.5921	0.5456	0.0788	0.027
H24	0.3417	0.4574	0.0491	0.023
H26	0.0969	0.3597	−0.0971	0.022
H27	−0.1469	0.3859	−0.1713	0.025
H28	−0.4879	0.3373	−0.1711	0.025
H29	−0.5867	0.2608	−0.0985	0.023
H30	−0.3406	0.2326	−0.0251	0.021
H31	0.6502	0.1057	0.0532	0.020
H32	0.8402	0.0496	−0.0163	0.022
H33	0.6743	0.0304	−0.1056	0.022
H34	0.3219	0.0703	−0.1221	0.023
H35	0.1460	0.1250	−0.0497	0.022
H2	0.243 (9)	0.152 (3)	0.256 (2)	0.036 (16)
H17	0.222 (10)	0.372 (4)	−0.010 (3)	0.05 (2)

Table A 3.3: Anisotropic displacement parameters (Å^2) for [VO(dbm)$_2$py]. The anisotropic displacement factor exponent takes the form: -2π^2[h^{2}a^{*2}U^{11} + … + 2hka*b*U^{23}].

Atom	U^{11}	U^{22}	U^{33}	U^{12}	U^{13}	U^{23}
C1	0.017 (2)	0.015 (2)	0.016 (2)	−0.0016 (17)	0.0019 (16)	0.0003 (17)
C2	0.020 (2)	0.017 (2)	0.014 (2)	−0.0002 (18)	0.0013 (16)	0.0023 (17)
C3	0.016 (2)	0.011 (2)	0.017 (2)	−0.0043 (16)	−0.0029 (16)	0.0013 (16)
C4	0.022 (2)	0.012 (2)	0.018 (2)	0.0003 (17)	0.0052 (17)	0.0017 (17)
C5	0.022 (2)	0.017 (2)	0.020 (2)	0.0001 (18)	0.0046 (18)	0.0006 (18)
C6	0.022 (2)	0.020 (2)	0.029 (3)	0.0023 (19)	0.007 (2)	0.004 (2)
C7	0.034 (3)	0.018 (2)	0.029 (3)	0.006 (2)	0.016 (2)	−0.002 (2)
C8	0.033 (3)	0.018 (2)	0.021 (2)	−0.005 (2)	0.007 (2)	−0.0036 (19)
C9	0.020 (2)	0.019 (2)	0.020 (2)	−0.0033 (18)	0.0033 (18)	0.0003 (18)
C10	0.016 (2)	0.012 (2)	0.015 (2)	−0.0002 (16)	−0.0040 (16)	−0.0026 (16)
C11	0.022 (2)	0.016 (2)	0.016 (2)	−0.0001 (18)	0.0010 (17)	−0.0017 (17)
C12	0.036 (3)	0.016 (2)	0.014 (2)	0.001 (2)	−0.0016 (19)	0.0009 (17)
C13	0.027 (2)	0.016 (2)	0.020 (2)	0.0049 (19)	−0.0075 (19)	−0.0014 (18)
C14	0.019 (2)	0.019 (2)	0.021 (2)	0.0041 (18)	−0.0039 (18)	−0.0037 (18)
C15	0.019 (2)	0.013 (2)	0.017 (2)	−0.0016 (17)	−0.0039 (17)	−0.0001 (17)
C16	0.017 (2)	0.014 (2)	0.017 (2)	0.0007 (17)	0.0025 (16)	−0.0032 (17)
C17	0.021 (2)	0.014 (2)	0.017 (2)	−0.0026 (17)	−0.0024 (17)	0.0041 (17)
C18	0.017 (2)	0.017 (2)	0.014 (2)	0.0051 (17)	0.0003 (16)	0.0025 (17)
C19	0.019 (2)	0.015 (2)	0.0129 (19)	−0.0031 (17)	−0.0006 (16)	−0.0005 (16)
C20	0.023 (2)	0.017 (2)	0.016 (2)	0.0024 (18)	0.0017 (17)	−0.0017 (17)
C21	0.021 (2)	0.025 (3)	0.022 (2)	0.000 (2)	−0.0018 (18)	−0.002 (2)
C22	0.025 (2)	0.020 (2)	0.024 (2)	−0.009 (2)	0.0007 (19)	−0.0027 (19)
C23	0.031 (3)	0.013 (2)	0.024 (2)	−0.0013 (19)	0.001 (2)	−0.0003 (18)
C24	0.023 (2)	0.018 (2)	0.016 (2)	−0.0012 (18)	0.0000 (17)	0.0004 (17)
C25	0.016 (2)	0.011 (2)	0.016 (2)	0.0028 (16)	−0.0026 (16)	−0.0015 (16)
C26	0.018 (2)	0.014 (2)	0.023 (2)	0.0002 (18)	−0.0021 (17)	0.0002 (18)
C27	0.028 (2)	0.018 (2)	0.017 (2)	0.0007 (19)	−0.0016 (18)	0.0058 (18)
C28	0.024 (2)	0.016 (2)	0.022 (2)	0.0023 (18)	−0.0051 (18)	0.0027 (18)
C29	0.019 (2)	0.019 (2)	0.020 (2)	0.0029 (18)	−0.0016 (17)	−0.0003 (18)
C30	0.018 (2)	0.016 (2)	0.018 (2)	0.0012 (17)	−0.0013 (17)	0.0008 (17)
C31	0.018 (2)	0.011 (2)	0.021 (2)	−0.0017 (17)	−0.0009 (17)	0.0006 (17)
C32	0.020 (2)	0.015 (2)	0.020 (2)	−0.0010 (18)	0.0041 (17)	0.0033 (17)
C33	0.023 (2)	0.015 (2)	0.018 (2)	−0.0019 (18)	0.0030 (18)	−0.0004 (17)

C34	0.025 (2)	0.019 (2)	0.013 (2)	−0.0013 (19)	−0.0001 (17)	−0.0014 (17)
C35	0.021 (2)	0.016 (2)	0.017 (2)	−0.0002 (18)	−0.0024 (17)	−0.0009 (17)
N1	0.0171 (18)	0.0140 (18)	0.0140 (17)	−0.0003 (14)	0.0022 (14)	0.0022 (14)
O1	0.0182 (15)	0.0199 (17)	0.0176 (15)	−0.0019 (13)	0.0029 (12)	0.0034 (13)
O2	0.0208 (16)	0.0203 (16)	0.0137 (15)	0.0052 (13)	0.0004 (12)	−0.0002 (12)
O3	0.0169 (15)	0.0182 (16)	0.0144 (15)	0.0022 (12)	−0.0005 (12)	0.0002 (12)
O4	0.0184 (15)	0.0160 (16)	0.0167 (15)	0.0003 (12)	−0.0007 (12)	0.0026 (12)
O5	0.0170 (15)	0.0150 (15)	0.0170 (15)	−0.0002 (12)	0.0003 (12)	0.0037 (12)
V1	0.0164 (4)	0.0138 (4)	0.0134 (3)	0.0007 (3)	−0.0003 (3)	0.0013 (3)

Table A 3.4: Complete listing of bond lengths (Å) for [VO(dbm)$_2$py].

Bond	Distance	Bond	Distance
C1—O2	1.272 (5)	C20—C21	1.374 (6)
C1—C2	1.402 (6)	C20—H20	0.9500
C1—C4	1.488 (6)	C21—C22	1.389 (7)
C2—C3	1.390 (6)	C21—H21	0.9500
C2—H2	0.97 (6)	C22—C23	1.388 (7)
C3—O3	1.276 (5)	C22—H22	0.9500
C3—C10	1.499 (6)	C23—C24	1.393 (6)
C4—C5	1.392 (6)	C23—H23	0.9500
C4—C9	1.397 (6)	C24—H24	0.9500
C5—C6	1.387 (6)	C25—C30	1.392 (6)
C5—H5	0.9500	C25—C26	1.394 (6)
C6—C7	1.395 (7)	C26—C27	1.390 (6)
C6—H6	0.9500	C26—H26	0.9500
C7—C8	1.388 (7)	C27—C28	1.380 (7)
C7—H7	0.9500	C27—H27	0.9500
C8—C9	1.391 (6)	C28—C29	1.383 (6)
C8—H8	0.9500	C28—H28	0.9500
C9—H9	0.9500	C29—C30	1.393 (6)
C10—C15	1.400 (6)	C29—H29	0.9500
C10—C11	1.401 (6)	C30—H30	0.9500
C11—C12	1.384 (6)	C31—N1	1.332 (6)
C11—H11	0.9500	C31—C32	1.388 (6)
C12—C13	1.383 (7)	C31—H31	0.9500
C12—H12	0.9500	C32—C33	1.384 (6)

C13—C14	1.387 (7)	C32—H32	0.9500
C13—H13	0.9500	C33—C34	1.388 (6)
C14—C15	1.382 (6)	C33—H33	0.9500
C14—H14	0.9500	C34—C35	1.379 (6)
C15—H15	0.9500	C34—H34	0.9500
C16—O4	1.271 (5)	C35—N1	1.354 (5)
C16—C17	1.401 (6)	C35—H35	0.9500
C16—C19	1.505 (6)	N1—V1	2.154 (4)
C17—C18	1.383 (6)	O1—V1	1.612 (3)
C17—H17	0.99 (7)	O2—V1	2.004 (3)
C18—O5	1.284 (5)	O3—V1	1.994 (3)
C18—C25	1.492 (6)	O4—V1	2.138 (3)
C19—C20	1.381 (6)	O5—V1	1.994 (3)
C19—C24	1.398 (6)		

Table A 3.5: Complete listing of bond angles (°) for [VO(dbm)₂py].

Angle	Value	Angle	Value
O2—C1—C2	124.8 (4)	C23—C22—H22	120.1
O2—C1—C4	115.4 (4)	C21—C22—H22	120.1
C2—C1—C4	119.9 (4)	C22—C23—C24	120.3 (4)
C3—C2—C1	124.2 (4)	C22—C23—H23	119.9
C3—C2—H2	123 (3)	C24—C23—H23	119.9
C1—C2—H2	112 (3)	C23—C24—C19	119.1 (4)
O3—C3—C2	124.8 (4)	C23—C24—H24	120.4
O3—C3—C10	114.7 (4)	C19—C24—H24	120.4
C2—C3—C10	120.5 (4)	C30—C25—C26	119.0 (4)
C5—C4—C9	119.5 (4)	C30—C25—C18	119.2 (4)
C5—C4—C1	118.7 (4)	C26—C25—C18	121.8 (4)
C9—C4—C1	121.8 (4)	C27—C26—C25	120.7 (4)
C6—C5—C4	120.7 (4)	C27—C26—H26	119.6
C6—C5—H5	119.6	C25—C26—H26	119.6
C4—C5—H5	119.6	C28—C27—C26	119.4 (4)
C5—C6—C7	119.7 (5)	C28—C27—H27	120.3
C5—C6—H6	120.1	C26—C27—H27	120.3
C7—C6—H6	120.1	C27—C28—C29	120.9 (4)

C8—C7—C6	119.6 (4)	C27—C28—H28	119.5
C8—C7—H7	120.2	C29—C28—H28	119.5
C6—C7—H7	120.2	C28—C29—C30	119.5 (4)
C7—C8—C9	120.8 (5)	C28—C29—H29	120.2
C7—C8—H8	119.6	C30—C29—H29	120.2
C9—C8—H8	119.6	C25—C30—C29	120.4 (4)
C8—C9—C4	119.6 (4)	C25—C30—H30	119.8
C8—C9—H9	120.2	C29—C30—H30	119.8
C4—C9—H9	120.2	N1—C31—C32	123.2 (4)
C15—C10—C11	119.0 (4)	N1—C31—H31	118.4
C15—C10—C3	118.8 (4)	C32—C31—H31	118.4
C11—C10—C3	122.2 (4)	C33—C32—C31	118.6 (4)
C12—C11—C10	120.4 (4)	C33—C32—H32	120.7
C12—C11—H11	119.8	C31—C32—H32	120.7
C10—C11—H11	119.8	C32—C33—C34	118.8 (4)
C13—C12—C11	120.1 (4)	C32—C33—H33	120.6
C13—C12—H12	120.0	C34—C33—H33	120.6
C11—C12—H12	120.0	C35—C34—C33	119.0 (4)
C12—C13—C14	120.1 (4)	C35—C34—H34	120.5
C12—C13—H13	120.0	C33—C34—H34	120.5
C14—C13—H13	120.0	N1—C35—C34	122.6 (4)
C15—C14—C13	120.4 (4)	N1—C35—H35	118.7
C15—C14—H14	119.8	C34—C35—H35	118.7
C13—C14—H14	119.8	C31—N1—C35	117.8 (4)
C14—C15—C10	120.2 (4)	C31—N1—V1	122.6 (3)
C14—C15—H15	119.9	C35—N1—V1	119.2 (3)
C10—C15—H15	119.9	C1—O2—V1	127.5 (3)
O4—C16—C17	124.0 (4)	C3—O3—V1	126.5 (3)
O4—C16—C19	116.1 (4)	C16—O4—V1	129.3 (3)
C17—C16—C19	119.9 (4)	C18—O5—V1	132.9 (3)
C18—C17—C16	124.0 (4)	O1—V1—O3	96.55 (15)
C18—C17—H17	119 (4)	O1—V1—O5	97.63 (15)
C16—C17—H17	116 (4)	O3—V1—O5	165.76 (13)
O5—C18—C17	124.9 (4)	O1—V1—O2	98.43 (15)
O5—C18—C25	115.6 (4)	O3—V1—O2	88.31 (13)
C17—C18—C25	119.6 (4)	O5—V1—O2	90.95 (13)

C20—C19—C24	120.0 (4)		O1—V1—O4	176.86 (15)
C20—C19—C16	118.9 (4)		O3—V1—O4	82.08 (13)
C24—C19—C16	121.1 (4)		O5—V1—O4	83.69 (12)
C21—C20—C19	120.7 (4)		O2—V1—O4	84.38 (13)
C21—C20—H20	119.7		O1—V1—N1	93.06 (15)
C19—C20—H20	119.7		O3—V1—N1	89.73 (14)
C20—C21—C22	120.0 (4)		O5—V1—N1	88.17 (13)
C20—C21—H21	120.0		O2—V1—N1	168.49 (14)
C22—C21—H21	120.0		O4—V1—N1	84.12 (13)
C23—C22—C21	119.8 (4)			

A 4. Supplementary Data for (C$_9$H$_{17}$O$_2$)[VO$_2$(cupf)$_2$]

Table A 4.1: Atomic coordinates and equivalent isotropic displacement parameters (Å^2) for (C$_9$H$_{17}$O$_2$)[VO$_2$(cupf)$_2$]. U(eq) is defined as one third of the trace of the orthogonalized U^{ij} tensor.

Atom	x	y	z	U$_{eq}$
C1	0.65143 (15)	0.49101 (14)	0.49344 (14)	0.0157 (4)
C2	0.62000 (16)	0.53897 (15)	0.57583 (14)	0.0171 (4)
C3	0.57824 (17)	0.63023 (15)	0.56345 (15)	0.0209 (4)
C4	0.56722 (18)	0.67257 (16)	0.46947 (16)	0.0233 (5)
C5	0.60027 (18)	0.62323 (16)	0.38817 (15)	0.0231 (5)
C6	0.64355 (17)	0.53243 (16)	0.39922 (14)	0.0202 (4)
C7	0.55494 (16)	0.03738 (15)	0.63376 (13)	0.0162 (4)
C8	0.55489 (17)	−0.05966 (15)	0.61567 (15)	0.0200 (4)
C9	0.45830 (18)	−0.11022 (16)	0.62177 (15)	0.0227 (4)
C10	0.36398 (18)	−0.06402 (16)	0.64379 (15)	0.0231 (5)
C11	0.36595 (17)	0.03348 (16)	0.66072 (15)	0.0214 (4)
C12	0.46228 (17)	0.08525 (15)	0.65702 (14)	0.0184 (4)
C13	1.16068 (18)	0.24404 (14)	0.77446 (15)	0.0168 (4)
C14	1.08952 (17)	0.15728 (14)	0.78072 (14)	0.0166 (4)
C15	1.03572 (15)	0.15290 (14)	0.87856 (14)	0.0134 (4)
C16	0.94109 (17)	0.08141 (15)	0.86972 (15)	0.0193 (4)
C17	1.11801 (17)	0.12509 (16)	0.96624 (15)	0.0204 (4)
C18	1.04992 (16)	0.33988 (14)	0.88795 (13)	0.0135 (4)

C19	1.13612 (17)	0.35139 (16)	0.97784 (14)	0.0199 (4)
C20	0.96695 (18)	0.42105 (15)	0.88620 (15)	0.0195 (4)
C21	1.10262 (16)	0.33667 (14)	0.78942 (14)	0.0150 (4)
N1	0.69629 (13)	0.39744 (12)	0.50905 (11)	0.0150 (3)
N2	0.69833 (14)	0.33810 (12)	0.43646 (12)	0.0170 (3)
N3	0.74397 (14)	0.04851 (12)	0.62234 (12)	0.0186 (4)
N4	0.65314 (14)	0.09283 (12)	0.62638 (11)	0.0151 (3)
O1	0.93080 (12)	0.26310 (10)	0.58913 (10)	0.0174 (3)
C18	1.04992 (16)	0.33988 (14)	0.88795 (13)	0.0135 (4)
C19	1.13612 (17)	0.35139 (16)	0.97784 (14)	0.0199 (4)
C20	0.96695 (18)	0.42105 (15)	0.88620 (15)	0.0195 (4)
C21	1.10262 (16)	0.33667 (14)	0.78942 (14)	0.0150 (4)
N1	0.69629 (13)	0.39744 (12)	0.50905 (11)	0.0150 (3)
N2	0.69833 (14)	0.33810 (12)	0.43646 (12)	0.0170 (3)
N3	0.74397 (14)	0.04851 (12)	0.62234 (12)	0.0186 (4)
N4	0.65314 (14)	0.09283 (12)	0.62638 (11)	0.0151 (3)
O1	0.93080 (12)	0.26310 (10)	0.58913 (10)	0.0174 (3)
O2	0.81861 (12)	0.26285 (10)	0.74284 (10)	0.0167 (3)
O3	0.73344 (12)	0.37361 (10)	0.60237 (9)	0.0176 (3)
O4	0.74355 (12)	0.25832 (9)	0.46507 (10)	0.0159 (3)
O5	0.82510 (11)	0.10799 (11)	0.61008 (11)	0.0189 (3)
O6	0.64683 (11)	0.18494 (10)	0.62151 (10)	0.0179 (3)
O7	1.25554 (14)	0.23940 (12)	0.75695 (13)	0.0280 (4)
O8	0.98370 (14)	0.24893 (10)	0.89575 (12)	0.0210 (3)
V1	0.80548 (3)	0.24906 (2)	0.62185 (2)	0.01151 (12)

Table A 4.2: Hydrogen coordinates and isotropic displacement parameters ($Å^2$) for $(C_9H_{17}O_2)[VO_2(cupf)_2]$.

Atom	*x*	*y*	*z*	U_{eq}
H2	0.6270	0.5096	0.6396	0.021
H3	0.5570	0.6641	0.6192	0.025
H4	0.5373	0.7348	0.4609	0.028
H5	0.5930	0.6523	0.3243	0.028
H6	0.6672	0.4993	0.3440	0.024
H8	0.6193	−0.0910	0.5995	0.024

H9	0.4570	−0.1770	0.6107	0.027
H10	0.2982	−0.0989	0.6473	0.028
H11	0.3010	0.0652	0.6750	0.026
H12	0.4644	0.1517	0.6701	0.022
H14A	1.1346	0.0995	0.7751	0.020
H14B	1.0316	0.1576	0.7239	0.020
H16A	0.9689	0.0182	0.8549	0.029
H16B	0.8858	0.1011	0.8159	0.029
H16C	0.9080	0.0792	0.9327	0.029
H17A	1.1849	0.1630	0.9648	0.031
H17B	1.1358	0.0574	0.9616	0.031
H17C	1.0863	0.1371	1.0287	0.031
H19A	1.1653	0.4163	0.9791	0.030
H19B	1.1958	0.3060	0.9726	0.030
H20A	0.9111	0.4127	0.8294	0.029
H20B	1.0046	0.4819	0.8799	0.029
H20C	0.9319	0.4206	0.9482	0.029
H21A	1.0450	0.3463	0.7333	0.018
H21B	1.1557	0.3896	0.7885	0.018
H8A	0.955 (2)	0.2501 (15)	0.965 (2)	0.016 (6)

Table A 4.3: Anisotropic displacement parameters (Å^2) for ($C_9H_{17}O_2$)[VO_2(cupf)$_2$]. The anisotropic displacement factor exponent takes the form: $-2\pi^2[h^2a^{*2}U^{11} + \ldots + 2hka^*b^*U^{23}]$.

Atom	U^{11}	U^{22}	U^{33}	U^{12}	U^{13}	U^{23}
C1	0.0123 (9)	0.0172 (10)	0.0173 (9)	−0.0015 (7)	−0.0004 (7)	0.0013 (7)
C2	0.0152 (9)	0.0202 (10)	0.0159 (8)	−0.0011 (8)	0.0019 (7)	0.0018 (7)
C3	0.0185 (10)	0.0207 (11)	0.0238 (10)	0.0010 (8)	0.0036 (8)	0.0002 (8)
C4	0.0198 (10)	0.0203 (11)	0.0292 (11)	0.0014 (8)	−0.0003 (8)	0.0058 (8)
C5	0.0227 (11)	0.0243 (12)	0.0213 (10)	−0.0020 (9)	−0.0017 (8)	0.0085 (8)
C6	0.0203 (10)	0.0222 (11)	0.0176 (9)	−0.0040 (8)	0.0003 (8)	0.0015 (8)
C7	0.0170 (10)	0.0189 (10)	0.0124 (8)	−0.0005 (8)	0.0009 (7)	0.0014 (7)
C8	0.0201 (10)	0.0195 (11)	0.0204 (9)	0.0016 (8)	0.0017 (8)	−0.0020 (8)
C9	0.0259 (11)	0.0184 (11)	0.0233 (10)	−0.0034 (9)	0.0007 (8)	−0.0029 (8)
C10	0.0226 (11)	0.0269 (12)	0.0200 (9)	−0.0056 (9)	0.0029 (8)	−0.0023 (8)
C11	0.0178 (10)	0.0261 (11)	0.0207 (9)	0.0026 (8)	0.0048 (8)	0.0004 (8)

C12	0.0205 (10)	0.0183 (10)	0.0168 (9)	0.0021 (8)	0.0033 (7)	0.0007 (7)
C13	0.0181 (10)	0.0204 (11)	0.0123 (9)	0.0003 (7)	0.0035 (7)	0.0024 (7)
C14	0.0198 (10)	0.0139 (10)	0.0174 (9)	0.0027 (8)	0.0071 (7)	−0.0001 (7)
C15	0.0130 (9)	0.0115 (9)	0.0165 (8)	0.0028 (7)	0.0051 (7)	0.0033 (7)
C16	0.0212 (10)	0.0121 (10)	0.0253 (10)	−0.0023 (8)	0.0050 (8)	0.0015 (7)
C17	0.0177 (10)	0.0221 (11)	0.0217 (9)	0.0065 (8)	0.0030 (8)	0.0097 (8)
C18	0.0148 (9)	0.0129 (9)	0.0129 (8)	−0.0035 (7)	0.0018 (7)	0.0011 (6)
C19	0.0209 (10)	0.0233 (11)	0.0150 (9)	−0.0081 (8)	−0.0009 (7)	−0.0007 (7)
C20	0.0252 (11)	0.0121 (10)	0.0217 (9)	0.0002 (8)	0.0045 (8)	−0.0012 (7)
C21	0.0165 (9)	0.0147 (10)	0.0141 (8)	−0.0031 (7)	0.0037 (7)	0.0024 (7)
N1	0.0146 (8)	0.0184 (9)	0.0119 (7)	−0.0012 (6)	0.0004 (6)	0.0015 (6)
N2	0.0154 (8)	0.0201 (9)	0.0155 (7)	−0.0015 (7)	0.0010 (6)	−0.0007 (6)
N3	0.0168 (9)	0.0172 (9)	0.0218 (8)	0.0011 (7)	0.0019 (7)	−0.0009 (6)
N4	0.0178 (8)	0.0136 (8)	0.0138 (7)	0.0012 (6)	0.0015 (6)	−0.0001 (6)
O1	0.0146 (7)	0.0245 (8)	0.0135 (6)	−0.0012 (6)	0.0030 (5)	−0.0009 (5)
O2	0.0163 (7)	0.0212 (8)	0.0124 (6)	0.0024 (5)	0.0004 (5)	0.0004 (5)
O3	0.0219 (7)	0.0190 (7)	0.0114 (6)	0.0026 (6)	−0.0015 (5)	0.0011 (5)
O4	0.0167 (7)	0.0178 (8)	0.0131 (6)	0.0001 (5)	0.0007 (5)	−0.0012 (5)
O5	0.0148 (7)	0.0186 (8)	0.0236 (7)	0.0010 (6)	0.0036 (5)	−0.0018 (5)
O6	0.0187 (7)	0.0136 (7)	0.0213 (7)	0.0027 (5)	0.0022 (5)	0.0013 (5)
O7	0.0194 (8)	0.0339 (10)	0.0329 (9)	0.0013 (6)	0.0131 (7)	0.0059 (7)
O8	0.0218 (8)	0.0186 (8)	0.0228 (8)	0.0000 (5)	0.0037 (6)	0.0006 (5)
V1	0.01081 (19)	0.0136 (2)	0.00998 (18)	0.00075 (11)	0.00043 (13)	0.00021 (10)

Table A 4.4: Complete listing of bond lengths (Å) for (C$_9$H$_{17}$O$_2$)[VO$_2$(cupf)$_2$].

Bond	Distance	Bond	Distance
C1—C2	1.389 (3)	C15—C16	1.531 (3)
C1—C6	1.392 (3)	C16—H16A	0.9800
C1—N1	1.433 (3)	C16—H16B	0.9800
C2—C3	1.385 (3)	C16—H16C	0.9800
C2—H2	0.9500	C17—H17A	0.9800
C3—C4	1.395 (3)	C17—H17B	0.9800
C3—H3	0.9500	C17—H17C	0.9800
C4—C5	1.394 (3)	C18—O8	1.524 (2)
C4—H4	0.9500	C18—C20	1.528 (3)
C5—C6	1.384 (3)	C18—C19	1.532 (3)

C5—H5	0.9500	C18—C21	1.539 (2)
C6—H6	0.9500	C19—H19A	0.9800
C7—C8	1.385 (3)	C19—H19B	0.9800
C7—C12	1.386 (3)	C19—H19C	0.9800
C7—N4	1.448 (3)	C20—H20A	0.9800
C8—C9	1.392 (3)	C20—H20B	0.9800
C8—H8	0.9500	C20—H20C	0.9800
C9—C10	1.387 (3)	C21—H21A	0.9900
C9—H9	0.9500	C21—H21B	0.9900
C10—C11	1.389 (3)	N1—N2	1.289 (2)
C10—H10	0.9500	N1—O3	1.336 (2)
C11—C12	1.394 (3)	N2—O4	1.292 (2)
C11—H11	0.9500	N3—N4	1.283 (2)
C12—H12	0.9500	N3—O5	1.324 (2)
C13—O7	1.214 (3)	N4—O6	1.298 (2)
C13—C14	1.507 (3)	O1—V1	1.6562 (16)
C13—C21	1.508 (3)	O2—V1	1.6353 (15)
C14—C15	1.538 (2)	O3—V1	1.9661 (16)
C14—H14A	0.9900	O4—V1	2.1757 (16)
C14—H14B	0.9900	O5—V1	2.0053 (17)
C15—O8	1.521 (2)	O6—V1	2.1455 (16)
C15—C17	1.524 (3)	O8—H8A	1.04 (3)

Table A 4.5: Complete listing of bond angles (°) for (C$_9$H$_{17}$O$_2$)[VO$_2$(cupf)$_2$].

Angle	Value	Angle	Value
C2—C1—C6	121.98 (19)	H17A—C17—H17B	109.5
C2—C1—N1	117.54 (17)	C15—C17—H17C	109.5
C6—C1—N1	120.45 (17)	H17A—C17—H17C	109.5
C3—C2—C1	118.89 (18)	H17B—C17—H17C	109.5
C3—C2—H2	120.6	O8—C18—C20	105.51 (15)
C1—C2—H2	120.6	O8—C18—C19	111.27 (15)
C2—C3—C4	120.28 (19)	C20—C18—C19	109.72 (16)
C2—C3—H3	119.9	O8—C18—C21	108.10 (15)
C4—C3—H3	119.9	C20—C18—C21	110.40 (16)
C5—C4—C3	119.7 (2)	C19—C18—C21	111.66 (16)

C5—C4—H4	120.2	C18—C19—H19A	109.5
C3—C4—H4	120.2	C18—C19—H19B	109.5
C6—C5—C4	120.92 (19)	H19A—C19—H19B	109.5
C6—C5—H5	119.5	C18—C19—H19C	109.5
C4—C5—H5	119.5	H19A—C19—H19C	109.5
C5—C6—C1	118.22 (19)	H19B—C19—H19C	109.5
C5—C6—H6	120.9	C18—C20—H20A	109.5
C1—C6—H6	120.9	C18—C20—H20B	109.5
C8—C7—C12	122.18 (19)	H20A—C20—H20B	109.5
C8—C7—N4	120.19 (18)	C18—C20—H20C	109.5
C12—C7—N4	117.62 (19)	H20A—C20—H20C	109.5
C7—C8—C9	118.47 (19)	H20B—C20—H20C	109.5
C7—C8—H8	120.8	C13—C21—C18	112.86 (16)
C9—C8—H8	120.8	C13—C21—H21A	109.0
C10—C9—C8	120.6 (2)	C18—C21—H21A	109.0
C10—C9—H9	119.7	C13—C21—H21B	109.0
C8—C9—H9	119.7	C18—C21—H21B	109.0
C9—C10—C11	119.8 (2)	H21A—C21—H21B	107.8
C9—C10—H10	120.1	N2—N1—O3	121.49 (16)
C11—C10—H10	120.1	N2—N1—C1	121.32 (16)
C10—C11—C12	120.6 (2)	O3—N1—C1	117.17 (15)
C10—C11—H11	119.7	N1—N2—O4	112.10 (15)
C12—C11—H11	119.7	N4—N3—O5	111.55 (17)
C7—C12—C11	118.3 (2)	N3—N4—O6	121.96 (17)
C7—C12—H12	120.8	N3—N4—C7	118.37 (17)
C11—C12—H12	120.8	O6—N4—C7	119.65 (16)
O7—C13—C14	122.73 (18)	N1—O3—V1	116.96 (11)
O7—C13—C21	123.30 (18)	N2—O4—V1	115.97 (11)
C14—C13—C21	113.95 (18)	N3—O5—V1	121.07 (12)
C13—C14—C15	112.58 (16)	N4—O6—V1	111.68 (11)
C13—C14—H14A	109.1	C15—O8—C18	119.85 (15)
C15—C14—H14A	109.1	C15—O8—H8A	109.7 (12)
C13—C14—H14B	109.1	C18—O8—H8A	106.4 (12)
C15—C14—H14B	109.1	O2—V1—O1	104.78 (7)
H14A—C14—H14B	107.8	O2—V1—O3	91.37 (6)
O8—C15—C17	111.33 (16)	O1—V1—O3	106.01 (7)

179

O8—C15—C16	105.47 (15)	O2—V1—O5	101.31 (7)
C17—C15—C16	109.15 (16)	O1—V1—O5	88.51 (7)
O8—C15—C14	108.68 (15)	O3—V1—O5	157.74 (6)
C17—C15—C14	111.55 (16)	O2—V1—O6	92.65 (6)
C16—C15—C14	110.49 (16)	O1—V1—O6	156.61 (6)
C15—C16—H16A	109.5	O3—V1—O6	88.74 (6)
C15—C16—H16B	109.5	O5—V1—O6	72.61 (6)
H16A—C16—H16B	109.5	O2—V1—O4	162.11 (7)
C15—C16—H16C	109.5	O1—V1—O4	88.47 (7)
H16A—C16—H16C	109.5	O3—V1—O4	73.16 (5)
H16B—C16—H16C	109.5	O5—V1—O4	90.84 (6)
C15—C17—H17A	109.5	O6—V1—O4	78.38 (5)
C15—C17—H17B	109.5		

A 5.   Supplementary Data for Kinetic Measurements in Chapter 6.

The tables in this section give the observed first-order rate constants for the reactions described in Chapter 6. The ligand concentrations are given in mol.dm^{-3}; the first-order rate constant, k_{obs} is given in the unit s^{-1}; temperatures are given in °C.

Table A 5.1: Plot of Abs (λ= 360 nm) vs. pH of 0.90 mM [VO(O$_2$)$_2$bpy]⁻ in 0.10 M sodium phosphate buffer solution, µ= 1.0 M at 25 °C.

pH	Abs
6.5	0.780
6.0	0.776
5.5	0.757
5.0	0.671
4.5	0.590
4.0	0.550
3.5	0.535
3.0	0.510

Table A 5.2: Temperature and 2,3-dipic concentration dependence of the pseudo-first order rate constant for the substitution reaction between 0.90 mM [VO(O$_2$)$_2$bpy]$^-$ and 2,3-dipic in 0.10 M sodium phosphate buffer solution, μ= 1.0 M, pH 5.0.

[2,3-dipic]	k_{obs} (s^{-1})	k_{obs} (s^{-1})	k_{obs} (s^{-1})	k_{obs} (s^{-1})
	15 ℃	25 ℃	35 ℃	45 ℃
0.06	0.001059(4)	0.0034(2)	0.0098(2)	0.0181(2)
0.08	0.001115(5)	0.00326(3)	0.0101(3)	0.0189(1)
0.12	0.001192(5)	0.00375(2)	0.0108(2)	0.0211(1)
0.14	0.001248(7)	0.00357(2)	0.0118(5)	0.0221(3)
0.16	0.001282(9)	0.00369(2)	0.0118(3)	0.0231(2)
0.18	0.001299(1)	0.00382(3)	0.011634(2)	0.024(1)
0.2	0.00133(1)	0.00389(2)	0.0125(4)	0.0248(6)
0.25	0.00143(2)	0.00418(5)	0.013(6)	0.0267(2)

Table A 5.3: pH and 2,3-dipic concentration dependence of the pseudo-first order rate constant for the substitution reaction between 0.90 mM [VO(O$_2$)$_2$bpy]$^-$ and 2,3-dipic in 0.10 M sodium phosphate buffer solution, μ= 1.0 M at 25 ℃, pH 7.5.

[2,3-dipic] (M)	k_{obs} (s^{-1})
0.03	0.0011(2)
0.04	0.001(3)
0.06	0.000878(2)
0.08	0.000777(1)
0.12	0.00053(1)
0.16	0.000439(9)

Table A 5.4: pH and 2,3-dipic concentration dependence of the pseudo-first order rate constant for the substitution reaction between 0.90 mM [VO(O$_2$)$_2$bpy]$^-$ and 2,3-dipic in 0.10 M sodium phosphate buffer solution, μ= 1.0 M at 25 ℃, pH 6.5.

[2,3-dipic] (M)	k_{obs} (s^{-1})
0.03	0.00234(4)
0.04	0.0008(5)
0.06	0.00185(6)
0.08	0.000533(3)
0.12	0.001679(2)
0.16	0.001586(1)
0.2	0.00132(2)
0.25	0.00234(4)

Table A 5.5: pH and 2,3-dipic concentration dependence of the pseudo-first order rate constant for the substitution reaction between 0.90 mM [VO(O$_2$)$_2$bpy]$^-$ and 2,3-dipic in 0.10 M sodium phosphate buffer solution, μ= 1.0 M at 25 ℃, pH 4.5.

[2,3-dipic] (M)	k$_{obs}$ (s^{-1})
0.06	0.0171(2)
0.12	0.01799(3)
0.18	0.0192(3)
0.25	0.0199(3)

Table A 5.6: pH and 2,3-dipic concentration dependence of the pseudo-first order rate constant for the substitution reaction between 0.90 mM [VO(O$_2$)$_2$bpy]$^-$ and 2,3-dipic in 0.10 M sodium phosphate buffer solution, μ= 1.0 M at 25 ℃, pH 4.0.

[2,3-dipic] (M)	k$_{obs}$ (s^{-1})
0.06	0.0292(6)
0.08	0.0301(6)
0.12	0.0315(7)
0.16	0.0321(8)
0.18	0.0325(7)
0.2	0.033(9)
0.25	0.034(7)

Table A 5.7: pH and 2,3-dipic concentration dependence of the pseudo-first order rate constant for the substitution reaction between 0.90 mM [VO(O$_2$)$_2$bpy]$^-$ and 2,3-dipic in 0.10 M sodium phosphate buffer solution, μ= 1.0 M at 25 ℃, pH 3.5.

[2,3-dipic] (M)	k$_{obs}$ (s^{-1})
0.06	0.035(1)
0.12	0.036(1)
0.18	0.038(1)
0.25	0.039(2)

Table A 5.8: pH and 2,3-dipic concentration dependence of the pseudo-first order rate constant for the substitution reaction between 0.90 mM [VO(O$_2$)$_2$bpy]$^-$ and 2,3-dipic in 0.10 M sodium phosphate buffer solution, μ= 1.0 M at 25 ℃, pH 3.0.

[2,3-dipic] (M)	k$_{obs}$ (s^{-1})
0.06	0.037(2)
0.12	0.034(1)
0.18	0.035(2)
0.25	0.033(2)

Table A 5.9: Formation and disappearance of vanadium species as followed via ^{51}V NMR for the substitution reaction between 0.90 mM [VO(O$_2$)$_2$bpy]$^-$ and 2,3-dipic in 0.10 M sodium phosphate buffer solution, μ= 1.0 M at 20 °C, pH 5.0.

Disappearance of [VO(O$_2$)$_2$bpy]$^-$		Formation of [VO(O$_2$)(2,3-dipic)$_2$]$^-$	
Time (x 10^3 s)	Peak Height (mm)	Time (x 10^3 s)	Peak Height (mm)
200	45.0	200	1.0
400	37.0	400	5.0
600	29.0	600	8.0
800	23.0	800	11.0
1000	22.0	1000	13.0
1200	14.0	1200	15.0
1400	12.0	1400	16.0
1600	10.0	1600	18.0
1800	7.0	1800	17.5
2000	5.5	2000	19.0
2200	5.0	2200	18.5
2400	4.0	2400	19.0
2600	3.5	2600	19.5
2800	3.0	2800	20.0
3000	3.0	3000	20.0
3200	2.5	3200	20.0
3400	2.5	3400	21.0
3600	2.5	3600	21.0
3800	2.0	3800	21.0